Establishment of intraportal islet allotransplantation in a diabetic pig model

von Johanna Pilz

Inaugural-Dissertation zur Erlangung der Doktorwürde

der Tierärztlichen Fakultät der Ludwig-Maximilians-Universität München

Establishment of intraportal islet allotransplantation in a diabetic pig model

von Johanna Pilz

aus München

München 2024

Aus dem Veterinärwissenschaftlichen Department

der Tierärztlichen Fakultät

der Ludwig-Maximilians-Universität München

Lehrstuhl für Molekulare Tierzucht und Biotechnologie

Arbeit angefertigt unter der Leitung von

Prof. Dr. Elisabeth G. Kemter

Mitbetreuung durch Univ.-Prof. Dr. Eckhard Wolf

Gedruckt mit Genehmigung der Tierärztlichen Fakultät

der Ludwig-Maximilians-Universität München

Dekan:	Univ.-Prof. Dr. Reinhard K. Straubinger, Ph.D.
Berichterstatter:	Prof. Dr. Elisabeth G. Kemter
Korreferent/en:	Priv.-Doz. Dr. Roswitha Dorsch
	Univ.-Prof. Dr. Andreas F. Parzefall
	Univ.-Prof. Dr. Holm Zerbe
	Univ.-Prof. Dr. Heidrun Potschka

Tag der Promotion: 6. Juli 2024

Für meine Eltern,

die mir stets Vorbild und Unterstützung sind.

Parts of this work have been published in a peer-reviewed journal or were presented at international congresses:

Publication in peer-reviewed journal:

Functional maturation and longitudinal imaging of intraportal neonatal porcine islet grafts in genetically diabetic pigs

J. Pilz*, N. Gloddek*, F. Lindheimer, M. J. Lindner, D. Puhr-Westerheide, M. Ümütlü, C. Cyran, M. Seidensticker, S. Renner, D. Merkus, R. Lindner, M. Kraetzl, D. Teupser, P. Bartenstein, S. I. Ziegler, E. Wolf, E. Kemter

American Journal of Transplantation; DOI: 10.1016/j.ajt.2024.02.026

* contributed equally

The following abstracts were submitted for presentation at international congresses:

Intraportal transplantation of neonatal porcine islets cures diabetes mellitus of *INS*^{C94Y} transgenic pigs

J. Pilz*, N. Gloddek*, D. Puhr-Westerheide, M. Ümütlü, E. Wolf, E. Kemter

IPITA-IXA-CTMR Joint Congress 2023; San Diego, USA

Transplantation, 107(10S2): p 31, October 2023.
DOI: 10.1097/01.tp.0000993896.67852.87

[^{68}Ga]Ga-DOTA-Exendin-4 PET/CT detects increased liver signal of transplanted neonatal islet cell clusters in diabetic pig recipients

N. Gloddek*, J. Pilz*, F. Lindheimer, M. Lindner, P. Bartenstein, S. Ziegler, D. Puhr-Westerheide, E. Wolf, E. Kemter

IPITA-IXA-CTMR Joint Congress 2023; San Diego, USA

Transplantation, 107(10S2): p 138, October 2023.
DOI: 10.1097/01.tp.0000994536.09032.fc;

[^{68}Ga]-DOTA-Exendin-4 PET/CT non-invasive imaging for detection of reduced β-cell volume in a diabetic pig model

J. Pilz*, N. Gloddek*, F. Lindheimer* , M. Lindner, I. Berg, A. Bollenbacher, P. Bartenstein, S. Ziegler, E. Wolf, E. Kemter

The Swine in Biomedical Research Conference 2022; Madison, USA

* contributed equally

TABLE OF CONTENTS

INDEX OF ABBREVIATIONS

ALT	Alanine aminotransferase
ALX	Alloxan
AP	Alkaline phosphatase
APIs	Adult porcine islets
ASA	Acetylic salicylic acid
AST	Aspartate aminotransferase
ATG	Antithymocyte globulin
BCM	Beta-cell mass
bidist.	Bidistilled
BMI	Body mass index
BW	Body weight
[^{11}C]5-HTP	[^{11}C]5-hydroxytryptophan
CITR	Collaborative Islet Transplant Registry
CITRAT	Citrat-0.5% Tween®20 buffer
CMV	Cytomegalovirus
CNI	Calcineurin inhibitor
CRP	C-reactive protein
CT	Computed tomography
DAB	3,3'-diaminobenzidine
DAPI	4',6-diamidino-2-phenylindole
DOTA	1,4,7,10-tetraazacyclododecane-1,4,7,10-tetraacetic acid
EDTA	Ethylenediaminetetraacetic acid
EPITA	European Pancreas and Islet Transplant Association
ER	Endoplasmic reticulum
FBG	Fasted blood glucose
[^{18}F]FDG	[^{18}F]Fluorodeoxyglucose
Ga	Gallium
GADA	Glutamic acid decarboxylase antibodies
GCG	Glucagon

GGT	Gamma-glutamyl transferase
GIP	Glucose-dependent insulinotropic polypeptide
GLP-1	Glucagon-like peptide-1
GLP-1R	Glucagon-like peptide-1 receptor
GLUT2	Glucose transporter 2
HbA1c	Hemoglobin A1c
H&E	Hematoxylin & Eosin
HIAR	Heat-induced antigen retrieval
HLA	Human leukocyte antigen
HRP	Horseradish peroxidase
HTK	Histidine-tryptophan ketoglutarate
IAA	Insulin autoantibodies
IA-2A	Islet antigen-2 autoantibodies
IAK	Islet-after-kidney
IBMIR	Instant blood-mediated inflammatory reaction
ICC	Islet cell cluster
IEQ	Islet equivalent
IF	Immunofluorescence
IgG	Immunoglobulin G
i.m.	Intramuscular
IHC	Immunohistochemistry
INS	Insulin
IPITA	International Pancreas and Islet Transplant Association
ITA	Islet transplant alone
ITx	Islet transplantation
i.v.	Intravenously
JPIs	Juvenile porcine islets
KAI	Kidney-after-islet
LAIA	Long-acting insulin analog
mAb	Monoclonal antibody

ME	Methacarn
MHC	Major histocompatibility complex
MIDY	Mutant *INS*-gene induced diabetes of youth
MMF	Mycophenolate mofetil
MRI	Magnet resonance imaging
MSC	Mesenchymal stromal cell
mTOR	Mammalian target of rapamycin
NHPs	Non-human primates
NPIs	Neonatal porcine islets
NS	Neutral serum
NSG	NOD-*scid* gamma
OD	Optical density
OGTT	Oral glucose tolerance test
pAb	Polyclonal antibody
PBS	Phosphate-buffered salt solution
PET	Positron emission tomography
PET/CT	Positron emission tomography/computed tomography
PFA	Paraformaldehyde
pH	Hydrogen ion concentration
PIPIT	Percutaneous intraportal pancreatic islet transplantation
PMN	Polymorphonuclear leukocyte
PNDM	Permanent neonatal diabetes mellitus
ROS	Radical oxygen species
RT	Room temperature
SAIA	Short-acting insulin analog
s.c.	subcutaneously
SD	Standard deviation
SEM	Standard error of the mean
SIK	Simultaneous-islet-and-kidney
SPECT	Single photon emission computed tomography

SPIO	superparamagnetic iron oxide
SST	Somatostatin
STZ	Streptozotocin
SUV	Standard uptake value
SYP	Synaptophysin
TAC	Tacrolimus
TBS	Tris-buffer salt solution
T1D	Type 1 diabetes
T2D	Type 2 diabetes
TF	Tissue factor
TRIS	Tris-EDTA-0.5% Tween®20 buffer
Tx	Transplantation
Txd	Transplantation day
ULN	Upper limit of the normal
UPR	Unfolded protein response
VOI	Volume of interest
WT	Wildtype
ZnT8A	Zinc Transporter-8 Autoantibody
+	Positive

Chemical structural formulas

EtOH	Ethanol
HCl	Hydrochloric acid
H_2O_2	Hydrogen peroxide
KH_2PO_4	Potassium dihydrogen phosphate
KCl	Potassium chloride
NaCl	Sodium chloride
NaOH	Caustic soda
Na_2HPO_4	Disodium hydrogen phosphate
NO	Nitric oxide

Units

cm	Centimeter
G	Gauge
g	Gram
h	Hour
IU	International Unit
kg	Kilogram
KIU	Kallikrein-Inhibitor-Unit
l	Liter
M	Molar
MBq	Megabecquerel
mg	Milligram
min	Minute
ml	Milliliter
µl	Microliter
mm	Millimeter
µm	Micrometer
mmHg	Millimeter of mercury
mmol	Millimole
µmol	Micromole
nmol	Nanomole
sec	Second
U	Unit
°C	Degree Celsius

I. INTRODUCTION

Type 1 diabetes (T1D) is a chronic autoimmune disease, which is characterized by the destruction of insulin-producing beta cells in the pancreatic islets of Langerhans (reviewed in ZAJEC et al., 2022). Although there has been a great increase in knowledge about the pathophysiology of the disease and significant improvements in treatment and management, T1D remains a serious burden for those affected (reviewed in QUATTRIN, MASTRANDREA & WALKER, 2023). T1D patients are dependent on a lifelong supply of exogenous insulin (reviewed in KATSAROU et al., 2017). While exogenous insulin therapy can prevent hyperglycemia and slow the onset of complications, it is not a curative treatment for T1D and cannot fully restore glucose homeostasis, which is why diabetes-associated complications cannot be completely prevented (reviewed in RICHARDS et al., 2020). As a result, T1D patients still have a lower life expectancy compared to the general population (reviewed in PIEMONTI, 2022).

In recent years, transplantation of pancreatic islets (ITx) has emerged as a promising strategy for curing insulin-dependent diabetes by providing a beta-cell replacement (reviewed in RICKELS & ROBERTSON, 2019). ITx is primarily aimed at T1D patients affected by repeated, severe hypoglycemic episodes in combination with impaired hypoglycemic awareness, or for those suffering from high glycemic instability (reviewed in VANTYGHEM et al., 2019). The portal vein represents the standard transplantation site for ITx and can be accessed in a minimally invasive procedure using imaging techniques and interventional radiology (reviewed in DELAUNE et al., 2017; reviewed in VENTURINI et al., 2018). Despite the great potential of ITx as a curative treatment for T1D, several hurdles limit its broad clinical application, in particular the shortage of donor organs and a pronounced loss of islet graft mass after transplantation (reviewed in WALKER, APPARI & FORBES, 2022).

The fate of the transplanted islets after ITx can so far only be determined indirectly based on functional parameters, which do not allow reliable conclusions to be drawn about the viable beta-cell mass (BCM). However, detecting changes in the viable BCM is crucial for timely therapeutic intervention in the event of graft loss

and thus for optimizing the ITx outcome. This results in an urgent need for non-invasive monitoring procedures for the quantitative recording of BCM (reviewed in RICHARDS et al., 2020). Biomedical imaging such as positron emission tomography/computed tomography (PET/CT) represents a highly promising approach in this context (JANSEN et al., 2023).

Animal models are a valuable tool in research to gain a better understanding of the pathophysiology of human diseases and to develop novel therapeutic strategies (reviewed in ROBINSON et al., 2019). ITx research requires diabetic animal models, which can be generated based on genetic modification, chemical induction or surgical intervention (reviewed in SAKATA et al., 2012). Pigs share many anatomical, physiological and pathophysiological similarities with humans, which is why porcine models have a high translational value (reviewed in WOLF et al., 2014). Transgenic *INS*^{C94Y} pigs develop a stable, insulin-dependent diabetic phenotype without further intervention due to a mutation in the insulin gene, making them particularly suitable for ITx studies (RENNER et al., 2013). Neonatal porcine islets (NPIs) are of great interest for xenotransplantation, which explains the great research efforts in this field (reviewed in COE, MARKMANN & RICKERT, 2020). NPIs are characterized by the fact that they are immature when isolated, so that *in vitro* and *in vivo* maturation is required to achieve full functionality (reviewed in KEMTER & WOLF, 2018).

In this study, wildtype (WT) pigs received an intraportal islet transplant consisting of NPIs to establish a pig islet allotransplantation model. Subsequently, an intraportal ITx with NPIs was performed in diabetic, transgenic *INS*^{C94Y} pigs to evaluate the effect of NPI transplantation on their blood glucose levels. An observation period of these pigs of up to four months was aimed for, in order to take into account the need for *in vivo* maturation of the NPIs. ITx was accompanied by daily immunosuppressive and antithrombotic treatment. Non-invasive longitudinal [^{68}Ga]Ga-DOTA-Exendin-4 PET/CT imaging was performed to evaluate the feasibility of this approach for morphological imaging of viable BCM. This was followed by a detailed histological analysis of the transplant-containing liver to determine graft distribution and properties and to investigate immunological processes after ITx.

II. REVIEW OF THE LITERATURE

1. Type 1 diabetes

T1D is an autoimmune disease and is considered one of the most common metabolic and endocrinological diseases in children and young adults. For instance, in Germany about 3,100 patients between the ages of 0 and 17 years are newly diagnosed with T1D every year (reviewed in SHOJAEIAN & MEHRI-GHAHFARROKHI, 2018; DANIEL, 2019). There are currently about 373,000 diagnosed T1D cases in Germany, which corresponds to about 0.4% of the total German population. Around 32,000 of these are children and adolescents (DANIEL, 2019). Worldwide, 8.75 million people were affected by T1D in 2022, with 530,000 new diagnosed cases. One fifth of those affected come from low-income and low-middle income countries. 17% of T1D patients are younger than 20 years, 64% are between 20 and 59 years old and 19.9% are 60 years or older. In 2022, there were 182,000 deaths caused by T1D (OGLE et al., 2022). Of note, there was a continuous increase of T1D incidence in the past years and a further increase of 60-107% in prevalent T1D cases is predicted by 2040 (GREGORY et al., 2022).

Several environmental factors are linked to the development of T1D, including for example early childhood contact with viruses that cause islet inflammation (such as enteroviruses), infant and adult dietary patterns, vitamin D supply, overweight and composition of gut microbiome (reviewed in REWERS & LUDVIGSSON, 2016; reviewed in DIMEGLIO, EVANS-MOLINA & ORAM, 2018). Genetic factors also play an important role in the development of the disease, where the highest genetic risk is associated with genes encoding Human Leukocyte Antigens (HLA), especially the HLA haplotypes DR3 and DR4 for white people (reviewed in NOBLE, 2015; reviewed in DIMEGLIO, EVANS-MOLINA & ORAM, 2018). T1D is mainly caused by autoimmune mediated destruction of pancreatic beta cells leading to insufficient insulin production (type 1a), only < 10% of patients are classified as idiopathic without autoimmune mechanisms (type 1b). The development of hyperglycemia and onset of diabetic symptoms typically emerges after a considerable latency phase, due to the substantial percentage of beta cells, that first has to be destroyed or impaired (reviewed in PASCHOU et al., 2018). The more prevalent type 2 diabetes (T2D) results from resistance to secreted insulin

accompanied by an insufficient compensatory insulin secretion response (reviewed in MAAHS et al., 2010). T1D is the consequence of an insulitis that is based on innate immune mechanisms. This involves the activation of pattern recognition receptors by endogenous and exogenous ligands, followed by production of interferons by beta cells and other islet cells, finally resulting in the recruitment of immune cells (ZAJEC et al., 2022). Macrophages are the first infiltrating cell type present in the inflamed islets. As the insulitis progresses, they are supplemented by $CD8^+$ T cells, and to a lesser extent by $CD20^+$ B cells and $CD4^+$ T cells. As a result, beta cells are destroyed by immunological cascades, mediated by immune cells infiltrating in and around the islets (reviewed in RODRIGUEZ-CALVO, RICHARDSON & PUGLIESE, 2018; reviewed in ZAJEC et al., 2022). In addition, beta cells themselves are seen as contributors to the pathogenetic processes of T1D, making them accomplices rather than victims of the immune system (reviewed in SAHIN, LEE & ENGIN, 2021). This observation results from the fact that islet autoreactive $CD8^+$ T cells also exist in healthy individuals, which implicates, that autoimmune processes are activated in the targeted tissue (reviewed in MALLONE & EIZIRIK, 2020; reviewed in ROEP et al., 2021). Characteristic for beta cells of T1D patients are elevated STAT1 levels and overexpression of HLA class I, promoting the immigration of $CD8^+$ T cells and thus amplifying their vulnerability to autoimmune-driven destruction (RICHARDSON et al., 2016; reviewed in DIMEGLIO, EVANS-MOLINA & ORAM, 2018). In addition to these beta-cell abnormalities, beta-cell endoplasmic reticulum (ER) stress and a misguided unfolded protein response (UPR) are seen as main initiators and drivers in the pathogenesis of T1D (reviewed in BROZZI & EIZIRIK, 2016; reviewed in SAHIN, LEE & ENGIN, 2021). Beta cells require a complex ER system based on their synthesis and secretion function of insulin and are *per se* susceptible to biosynthetic stress (reviewed in ROEP et al., 2021; reviewed in SAHIN, LEE & ENGIN, 2021). When exposed to stressors (e.g. viral infection, oxidative stress, etc.), the synthesis and folding performance of ER is disturbed, leading to accumulation of misfolded protein in the ER, and thus to activation of the UPR (reviewed in CAO et al., 2020). While being an important mechanism for relieving ER stress and preventing cell death in the physiological state, a misdirected UPR can promote cell death in the

event of chronic, excessive ER stress (reviewed in ENGIN, 2016; reviewed in CAO et al., 2020).

The clinical manifestation of T1D occurs in a first minor epidemiological peak at about five years of age and then mainly before the onset of puberty. In general, however, T1D can occur in any age group. Classic symptoms include polyuria, polydipsia and weight loss over a period of 2-6 weeks (KORDONOURI & KERNER, 2021). The following clinical parameters are used as a standard for the diagnosis of (pre-)diabetes: (A) fasted blood glucose (FBG) increased at two days (physiological: < 100 mg/dl), (B) non-fasting blood glucose ('random glucose') increased (≥ 200 mg/dl) at two days or associated with typical diabetes mellitus symptoms, (C) oral glucose tolerance test (OGTT) altered (2-h-glucose after 75g glucose intake ≥ 140 mg/dl), and (D) hemoglobin A1c (HbA1c) increased (indicates averaged blood glucose levels over several weeks; diagnostic: ≥ 6.5%) (HARREITER & RODEN, 2023). If there is a first-degree relative affected by T1D, screening for diabetes-associated autoantibodies (IAA, GADA, IA-2A, ZnT8A) is recommended (reviewed in YU, ZHAO & STECK, 2017; HARREITER & RODEN, 2023). If at least two of these autoantibodies are present, this indicates a > 80% risk of developing T1D within 15 years. Antibodies against IAA are usually the first to be detected in young children, while antibodies against GADA appear mainly first in adolescents and young adults (reviewed in YU, ZHAO & STECK, 2017; HARREITER & RODEN, 2023).

T1D leads to absolute insulin deficiency (reviewed in KATSAROU et al., 2017). In order to treat insulin deficiency and to prevent acute (hyper- and hypoglycemic events) and long-term complications of T1D (secondary diabetic lesions of the cardiovascular, cerebrovascular, and renal system, diabetic retinopathy, for instance), lifelong replacement therapy with an exogenous insulin source is required (reviewed in MALIK & TAPLIN, 2014; DE BEAUFORT, BESANÇON & BALDE, 2018). If diabetes remains untreated, there is a risk of potentially life-threatening diabetic ketoacidosis (MAGLIANO, BOYKO & BALKAU, 2021). Depending on the chemical structure, a distinction is made between human insulin and insulin analogs and, depending on the pharmacokinetic properties, between long-acting (basal), short-acting (bolus) and premixed preparations (BIRKENFELD et al., 2021). Intensified insulin therapy, consisting of at least three

insulin injections per day and use of long-acting and short-acting insulin to mimic basal and prandial insulin secretion, should be the standard therapy for T1D to slow the progression of diabetes-associated long-term complications (HAAK et al., 2018). So far, the most common method for administering insulin has been through subcutaneous injection, using e.g. syringes, pens and pumps (reviewed in SHAH et al., 2016). Despite continuous refinement of insulin replacement therapy, there are patients with poor control of glucose levels that are suffering from unaware events of life threatening hypoglycemic episodes, a state that is also called Brittle diabetes (see section 2.2). These patients are candidates for allogeneic ITx (reviewed in VANTYGHEM et al., 2019; reviewed in DUAN et al., 2023).

2. Pancreatic islet transplantation

2.1. Islet transplantation - past till present

The first beta-cell replacement therapy was carried out in 1893 by Watson-Williams and Harsant in Bristol, who xenotransplanted sheep pancreatic tissue into a patient with acute ketoacidosis. The patient died three days after the procedure (SHAPIRO, 2002; reviewed in GAMBLE et al., 2018). ITx studies were re-initiated in 1972 by Paul E. Lacy, who achieved glycemic control in chemically induced diabetic rats by allogeneic intraperitoneal and intramuscular (i.m.) ITx (BALLINGER & LACY, 1972; reviewed in GAMBLE et al., 2018). In 1973, ITx induced normoglycemia in chemically induced diabetic mice and the hepatic portal vein was first used as transplantation (Tx) site in rodent models (RECKARD & BARKER, 1973; reviewed in CZARNECKA et al., 2023). In 1980, successful intraportal auto-ITx after (near-)total pancreatectomy was performed in ten human patients suffering from chronic pancreatitis, with three achieving insulin independence for one, nine and 38 months, respectively (NAJARIAN et al., 1980; reviewed in GAMBLE et al., 2018).

The introduction of the “Automated Method” for human islet isolation by Dr. Camillo Ricordi represents a next turning point in clinical ITx and remains the gold standard for human islet isolation till today (RICORDI, LACY & SCHARP, 1989; reviewed in GAMBLE et al., 2018). This approach involves mechanically improved enzymatic degradation of the pancreatic tissue through the use of a

dissociation/filtration chamber. This ensures that pancreatic islets are removed directly from the digestion system, preventing overdigestion and maintaining the integrity of the endocrine cell clusters (reviewed in PIEMONTI & PILEGGI, 2013).

A total of 267 ITx procedures were performed in patients from 1980-1999, however, less than 8% of these led to insulin independence for more than one year. With the Edmonton protocol, introduced by Shapiro et al. in 2000, ITx became a clinical feasible procedure (reviewed in GAMBLE et al., 2018). Until 2000, immunosuppression after ITx mainly involved the use of antilymphocyte drugs combined with cyclosporine, azathioprine and glucocorticoids (SHAPIRO et al., 2000). Steroids are known for their diabetogenic effect and prednisolone appears to have at least a toxic long-term effect on islet engraftment and function (ZENG et al., 1993; SHAPIRO et al., 2000). The Edmonton protocol therefore dispenses with the use of glucocorticoids. Instead, immunosuppressive treatment is based on sirolimus, low-dose tacrolimus (TAC) and daclizumab (SHAPIRO et al., 2000; reviewed in GAMBLE et al., 2018). This new immunosuppressive regime in combination with an adequate islet graft mass (mean 11,547 ± 1,604 islet equivalents (IEQs)/kg body weight (BW)) was able to achieve stable insulin independence (follow-up: 4.4 – 14.9 months) in seven T1D patients and reliably prevent hypoglycemic episodes after intraportal ITx (SHAPIRO et al., 2000).

Since the publication of the Edmonton protocol, numerous countries worldwide have progressed in utilizing allogeneic ITx as a treatment for T1D patients facing severe hypoglycemia, hypoglycemia unawareness, or significant glycemic instability (reviewed in RICKELS & ROBERTSON, 2019). Hering and coworkers were able to achieve insulin independence for at least one year in eight out of eight patients through improvements in perioperative management (strong induction immunotherapy and less diabetogenic maintenance immunosuppression). In this study an islet graft was based on only one donor organ per ITx recipient, as opposed to the 2-4 donor pancreata per recipient used in the Edmonton protocol (HERING et al., 2005; reviewed in RICKELS & ROBERTSON, 2019).

In 2001, the Collaborative Islet Transplant Registry (CITR) was established to compile data from the majority of human-to-human ITx programs in North America (period 1999-2020) and additionally from Europe and Australia (period 2006-2015)

(reviewed in GAMBLE et al., 2018; CITR, 2022). The latest report of 2022 postulates a total of 1,399 allo-ITx patients in the period of 1999-2020, thereof 1,108 islet transplant alone (ITA) recipients and 291 islet-after-kidney (IAK), simultaneous-islet-kidney (SIK) or kidney-after-islet (KAI) transplant recipients. Within the ITA patients, 19.6% are insulin independent, 29% insulin dependent with preserved graft function and 19.7% without graft function. No data is available for 31.7% (CITR, 2022).

Over the past years, advancements in ITx have been considerable, marked by numerous enhancements such as improved islet preparation methods, refined culture techniques, safer transplant procedures and more potent anti-inflammatory and immune-modulating interventions (reviewed in GAMBLE et al., 2018). In 2022, the largest single-center cohort study on long-term outcomes after ITx was published by Marfil-Garza et al. with 255 patients from Edmonton, Canada (MARFIL-GARZA et al., 2022; reviewed in CZARNECKA et al., 2023). This study illustrates the long-term safety of ITx therapy despite chronic immunosuppression (reviewed in CZARNECKA et al., 2023).

Launched in 2008, the University Hospital of Dresden currently hosts the only active clinical ITx program in Germany. This is attributed to a highly complex regulatory situation (LUDWIG et al., 2015; DGFG, 2022).

An overview about important discoveries and landmarks of clinical ITx history is provided in **Figure 1**.

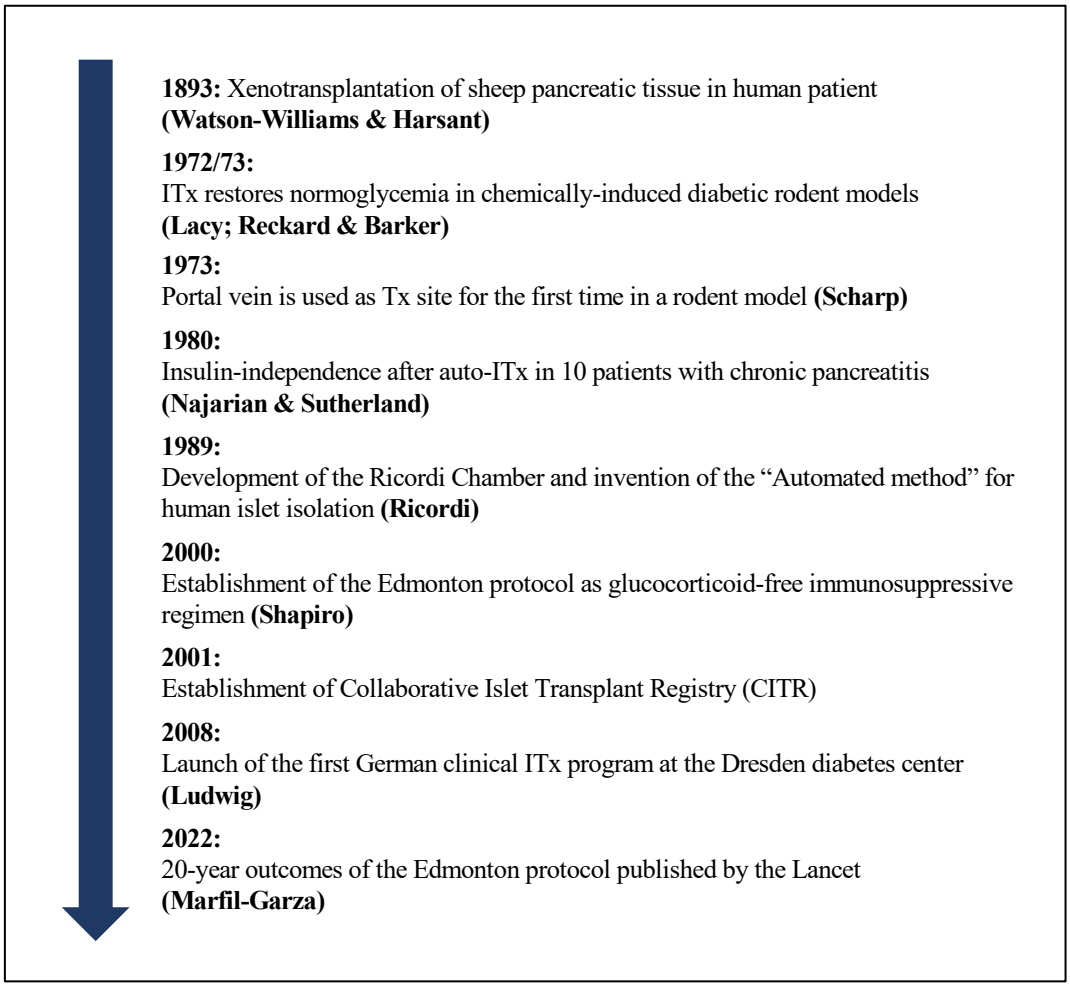

Figure 1: *Selected important discoveries and landmarks of clinical ITx history.*

Author's own figure, adapted from Czarnecka et al., 2023;
Additional information from Gamble et al., 2018 and DGFG, 2022.

2.2. Indications for islet transplantation

Currently, the main indication for an allogeneic ITx is T1D (reviewed in PIEMONTI, 2022). Although patients with T1D can be treated symptomatically with exogenous insulin therapy, insulin injections cannot replace the physiologic pancreatic secretion patterns of insulin, glucagon and somatostatin required for proper glucose homeostasis (reviewed in JOHNSON & JONES, 2012). This is clinically highly relevant, as studies have shown that there is a close correlation between the quality of glucose control and the development of diabetic complications (NATHAN et al., 1993; reviewed in JOHNSON & JONES, 2012; LAITEERAPONG et al., 2019).

However, intensive insulin therapy required to counteract this, increases the risk of life-threatening hypoglycemic events (DCCT, 1997; reviewed in JOHNSON & JONES, 2012). ITx as beta-cell replacement therapy can overcome these limitations of insulin therapy (NOGUCHI, 2009).

ITx is also a very effective measure to correct hypoglycemia and is therefore primarily aimed at T1D patients with events of severe recurrent hypoglycemia that cannot be prevented even with intensive medical care (reviewed in OTHONOS & CHOUDHARY, 2017), also known as brittle diabetes (GANGEMI et al., 2008; RICORDI & JAPOUR, 2019). The current valid classification of hypoglycemia as mild or severe is not determined by precise blood glucose thresholds, but rather by an individual's capacity for self-treatment (HAAK et al., 2019). A severe hypoglycemic state is characterized by severe cognitive dysfunction (convulsion or coma), which requires external intervention and the administration of glucose, glucagon, or other corrective measures (reviewed in URAKAMI, 2020). In addition to coma and seizures, severely low blood sugar can also lead to heart attacks and even death. The primary goal of ITx is therefore to address a heightened vulnerability to severe hypoglycemia and irregularities in glycemic control, which lead to a mortality of 8% (reviewed in PIEMONTI, 2022).

ITx can also be performed as IAK or SIK transplantation in uremic T1D patients affected by chronic kidney failure (reviewed in VENTURINI et al., 2018; MARKMANN et al., 2021; reviewed in PIEMONTI, 2022). For IAK transplantation, patient selection is not as strict as for ITA recipients as these patients already undergo chronic immunosuppressive treatment due to the kidney graft (reviewed in SHAPIRO, POKRYWCZYNSKA & RICORDI, 2017).

Apart from T1D, pancreatogenic types of diabetes (caused by e.g. chronic pancreatitis, tumors or pancreatectomy), cystic fibrosis-related diabetes or advanced insulinopenic T2D may also be indications for ITx. This is indicated when these patients suffer from glycemic instability and therapy-resistant hypo- and hyperglycemia caused by beta-cell failure (reviewed in RICKELS et al., 2018; reviewed in RICKELS & ROBERTSON, 2019; reviewed in PIEMONTI, 2022). If the transplanted islets are the patient's own islets obtained after pancreatectomy, this is referred to as autologous ITx (reviewed in PIEMONTI, 2022).

2.3. Procedure of clinical islet transplantation in T1D patients

2.3.1. Pancreas procurement and islet isolation

Human islet grafts for allogeneic ITx are currently derived from pancreata that are obtained from deceased organ donors (reviewed in SHAPIRO, POKRYWCZYNSKA & RICORDI, 2017). The implementation of certain criteria when selecting the donor, such as the use of steroids, vasopressors (pitressin), male gender, BMI > 25 kg/m^2, minimum glycemia < 150 mg/dl and local explantation team, has a decisive influence on the success and outcome of the ITx procedure (PONTE et al., 2007; reviewed in SHAPIRO, POKRYWCZYNSKA & RICORDI, 2017). The collection of donor pancreas requires the utmost care to preserve the integrity of the pancreatic capsule while minimizing processing time and maximizing the flow of oxygenated blood in the pancreas prior to clamping the aorta, referred to as warm ischemia time (reviewed in SHAPIRO, POKRYWCZYNSKA & RICORDI, 2017; DE PAEP et al., 2021). Removal of the pancreas is usually performed en bloc with the duodenum and spleen. Subsequently the organ is transferred to an islet isolation facility, preserved in University of Wisconsin or histidine-tryptophan ketoglutarate (HTK) solution at 4°C (reviewed in KIN & SHAPIRO, 2010; reviewed in SHAPIRO, POKRYWCZYNSKA & RICORDI, 2017). The islet isolation facility for clinical ITx has to be accredited according to Current Good Manufacturing Practices. The cold ischemia time of the donor pancreas during collection, preservation and transport should be reduced to a minimum and be less than eight hours (reviewed in RICKELS & ROBERTSON, 2019). In the islet isolation facility, the following steps are taken to obtain transplantable islets from donor pancreas: (1) intraductal distention of the pancreas by injection of collagenase solution into the cannulated pancreatic duct (reviewed in KIN & SHAPIRO, 2010), (2) enzymatic digestion and mechanically separation of pancreatic tissue by using the Ricordi method (RICORDI et al., 1988; reviewed in RICKELS & ROBERTSON, 2019), (3) purification of islets by centrifugation and (4) finally cultivation of islets for 36-72h before ITx, to reduce immunogenic and inflammatory properties of the islet graft by increasing purity of islets (reviewed in SHAPIRO, POKRYWCZYNSKA & RICORDI, 2017; reviewed in RICKELS & ROBERTSON, 2019) **(Fig. 2)**.

The minimum amount of IEQs should be 5,000 IEQs/kg BW for each islet allograft and > 6,000-7,000 if a single donor organ is used (reviewed in SHAPIRO, 2012; reviewed in SHAPIRO, POKRYWCZYNSKA & RICORDI, 2017).

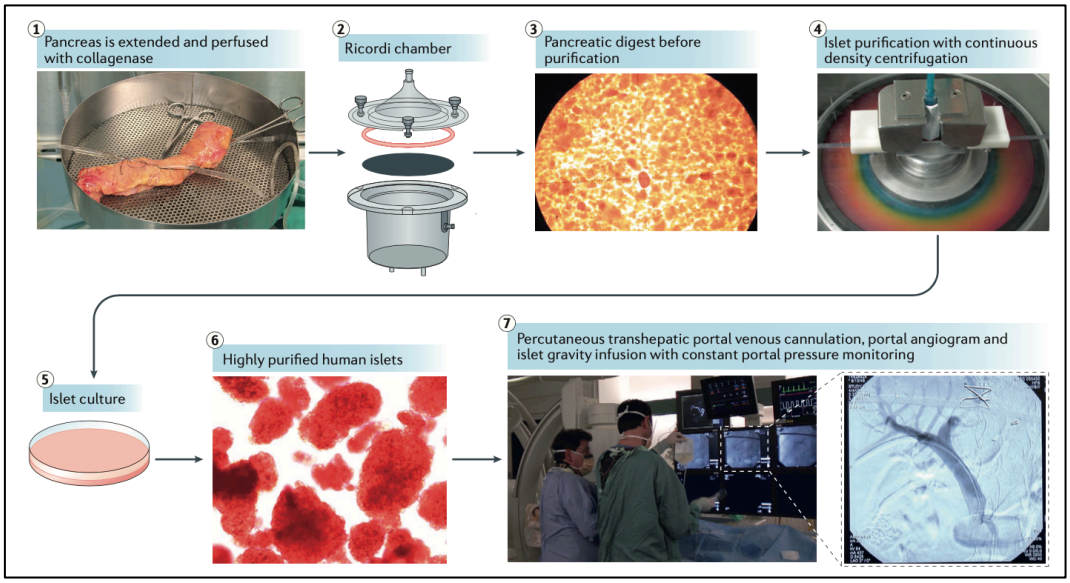

Figure 2: *From donor organ to islet graft.*

(1) *Distention of pancreas by intraductal administration of collagenase solution.* ***(2)*** *Digestion of pancreatic tissue in Ricordi chamber.* ***(3)*** *Digest before purification (islets stained red by dithizone dye).* ***(4)*** *Purification of islets by centrifugation.* ***(5)*** *Islet cultivation.* ***(6)*** *Purified human islets (staining: dithizone-red) ready for clinical use.* ***(7)*** *Intraportal ITx.*

Image source: Shapiro et al., 2017; Figure legend: Adapted from Shapiro et al., 2017.

Reproduced with permission from Springer Nature.

2.3.2. Percutaneous intraportal pancreatic islet transplantation (PIPIT)

The islet graft is resuspended in transplantation medium, transferred in a sterile infusion bag containing 70 IU/kg BW heparin and administered into the percutaneously catheterized portal vein (reviewed in SHAPIRO, POKRYWCZYNSKA & RICORDI, 2017). Percutaneous transhepatic catheterization of the portal vein for ITx using a combined CT- and fluoroscopy-guided technique was described in 1999 (WEIMAR et al., 1999). Since then it has been further developed and is considered a safe, effective transplantation method (VENTURINI et al., 2005; reviewed in SHAPIRO, POKRYWCZYNSKA & RICORDI, 2017). Compared to pancreas transplantation, PIPIT is a minimally invasive procedure that involves distinct less surgical risk (reviewed in WOJTUSCISZYN et al., 2019; reviewed in BERNEY et al., 2022).

Prior to PIPIT, the patient undergoes radiological, clinical and biochemical examinations to determine whether the inclusion and exclusion criteria for the procedure are met (reviewed in VENTURINI et al., 2018) **(Table 1)**.

PIPIT inclusion criteria	**PIPIT exclusion criteria**
Diabetes duration ≥ 5 years	Diabetes duration ≤ 5 years
No endogenous C-peptide secretion (insulin biosynthesis and secretion marker)	C-peptide secretion (stimulated C-peptide level > 0.5 ng/dL)
Therapy-resistant severe glycemic instability with frequent episodes of undetected hypoglycemia, progression of diabetic complications despite exogenous insulin therapy	Untreated proliferative diabetic retinopathy
	Portal hypertension
	Cardiovascular disease
	Active infection (incl. hepatitis C, hepatitis B, HIV, tuberculosis)
	Abuse of alcohol or substance
	Pregnancy, intent of future pregnancy

Table 1: *Inclusion and exclusion criteria for PIPIT as ITA.*

Adapted from Venturini et al., 2018.

Interventional radiology plays a key role in PIPIT, as it enables minimally invasive access to the portal vein, which therefore does not have to be opened up surgically (reviewed in GABA, GARCIA-ROCA & OBERHOLZER, 2012). Before PIPIT, patients are usually given antimicrobial and antiviral therapy, as contaminated islets can potentially cause septicemia and because of immunosuppression leading to an increased sensitivity to pathogens (TAYLOR et al., 1994; reviewed in VENTURINI et al., 2018; reviewed in PIEMONTI, 2022). PIPIT is usually carried out in an angiographic facility under sterile conditions and moderate intravenous sedation. Cardiac and hemodynamic parameters and oxygen saturation are recorded during the procedure (reviewed in VENTURINI et al., 2018). The hepatic portal vein is currently the clinically state-of-the-art transplantation site for islets. This is due to the fact that the portal vein is easily and minimally invasively accessible and insulin secretion from the transplanted islets occurs into the portal vein, which prevents systemic hyperinsulinemia (reviewed in RAJAB, 2010; reviewed in VENTURINI et al., 2018). In addition, this ITx site recapitulates the physiological route of insulin secretion from the pancreatic islets of Langerhans into the portal

vein, with hepatocytes being the initial targeted structure for insulin (EDGERTON et al., 2021; reviewed in CALDARA et al., 2023).

The ITx process is carried out in the following steps: (1) Ultrasound or fluoroscopy guided percutaneous puncture of a portal vein branch, approaching intercostal from the right side, using 22G needle and providing local anesthesia. (2) Advancing a 0.018-inch guidewire through the needle into the main branch of the portal vein and positioning a straight end-hole 4-F catheter. (3) Portography to check the position of the catheter and to determine the pressure (normally 6-12 mmHg) and patency of the portal vein. (4) Gentle islet infusion either by gravity or by syringe injection (20-30 min). (5) Repetition of the portal pressure measurement (increase normally 1-2 mmHg) and final portography. (6) Retraction of the catheter under fluoroscopic guidance and embolization of the puncture tract with hemostatic agents, e.g. gelfoam torpedoes, to reduce the hemorrhagic risk (OWEN et al., 2003; VENTURINI et al., 2005; reviewed in VENTURINI et al., 2018).

If percutaneous access to the portal vein is not possible, e.g. in the case of a large hepatic hemangioma, an open ITx procedure can be performed as an alternative (SHAPIRO & RICORDI, 2014).

PIPIT requires anticoagulant measures to prevent acute thrombosis of the portal vein. This can be achieved for example by administration of 1,500 - 2,000 IU heparin with islet infusion and subsequently 6,000 IU/day enoxaparin subcutaneously (s.c.) for seven days (reviewed in VENTURINI et al., 2005; VENTURINI et al., 2018).

2.3.3. Posttransplant management

Posttransplant management includes an immediate-post-PIPIT imaging with ultrasound to rule out early bleeding. Doppler ultrasound examinations are usually carried out on day one, three and seven post ITx (reviewed in VENTURINI et al., 2018). In this way, the two main acute complications, bleeding and, more rarely, portal vein thrombosis, can be diagnosed (RYAN et al., 2005; reviewed in VENTURINI et al., 2018). Late-post-PIPIT imaging is used to detect long-term effects of PIPIT induced by the islet transplant or immunosuppression (reviewed in VENTURINI et al., 2018).

For example, chronic immunosuppression can promote neoplasia and infections, e.g. with the cytomegalovirus (CMV), the consequences of which can be detected in CT scans, e.g. pneumonitis or myocarditis. This is clinically relevant as CMV infections can also damage the islet transplant (ECKHARD et al., 2002; reviewed in VENTURINI et al., 2018). Another long-term effect may be hepatic steatosis, which can be detected from six months post-PIPIT onwards by magnet resonance imaging (MRI) and ultrasound (reviewed in VENTURINI et al., 2018). It is caused by local insulin production of engrafted islets, which promotes lipogenesis and inhibits lipolysis, leading to fat deposition (KILWORTH, CRANE & MASTERS, 1985; reviewed in VENTURINI et al., 2018). Hepatic steatosis diagnosed by ultrasound may be an indicator of islet graft exhaustion, although a negative ultrasound does not rule this out and the connection between hepatic steatosis and graft function is not fully known (VENTURINI et al., 2015; reviewed in VENTURINI et al., 2018).

Other clinical parameters that are regularly evaluated after PIPIT, e.g. to detect unfavorable effects of immunosuppressants or general effects of ITx on the organism, are hematological parameters (cell blood counts), kidney function, liver function and immune monitoring (reviewed in PIEMONTI, 2022).

2.4. Immunosuppressive treatment

To avoid allograft rejection after ITx, immunosuppressive treatment of the recipient is required (VAN BELLE & VON HERRATH, 2008). No official standard therapy for immunosuppression after ITx is currently available and CITR data show a dynamic-variable approach to immunosuppression during the last years, with different combinations of agents (BARTON et al., 2012; CITR, 2022; reviewed in PIEMONTI, 2022). Since the establishment of the glucocorticoid-free immunosuppression regimen in the Edmonton protocol, several adjustments have been made to improve the tolerability of immunosuppression and minimize adverse effects on the islet graft, e.g. by substituting sirolimus with mycophenolate mofetil (MMF) (reviewed in SHAPIRO, 2011).

In general, immunosuppressant therapies are classified as induction or maintenance regime (reviewed in PARLAKPINAR & GUNATA, 2021).

Table 2 provides an overview of the most commonly used immunosuppressant drugs in terms of ITx. Currently, most ITx immunosuppression regimens include induction therapy for T-lymphocyte depletion, e.g. with antithymocyte globulin (ATG), anti-CD52-monoclonal antibody (mAb) (alemtuzumab) or IL-2 receptor antagonists (e.g. basiliximab) (MATSUMOTO et al., 2011; BROOKS et al., 2013; NIJHOFF et al., 2016; reviewed in RICKELS & ROBERTSON, 2019). Immunosuppression via T-lymphocyte depletion is more effective than via IL-2 receptor antagonists (BRENNAN & SCHNITZLER, 2008; HAYNES et al., 2014; reviewed in RICKELS & ROBERTSON, 2019). In addition, the combination of anti-T-lymphocyte agents with a TNF-α inhibitor, such as etanercept has a positive effect on the long-term insulin independence in contrast to when IL-2 inhibitors are used (BELLIN et al., 2012; reviewed in RICKELS & ROBERTSON, 2019). IL-2 antagonists are the agents of choice for repeated infusions to minimize adverse effects of immunosuppression and in case of allergy to T cell depleting agents (SOLEIMANPOUR et al., 2011; HERING et al., 2016; reviewed in RICKELS & ROBERTSON, 2019). For the maintenance of immunosuppression, a combination of a calcineurin inhibitor (CNI), mainly TAC, and MMF is used as standard. This combination has largely replaced the mammalian target of rapamycin (mTOR) inhibitor sirolimus, which was originally combined with TAC in the Edmonton protocol (CITR, 2022; reviewed in WALKER, APPARI & FORBES, 2022).

Overall, complications of immunosuppression in ITx, such as malignant degenerations and infections, occur relatively rarely (reviewed in REID, BAXTER & FORBES, 2021). The CITR report documents the correlation between immunosuppression and the occurrence of complications such as neoplasia and mortality. By 2022, for example, 12.2% of all neoplasms that occurred in all ITx patients were definitely linked to immunosuppression and ten out of 77 reported deaths post-ITx were possibly or certainly related to immunosuppression (CITR, 2022). Nevertheless, there are still considerable side effects of immunosuppressants, such as nephrotoxicity, cardiovascular diseases or neuropathies that can be triggered especially by CNIs (ARNOLD et al., 2013; reviewed in BAMOULID et al., 2015; reviewed in REID, BAXTER & FORBES, 2021). This is why the potential risks of chronic immunosuppression must always be weighed against the benefits of ITx therapy and this assessment must be adapted

to the latest developments in the field of both diabetes therapy and immunosuppression (reviewed in SHAPIRO, 2011). In addition, alternative immunosuppressants such as everolimus or belatacept should also be considered and further researched (POSSELT et al., 2010; SAGESHIMA et al., 2014; reviewed in WALKER, APPARI & FORBES, 2022).

Category	Agent	Mechanism of action	Use
Induction	Daclizumab	IL-2 inhibitor, mAb	Early induction agent
	Alemtuzumab	Anti-CD52, mAb	Main induction agent currently used for first ITx
	Basiliximab	IL-2 receptor antagonist, mAb	Potential induction agent for ITx
	Antithymocyte globulin (ATG)	Anti-T-cell antibody preparation	Induction agent; used combined with etanercept
	Etanercept	TNF-α inhibitor	As combination with alemtuzumab or ATG for initial induction
Maintenance	Tacrolimus	Calcineurin inhibitor → reduction of IL-2 up-regulation	Main maintenance immunosuppression agent
	Mycophenolate mofetil	Inhibition of inosine monophosphate dehydrogenase	Main maintenance adjunct to TAC
	Sirolimus	mTOR inhibitor → inhibition of IL-2	Alternative to MMF; alternative to TAC in patients with declining renal function

Table 2: *Most commonly used immunosuppressive agents in ITx.*

Adapted from Reid et al., 2021.

2.5. Monitoring of the islet graft

Regular evaluations of the islet graft function are crucial after ITx to determine if further islet loading (second or third transplant) is required or if there are signs of graft rejection (reviewed in CANTLEY et al., 2023).

There are several metabolic parameters that allow conclusions to be drawn about islet graft function. This includes standard parameters like fasted and postprandial blood glucose, basal and stimulated C-peptide as a marker for insulin production, HbA1c levels, development of exogenous insulin need, as well as stimulated parameters, e.g. response on Mixed Meal, intravenous glucose or

intravenous arginine. In addition, indices like the BETA2 score derived from a combination of several parameters are useful for clinical evaluation. However, there is no standardized method for determining islet graft function and clinical outcome, which is a weakness of beta-cell replacement therapy, that reduces its acceptance as a treatment method (reviewed in PIEMONTI, 2022).

To fill this gap, in 2017, IPITA and EPITA jointly introduced the Igls Score **(Table 3)**, to standardize the evaluation of beta-cell replacement therapy success, which includes the parameters HbA1c, severe hypoglycemic episodes, insulin requirement and C-peptide (reviewed in RICKELS et al., 2018; reviewed in PIEMONTI, 2022).

Beta cell functional status	**HbA1c % (mmol/mol)**	**Severe hypoglycemia (events/year)**	**Insulin requirements ($U \cdot kg^{-1}d^{-1}$)**	**C-peptide**	**Treatment success**
Optimal	≤ 6.5 (48)	None	None	> Baseline and > 0.5 ng/ml fasting or stimulated	Yes
Good	< 7.0 (53)	None	< 50% Baseline and < $0.5 U \cdot kg^{-1}d^{-1}$	> Baseline and > 0.5 ng/ml fasting or stimulated	Yes
Marginal	Baseline	< Baseline	≥ 50% Baseline	> Baseline and > 0.5 ng/ml fasting or stimulated	No
Failure	Baseline	Baseline	Baseline	Baseline	No

Table 3: *Igls definition for functional and clinical outcome of beta-cell replacement therapies. Adapted from Rickels et al., 2018 and Piemonti, 2022.*

Assessments of the islet graft function, as with C-peptide and HbA1c, is limited to an indirect representation of BCM, since function does not allow direct quantification of BCM (reviewed in ORAM, SIMS & EVANS-MOLINA, 2019; JANSEN et al., 2023). Furthermore, metabolic tests can only indicate adverse changes in the transplant with a delay and as a consequence of beta-cell loss, when the time frame for therapeutic countermeasures has already been exceeded (reviewed in BERNEY & TOSO, 2006; reviewed in ERIKSSON & ALAVI, 2012).

Biomedical imaging is a promising approach for the quantification of BCM and could therefore provide important insights into the survival of islets after ITx (JANSEN et al., 2023). Imaging techniques that are of interest in this context are mainly MRI, PET and single photon emission computed tomography (SPECT) (reviewed in ERIKSSON & ALAVI, 2012).

PET as a highly sensitive molecular imaging technique is based on the simultaneous detection of annihilation photons following positron decay (reviewed in ZATCEPIN & ZIEGLER, 2023) **(Fig. 3)**. It enables to visualize, characterize, and quantify biological processes at cellular and molecular levels in a noninvasive way (reviewed in JIN et al., 2022). PET imaging is supplemented by a CT or MRI to obtain additional anatomical information (reviewed in ARIFIN & BULTE, 2021). Since specific targets can be visualized, this imaging modality is particularly attractive for longitudinal quantification of BCM (reviewed in ERIKSSON & ALAVI, 2012). Molecular detection is based on the use of radiopharmaceuticals, consisting of a targeting ligand (e.g. a small molecule, peptide, antibody, or nanoparticle), that are linked with a radionuclide. This linkage is sometimes mediated by a connecting piece (reviewed in JIN et al., 2022) **(Fig. 3)**.

Radionuclides for labeling islet-targeting-ligands are for example ^{125}In, ^{99m}Tc, ^{68}Ga, or ^{18}F (reviewed in ARIFIN & BULTE, 2021). When labeling islets, there are various approaches that provide information about the islet graft at different transplantation phases and timepoints, e.g. *ex vivo* labeling or *in vivo* targeting of islets (reviewed in ERIKSSON & ALAVI, 2012). A promising approach to image beta cells and thus transplanted islets by *in vivo* targeting is the use of glucagon-like peptide-1 (GLP-1) receptor analogs, such as exendin-3 or exendin-4 (reviewed in ERIKSSON & ALAVI, 2012; BROM et al., 2014; BOSS et al., 2020; JANSEN et al., 2023; LINDHEIMER et al., 2023). The GLP-1 receptor (GLP-1R) is specifically and highly expressed on pancreatic beta cells of humans, mice, rats and pigs (TORNEHAVE et al., 2008; RENNER et al., 2010; reviewed in ERIKSSON & ALAVI, 2012). Endogenous GLP-1 is postprandial secreted by intestinal L-cells. Receptor binding leads to stimulated, glucose-dependent insulin synthesis and release (reviewed in LEECH et al., 2011; reviewed in MELONI et al., 2013).

Since endogenous GLP-1 is degraded to a biologically inactive form within minutes, synthetic GLP-1 analogs such as exendin are used for nuclear medical imaging (VILSBØLL et al., 2003; GOTTHARDT et al., 2006; WILD et al., 2010; NALIN et al., 2014).

Depending on the radionuclide selected, *in vivo* imaging of islets can be carried out with PET or SPECT. Of note, PET has a 2-3 times higher sensitivity and spatial resolution than SPECT and the PET radiotracers have a shorter decay time. On the other hand, SPECT is lower in costs (reviewed in RAHMIM & ZAIDI, 2008; reviewed in ARIFIN & BULTE, 2021).

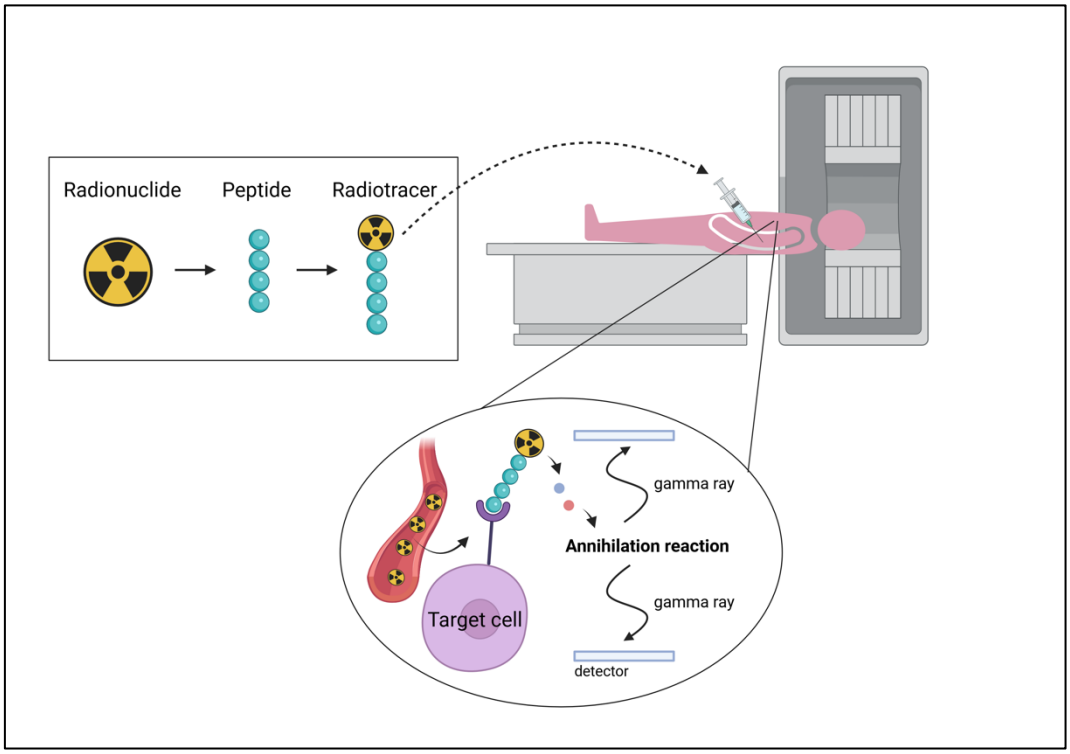

Figure 3: *Basic principles of PET molecular imaging.*

Author's own figure, adapted from Jin et al., 2022; Created with Biorender.com.

2.6. Challenges and future directions in islet transplantation

ITx faces a number of challenges that currently limit its potential as a curative therapy for T1D, including low transplant availability due to the lack of human donor organs and sparse islet yield, inflammation, auto-, and allogenic immune rejection, toxic effects of chronic immunosuppression, hypoxia and ischemia/reperfusion injury (reviewed in WALKER, APPARI & FORBES, 2022) **(Fig. 5)**. Despite the many advances that have been made, 50-70% of the islets are still lost in the early phase after ITx (reviewed in DELAUNE et al., 2017).

2.6.1. Oxidative stress, ischemia/reperfusion injury, hypoxia

In general, the transplanted islets are exposed to dynamic changes in structure and function in the first few days after ITx. This is associated with islet graft dysfunction and substantial islet loss before tissue remodeling and engraftment occur, with T1D or hyperglycemia having a negative effect on islet survival (DAVALLI et al., 1996; BIARNÉS et al., 2002; reviewed in WALKER, APPARI & FORBES, 2022).

In addition, islets are exposed to oxidative stress during the entire ITx process, which negatively affects islet viability and function. Therefore the use of antioxidants, such as metallothionein and glutathione peroxidase, in the ITx process (e.g. during islet graft preparation and islet infusion) might represent an important starting point for improving the ITx outcome (CHEN et al., 2001; LI, CHEN & EPSTEIN, 2004; MYSORE et al., 2005; reviewed in EGUCHI et al., 2022; reviewed in WALKER, APPARI & FORBES, 2022).

Another key factor contributing to islet mass loss is ischemia/reperfusion injury, which is due to the restoration of blood flow to a transiently oxygen deprived graft (DU et al., 2013; reviewed in DELAUNE et al., 2017). Therefore, agents such as adiponectin or diazoxide are being researched for their protective effect against ischemia/reperfusion injury (DU et al., 2013; WANG et al., 2015; WANG et al., 2022).

Hypoxia represents a further challenge in ITx (reviewed in WALKER, APPARI & FORBES, 2022). This is based on the discrepancy that naive islets in the pancreas have a very high oxygenation need (5-15% of the pancreatic blood volume is used

by the islets, oxygen tension 40 mmHg), but at the time of ITx they are avascular and are therefore initially only supplied with oxygen via diffusion (CARLSSON et al., 2001; reviewed in DELAUNE et al., 2017). Revascularization starts a few days after ITx. 10-14 days after ITx, the islets are considered to be fully revascularized (MENGER et al., 1989; VAJKOCZY et al., 1995a; VAJKOCZY et al., 1995b; reviewed in JANSSON & CARLSSON, 2002; JONES et al., 2007; reviewed in DELAUNE et al., 2017).

In addition, the portal vein system is characterized by a low oxygen tension (reviewed in VAN DER WINDT et al., 2008; reviewed in DELAUNE et al., 2017). Hypoxia is a well-known apoptosis trigger in beta cells and therefore contribute to islet loss after ITx (EMAMAULLEE et al., 2005; reviewed in VAN DER WINDT et al., 2008). This is one of the reasons why the portal vein is being questioned as the current standard ITx site and why intensive research for evaluation of alternative ITx sites, like the omentum or the gastric submucosa are ongoing (ECHEVERRI et al., 2009; DE MESQUITA et al., 2018; LU et al., 2019; reviewed in DAMYAR et al., 2021; reviewed in WALKER, APPARI & FORBES, 2022).

2.6.2. Immunological challenges – IBMIR

Immunological challenges pose additional obstacles to the success of ITx, encompassing issues such as allo- and autogenic graft rejection, as well as the instant blood-mediated inflammatory reaction (IBMIR) (reviewed in WALKER, APPARI & FORBES, 2022).

As known from other organ transplantations, immune-mediated graft rejection can also occur after ITx, representing a significant factor contributing to the loss of function of transplanted islets (reviewed in CHEN et al., 2023; LANDSTRA et al., 2023). This is due to pre-ITx or ITx-induced auto- and allo-specific cellular immune responses (CAMPBELL et al., 2007; HILBRANDS et al., 2009; PIEMONTI et al., 2013; reviewed in PIEMONTI, 2022), accompanied by non-specific, innate immune mechanisms (CITRO et al., 2012; reviewed in CITRO, CANTARELLI & PIEMONTI, 2013; reviewed in PIEMONTI, 2022). The main cell types involved in immune-mediated rejection after ITx are macrophages, $CD4^+$ T helper cells, $CD8^+$ cytotoxic T cells and B cells. In addition to these effector cells, regulatory

immune cells, e.g. regulatory T cells, are involved in the immune process to regulate and limit the extent of immunological and inflammatory processes and prevent autoimmunity (reviewed in CHEN et al., 2023).

Allo-rejection is due to incompatibility of the recipient with the donor HLA, a phenomenon that is particularly explosive in the case of multiple donors (reviewed in RICKELS & ROBERTSON, 2019). Allo-rejection can occur acutely if pre-sensitization to the donor HLA has already occurred with the formation of alloantibodies, or chronically if *de novo* alloantibodies are formed after ITx (LOBO et al., 2005; MOHANAKUMAR et al., 2006; reviewed in RICKELS & ROBERTSON, 2019). In T1D patients, reoccurrence of autoreactivity against islet autoantigens even under immunosuppression can also potentially lead to rejection of the islet graft (STEGALL et al., 1996; TYDÉN et al., 1996; ROEP et al., 1999; VENDRAME et al., 2010; reviewed in RICKELS & ROBERTSON, 2019).

IBMIR is an inflammatory process occurring in the first days after intraportal ITx (reviewed in KOURTZELIS et al., 2015). When islets were exposed to allogeneic blood *in vitro* and *in vivo*, Bennet and coworkers observed platelet activation, recruitment of immune cells and activation of the coagulation and complement system, respectively (BENNET et al., 1999; reviewed in KANAK et al., 2014). In addition, they found that the cascade can be attenuated by the use of heparin and a soluble complement receptor, which is why they proposed these agents for clinical use (BENNET et al., 1999). The main initiator of IBMIR is tissue factor (TF), which is expressed on the surface of the islets, inducing platelet binding and activation and leading to a clot reaction and intensive recruitment of immune cells (reviewed in KANAK et al., 2014; reviewed in GAMBLE et al., 2018). The driver of this coagulative reaction is thrombin, which is initially formed on the basis of the islet-expressed TF and later amplified by the activated platelets, resulting in the formation of a fibrin capsule around the islets (MOBERG et al., 2002; OZMEN et al., 2002). In addition to coagulation, complement activation and secretion of chemokines contribute to IBMIR, leading to infiltration of the islets with leukocytes (mainly polymorphonuclear leukocytes (PMNs)), which release proinflammatory cytokines.

This results in a disruption of islet integrity and ultimately islet loss (MOBERG, KORSGREN & NILSSON, 2005; reviewed in NILSSON, EKDAHL & KORSGREN, 2011; reviewed in KANAK et al., 2014) **(Fig. 4)**. It is assumed that more than 50% of the transplanted islet mass is lost in the first period directly after ITx, whereby the innate IBMIR is significantly involved (KOSINOVA et al., 2019). Similar to the allogeneic setting, IBMIR also leads to tissue loss in xenogeneic settings, which has been demonstrated both *in vitro* and *in vivo* in transplantation of porcine islets to mice and to non-human primates (NHPs) (BENNET et al., 2000; GOTO et al., 2004; reviewed in NILSSON, EKDAHL & KORSGREN, 2011; LIUWANTARA et al., 2016).

Therefore, intensive research has been conducted to overcome IBMIR. These approaches encompass the use of heparin or thrombin-inhibitors such as melagatran, knocking down TF or using engineered pancreatic islets expressing streptavidin-thrombomodulin (OZMEN et al., 2002; KOH et al., 2010; MA et al., 2012; reviewed in WALKER, APPARI & FORBES, 2022; ZHANG et al., 2022; TURAN et al., 2023). In order to reduce inflammation in general, ITx should be accompanied by administration of anti-inflammatory agents, e.g. infliximab, anakinra, etanercept or a combination thereof (reviewed in SZEMPRUCH et al., 2019; reviewed in WALKER, APPARI & FORBES, 2022).

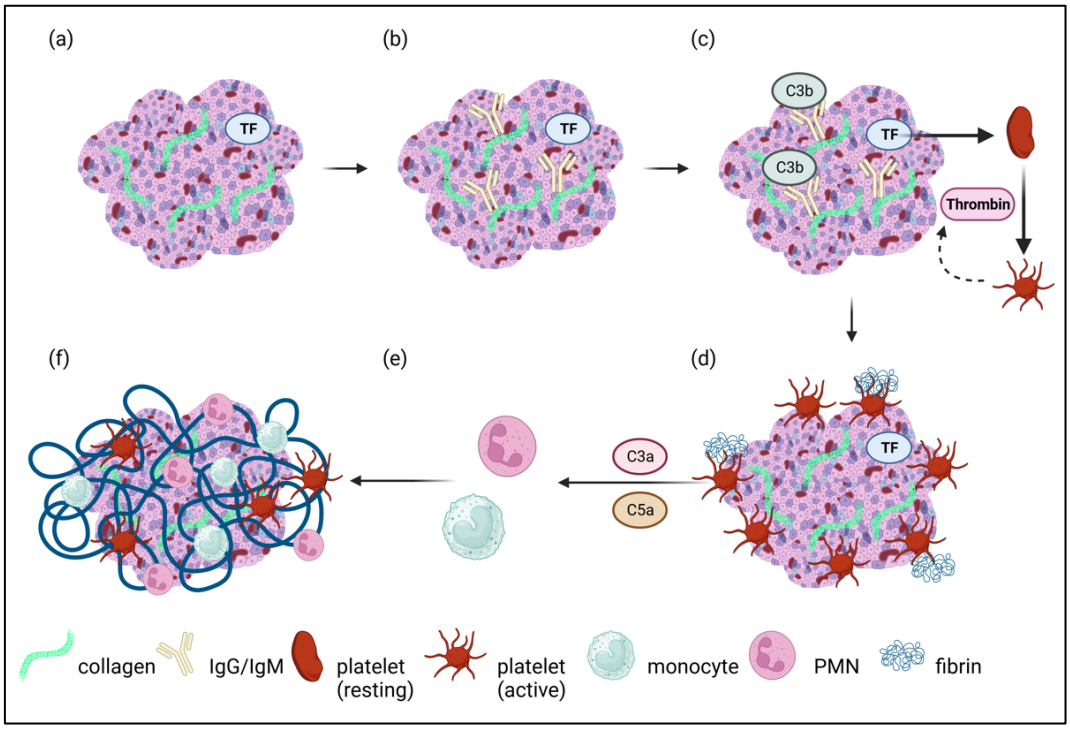

Figure 4: *Simplified schema of IBMIR.*

(a, b) *Complement activation by binding of IgG and IgM to surface structures of the islets, such as collagen.* ***(c)*** *Deposition of complement factor C3b. Platelet activation by formation of thrombin due to islet expressed TF. Amplification of thrombin formation by activated platelets.* ***(d)*** *Binding of activated platelets to islets. Formation of fibrin.* ***(e)*** *Complement activation and formation of C3a and C5a due to activated platelets with subsequent recruitment and activation of monocytes and PMNs.* ***(f)*** *Encapsulation of islets by fibrin, entrapment of platelets, monocytes, PMNs, infiltration of islets by monocytes and PMNs resulting in disruption of islet integrity and islet loss.*

Author's own figure, adapted from Nilsson et al., 2011;
Figure legend: Adapted from Nilsson et al., 2011; Created with Biorender.com.

There are several approaches to counter immunological hurdles of ITx (reviewed in WALKER, APPARI & FORBES, 2022). One example are encapsulation technologies (reviewed in DIMITRIOGLOU et al., 2019; reviewed in WALKER, APPARI & FORBES, 2022). These devices create a semi-permeable barrier between the host and the therapeutic tissue, providing it with immunological protection and therefore preventing graft rejection (reviewed in DESAI & SHEA, 2017; reviewed in ERNST, WANG & MA, 2018). Other approaches to overcome immunological hurdles are e.g. HLA silencing, the use of regulatory T cells or the co-culture/co-transplantation of islets with mesenchymal stromal cells (MSCs), due to their anti-inflammatory and angiogenesis-promoting effects (HACKE et al., 2009; GOŁĄB et al., 2014; reviewed in KEMTER & WOLF, 2018; FORBES et al., 2020; reviewed in WALKER, APPARI & FORBES, 2022).

2.6.3. Organ donor shortage & alternative islet sources

A major limitation of ITx is that human donor organs are currently required for ITx, and the supply of donor organs cannot meet the demand (reviewed in MATSUMOTO & SHIMODA, 2020). This is further exacerbated by low islet yield, as the islet isolation processes cause a reduction of the estimated one million islets of a donor pancreas by more than 50% (reviewed in WALKER, APPARI & FORBES, 2022).

There are various approaches to overcoming the organ donor shortage, e.g. the improvement of the human islet yield through non-thermic pancreas perfusion or an expansion of the criteria for organ donor selection (BTS, 2019; reviewed in WALKER, APPARI & FORBES, 2022; ROODEN et al., 2023). The main focus, however, is on the development of alternative islet sources such as stem-cell derived islets or xenogeneic porcine islets (reviewed in COE, MARKMANN & RICKERT, 2020; reviewed in WALKER, APPARI & FORBES, 2022; reviewed in CZARNECKA et al., 2023).

Stem-cell-derived islet-like cells can be generated based on human embryonic stem cells or induced pluripotent stem cells (D'AMOUR et al., 2006; TAKAHASHI & YAMANAKA, 2006; KROON et al., 2008; PAGLIUCA et al., 2014; reviewed in CZARNECKA et al., 2023). Fully functional pancreatic beta cells derived from human pluripotent stem cells were generated *in vitro* by Pagliuca and coworkers in 2014 and formed the basis for clinical transplantation studies in humans (PAGLIUCA et al., 2014; reviewed in CZARNECKA et al., 2023).

Another promising approach to overcome organ donor shortage is porcine islet xenotransplantation. The progress in genetic editing technology has paved the way for creating porcine islet donors with multiple genetic modifications. These modifications involve genetic depletion of certain carbohydrate xeno-antigens (αGal, Neu5Gc, and Sd(a)), whose presence are associated with complement and coagulation activation in humans. In addition, genetically modifying islet donor pigs to express human immune regulatory proteins lead to enhanced immunological compatibility to overcome cellular rejection (reviewed in KEMTER, DENNER & WOLF, 2018; reviewed in COE, MARKMANN & RICKERT, 2020).

Porcine islets have different characteristics depending on the age of the donor pig, so that a distinction is proposed between NPIs (1-3 days), juvenile (18-21 days) and adult (> 2 years) porcine islets (JPIs, APIs). Insulin secretion rates are higher in APIs than in NPIs (SMITH et al., 2018; VANDERSCHELDEN et al., 2019). NPIs consist of immature islet-like cell cluster in which insulin production is low compared to mature islets, which implies that *in vitro* or *in vivo* maturation is necessary to reach their full functionality (KORSGREN, CHRISTOFFERSON & JANSSON, 1999; reviewed in KEMTER & WOLF, 2018; VANDERSCHELDEN et al., 2019). However, NPIs are characterized by several advantages over APIs, which include higher resistance to hypoxia, lower immunogenicity, increased *in vitro* stability and enhanced *in vivo* cell proliferation capacity post ITx (BLOCH et al., 1999; YOON et al., 1999; TRIVEDI et al., 2001; reviewed in KEMTER & WOLF, 2018; VANDERSCHELDEN et al., 2019). In addition, NPIs are the most cost-efficient option (US$ per islet API *vs.* JPI and NPI: $0.09 *vs.* $0.04 and $0.02, respectively) (reviewed in KEMTER & WOLF, 2018; VANDERSCHELDEN et al., 2019). The efficacy of transplanted NPIs to restore normoglycemia has been demonstrated in mice and NHPs (YOON et al., 1999; HAWTHORNE et al., 2022). Some studies with porcine xenotransplantation in humans have already been carried out, using e.g. encapsulated WT islets, but although some improvements in glycemic control have been seen, a breakthrough has not yet been achieved (GROTH et al., 1994; ELLIOTT et al., 2000; VALDÉS-GONZÁLEZ et al., 2005; WANG et al., 2011; MATSUMOTO et al., 2014; MOROZOV et al., 2017; reviewed in COE, MARKMANN & RICKERT, 2020). In order to bring islet xenotransplantation to the clinic, a number of persistent barriers still need to be overcome, with the main focus being on further genetic optimization of donor pigs and development of long-term functioning islets in the presence of clinically relevant immunosuppression (reviewed in COE, MARKMANN & RICKERT, 2020).

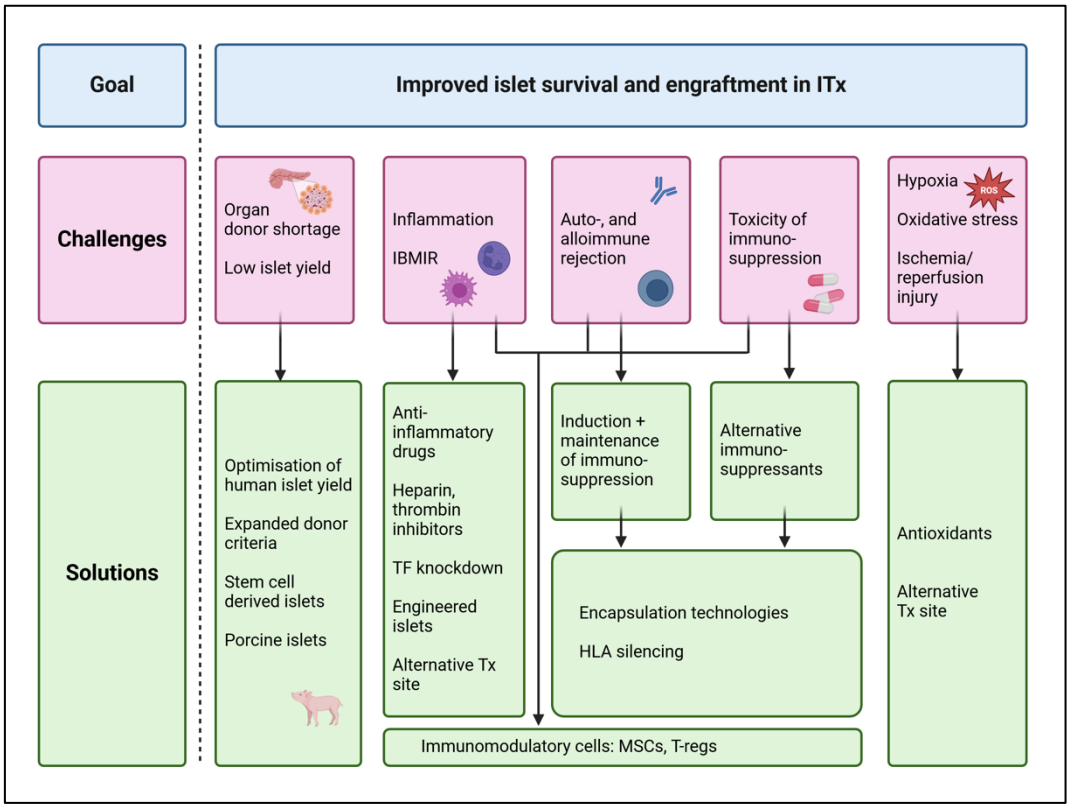

Figure 5: *Challenges and future directions of ITx.*

Author's own figure, adapted from Walker et al., 2022;
Additional information: Ma et al., 2012; Turan et al., 2023; Created with Biorender.com.

3. Animal models in diabetes research - Selecting the most suitable ITx recipient model

Animal models play a very important role in preclinical research of diabetes mellitus and ITx. Most work in this field is performed on rodents, but also in large animal models such as NHPs and increasingly also in pigs (reviewed in REES & ALCOLADO, 2005; LUDWIG et al., 2020; reviewed in BERGEN, 2022).

Animal models are used in this context to gain a better understanding of the pathophysiological processes of the disease, but also to develop new therapeutic agents and treatment methods (reviewed in AL-AWAR et al., 2016). T1D symptomatology can be achieved by genetic background (spontaneous mutation or genetic modification), chemical induction or surgical intervention (pancreatectomy) (reviewed in WOLF et al., 2014; reviewed in AL-AWAR et al., 2016; LUDWIG et al., 2020) **(Fig. 6)**.

Models for diet-induced metabolic disorders of glucose metabolism are not relevant as recipients for ITx and therefore not mentioned below.

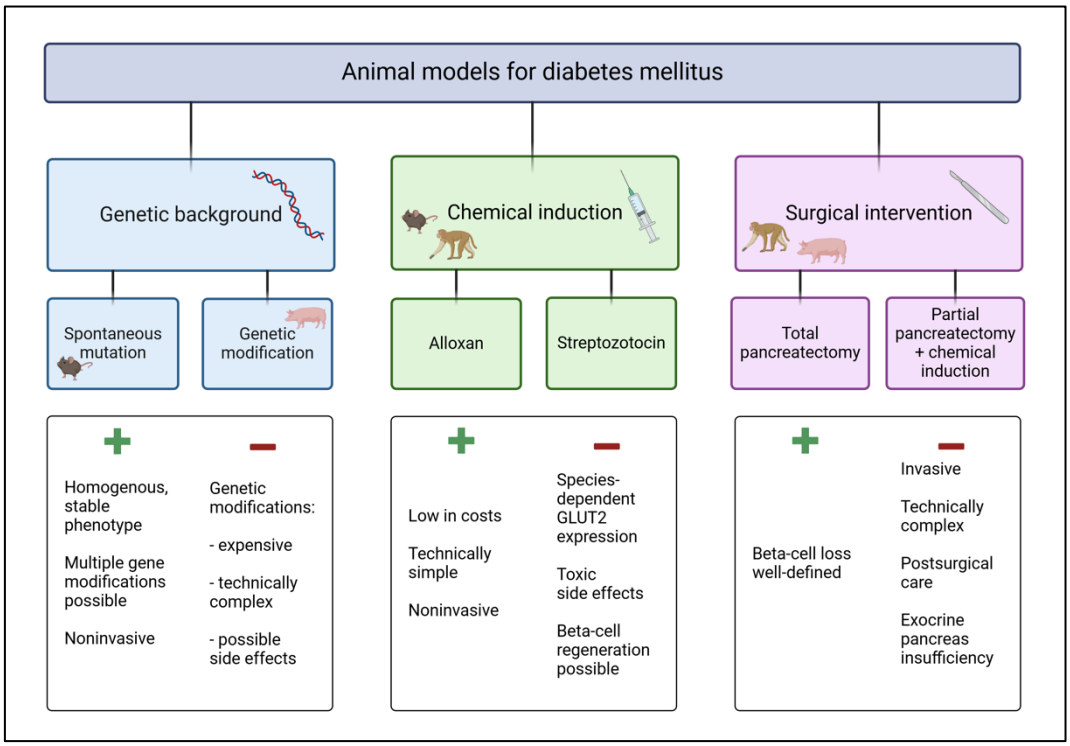

Figure 6: *Overview of animal models for diabetes mellitus.*

Author's own figure, adapted from Al-Awar et al., 2016 and Renner et al., 2020; Additional information: King et al., 2012, Wolf et al. 2014, Ludwig et al., 2020; Created with Biorender.com.

3.1. Chemical diabetes induction

Diabetes can be induced chemically by streptozotocin (STZ) and alloxan (ALX) (reviewed in AL-AWAR et al., 2016). These two agents are toxic glucose analogs, primarily accumulating in pancreatic beta cells through the uptake via glucose transporter 2 (GLUT2) (reviewed in LENZEN, 2008).

STZ is an antibiotic agent obtained from *Streptomyces achromogenes var. streptozoticus* with additional antitumor, mutagenic and diabetogenic properties (REUSSER, 1971). The diabetogenic effect of STZ is based on its predominant uptake by and subsequent destruction of pancreatic beta cells (FURMAN, 2021). Of note, STZ can also have a dose-dependent toxic effect on other cell types than beta cells (reviewed in DEEDS et al., 2011; reviewed in GOYAL et al., 2016; NØRGAARD et al., 2020). STZ is toxic for beta cells primarily due to its alkylating

properties, leading to fragmentation of the DNA, and to a lesser extent by formation of DNA-damaging nitric oxide (NO) and radical oxygen species (ROS) (reviewed in SZKUDELSKI, 2001) **(Fig. 7)**.

Chemical diabetes induction can be achieved either by a single high-dose administration of the beta-cell toxin or by multiple low-dose injections (reviewed in KING, 2012) **(Fig. 8)**. STZ diabetes induction is applicable in various species, e.g. in mice (ZHENG et al., 2019; ZHONG et al., 2022), rats (PAMIDI & SATHEESHA NAYAK, 2012; HAO et al., 2021), rabbits (JAVADI, ASRI-REZAEI & ALLAHVERDIZADEH, 2014; DING et al., 2022), dogs (JAVED et al., 2014; AL HEZAIMI et al., 2021), guinea pigs (CELLINI, ZAURA JUKIC & LEPARD, 2011; PODELL et al., 2017), pigs (LI, CUI & YANG, 2020; NIU et al., 2020) and NHPs (FROST et al., 2015; HAWTHORNE et al., 2022). However, its robustness varies between species as it is dependent on GLUT2 abundance on beta cells (reviewed in GOYAL et al., 2016). Consequently, a strong diabetogenic effect occurs for instance in rodents due to a high GLUT2 density on beta cells, while humans and also pigs are largely resistant to the diabetogenic effect of STZ due to sparse/absent GLUT2 expression on their beta cells (DUFRANE et al., 2006; reviewed in LENZEN, 2008; reviewed in GOYAL et al., 2016; reviewed in RENNER et al., 2020).

ALX has a diabetogenic effect through two mechanisms: firstly, it inhibits glucokinase, leading to reduced ATP production and thus decreasing glucose-induced insulin secretion (MEGLASSON et al., 1986; LENZEN, FREYTAG & PANTEN, 1988; reviewed in LENZEN, 2008). Secondly, in the presence of intracellular thiols, especially glutathione, ALX induces the formation of ROS (superoxide radicals, hydrogen peroxide, hydroxyl radicals) as part of a cyclic redox reaction, whereby hydroxyl radicals finally cause the selective destruction of beta cells (reviewed in SZKUDELSKI, 2001; reviewed in LENZEN, 2008) **(Fig. 7)**. The diabetogenic effect of ALX is species-dependent, among the sensitive species, rats are the most commonly used (reviewed in RADENKOVIĆ, STOJANOVIĆ & PROSTRAN, 2016). ALX-induced diabetes can also be achieved in mice (MILLMAN et al., 2016; OU et al., 2016), rabbits (FU et al., 2016; JEONG et al., 2018), pigs (KING et al., 2011; BADIN et al., 2018) and dogs (ESIEVO et al., 2021; HAN et al., 2022). Cats are resistant to the diabetogenic effect of ALX, but ALX-

induced kidney damage also occurs in this species. A dose-dependent (< 40 mM) resistance to ALX has also been reported in guinea pigs (GORRAY & FUJIMOTO, 1983; HATCHELL et al., 1986; reviewed in RADENKOVIĆ, STOJANOVIĆ & PROSTRAN, 2016). The low GLUT2 expression on beta cells in pigs limits the use of GLUT2-dependent beta-cell toxins for diabetes induction in this species (DUFRANE et al., 2006; reviewed in RENNER et al., 2020)

The advantages of chemical diabetes induction are that it is low in costs, easy to perform, and a non-invasive procedure (reviewed in RENNER et al., 2020). In general, STZ is the more commonly used agent for chemical diabetes induction. However, there are scenarios in which ALX is preferred, for example because of its lower mortality rate. The toxic effect of ALX on beta cells may be partially reversible, therefore, ALX should be considered for short-term studies only, while STZ, with its more stable effect on beta-cell destruction, can be used for short-term and long-term experiments (reviewed in RADENKOVIĆ, STOJANOVIĆ & PROSTRAN, 2016). Nevertheless, the possibility of beta-cell regeneration represents a decisive limitation of chemically induced diabetes models (reviewed in KING, 2012; reviewed in GRAHAM & SCHUURMAN, 2015). ALX and STZ both have toxic effects on organs other than the pancreas. In this context, the liver and kidneys are particularly affected, as these organs also express GLUT2 transporters (reviewed in RADENKOVIĆ, STOJANOVIĆ & PROSTRAN, 2016).

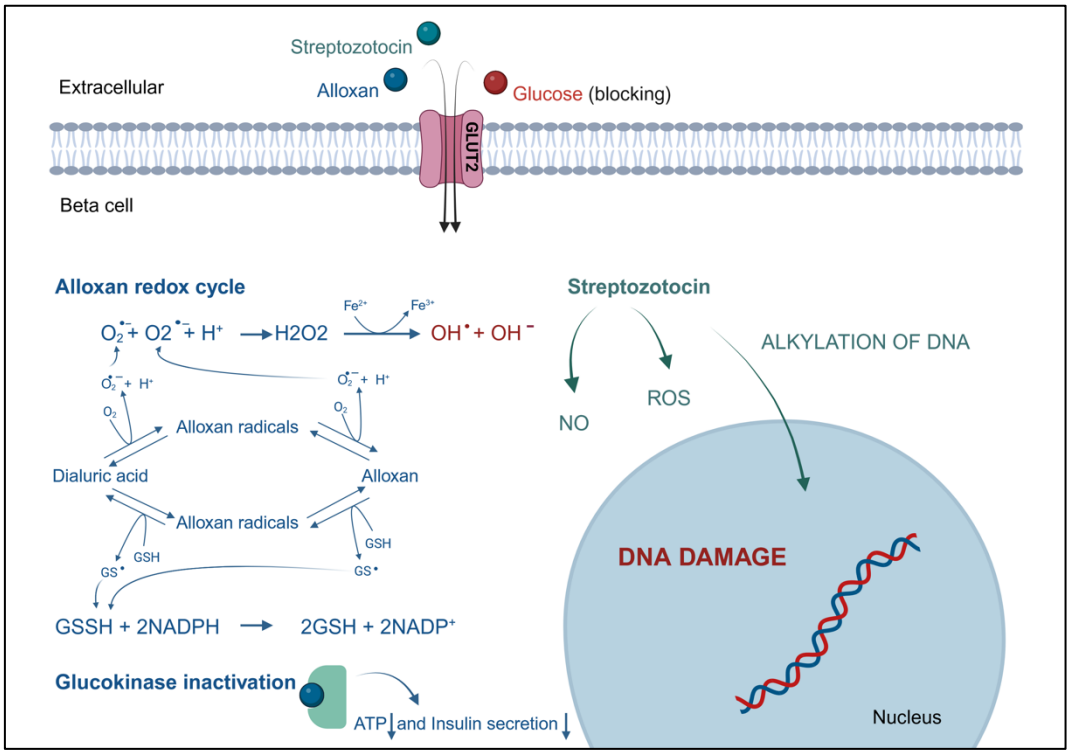

Figure 7: *Mode of action of ALX and STZ.*

H2O2: hydrogen peroxide; $O_2^{\bullet -}$: superoxide radicals; $OH^{\bullet}$: hydroxyl radicals (Lenzen, 2008);

Author's own figure, adapted from Radencović et al., 2016; Created with Biorender.com.

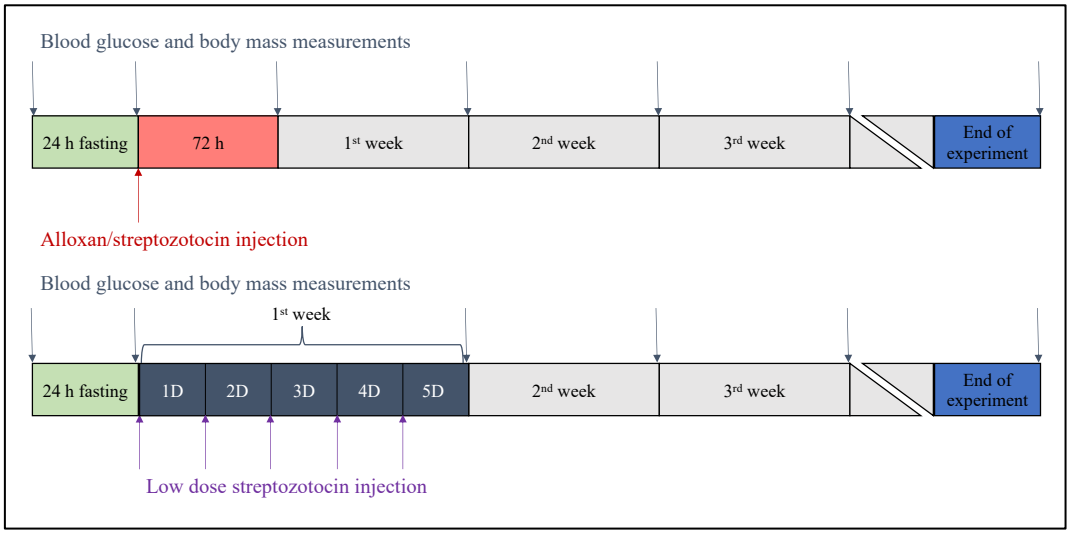

Figure 8: *Exemplary illustration of chemical diabetes induction with ALX and STZ in a susceptible species.*

Author's own figure, adapted from Radencović et al., 2016.

3.2. Diabetes induction by surgical intervention

Diabetes can be induced surgically by removal of the pancreas (pancreatectomy) (reviewed in SAKATA et al., 2012). In addition to the removal of the entire pancreas (total pancreatectomy), there is also partial pancreatectomy combined with the administration of STZ (WISE, GORDON & JOHNSON, 1985; HE et al., 2011; reviewed in KING, 2012). Surgical diabetes induction is mainly performed in large animal models such as pigs and NHPs (MOREL et al., 1991; MELLERT et al., 1998; reviewed in KING, 2012; LUDWIG et al., 2020). In pigs, a simultaneous splenectomy can facilitate the access to the pancreas. Pancreatectomy addresses the limitations of chemical diabetes induction in large animals, such as uncertain efficacy, potential beta-cell regeneration and toxic side effects (HEINKE et al., 2016). However, its use is technically demanding and is an invasive procedure for the animal that requires intensive post-operative care. Furthermore, pancreatectomy can lead to severe hypoglycemia due to a combined insulin and glucagon shortage and is also associated with exocrine pancreatic insufficiency (HE et al., 2011; reviewed in KING, 2012; HEINKE et al., 2016; reviewed in RENNER et al., 2020).

3.3. Genetically diabetic rodent models

There are plentiful genetically modified rodent models described in the field of diabetes research, based on either spontaneous mutation and selective breeding or on targeted genetic modifications (reviewed in KING, 2012). Examples of insulin-deficient diabetes models are described below.

The *BB rat model*, as the most thoroughly investigated diabetes rat model, originates from a Canadian population of outbred Wistar rats. It is based on pancreatic insulitis, that occurred spontaneously in founder rats, leading to destruction of beta cells and therefore to hyperglycemia and ketoacidosis (reviewed in MORDES et al., 2004).

The *LEW.1AR1/Ztm-iddm rat model* exhibits autoimmune-mediated destruction of beta cells due to a spontaneous mutation that appeared in a congenic Lewis rat strain with a defined major histocompatibility complex (MHC)

haplotype (RT1.A^a B/D^u C^u). The mutation caused diabetic symptoms with an incidence of 20% (LENZEN et al., 2001).

The *NOD mouse model* originally goes back to a cataract mouse line with a JcI-ICR background and was established through selective breeding methods (reviewed in HANAFUSA et al., 1994). It was first described by Makino and coworkers (MAKINO et al., 1980). In this model, diabetes emerged spontaneously, caused by autoimmune processes, with the pathophysiology being comparable to that of T1D in humans. Similar to humans, the MHC locus is a decisive factor for susceptibility to autoimmune diabetes in the mouse model as well, with a shared amino acid substitution located in an MHC class II gene (CHEN, MATHEWS & DRIVER, 2018; reviewed in AUBIN et al., 2022).

The *Akita mouse model* emerged from a spontaneous arisen $Ins^{2+/C96Y}$ mutation in the insulin *(Ins)* 2 gene in a C57BL/6NSIc mouse (reviewed in AL-AWAR et al., 2016). This mutation leads to the exchange of a nucleotide, thereby disrupting the disulfide bridge between the A chain and the B chain of the insulin protein (YOSHINAGA et al., 2005). In consequence, mutant insulin undergoes improper proinsulin processing, leading to aggregation of misfolded proteins in the ER and triggering ER stress. As a result, beta-cell apoptosis occurs, resulting in onset of insulin-dependent diabetes at an age of 3-4 weeks (reviewed in AL-AWAR et al., 2016). As there is no beta-cell autoimmunity in this model and the mice are still insulin sensitive, it is particularly suitable for research into ITx (MATHEWS, LANGLEY & LEITER, 2002).

3.4. Genetically diabetic pig models

Pigs are recognized as a primary animal species employed in translational research. The distinct benefits of using pigs stem from their anatomical and physiological traits in areas such as cardiovascular, urinary, integumentary and digestive systems, which closely resemble those of humans (reviewed in SWINDLE et al., 2012). With regard to the pancreas organ, there are largely anatomic similarities between humans and pigs, although there are differences in the efferent pancreatic duct system (reviewed in WOLF et al., 2014).

Of note, islet anatomy, development and islet cell properties have a higher similarity between humans and pigs compared to that between humans and rodents (reviewed in ARROJO E DRIGO et al., 2015; KIM et al., 2020c; TRITSCHLER et al., 2022). In addition, pigs show an early onset of sexual maturity at an age between five and eight months, a brief generation interval of 12 months, high numbers of offspring (10-12 piglets/litter) and are all season breeders, which make them an attractive animal model for translational research. Further, genetic modifications can be performed in pigs by default (reviewed in AIGNER et al., 2010; reviewed in WOLF et al., 2014).

To study the pathophysiology of diabetes in a large animal model, several genetically modified pig models were developed (reviewed in WOLF et al., 2014; reviewed in RENNER et al., 2020). One example is the $GIPR^{dn}$ model (RENNER et al., 2010). These pigs express a beta cell specific dominant-negative glucose-dependent insulinotropic polypeptide (GIP) receptor that can bind the incretin hormone GIP with the same affinity as the WT GIP receptor. This results in a reduced insulinotropic action of GIP, which leads to the development of a prediabetic state (reviewed in WOLF et al., 2014).

Transgenic pigs, characterized by the expression of a dominant-negative human hepatocyte nuclear factor 1α were generated as a model for Maturity Onset Diabetes of the Young 3 (UMEYAMA et al., 2009; reviewed in WOLF et al., 2014).

Another example for genetically diabetic pigs is the INS^{C94Y} transgenic pig model for permanent neonatal diabetes mellitus (PNDM) according to Renner et al. (RENNER et al., 2013). PNDM in human patients is defined as diabetes that occurs at the age of ≤ six months and persists for life (reviewed in HUANG et al., 2014). A significant number of PNDM cases are caused by mutations in the *INS* gene, which are then referred to as mutant *INS* gene-induced diabetes of youth (MIDY) (reviewed in WOLF et al., 2014; KIM et al., 2015). MIDY in humans is defined as autosomal dominant diabetes with early onset, insulin deficiency and absence of autoantibodies against pancreatic beta cells (reviewed in LIU et al., 2010). MIDY/PNDM is caused by at least 26 missense mutations in the *INS* gene (STØY et al., 2007; AHAMED et al., 2008; COLOMBO et al., 2008; EDGHILL et al., 2008; MOLVEN et al., 2008; POLAK et al., 2008; reviewed in LIU et al., 2010).

INS^{C94Y} transgenic pigs (MIDY pigs) were generated by a guanine-arginine base exchange in the porcine *INS* gene, resulting in an exchange from cysteine to tyrosine at amino acid position 94 (RENNER et al., 2013) **(Fig. 9)**. Porcine *INS*^{C94Y} matches human *INS*^{C96Y}, a mutation variant that occurs in MIDY, because the human C-peptide comprises two more amino acids compared to porcine C-peptide. Analogue to murine *Ins*$^{2+/C96Y}$ in the Akita mouse model, porcine *INS*^{C94Y} and human *INS*^{C96Y} provoke an impaired proinsulin folding due to an abolished B-A interchain disulfide bridge within the insulin molecule. This interferes with proinsulin trafficking, since WT proinsulin and mutant proinsulin build high molecular complexes. As a consequence, misfolded insulin accumulates in the ER, triggering ER stress and ultimately resulting in beta-cell demise (reviewed in LIU et al., 2010; reviewed in WOLF et al., 2014; reviewed in LIU et al., 2015).

MIDY pigs have significantly increased random blood glucose values, which are already detectable within the first 24 hours after birth. FBG values are also continuously and significantly increased in MIDY pigs compared to WT pigs. Furthermore, they show the following characteristics compared to their littermates at an age of 4.5 months: A 41% reduced BW, 72% decreased BCM, equivalent to approximately 53% when normalized to BW, along with a 60% decrease in fasting insulin levels. According to the reduced growth rate from two months of age, MIDY pigs exhibit proportionally reduced weights of most organs, including the pancreas. This does not include kidney weight, which is only reduced by 15% and therefore significantly increased in relative terms. Beta cells from MIDY pigs show reduced insulin secretory granules and a greatly expanded ER. Cataract emerges from eight days of age onwards. No pathological changes associated with diabetes in the kidney or nervous system are present within one year. The MIDY pig model is characterized by a stable diabetic phenotype that can be treated symptomatically with exogenous insulin, making it attractive for example for insulin therapy or ITx studies (RENNER et al., 2013; reviewed in WOLF et al., 2014).

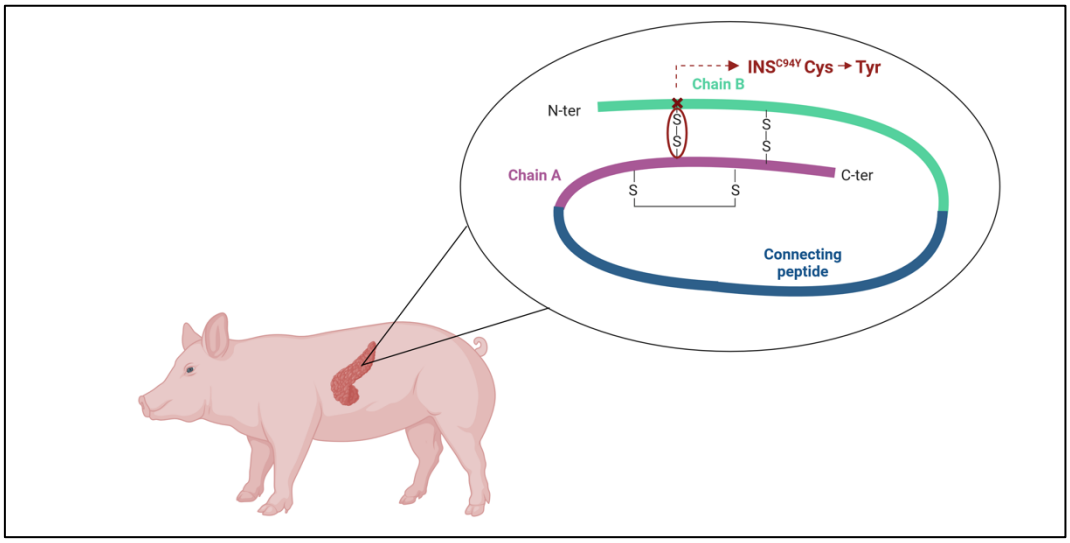

Figure 9: *INS^{C94Y} transgenic pig as a porcine MIDY model.*

Cysteine → Tyrosine mutation in the insulin gene at amino acid position 94 (Renner et al. 2013); Author's own figure, adapted from Renner et al., 2020; Created with BioRender.com.

Genetic diabetes models are characterized by a homogeneous, stable phenotype, are non-invasive and allow the implementation of multiple genetic modifications. On the other hand, genetic modifications are associated with high financial outlay, are technically demanding procedures and can lead to unplanned side effects (reviewed in RENNER et al., 2020)

3.5. Diabetic animal models used for ITx studies

As with ITx in humans, protection of the transplant against immunological rejection is also required in animal models for ITx. Suppression of the immune system in ITx studies can be achieved either by usage of genetically modified immunodeficient animal models as recipients, as the NOD-*scid* gamma (NSG) mouse model, or by application of an immunosuppressive therapeutic regime (ESTIL LES et al., 2018; KIM et al., 2019; BERTERA et al., 2020; HAWTHORNE et al., 2022; reviewed in WAGNER et al., 2022; LINDHEIMER et al., 2023). Currently, ITx studies are mostly conducted in mice and NHPs, pigs have been sporadically utilized as recipient species so far (LAMPE, SUTHERLAND & NAJARIAM, 1976; MELLERT et al., 1998; reviewed in SAKATA et al., 2012; reviewed in GRAHAM & SCHUURMAN, 2015) **(Table 4)**.

Species	**Immunosuppression**	**Diabetes induction**	**References**
Mouse	- Genetic immunodeficiency - Immunosuppressive regime	- Chemical induction (STZ) - Genetic background (spontaneous) • NOD • Akita	(MATHEWS, LANGLEY & LEITER, 2002; reviewed in SAKATA et al., 2012; reviewed in CANTARELLI et al., 2013; KIKAWA et al., 2014; BUERCK et al., 2017; reviewed in NAGAYA et al., 2021; reviewed in WAGNER et al., 2022; LINDHEIMER et al., 2023; LEI et al., 2024)
NHPs	Immunosuppressive regime	- Chemical induction (STZ) - Surgical induction	(SAKATA et al., 2012; SHIN et al., 2017; reviewed in BERTERA et al., 2020; KIM et al., 2020a; GRAHAM et al., 2022; HAWTHORNE et al., 2022)

Table 4: *Commonly used diabetic animal models in ITx research.*

III. OBJECTIVES

This study focuses on the following objectives:

1. Establishment of a novel intraportal islet allotransplantation model of NPIs in a group of three WT pigs.

2. Implementation of intraportal islet allotransplantation in four diabetic transgenic *INS*^{C94Y} pigs to assess *in vivo* maturation and long-term functionality of the islet graft.

3. Evaluation of the feasibility of [^{68}Ga]Ga-DOTA-Exendin-4 PET/CT imaging for *in vivo* monitoring of intraportal islet grafts in genetically diabetic ITx recipient pigs.

The establishment of [^{68}Ga]Ga-DOTA-Exendin-4 PET/CT imaging of endogenous beta cells in pigs as prerequisite for imaging of intraportal islet grafts was the focus of the scientific work of the dissertation of Ms. Nicol Gloddek.

4. Histological validation of ITx outcome by assessment of islet transplant distribution and properties

5. Characterization and quantification of immunological processes in the graft-bearing livers.

The study was designed as an orientation study. Parts of this dissertation are also described in (PILZ et al., 2024).

IV. ANIMALS, MATERIALS AND METHODS

1. Animals

All animal experiments were performed according to the German Animal Welfare Act and Directive 2010/63/EU on the protection of animals used for scientific purposes and were approved by the responsible animal welfare authority (Government of Upper Bavaria, ROB-55.2-2532.Vet_02-20-45).

Neonatal WT piglets between one and seven days of age served as NPI donors for ITx. The establishment of the ITx method was carried out in two male and one female WT pigs (age: 88-134 days, BW: 28-55 kg), referred to as WT group. The long-term experiments were performed with four female transgenic *INS*^{C94Y} pigs with diabetic phenotype (age: 81-137 days, BW: 18-48.5 kg), referred to as MIDY group. Observation period in the WT group was 7-31 days and in the MIDY group 71-103 days. Properties of graft recipient pigs are provided in **Table 5**. Breeding and rearing until at least ten weeks of age took place at the Center for Innovative Medical Models, Chair for Molecular Animal Breeding and Biotechnology, LMU Munich in conventional pig indoor housing under designated pathogen free hygiene conditions. The ITx experiments were carried out at the Walter-Brendel-Center, LMU Munich, where the pigs had access to a littered stable and a covered run including enrichment material. Access to the animal housing was available through a hygiene gate.

Animal-ID	Genotype	Sex	BW (kg)	Age at ITx (days)	Observation period
11821	WT	♂	55	134	7 days
11822	WT	♂	28	88	7 days
12401	WT	♀	47	109	31 days
12580	*INS*^{C94Y}	♀	29	116	103 days
12582	*INS*^{C94Y}	♀	48.5	137	83 days
13062	*INS*^{C94Y}	♀	24.5	95	100 days
13064	*INS*^{C94Y}	♀	18	81	71 days

Table 5: *Properties of experimental animals.*

Weaning took place at the age of four weeks. WT pigs were offered then with *ad libitum* feeding, to the diabetic pigs a restrictive feeding regimen **(Table 6)** was applied.

The animals were fed with a commercial pig feed (Breeding-feed-LMU; Vilstalmühle). Pigs were fed once per day from the start of experiments and had free access to tap water at all times.

Age (weeks)	Amount of feed (kg/day)
4 - 7	0.5
8 - 9	0.8
10 - 11	1
12 - 13	1.4
14 - 15	1.75
> 16	2

Table 6: *Feeding regime of diabetic pigs.*

In addition, existing blood samples from WT pig #11855 **(Table 7)** and one male transgenic *INS*^{C94Y} pig (Animal-ID: #13057, age at necropsy: 121 days) served as controls for alanine aminotransferase (ALT) and C-reactive protein (CRP) measurements. Neither pig underwent ITx.

For histological analysis of the hepatic macrophage abundance after ITx, existing samples from two WT and three diabetic pigs, none of which received ITx, were used as controls **(Table 7)**.

Animal ID	Genotype	Sex	Age at necropsy (days)
11855	WT	♀	138
12224	WT	♂	197
11985	*INS*^{C94Y}	♀	144
12348	*INS*^{C94Y}	♂	148
11863	*INS*^{C94Y}/*INS*-eGFP-2760	♀	92

Table 7: *Properties of control animals for histological analysis of hepatic macrophage abundance.*

2. Materials

2.1. Devices

Accu-jet® pro pipette controller	Brand; Germany
Avanti™ 30 Centrifuge	Beckman Coulter; USA
Axioscan 7 Microscope Slide Scanner	Zeiss; Germany
Biograph True-Point 64 PET/CT	Siemens; Germany
Combimag RCH magnetic stirrer	IKA-Works Inc.; USA
CoMo-170/-300M	NuviaTech Instruments; France
Embedding molds premium	Medite Medical GmbH; Germany
Excelsior AS A82310100	Thermo Fisher Scientific; USA
Five Easy F20 pH meter	Mettler Toledo; USA
FreeStyle Freedom Lite system	Abott; USA
Grant Sub 14 water bath	CLF; Germany
Heating Thermal Pet Pad (MHP-E1220)	Anpan; China
Incubator ED056-230V	Binder GmbH; Germany
Leica microscope type DMC4500 (12730517)	Leica Microsystems; Switzerland
Microm HM 325 rotary microtome	Thermo Fisher Scientific; USA
Microwave MS-196VUT	LG; South Korea
Milli-Q® water system	Millipore; USA
MJ-3000 scale	Chyo; country information not available
MyLab™ X8VET ultrasound	Esaote; Italy
NanoZoomer S60, model C13210-04	Hammatsu Photonics K. K.; Japan
Olympus microscope model BX43F	Olympus; Japan
Pipets Pipetman	Gilson; USA

SC 9000XL patient monitor	Siemens; Germany
Servo Ventilator 900C	Siemens-Elema; Sweden
TES 99 modular paraffin embedding system	Medite Medical GmbH; Germany
Tissue cool plate COP 30	Medite Medical GmbH; Germany
Tissue float bath 1052	GFL; Germany
Veterinary Pulse Oximeter	Henry Schein Inc.; USA
Vortexer MS1 minishaker	IKA-Works Inc.; USA
Ziehm vision mobile C-arm #91554	Ziehm Imaging; Germany

2.2. Consumables

Aquasonic 100 ultrasound transmission gel	Parker Laboratories; USA
BD Micro-Fine Ultra™ needles, 12.7 mm	Becton Dickinson; USA
Braunol®, Antiseptic solution	Braun; Germany
Cobra (C2) 4F catheter, 65 cm	Cordis; USA
Cover cloth Foliodrape®	Hartmann Group; Germany
Cover slips 24 x 40 mm	Epredia; USA
Embedding cassettes UniLink	Engelbrecht Medizin- & Labortechnik; Germany
Endotracheal tubes, single-use (3.0 – 4.5)	Henry Schein Inc.; USA
EV3 N180801, Nitrex Guidewire, 0.018 inch	Medical Cart; Hungary
Falcon® 50 ml	Greiner Holding; Austria
Feather® Stitch scalpel No. 11	FEATHER® Safety Razor Co Ltd.; Japan
Glidewire®, 180 cm	Terumo; Japan

Heidelberg extension line 75 cm	Covetrus; USA
Histoplast PE Paraffin	Epredia; Netherlands
Microtome blades S35	FEATHER® Safety Razor Co Ltd.; Japan
Microvette® 200 EDTA K3E	Sarstedt AG & Co. KG; Germany
Needles (18G, 20G)	Braun; Germany
Neff Percutaneous Access Set	COOK® Medical; USA
Imeron® 300 M	Bracco Imaging Deutschland GmbH; Germany
Intrafix® SafeSet	Braun; Germany
Parafilm®	Bemis; USA
Pipette tips (10 µl, 200 µl, 1000 µl)	Sarstedt AG & Co. KG; Germany
Safe-Lock reaction tubes	Eppendorf; Germany
Serological pipettes (5 ml, 10 ml)	Sarstedt AG & Co. KG; Germany
Single-use razors	Wilkinson Sword; UK
S-Monovette® (K3 EDTA, Serum)	Sarstedt AG & Co. KG; Germany
Solofix® blood lancets	Braun; Germany
Spongostan®	Ferrosan Medical devices; Denmark
StarFrost® microscope slides	Engelbrecht Medizin- & Labortechnik; Germany
Syringes (1 ml, 5 ml, 10 ml, 20 ml)	Braun; Germany
Tape 4651, 50 mm	Tesa; Germany
TissueTek Disposable Molds (25 mm x 20 mm x 5 mm)	Sakura Finetek; USA
TissueTek O.C.T.™	Sakura Finetek; USA
Tourniquet Stripp-Quick	KaWe Medizintechnik; Germany
Vasofix® Braunüle (G20, G22)	Braun; Germany

2.3. Drugs

Aspirin® 100 mg, (acetylsalicylic acid)	Bayer AG; Germany
Azaporc® 40 mg/ml, (azaperone)	Serumwerk BernburgAG; Germany
CellCept® 1 g/5 ml (mycophenolate mofetil)	Roche; Switzerland
Enerlyte® Plus	Virbac; France
Fentadon® 50 µg/ml (fentanyl)	Dechra; UK
Heparin-Natrium® 5,000 IU/ml (heparin)	Braun; Germany
Ketamidor® 100 mg/ml (ketamine)	WDT; Germany
Lantus® 100 IU/ml (long-acting insulin analog)	Sanofi; France
Metacam® 20 mg/ml (meloxicam)	Boehringer Ingelheim; Germany
Morphasol® 4 mg/ml (butorphanol)	Livisto; Germany
Narcoren®16 g/100 ml (pentobarbital)	Boehringer Ingelheim; Germany
NaCl 0.9% (physiological saline solution)	Braun; Germany
Novorapid® 100 IU/ml (short-acting insulin analog)	NovoNordisk; Denmark
Perenterol® forte 250 mg	Medice; Germany
Prograf® 5 mg (tacrolimus)	Astellas Pharma GmbH; Germany
Rompun® 2% (xylazine)	Bayer AG; Germany
Sevorane® 100% (sevoflurane)	Abbvie; USA
Stresnil® 40 mg/ml, (azaperone)	Elanco; USA
Ursotamin® 100 mg/ml (ketamine)	Serumwerk Bernburg AG; Germany

2.4. Chemicals and reagents

Acetic (glacial) acid, 100%	Carl Roth; Germany
Caustic soda (2N) (NaOH)	Carl Roth; Germany
Chloroform, 100%	Merck; Germany
Collagenase V #C9263	Sigma-Aldrich; USA

4’,6-diamidino-2-phenylindole (DAPI)	Biotium; USA
Disodium hydrogen phosphate (Na_2HPO_4), water free	Carl Roth; Germany
Eosin, 2%	Morphisto; Germany
Ethanol denatured, >99.8% (EtOH)	Carl Roth; Germany
Ethylenediaminetetraacetic acid (EDTA)	VWR; USA
Giemsa stock solution	Sigma-Aldrich; USA
Hematoxylin	Morphisto; Germany
Histokitt	Hecht Assistant®; Austria
Hydrochloric acid 25% (HCl)	Carl Roth; Germany
Hydrogen peroxide 35% (H_2O_2)	Carl Roth; Germany
Kernechtrot 0.1%	Morphisto; Germany
Methanol, 100%	Carl Roth; Germany
Meyer’s Hemalum	Sigma-Aldrich; USA
Natrium chloride (NaCl)	Carl Roth; Germany
Neutral serum	Biozol; Germany
Paraformaldehyde	Carl Roth; Germany
Potassium chloride (KCl)	Merck; USA
Potassium dihydrogen phosphate (KH_2PO_4)	Carl Roth; Germany
Proteinase K	Dako; Denmark
RNAlater™ solution	Invitrogen; USA
Tris ($C_4H_{11}NO_3$)	Carl Roth; Germany
Tri-sodium citrate dihydrate ($C_6H_5Na_3O_7$)	Carl Roth; Germany
Triton X100	Carl Roth; Germany
Tween®20	Carl Roth; Germany
Xylol	VWR; USA

2.5. Kits

Avidin/Biotin Blocking Kit	Vector Laboratories Inc.; USA
Avidin-Biotin Complex (ABC)	Vector Laboratories Inc.; USA
BCIP/NBT Substrate (AP)	Vector Laboratories Inc.; USA
3,3'-diaminobenzidine (DAB) Substrate Kit (HRP), with Nickel	Vector Laboratories Inc.; USA
ImmPACT® DAB Substrate Kit (HRP)	Vector Laboratories Inc.; USA
True View® Autofluorescence Quenching	Vector Laboratories Inc.; USA
Vectashield Vibrance®	Vector Laboratories Inc.; USA

2.6. Buffers, media and solutions

2.6.1. Pancreas procurement and NPI culture

Transport solution pancreas

25 ml HTK (Custodol®)	Dr. Franz Köhler Chemie GmbH; Germany
250 µl 1x penicillin/streptomycin #15140-122	Gibco, Thermo Fisher Scientific; USA
250 µl 1x amphotericin #15290-026	Gibco,Thermo Fisher Scientific; USA

Recovery medium of NPI culture (day 0, 1 and 2 of culture)

1:1 mixture of Ham's F12 and medium 199 #N6658 and #M4530	Sigma-Aldrich; USA
0.5% BSA #A9418	Sigma-Aldrich; USA
10 mmol/l glucose #G7021	Sigma-Aldrich; USA
10 mmol/l L-glutamine #G8540	Sigma-Aldrich; USA

10 mmol/l HEPES #15630-056	Gibco, Thermo Fisher Scientific; USA
10 mmol/l nicotinamide #N0636	Sigma-Aldrich; USA
0.062% glutathione #G6013	Sigma-Aldrich; USA
1x penicillin/streptomycin #15140-122	Gibco, Thermo Fisher Scientific; USA
1x amphotericin #15290-026	Gibco, Thermo Fisher Scientific; USA
25 U/ml heparin #H3149	Sigma-Aldrich; USA
0.5 mmol/l Pefabloc #0031682.02	Serva; Germany
100 KIU aprotinin #A3428	Sigma-Aldrich; USA
10 µmol/l Trolox™ #238813	Sigma-Aldrich; USA
1x BME vitamins #B6891	Sigma-Aldrich; USA
15.2 µmol/l zinc sulphate #Z0251	Sigma-Aldrich; USA
1 µmol/l Victoza® 6mg/ml (liraglutide)	Novo Nordisk; Denmark
1x ITS supplement #41400-045	Invitrogen; USA

Maturation medium of NPI culture (day 3 of culture onwards)

Ham's F10 #N6908	Sigma-Aldrich; USA
0.5% BSA #A9418	Sigma-Aldrich; USA
10 mmol/l glucose #G7021	Sigma-Aldrich; USA
10 mmol/l L-glutamine #G8540	Sigma-Aldrich; USA
10 µmol/l IBMX #I5879	Sigma-Aldrich; USA
10 mmol/l nicotinamide #N0636	Sigma-Aldrich; USA
1x penicillin/streptomycin #15140-122	Gibco, Thermo Fisher Scientific; USA
1.6 mmol/l CaCl2 #C7902	Sigma-Aldrich; USA
1 µmol/l Victoza® 6mg/ml (liraglutide)	Novo Nordisk; Denmark

1 µmol/l T3 analog #5552	Tocris; UK
50 nmol/l retinoic acid #0695	Tocris; UK

Transplantation medium

CMRL-1066 #P04-84600	PAN Biotech; Germany
0.5% Alburex®20 (human albumin)	CSL Behring; Germany
70 U/kg Heparin-Natrium 5.000 I.E./ml	Braun; Germany

2.6.2. Fixatives, histology, immunohistochemistry, immunofluorescence

Modified Carnoy fixative (Methacarn)

100 ml acetic acid (100%)
300 ml chloroform
600 ml methanol

Store dark at 4°C, use within one week.

PBS-buffered 4% Paraformaldehyde (PFA), pH 7.4:

40 g Paraformaldehyde
100 ml 10x PBS
950 ml Aqua bidistilled (bidist).
200 µl 5 M NaOH

Mix and solve at 50°C in water bath. Adjust pH to 7.4. Add Aqua bidist. to 1 l.
Store at 4°C.

Phosphate buffer A for Giemsa staining:

3.61 g KH_2PO_4
1000 ml Aqua bidist.

Store at 4°C.

Phosphate buffer B for Giemsa staining:

3.55 g Na_2HPO_4, water free

250 ml Aqua bidist.

Store at 4°C.

Giemsa-working-solution:

390 ml phosphate buffer A

10 ml phosphate buffer B

28 ml Giemsa stock solution

Mix buffer A and B and heat to 70-80°C before adding Giemsa stock solution.

Adjust pH to 5.0 and filter before use.

Citrate-0.5% Tween®20 buffer (CITRAT), pH 6.0 for immunohistochemistry/ immunofluorescence

2.94 g Tri-sodium citrate dihydrate

0.5 ml Tween®20

950 ml Aqua bidist.

HCl for adjusting pH to 6.0

Add Aqua bidist. to 1000 ml.

Tris-EDTA-0.5% Tween®20 buffer, pH 9.0 for immunohistochemistry (TRIS)

1.21 g Tris

2 ml 0.5 M EDTA (pH 8.0)

0.5 ml Tween®20

HCl for adjusting pH to 9.0

Add Aqua bidist. to 1000 ml.

10x Phosphate-buffered salt solution (PBS), pH 7.4

79.5 g NaCl

14.4 g Na_2HPO_4 (*2 H_2O)

2.0 g KCl

2.0 g KH_2PO_4

Mixed in 2,000 ml Aqua bidist.

Working-solution: stock solution was diluted 1:10 with Aqua bidist.

10x Tris-buffered salt solution (TBS), pH 7.6

83.33 g NaCl

60.57 g Tris

1 l Aqua bidist.

HCl for adjusting pH to 7.6

Working-solution: stock solution was diluted 1:10 with Aqua bidist.

2.7. Antibodies

Immunohistochemistry primary antibodies	
Mouse-anti-human-CD3 mAb #M725401-02	Dako; Denmark
Mouse-anti-CD45 mAb #60287-1-Ig	Proteintech; USA
Mouse-anti-human-Macrophages mAb #MCA874GA	Bio-Rad Laboratories; USA
Mouse-anti-Insulin mAb #I2018	Sigma-Aldrich; USA
Rabbit-anti-Glucagon polyclonal antibody (pAb) #15954-1-AP	Proteintech; USA
Rabbit-anti-Synaptophysin pAb #17785-1-AP	Proteintech; USA
Rat-anti-FoxP3 mAb #14-5773-82	Thermo Fisher Scientific; USA
Immunofluorescence primary antibodies	
Alexa Fluor™ 488-anti-Insulin mAb #53-5769-82	Invitrogen; USA
Guinea pig-anti-Glucagon pAb #M182	Takara Bio; Japan
Mouse-anti-Somatostatin mAb #sc-55565	Santa Cruz Biotechnology; USA
Rabbit-anti-Synaptophysin pAb #17785-1-A	Proteintech; USA
Immunohistochemistry secondary antibodies	
Biotinylated donkey-anti-rat IgG (H+L) pAb #712-065-153	Jackson ImmunoResearch; USA

Biotinylated goat-anti-mouse IgG (H+L) pAb #115-065-146	Jackson ImmunoResearch; USA
Goat-anti-mouse-IgG/HRP pAb #PO447	Dako; Denmark
Goat-anti-rabbit IgG/HRP pAb #PO448	Dako; Denmark
Immunofluorescence secondary antibodies	
AlexaFluor™ 555 donkey-anti-mouse IgG (H+L) pAb #A32773	Thermo Fisher Scientific; USA
AlexaFluor™ F647 donkey-anti-guinea pig IgG (H+L) pAb #706-605-148	Jackson ImmunoResearch; USA
DyLight755 donkey-anti-rabbit IgG (H+L) pAb #SA5-10043	Thermo Fisher Scientific; USA

2.8. Software

CellSens Dimension	Olympus; Japan
ChatGPT 3.5 (used for translation & grammar check)	Open AI; USA
DeepL version 24.1.2756848	DeepL GmbH; Germany
Leica Application Suite V4.12.0	Leica Microsystems; Switzerland
GraphPad Prism 5, 10	Graphpad Software; USA
Microsoft Office version 16.82	Microsoft Corporation; USA
PMOD version 4.005	PMOD Technologies GmbH; Switzerland
PROC MIXED SAS 9.4	SAS Institute; USA
QuPath-0.4.2	The University of Edinburgh; Scotland

3. Methods

3.1. Preparation of the islet graft

NPIs were used as islet transplant. Preparation procedure of the islet graft included pancreas procurement, NPI isolation and NPI *in vitro* maturation and started 6-7 days before ITx.

Pancreas donor animals were anaesthetized by intramuscular (i.m.) injection of azaperone (0.05 ml/kg BW; Azaporc® 40 mg/ml; Serumwerk Bernburg AG) and ketamine (0.2 ml/kg BW; Ursotamin® 100mg/ml; Serumwerk Bernburg AG). Analgesia was performed with i.m. administration of fentanyl (0.5 ml/10 kg; Fentadon® 50µg/ml; Dechra). The death was caused by exsanguation, to avoid detrimental impact of erythrocyte containing islets. Pancreas procurement was performed *post mortem* within ten minutes (warm ischemia time) under sterile conditions. Then, the organ was transferred immediately to cold HTK transport solution at 4°C. Cold ischemia time was three hours in maximum.
After mechanical shredding of the pancreas with scissors, tissue cell clusters were isolated by enzymatic pancreas digestion using collagenase-V (Sigma-Aldrich) and sieved trough a 500 µm mesh. After subsequent washing steps, isolates were then cultured for three days in recovery medium with full medium change at culture day one. From culture day three onwards, NPIs were cultured in maturation medium, with full medium change at day three, followed by half medium change every second day (KEMTER et al., 2017). NPI isolations and culture were carried out by Ms. Christina Blechinger and Ms. Florentine Stotz. At culture day six or seven, *in vitro* matured NPIs were used for allogeneic ITx. Shortly before the ITx, NPIs were transferred into islet transplantation medium. From there, a representative aliquot was taken to determine the total IEQ yield. The determination of IEQ yield was carried out by Mr. Martin Kraetzl.

3.2. Percutaneous intraportal pancreatic islet transplantation

ITx was carried out by PIPIT procedure as previously described elsewhere (VENTURINI et al., 2018) by Dr. Daniel Puhr-Westerheide from the Department of Radiology, LMU Munich, University Hospital.

3.2.1. Anesthesia and transplantation procedure

Following a 12-hour preoperative food abstinence, anesthesia of the ITx recipient pig was induced by i.m. injection of azaperone (0.05 ml/kg BW; Stresnil®; Elanco Animal Health) and ketamine (0.2 ml/kg BW; Ketamidor®; WDT) in the pig stable housing box. On the anesthetized animal a venous catheter (Vasofix® Braunüle (G20, G22); Braun) was placed in one of the ear veins for intravenous administration of medication. Anesthesia was deepened as needed with a mixture of ketamine and xylazine (3 ml xylazine (Rompun® 2%; Bayer Vital GmbH) + 7 ml ketamine). After being transferred to the animal surgery room, the pig was placed on a heating mat (Thermal Pet Pad Thermal MHP-E1220; Anpan) and connected to devices for monitoring anesthesia (SC 9000XL patient monitor; Siemens). Inhalation anesthesia with sevoflurane (1-2%; Sevorane®; Abbvie), provided by Servo Ventilator 900C (Siemens-Elema), was used to maintain anesthesia and was delivered via an endotracheal tube (3.0 – 4.5; Henry Schein Inc.) or alternatively, via an inhalation mask. The animal was connected to volume-controlled mechanical ventilation. During the entire procedure the animal was supplied with physiological saline solution (NaCl 0.9%; Braun) via an intravenous continuous drip for volume replenishment and the following parameters were continuously measured: ECG, O_2 saturation, respiratory rate, body temperature and, especially in diabetic animals, blood glucose.

The operating field was prepared with antiseptic solution (Braunol®; Braun) and covered with sterile drapes (Foliodrape®; Hartmann Group). First, the portal vein was visualized with ultrasound (MyLab™ X8VET; Esaote) and the right portal vein branch was percutaneously accessed under ultrasound guidance (transhepatic access) after a small skin incision (scalpel no. 11; Feather®) with a Neff Percutaneous Access Set (COOK® Medical) **(Fig. 10a)**. The access of the portal vein was confirmed by aspiration of blood and subsequent contrast agent

administration (approximately 3 ml; Imeron® 300M; Bracco) **(Fig. 10b)**. After placing a guide wire (EV3 Nitrex, diameter 0,018 inch; Medical ecart) into the portal vein under X-ray control (Ziehm vision mobile C-arm; Ziehm imaging) **(Fig. 10c)**, the Neff Set Sheath was advanced into the portal vein and the wire was exchanged to a 0,035 inch wire (Glidewire® 180cm; Terumo). Subsequently, a Cobra (C2) 4F catheter (65cm; Cordis) or the Neff set sheath was advanced **(Fig. 10d)** into the left main portal vein branch (or in the main portal vein) under fluoroscopy control, followed by an X-ray angiographic position control with a contrast agent run (approximately 10 ml; Imeron® 300M; Bracco) **(Fig. 10e**). The NPIs were slowly injected with a 20 ml syringe (Braun) over a period of around 20 minutes into a portal vein branch of the left liver lobe in all animals except one **(Fig. 10f).** In animal #13062, the islets were administered in the main branch of the portal vein. After NPI administration, the catheter was retracted and the puncture channel was closed with gelfoam sludge (Spongostan®; Ferrosan Medical devices; mixed with saline). An ultrasound and Doppler ultrasound were performed to visualize the intraportal islet graft, to rule out bleeding and to confirm the patency of the portal vein.

After completion of ITx, inhalation anesthesia was terminated and the pig was monitored during the recovery phase.

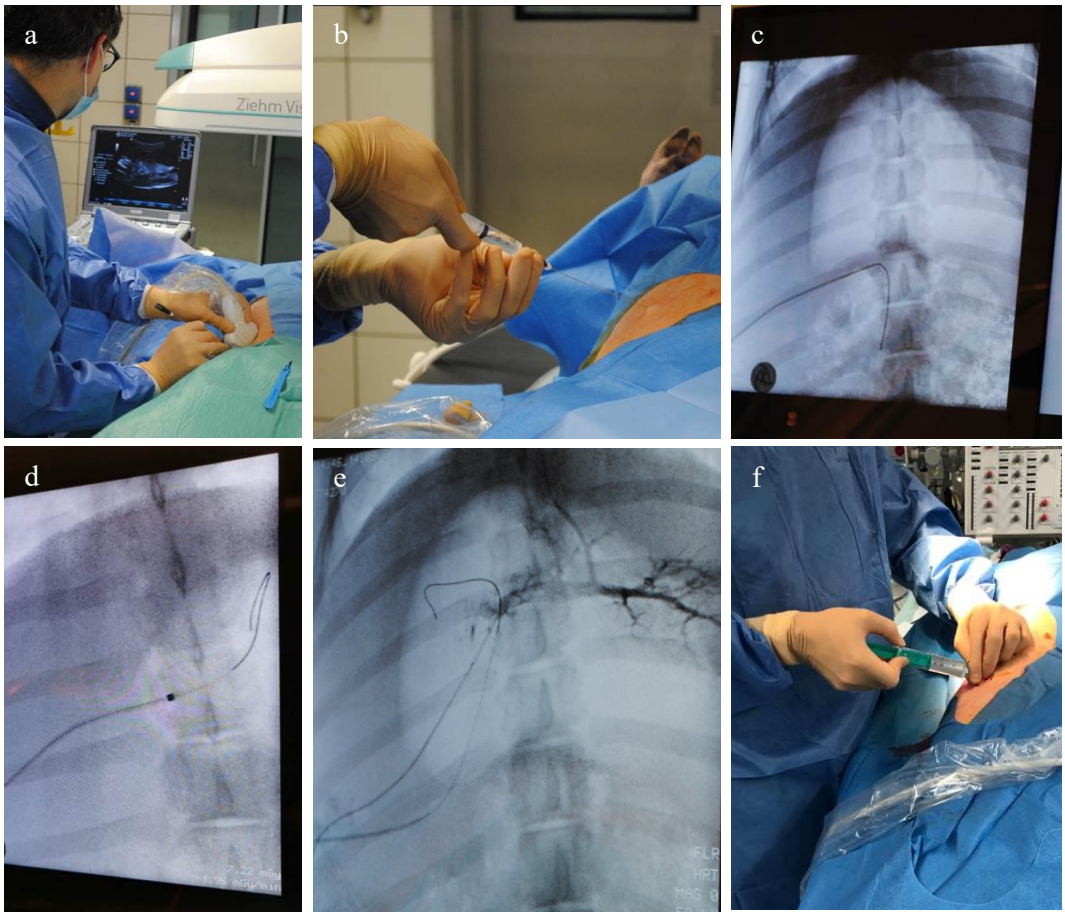

Figure 10: *Procedural steps during PIPIT.*

(a) *Ultrasound-guided puncture of the portal vein.* ***(b)*** *Aspiration of blood and administration of contrast agent to control the correct position of the catheter in the portal vein.* ***(c)*** *Advancement of guide wire under X-ray control.* ***(d)*** *Placement of the catheter in the left portal vein branch under fluoroscopy control.* ***(e)*** *X-ray angiographic position control.* ***(f)*** *Injection of islet graft.*

3.2.2. Concomitant drug therapy of the graft recipient pigs

ITx was accompanied by antithrombotic and immunosuppressive treatment. Oral immunosuppression started one day before ITx and consisted of TAC (0.25 mg/kg BW; Prograf® 5 mg; Astellas Pharma GmbH) and MMF (20 mg/kg BW; CellCept® 1g/5 ml; Roche) twice daily, as previously suggested elsewhere (JENSEN-WAERN, KRUSE & LUNDGREN, 2012). Of note, MMF is characterized by its bitter taste. TAC has to be absorbed by the small intestinal tract and can be degraded by the gastric environment. Therefore, it is formulated as a capsule, which should be swallowed directly. Thus, to ensure that the pigs absorbed the required amount of the active substance, the TAC dose was increased by up to 5 mg/day depending on the intake behavior, e.g. if the pigs chewed heavily on the capsules. To increase the oral intake of less palatable immunosuppressants, drugs where administered

together with palatable food, such as banana, based on the individual preferences of each pig. It should be noted that the dosage of immunosuppressants, in particular TAC, refers to the next decade in relation to BW, as finer dosage adjustments were only possible to a limited extent due to the formulation of the oral medication (TAC dosage form: 5mg/capsule). For antithrombotic prophylaxis the pigs received in total four injections of heparin (36 U/kg BW; Heparin-Natrium® 5,000 IU/ml; Braun), thereof one intravenously (i.v.) during PIPIT and three s.c. every 12 hours after PIPIT and additionally a daily dose of acetylsalicylic acid (ASA) (100 mg, Aspirin®; Bayer) orally, starting on transplantation day (Txd) one. Analgesia at PIPIT consisted of preemptive i.v. administration of butorphanol (0.01 ml/kg BW; Morphasol® 4mg/ml; Livisto) and i.m. administration of meloxicam (0.4 mg/kg BW; Metacam® 20 mg/ml; Boehringer Ingelheim). Postoperative analgesia was ensured with two doses of meloxicam (0.4 mg/kg BW; Metacam® 20 mg/ml; Boehringer Ingelheim) at 24-hour intervals. In case of diabetic recipient pigs, exogenous insulin replacement therapy was carried out to lower the FBG levels below 200 mg/dl. A combination of long-acting (Lantus®; Sanofi) and short-acting (Novorapid®; NovoNordisk) insulin analogs (LAIA and SAIA) was used for this purpose, with the dose being adjusted to the measured FBG values. The insulin preparations were administered s.c. (BD Micro-Fine Ultra™ needles, 12,7 mm; Becton Dickinson GmbH). The insulin therapy was started when the FBG values stably exceeded 200 mg/dl.

3.3. Observation period post islet transplantation

During the observation period, the animals underwent daily veterinary assessments and their general condition was recorded. The observation period in the WT group lasted between seven days and 31 days post ITx **(Table 5)**. The objective in this group was mainly to establish transplantation method, drug supply, and sampling procedure. The aim in the MIDY group was the long-term observation of *in vivo* maturation and function of the islet graft and the longitudinal islet graft [^{68}Ga]Ga-DOTA-Exendin-4 PET/CT imaging, so that this observation phase lasted between 71 and 103 days **(Table 5)**. The endpoint of the experiment in the MIDY group was determined based on the achieved results and considering animal welfare aspects,

including the overall health state of the animal. The study design is provided in **Figure 11.**

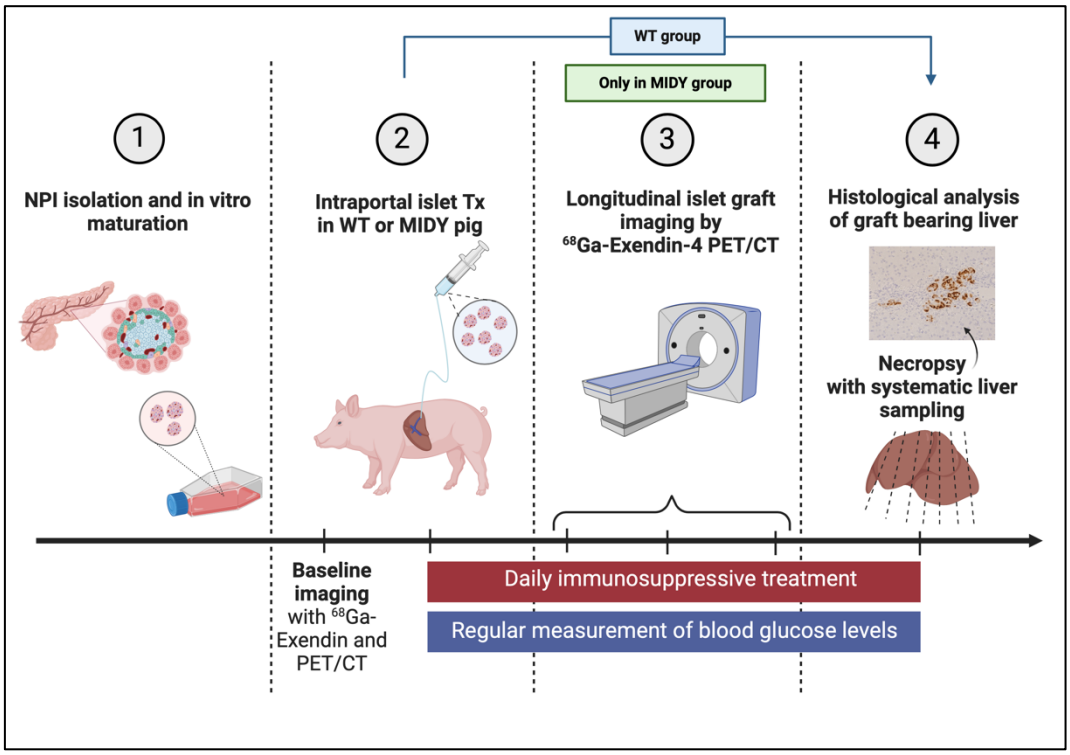

Figure 11: *Study design.*

(1) *Isolation and in vitro maturation of NPIs.* ***(2)*** *Intraportal transplantation of NPIs in WT and MIDY pigs. MIDY pigs underwent a baseline [^{68}Ga]Ga-DOTA-Exendin-4 PET/CT imaging prior to ITx.* ***(3)*** *Only in MIDY pigs: Longitudinal [^{68}Ga]Ga-DOTA-Exendin-4 PET/CT imaging up to three times, accompanied by daily immunosuppressive treatment and regular measurement of blood glucose levels.* ***(4)*** *Necropsy with systematic liver sampling and subsequent detailed histological analysis of graft bearing livers.*

Adapted from Pilz et al., 2024; Created with Biorender.com.

3.3.1. Clinical-chemical analyses of blood samples

In the MIDY group, FBG values were measured on a regular basis in the morning before feeding by puncturing the ear vein with a blood lancet (Solofix®; Braun), using the FreeStyle Freedom Lite system (Abott).

In addition, in WT and MIDY group, TAC levels were regularly examined **(Table 8)** based on EDTA-blood collected in Microvette® 200 EDTA K3E (Sarstedt). To determine TAC blood levels, trough levels are required, which are obtained by taking a blood sample when the TAC level is at its lowest, i.e. immediately before TAC administration (JENSEN-WAERN, KRUSE &

LUNDGREN, 2012). TAC blood concentration analysis was performed by the Institute for Laboratory Medicine, LMU Munich, University Hospital under supervision of Prof. Daniel Teupser. It was only partially possible to determine trough levels, especially when sampling had to be carried out on the awake, non-fixed animal. Nevertheless, non-trough samples were also submitted for analysis to obtain orientation values of TAC levels. Values obtained during the day in general anesthesia were also classified as trough levels since medication was omitted due to pre-anesthetic food abstinence.

In all ITx recipient animals, a clinical blood chemistry profile including liver enzymes, as well as CRP values were determined at several time points after ITx using serum or EDTA samples, collected in S-Monovette® Serum/K3 EDTA (Sarstedt). Clinical blood chemistry analysis was carried out by the Laboratory of the Clinic for Ruminants, LMU Munich. CRP and ALT values were measured by Dr. Birgit Rathkolb from Helmholtz Center Munich. The sampling times were mainly based on the performance of general anesthesia for PET/CT imaging **(Table 8)**.

Animal-ID	Blood sample for TAC measurement (ITx day)	Blood sample for CRP measurement (ITx day)	Blood sample for clinical-chemical blood profile (ITx day)
11821	0, 2, 7	7	2, 7
11822	-	7	7
12401	0, 15, 29	15, 29, 31	0, 15, 31
12580	Baseline, 0, 6, 13, 23, 27, 38, 76, 98, 103	103	0, 38, 76, 98, 103
12582	Baseline, 0, 6, 21	0, 52, 83	0, 52, 77, 83
13062	0, 7, 13, 21, 54, 89, 100	0, 54, 100	0, 100
13064	0, 6, 14, 21, 41, 71	0, 41, 71	0, 41, 71

Table 8: *Timepoints of blood sample collection.*

3.3.2. Longitudinal [^{68}Ga]Ga-DOTA-Exendin-4 PET/CT imaging

Longitudinal [^{68}Ga]Ga-DOTA-Exendin-4 PET/CT imaging in MIDY group was performed once prior to ITx (baseline) and up to three times post ITx. Radiotracer was synthesized as previously described (LINDHEIMER et al., 2023).

The radiotracer synthesis was carried out by Mr. Felix Lindheimer, Department of Nuclear Medicine, LMU Munich, University Hospital.

3.3.2.1. PET/CT imaging procedure

Prior to PET/CT imaging a food abstinence of at least six hours was performed. Anesthesia was induced with azaperone (0.05 ml/kg BW; Stresnil®; Elanco Animal Health) and ketamine (0.2 ml/kg BW; Ketamidor®; WDT) i.m.. Afterwards a catheter was placed in an ear vein of both ears (Vasofix® Braunüle (G20, G22); Braun). One catheter was used for the administration of anesthetic medication, while the other catheter was used for the injection of the radiotracer. A mixture of ketamine and xylazine (3 ml xylazine (Rompun® 2%; Bayer Vital GmbH) + 7 ml ketamine (Ketamidor®;WDT)) was given as needed to deepen the anesthesia. Placed on a heating mat (Thermal Pet Pad Thermal MHP-E1220; Anpan) the animal was connected to an ECG, a pulse oximeter (Veterinary Pulse Oximeter; Henry Schein Inc.) and a continuous drip infusion (NaCl 0.9%; Braun). Heart rate, respiratory rate, oxygen saturation, body temperature and blood glucose were continuously monitored. The radiotracer was injected intravenously (injected activity: 24.66 – 91.37 MBq; amount of peptide: 0.02 ± 0.005 µg/kg). Time interval between synthesis and injection was 34 minutes on average. For image acquisition, a Biograph True-Point 64 PET/CT device (Siemens) was used. The imaging included a dynamic PET scan with the axial field-of-view (21.6 cm) on the region of the liver, followed by a whole-body PET scan (20 min). Dynamic PET acquisition was initiated one minute before tracer injection. List-mode data were acquired over 60 minutes, sorted into 24 frames (11 x 1 min, 10 x 2 min, 3 x 10 min) and reconstructed using the software provided by Siemens: TrueX algorithm with 3 iterations and 21 subsets (voxel size (x, y, z): 2.67, 2.67, 3.0 [mm^3]), including corrections for scattered radiation and attenuation. The reconstructed data were filtered using a Gaussian filter with 5 mm full with at half maximum. For anatomical information and scatter as well as attenuation correction, low-dose CT scans without contrast agent were recorded for the axial field-of-view and whole-body regions. The animals were monitored during the recovery period after anesthesia, during which they were kept in a recovery box. The experimental procedure of PET/CT imaging in pigs is provided in **Figure 12.** The radioactivity

levels of the animals were checked the next day for radiation protection reasons, using CoMo-170/-300M (NuviaTech Instruments).

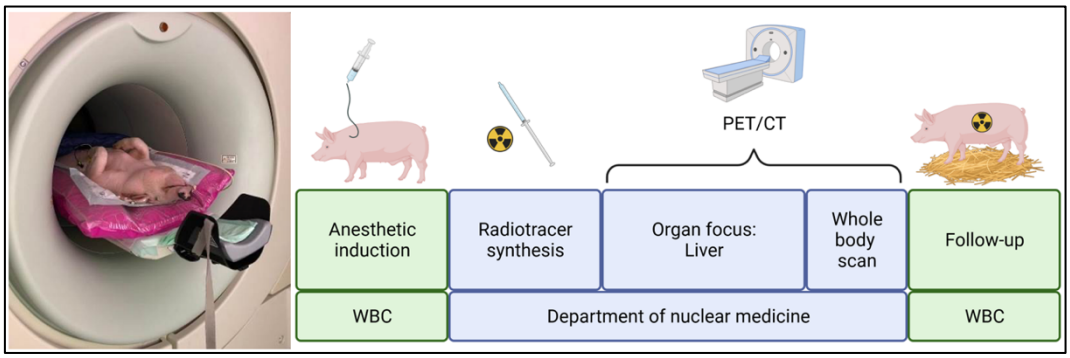

Figure 12: *Experimental procedure of [^{68}Ga]Ga-DOTA-Exendin-4 PET/CT imaging in pigs. WBC: Walter-Brendel-Center. Created with Biorender.com.*

3.3.2.2. [^{68}Ga]Ga-DOTA-Exendin-4 PET/CT image analysis

The analysis of the reconstructed PET/CT data was performed with PMOD software (version 4.005; PMOD Technologies). As measuring unit for activity concentration, the standard uptake value (SUV) was used. To determine this, the activity concentration values were normalized to the injected radioactivity and the BW.

For the baseline scans, a spherical volume of interest (VOI) (∅5mm) was used to measure the dynamic of SUVs in several organs (pancreas, kidney, liver and *longissimus dorsi* muscle) during the PET acquisition for reference and as proof-of-concept. Time-activity curves were created based on the measured SUVs.

Furthermore, whole-liver SUVs were measured in each MIDY pig before ITx (= baseline) and up to three times after ITx. For this purpose, the whole liver was manually plotted as a VOI in each data set **(Fig. 13)**. The whole-liver SUVs refer to the time point 55 minutes after tracer injection.

In addition, a hotspot analysis, as previously suggested elsewhere (JANSEN et al., 2023), was carried out in the manually plotted whole-liver volume. For this purpose, the mean value of the baseline whole-liver SUVs and twice their standard deviation (SD) were added, to determine a threshold value. By implementing this threshold, all liver regions with higher activity values were marked as VOI using the PMOD

iso-contouring function and their SUVs (= hotspot-liver SUVs) were determined at 55 minutes after tracer injection. Hotspot-SUVs were determined analogous to the whole-liver SUVs for each MIDY pig at baseline scan and for each PET/CT scan after ITx. Imaging time points are provided in **Table 9**.

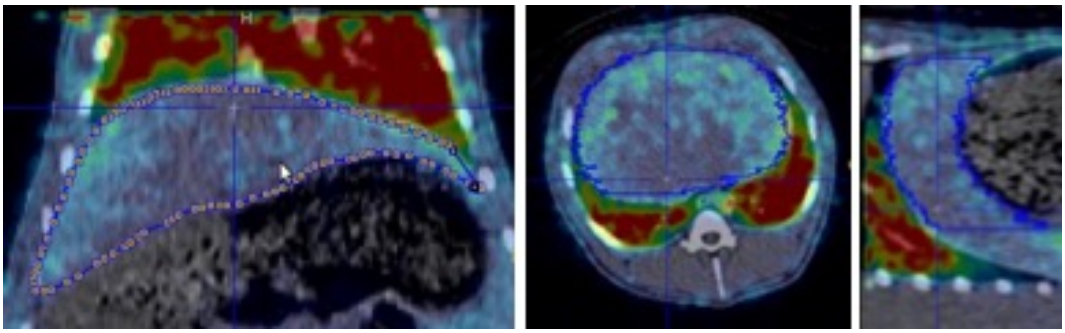

Figure 13: *Example of whole-liver VOI in coronal, axial and sagittal PET/CT images.*

Animal ID	Imaging timepoints (ITx days)
12580	Baseline, 38, 76, 98
12582	Baseline, 52, 77
13062	Baseline, 54, 89
13064	Baseline, 41, 71

Table 9: *Imaging time points of ITx MIDY pigs.*

3.4. Necropsy, sampling procedure and tissue processing

At the end of the observation period, in MIDY group within one week after the last PET/CT scan, the anaesthetized pigs were euthanized by an intravenous injection of pentobarbital (60 mg/kg; Narcoren®; Boehringer Ingelheim). Afterwards, the abdominal cavity was opened with a medial laparotomy and organ removal took place with special focus on the liver as graft bearing organ. Tissue sampling of the liver was performed according to a detailed sampling protocol. The liver sampling procedure was documented in a liver graph **(Fig. 14A)** (COURT et al., 2003). Before further processing, the liver was photographed from the cranial and caudal sides and for better orientation labeled with number tags according to liver sections (I-VIII) **(Fig. 14B)**.

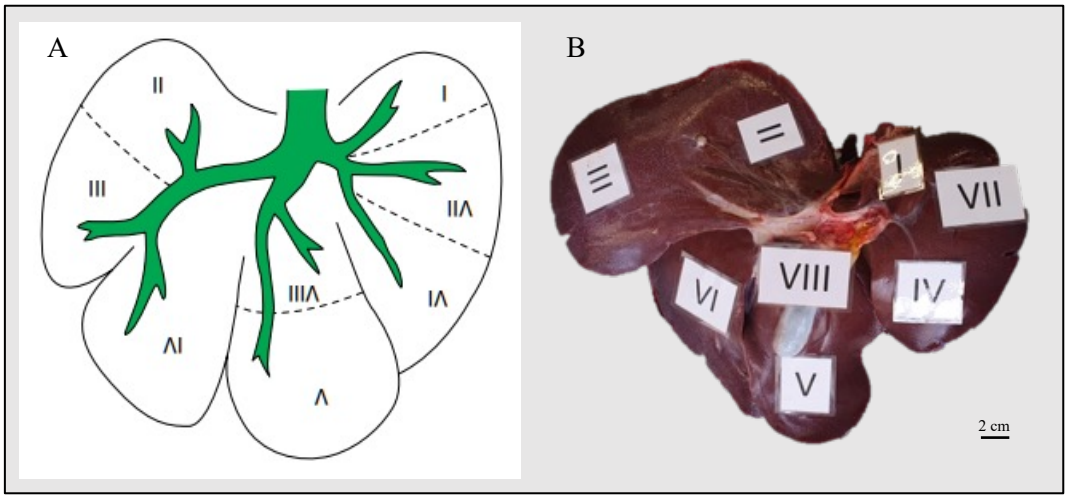

Figure 14: *Anatomical classification of the liver segments.*

(A) *Liver documentation graph according to Court et al., 2003.* ***(B)*** *Liver segments labelled according to liver documentation graph, MIDY pig #12582.*

Liver sampling was carried out according to the following scheme **(Fig. 15)**:

1. Starting at the left side of the liver, parallel, equivalent slices (thickness: ~ 2-3 cm) were cut from the organ from liver base to liver edge, numbered 1 to e.g. 17 (depending on the size of the organ).
2. The parallel slices were then cut into small pieces (size: ~ 2 cm x 2 cm x 1 cm), numbered a to e.g. f (depending on the size of the slice) starting from the base moving forward to the edge.
3. For every letter, e.g. “a”, one piece was taken for 4% PFA, methacarn and RNAlater® (Invitrogen) fixation, one piece was snap-frozen on dry ice and one piece was snap-frozen in Tissue-Tek® Cryomold (Sakura). The same order of fixation methods was applied to each piece.
4. At regular intervals, depending on the size of the organ, reserve strips were taken for 4% PFA fixation, e.g., every third strip.

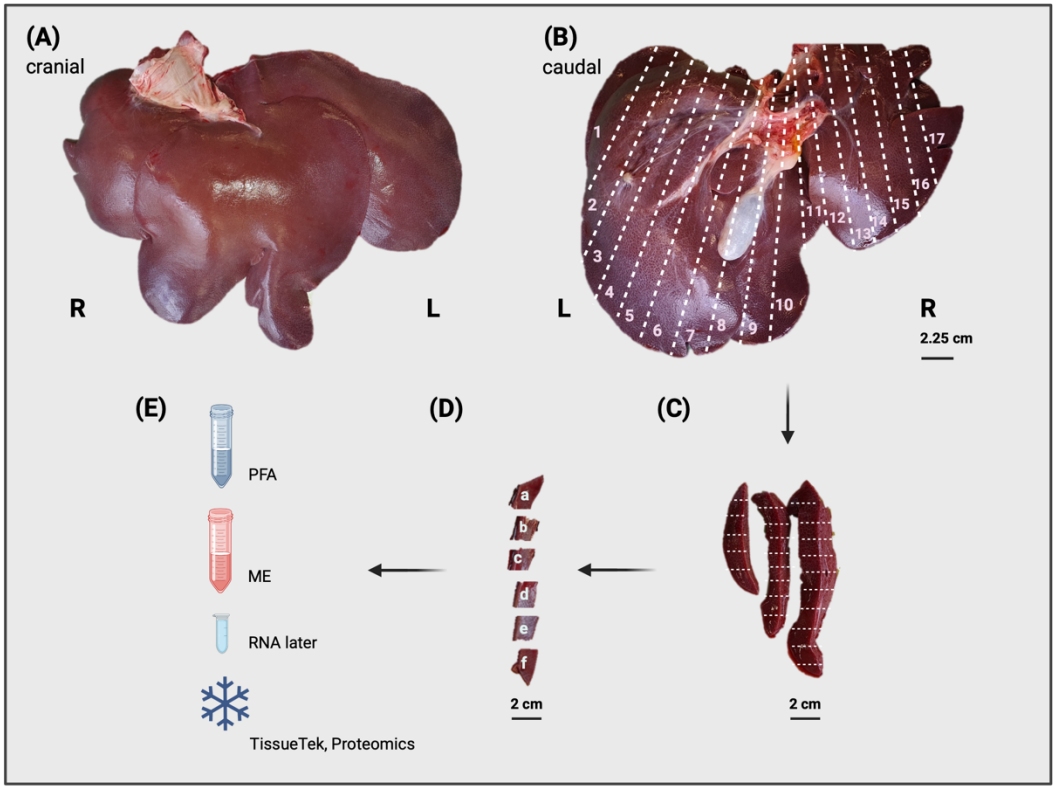

Figure 15: *Liver sampling procedure.*

(A) *Cranial view of the liver of MIDY pig #12582.* ***(B)*** *Caudal view of the liver of MIDY pig #12582.* ***(C)*** *Production of longitudinal strips labeled e.g. "1-17".* ***(D)*** *Subdivision into pieces labeled e.g. "a-f".* ***(E)*** *Preservation in various fixative solutions or as frozen samples.*

From Pilz et al., 2024.

In addition, samples were also taken from the pancreas, the heart, the lungs, the spleen and the kidneys. The tissue was preserved depending on the organ in the following solutions: 4% PFA, methacarn, and RNAlater® (Invitrogen). Furthermore, some tissue was frozen either directly on dry ice or in TissueTek® Cryomold (Sakura). Following the necropsy, the tissue remained for two hours in fixative solutions for initial fixation. Afterwards, it was cut into pieces (approximately 1.5 cm x 2 cm x 0.5 cm), that were put into labelled embedding cassettes (UniLink; Engelbrecht Medizin- & Labortechnik) which were then returned to new fixation solution at 4°C. Dry ice and TissueTek® samples were immediately stored at -80°C.

After 48 hour fixation in PFA and ME at 4°C, the fixed samples were prepared for paraffin-embedding. For this purpose, PFA-fixed samples were washed with tap water and ME-fixed samples with 70% Ethanol. Then they were further processed in the Excelsior AS A82310100 (Thermo Fisher Scientific) **(Table 10)**.

Reagent Group	Reagent	Time
Dehydrant Group	EtOH 70%	2x 1.5 h
	EtOH 90%	1.5 h
	EtOH 90%	1 h
	EtOH 100%	2x 1 h
Clearent Group	Xylol	3x 1 h
Infiltration Group	Paraffin	2x 1.75 h
	Paraffin	2 h

Table 10: *Worksteps of Excelsior AS A82310100.*

Adapted from (HORNASCHEWITZ, 2023).

Subsequently, paraffin (Histoplast PE; Epredia) embedding was performed with the TES 99 modular paraffin embedding system (Medite). 3 µm slices of the paraffin-embedded tissue were cut, using Microm HM 325 rotary microtome (Thermo Fisher Scientific). The slices were collected with microscope slides (StarFrost®; Engelbrecht) and stored at an incubator (ED056-230V; Binder GmbH) at 37°C. Cutting was carried out by Ms. Florentine Stotz and Ms. Christina Blechinger.

3.5. Histological and immunohistological analyses

Detailed histological examination of the islet graft-recipient organ liver were performed, including hematoxylin & eosin (H&E) **(Table 11)** and Giemsa staining **(Table 12)**, as well as immunohistochemistry (IHC) **(Table 13-15)** and immunofluorescence (IF) **(Table 16)**.

3.5.1. H&E staining

Procedure	Reagent	Time
Deparaffination	Xylol	20 min
Rehydration	100% EtOH 2x 96% EtOH 2x 70% EtOH	2 min (30 sec first cuvette, 90 sec second cuvette)
Washing	Aqua bidist.	10 sec
Staining	Hematoxylin	5 min
Washing	Tap water (floating)	5 min
Differentiation	0.5% HCl-EtOH	2 sec
Washing	Tap water (floating)	5 min
Counterstaining	2% Eosin	2 min
Washing	Aqua bidist.	10 sec
Dehydration	70% EtOH 96% EtOH 2x 100% EtOH 2x	2 min (30 sec first cuvette, 90 sec second cuvette)
Clearing	Xylol	Min. 5 min
Mounting	Histokitt	

Table 11: *Protocol for H&E staining.*

Adapted from Hornaschewitz, 2023.

3.5.2. Giemsa staining

Procedure	Reagent	Time
Deparaffination	Xylol	10 min
Rehydration	100% EtOH 2x 96% EtOH 2x 70% EtOH	2 min (30 sec first cuvette, 90 sec cuvette)
Washing	Aqua bidist.	10 sec
Staining	Giemsa working-solution	1 h at 65°C
Washing	Aqua bidist.	10 sec
Differentiation	0.5% acetic acid	1 sec (till color change)
Dehydration	96% EtOH 2x 100% EtOH 2x	2 min (30 sec first cuvette 90 sec second cuvette)
Clearing	Xylol	≥ 5 min
Mounting	Histokitt	

Table 12: *Protocol for Giemsa staining.*

3.5.3. Immunohistochemistry

Procedure	Reagent	Time
Deparaffination	Xylol 2x	2x 20 min
Rehydration	100% EtOH 2x 96% EtOH 2x 70% EtOH	10 sec each
Washing	Aqua bidist.	10 sec
Antigen retrieval	Heat-induced antigen retrieval (HIAR): TRIS or CITRAT buffer	TRIS: 18 min sub-boiling; CITRAT: 15 min sub-boiling
	Enzymatic antigen retrieval: Proteinase K	10 min
Cooling	Only after HIAR	30 min
Washing	1x TBS	10 min
Blocking	1% H_20_2 in 1x TBS	15 min
Washing	1x TBS	10 min
Biotin blocking (only liver tissue)	Avidin	15 min
	1x TBS	10 min
	Biotin	15 min
	1x TBS	10 min
Blocking	5% Neutral serum (NS) in 1x TBS	1 h at room temperature (RT)
Primary antibody	Antibody in 1x TBS	Overnight at 4°C
Washing	1x TBS	10 min
Secondary antibody	Antibody in 1x TBS	1 h at RT
Washing	1x TBS	10 min
Signal amplification	Avidin-biotin-complex (only when biotinylated secondary antibody is used) 1:100	30 min
Washing	1x TBS	10 min
Staining	DAB	Depending on antibody reactivity
Washing	Floating tap water	5 min
Counterstaining	Meyer's Hemalum	~ 30 sec
Washing	Floating tap water	5 min
Washing	Aqua bidist.	10 sec
Dehydration	70% EtOH 96% EtOH 2x 100% EtOH 2x	10 sec
Clearing	Xylol	≥ 5 min
Mounting	Histokitt	

Table 13: *Immunohistochemistry basic protocol.*

Primary antibody	Secondary antibody	Antigen retrieval	Neutral serum
Rabbit-anti-Synaptophysin 1:6,000	Goat anti-rabbit IgG/HRP 1:150	TRIS	Goat
Mouse-anti-Insulin 1:3,000	Biotinylated goat anti-mouse IgG 1:250 + 2% NS Pig	CITRAT	Goat
Rabbit-anti-Glucagon 1:12,000	Goat anti-rabbit IgG/HRP 1:150	CITRAT	Goat
Mouse-anti-human-Macrophages 1:200	Biotinylated goat anti-mouse IgG 1:250 + 2% NS Pig	Proteinase K	Goat
Mouse-anti-human-CD3 1:900	Biotinylated goat anti-mouse IgG 1:250 + 2% NS Pig	TRIS	Goat
Rat-anti-FoxP3 1:150	Biotinylated donkey anti-rat IgG 1:150	CITRAT	Donkey
Mouse-anti-CD45 1:1,200	Goat-anti-mouse-IgG/HRP 1:100 + 2% NS Pig	TRIS	Goat

Table 14: *Adaptions of basic IHC protocol to individual antibodies.*

1st antibody	2nd antibody	HIAR	NS	Staining	Counterstaining
Rabbit-anti-Synaptophysin 1:6,000	Goat-anti-rabbit IgG/AP 1:300	TRIS	Goat	BCIP	Kernecht-Rot
Mouse-anti-human-CD3 1:1,200	Goat-anti-mouse-IgG/HRP 1:100 + 2% NS pig			DAB	

Table 15: *Adaptions of basic IHC protocol for immunohistochemical co-staining of synaptophysin and CD3.*

3.5.4. Immunofluorescence

Procedure	Reagent	Time
Deparaffination	Xylol 2x	2x 20 min
Rehydration	100% EtOH 2x 96% EtOH 2x 70% EtOH	10 sec each
Washing	Aqua bidist.	10 sec
Antigen retrieval	HIAR: CITRAT buffer	15 min
Cooling		30 min
Washing	1x PBS	10 min
Washing	PBS-Triton X100 0.1%	10 min
Washing	1x PBS	5 min
Blocking	5% NS donkey in PBS- Tween®20 0.05%	1 h at RT
Primary antibody in 1x PBS	Guinea pig-anti-Glucagon 1:3,000 Rabbit-anti-Synaptophysin 1:4,000 Mouse-anti-Somatostatin 1:400	Overnight at 4°C
Washing	1x PBS-Tween®20 0.1%	2x 5min
Washing	1x PBS	5 min
Secondary antibody in 1x PBS	AF647 donkey-anti-guinea pig IgG 1:500 DyLight755 donkey-anti-rabbit IgG 1:1,200 AF555 donkey-anti-mouse IgG 1:1,000	1 h at RT
Washing	1x PBS-Tween®20 0.1%	2x 5 min
Washing	1x PBS	5 min
Antibody in 1x PBS	AF 488-anti-Insulin 1:350	2 h at RT
Washing	1x PBS-Tween®20 0.1%	2x 5 min
Washing	1x PBS	2x 5 min
Nuclear staining	DAPI	10 min
Washing	1x PBS	3x 5 min
Suppression of autofluorescence	Vector TrueView	5 min
Washing	1x PBS	2x 5 min
Mounting	Vectashield Vibrance + IF coverslip	

Table 16: *4-color IF staining protocol.*

3.6. Microscopic evaluation of ITx livers

Microscopic analyses and image acquisition of the stained livers were carried out with Leica type DMC4500 and Olympus model BX43F microscope, using Leica Application Suite V4.12.0 and Olympus CellSens Software, respectively. For IF, image acquisition was performed with Axioscan 7 device (Zeiss) and 20x objective by the Core Facility Pathology & Tissue Analytics at the Helmholtz Center Munich. The IHC slides stained for macrophages were scanned using the NanoZoomer S60 (Hammatsu Photonics K. K.) with the 20x objective at the Institute for Veterinary Pathology at the Center for Clinical Veterinary Medicine, LMU Munich by Mrs. Lisa Pichl under the supervision of Prof. Andreas Parzefall.

3.6.1. Analysis of graft localization and graft properties

Islet graft containing liver segments were identified by performance of synaptophysin (SYP) IHC and subsequent microscopic evaluation, which was performed with every PFA liver segment and formed the basis for the selection of liver segments for further histological examinations **(Table 17)**. The proportion of SYP, insulin (INS) and glucagon (GCG) positive (+) liver segments within all liver segments was determined by microscopic evaluation of the immunohistochemically stained liver segments. The occurrence of SYP+ (excluding nerves and neuronal cells), INS+ and GCG + islet cell clusters (ICCs) in every liver segment was graded in four scores (none (0) *vs.* 1-5 ICCs (I) *vs*. 6-15 ICCs (II) *vs.* > 15 ICCs (III) per slide). Representative sections were investigated by 4-color IF staining of SYP, INS, GCG and somatostatin (SST).

Target antigen	Target cell	Analyzed liver segments
Synaptophysin	Neuroendocrine cells	All PFA samples
Insulin	Beta cells	Graft bearing liver segments
Glucagon	Alpha cells	Graft bearing liver segments

Table 17: *Immunohistochemical analyses of graft distribution and function.*

3.6.2. Characterization of immunoreaction in the graft-bearing livers

In order to characterize the cells involved in the post-ITx immune response, a stepwise identification of individual cell types was performed. IHC against CD3 of graft-bearing livers was used to select representative liver segments for further evaluation with a high incidence of graft-infiltrating immune cell clusters **(Table 18)**.

Target antigen	Target cell	Analyzed liver segments
CD3	T cells	Graft bearing liver segments
CD45	Leukocytes	Representative liver segments
Fox P3	Regulatory T cells	Graft bearing liver segments
L1/Calprotectin	Macrophages	Graft bearing liver segments 5 liver segments without islet graft/animal

Table 18: *Immunohistochemical analyses of immunological processes in graft bearing livers.*

Periportal clusters of numerous CD3+ cells were considered as infiltrates. The occurrence of CD3+ cell infiltrates in the graft-containing livers was categorized into four grades (none (-) *vs*. 1-5 infiltrates (+) *vs.* 6-15 infiltrates (++) *vs.* >15 infiltrates (+++) per slide).

3.6.3. Morphometric analysis of macrophage abundance in ITx livers

For morphometric analysis of macrophage abundance in ITx livers, five islet-containing regions and five regions without islet transplant were chosen for each animal. Additionally, five liver sections of control pigs **(Table 7)**, that didn't receive an islet transplant were selected. It should be noted that the terms "macrophages" and "positive cells", which are used in the rest of this work, refer to cell cross-sectional profiles and do not indicate absolute numbers of cells. For identification of macrophages, calprotectin was immunohistochemically detected in the selected livers. The quantitative evaluation was carried out using QuPath software (The University of Edinburgh). First, the whole liver section was marked as the analysis area in the scans using the polygon function and refined by Wand tool. Larger vessel lumina were excluded from the analysis area **(Fig. 16)**. Then, a positive cell detection was performed (for technical details see **Table 19**). By using a triple intensity threshold, a distinction was made between weak, medium and

strong positive cells, based on the mean nucleus DAB optical density (OD). Strongly positive cells with mean OD > 0.6 per mm^2 were used as comparative value.

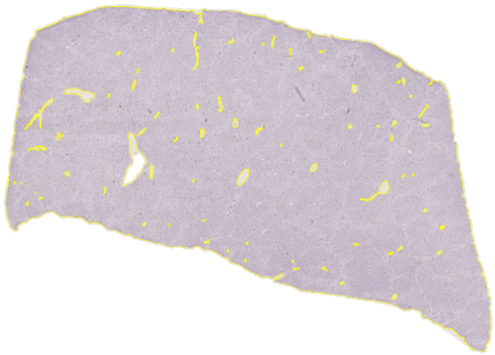

Figure 16: *Example for liver analysis area for positive cell detection.*

Setup parameters	Detection image	Optical density sum
	Requested pixel size	0.4404
Nucleus parameters	Background radius	8 µm
	Median filter radius	0 µm
	Sigma	1.5 µm
	Minimum area	8 μm^2
	Maximum area	100 μm^2
Intensity parameters	Threshold	0.1
	Max background intensity	2
Cell parameters	Cell expansion	0.03
Intensity threshold parameters (score compartment: Nucleus DAB OD mean)	Threshold 1+	0.2
	Threshold 2+	0.4
	Threshold 3+	0.6

Table 19: *Technical settings for QuPath positive cell detection.*

3.7. Graphics and statistical analyses

The graphics were created with Prism 5 and Prism 10 (GraphPad Software). For group plots, the mean and standard error of the mean (SEM) is shown, unless otherwise indicated in the graph.

For statistical analysis of whole-liver SUV and hotspot-liver SUV data PROC MIXED (SAS 9.4; SAS Institute) was used, considering both the effect of time after ITx and the random effect of individual recipient. QuPath results were analyzed with two-tailed Mann-Whitney-U tests. One Mann-Whitney-U test was carried out to compare the control group with the WT group and a second Mann-Whitney-U test was carried out to compare the control group with the MIDY group. Additionally, the islet-containing regions were compared to regions without islet transplant for both the WT group and the MIDY group using the Mann-Whitney U test.

Significance levels were set at $p < 0.05$ (*), $p < 0.01$ (**) and $p < 0.001$ (***).

V. RESULTS

1. Establishment of PIPIT in pigs

Isolation and *in vitro* maturation of the NPIs obtained from 9-15 donor pancreata resulted in an islet yield of 140,000 – 310,000 IEQs per batch **(Table 20)**. The NPIs were round and compact after the *in vitro* maturation period when used for PIPIT **(Fig. 17)**. The amount of transplanted IEQs ranged between 2,979 and 15,000 IEQs/kg BW. The left main branch of the portal vein was targeted as ITx site in order to have the right side of the liver available as a control. PIPIT was successfully performed in all seven pigs, with the transplantation site being the left main branch of the portal vein in six pigs and the main portal vein branch in pig #13062 **(Table 20)**. Evaluation of the liver by ultrasound after islet graft injection confirmed the presence of ICCs in the portal vein **(Fig. 18A)**. No ultrasonographical detectable signs of bleeding were observed. Doppler ultrasound analysis post-PIPIT confirmed the patency of the portal vein and a physiological hepatopetal **(Fig. 18B)**. Pig #11821 experienced anesthesia-induced respiratory depression and delayed awakening. There were no PIPIT-associated complications in the remaining pigs.

Animal ID	Number of donor organs	Islet yield in total [IEQs]	Transplanted IEQs/kg BW	Intraportal catheter position
11821	12	310,000	5,636	left main portal vein branch
11822	9	140,000	5,000	left main portal vein branch
12401	12	140,000	2,979	left main portal vein branch
12580	15	174,000	5,800	left main portal vein branch
12582	12	161,000	3,320	left main portal vein branch
13062	15	238,000	9,714	main portal vein branch
13064	14	300,000	15,000	left main portal vein branch

Table 20: *Number of donor organs, total islet yield, transplanted IEQs/kg BW and transplantation site.*

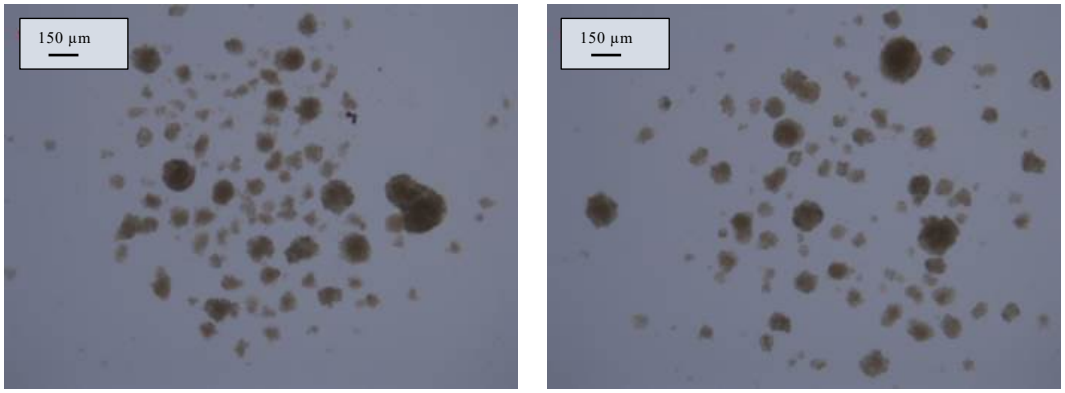

Figure 17: *Two examples of round, compact ICCs after in vitro maturation.*

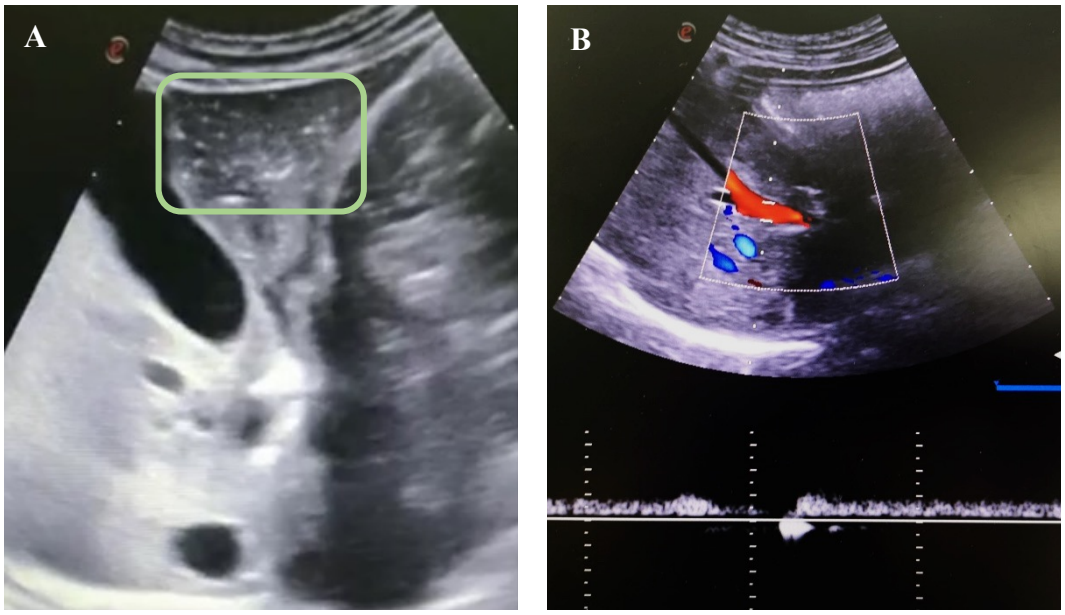

Figure 18: *Ultrasound control directly after ITx.*

(A) *Intravascular hyperechogenic spots confirmed the presence of ICCs in the portal vein system. No signs for bleeding were noted.* ***(B)*** *Doppler ultrasound confirmed the patency of the portal vein and physiological hepatopetal.*

2. Clinical outcome of islet transplantation

2.1. Overview of clinical ITx outcome

Animal ID	Survival (days)	General health state	Acceptance of oral drug intake	Blood parameters	Normo-glycemia achieved	Independence from exogenous insulin	Increase of liver signal in PET/CT imaging	Fate
11821	7	Un-remarkable	TAC and ASA accepted, MMF refused	Elevated AST and GGT value on Txd 2	-/-	-/-	-/-	Reached planned endpoint
11822	7	Un-remarkable	Refused all	Un-remarkable	-/-	-/-	-/-	Reached planned endpoint
12401	31	Un-remarkable	Irregular acceptance of TAC and MMF, ASA accepted	Elevated AST values from Txd 15 onwards	-/-	-/-	-/-	Monitoring period stopped due to rejection of immuno-suppression
12580	103	Intermittent diarrhea from Txd 31 onwards	TAC mostly accepted, MMF irregular, ASA accepted	Elevated TAC trough level and AST value on Txd 103	Yes	Yes	Yes	Monitoring period stopped due to weight loss prior end
12582	83	Intermittent diarrhea from Txd 18 onwards	TAC mostly accepted, MMF irregular, ASA accepted	Elevated GGT and AP values on Txd 0; Increased TAC trough level and AST value on Txd 83	Near-normo-glycemic range	No	Yes	Monitoring period stopped due to weight loss prior end
13062	100	Intermittent diarrhea from Txd 8 onwards	TAC mostly accepted, MMF irregular, ASA accepted	Elevated AP value on Txd 0	Yes	Yes	Yes	Monitoring period stopped due to weight loss prior end
13064	71	Occasional diarrhea, mostly un-remarkable	TAC mostly accepted, MMF irregular, ASA accepted	Elevated AST value on Txd 0; Increased CRP values from Txd 41 onwards	No	No	No	Gastro-intestinal emergency in anesthesia, not related to ITx

Table 21: *Overview of clinical ITx outcome.*

2.2. General health state

In the WT group, there were no effects of ITx on the general health state of the recipient pigs. #11821 and #11822 reached the planned endpoint. In #12401, the trial was terminated due to refusal of immunosuppressants. In the MIDY group, intermittent diarrhea occurred mainly in #12580, #12582 and #13062. The animals

were treated symptomatically with electrolytes (Enerlyte®; Virbac) and probiotics (Perenterol®; Medice) when diarrhea symptoms occurred. The general condition of the animals was undisturbed and the body temperature was constantly in the physiological range. Parasitological and bacteriological examinations remained unremarkable. In #13064, diarrhea symptoms occurred only sporadically. In #12580, #12582 and #13062 the experiments were stopped for animal welfare reasons due to weight loss. #13064 died due to a gastrointestinal emergency unrelated to ITx.

2.3. Immunosuppressive treatment regime and blood tacrolimus levels

For reduction of animal distress, both immunosuppressive drugs, TAC and MMF, as well as ASA were orally administered to the pigs. TAC trough levels of 5-15 ng/ml were targeted, as described elsewhere (JENSEN-WAERN, KRUSE & LUNDGREN, 2012). Measurements of #12580 and #12582 before starting immunosuppressive treatment served as control values and were < 2.5 ng/ml.

Establishment of PIPIT protocol was started with the animals of the WT group. #11822 refused consistently oral intake of both immunosuppressants. Therefore, there was no need to analyze the TAC levels in this animal and no graphs could be generated. #11821 refused MMF intake completely **(Fig. 19A1)** and accepted TAC intake constantly at a dosage of 30 mg/day **(Fig. 19A2)**. Two trough levels were determined for #11821: 4.8 ng/ml on medication day one and 15.4 ng/ml on medication day eight. On medication day two, 4.2 ng/ml was determined as non-trough level ~ 7 hours after administration of TAC. The values of #11821 were therefore largely within the target reference range **(Fig. 19A3)**. #12401 showed an irregular intake of MMF, with the targeted dose being reached on 16/31 (≙ 50%) treatment days **(Fig. 19B1)**. TAC uptake was even more inconsistent with the targeted dosage being reached on ten out of 32 days (≙ 31%) **(Fig. 19B2)**. In #12401, a trough level was measured on medication day one (4.8 ng/ml) and two non-trough values were measured on medication day 16 (8 ng/ml) and 30 (6.4 ng/ml), 7 and 7.5 hours after TAC administration, respectively. The values of #12401 were therefore in the lower reference range and it can be assumed that the lower limit was rather undercut **(Fig. 19B3)**.

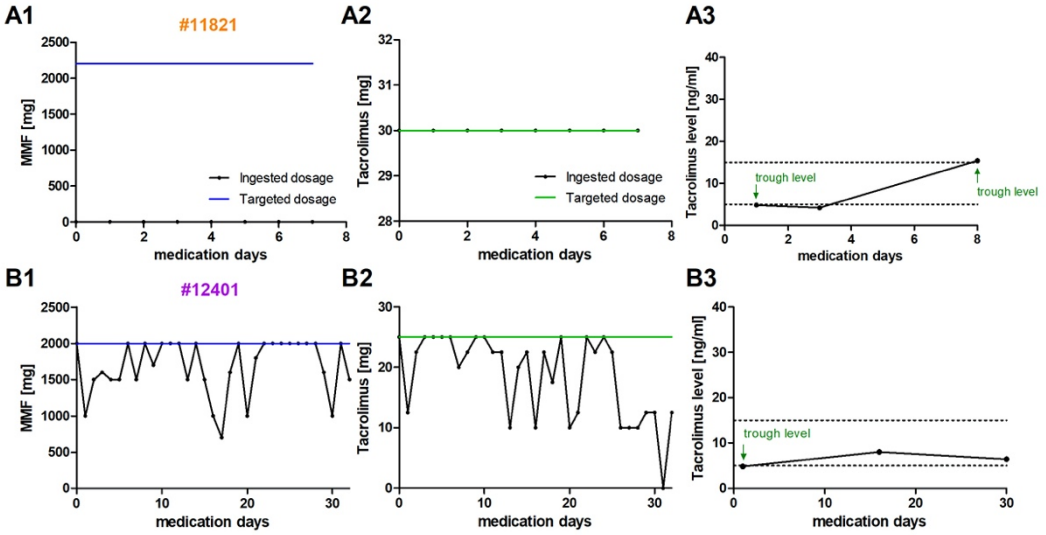

Figure 19: *Intake of MMF* ***(1)*** *and TAC* ***(2)****, and TAC blood levels* ***(3)*** *in WT group.*

(A1-3) *#11821, refused intake of MMF completely, accepted constantly the targeted dosage of TAC and trough- and non-trough levels were largely within reference range.* ***(B1-3)*** *#12401 showed irregular intake of both immunosuppressants. One trough level undercut the reference frame, non-trough-levels were in the lower range of reference frame.*

In the MIDY group, #12580 took the full MMF dose on 75/103 (≙ 73%) treatment days **(Fig. 20A1)**. This pig reached at least the targeted dosage of TAC on 82/103 (≙ 80%) treatment days. As it chewed heavily on the capsules, the dose of TAC was increased by 5 mg/day **(Fig. 20A2)**. TAC values were determined for #12580 on ten medication days. Of these, two measurements on day seven and 13 remained without value because the sample coagulated, four measurements on day 24 (27.9 ng/ml), day 28 (18.4 ng/ml), day 77 (34.6 ng/ml), and day 99 (34.8 ng/ml) do not correspond trough values and were measured 5-9.5 hours after TAC intake. Trough levels exist for medication day one (8.2 ng/ml), 39 (10 ng/ml) and 104 (22 ng/ml). In this animal, the reference limit was therefore exceeded by 7 ng/ml in one measurement (medication day 104) **(Fig. 20A3)**. #12582 completely accepted MMF on 38/83 (≙ 46%) treatment days **(Fig. 20B1)** and took up the minimum required dose of TAC on 68/83 (≙ 82%) treatment days. Chewing of the capsules was also observed in this animal, which explains the increase in dose by up to 5 mg **(Fig. 20B2)**. For #12582, seven TAC measurements were taken, five of which were non-trough levels on medication day seven (14.9 ng/ml), 22 (11.8 ng/ml), 29 (25.6 ng/ml), 53 (29.7 ng/ml) and 78 (18.5 ng/ml), which were measured 4.5-5.5 hours after TAC intake, and two trough levels on day one (8.7 ng/ml) and day 84 (23.3 ng/ml). Initially in the middle-upper reference range, the animal showed an

exceedance of the upper reference value by 8.3 ng/ml at its final trough level **(Fig. 20B3)**. In #13062, MMF was fully absorbed on 45/100 (≙ 45%) days **(Fig. 20C1)** and TAC on 94/100 (≙ 94%) days, on two days a dose adjustment was necessary **(Fig. 20C2)**. There were six TAC measurements for #13062. Non-trough levels in this animal were collected on medication day eight (36.7 ng/ml), 14 (15.2 ng/ml), 22 (20.1 ng/ml) and 55 (16 ng/ml), 5-6.5 hours after TAC intake. The trough values on day one (5.5 ng/ml) and 90 (10.5 ng/ml) were within the target reference range **(Fig. 20C3)**. MMF uptake in #13064, was irregular and was achieved on 31/71 (≙ 44%) treatment days **(Fig. 20D1)**. This pig showed a constant TAC intake, so that the minimum required amount could be achieved on 65/71 (≙ 91%) treatment days **(Fig. 20D2)**. For #13064, three TAC values could be determined in total, as the sample material on days seven, 15 and 42 was quantitatively insufficient for a measurement. One trough value was determined on day one (4.3 ng/ml), two non-trough levels were determined on day 22 (18.2 ng/ml) and day 72 (13.1 ng/ml) five and seven hours after TAC administration. Overall, this animal was therefore once confirmed slightly below the reference range and otherwise at least presumably within the reference range **(Fig. 20D4)**.

ASA was administered consistently to all pigs except #11822, which refused to take it in.

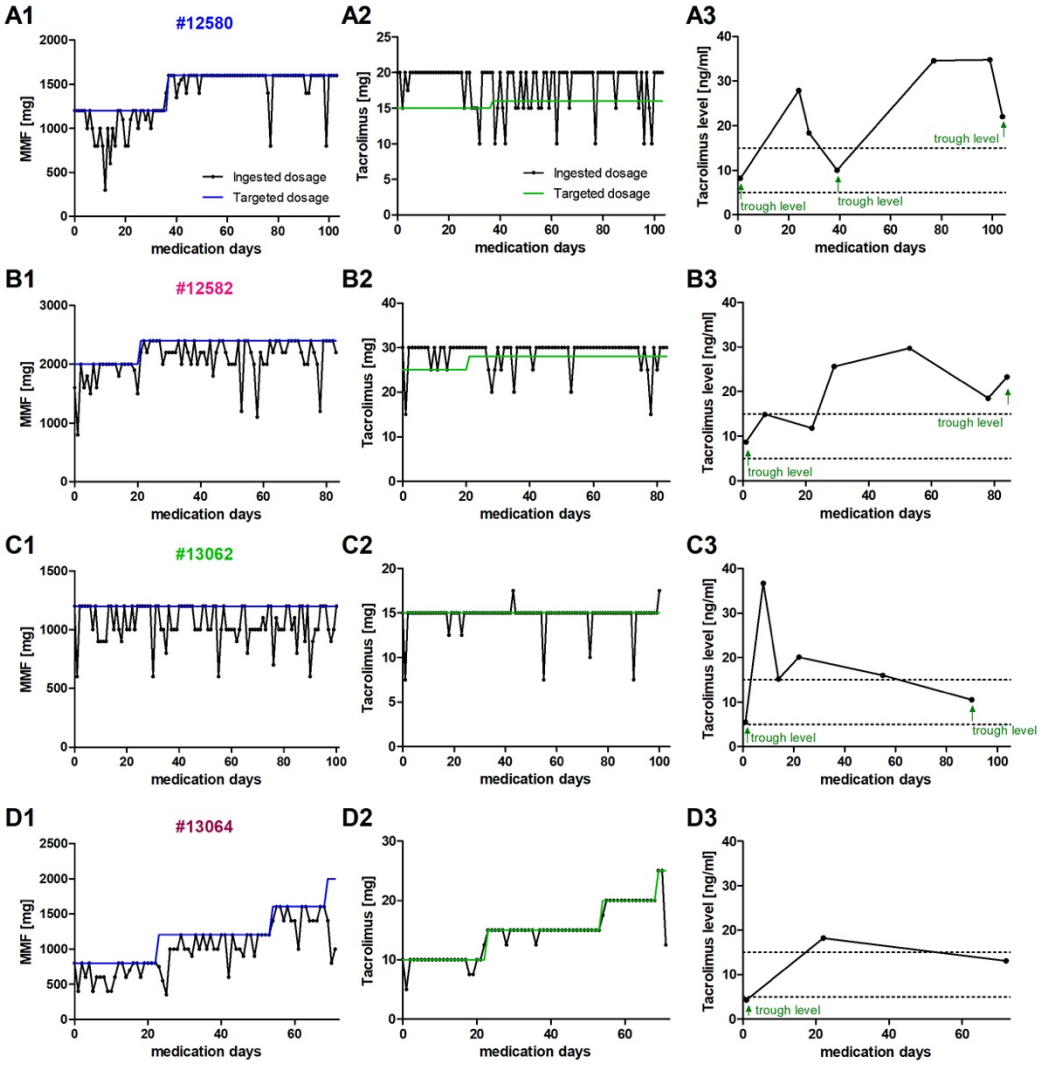

***Figure 20**: Intake of MMF **(1)** and TAC **(2)**, and TAC blood levels **(3)** in MIDY group.*

***(A1-3)** #12580, MMF uptake was irregular, targeted TAC dose was reached and slightly exceeded in most cases, two trough levels were within the reference frame, one trough level and non-trough levels exceeded reference frame. **(B1-3)** #12582, MMF uptake was irregular, ingested TAC dose exceeded targeted dose in most cases, one trough-level and two non-trough levels ranged in the reference frame, after the third measurement the levels were above the upper limit. **(C1-3)** #13062, inconstant MMF intake, ingested TAC dosage corresponded to targeted dosage in most cases, trough levels were within reference frame, non-trough levels were > 15 ng/ml. **(D1-3)** #13064, irregular MMF intake, ingested TAC dosage mostly matched targeted dosage, one trough level was slightly lower than bottom limit, the other values were (almost) in reference frame.*

In total, the WT pigs accepted the targeted dosage of TAC on 44% ± 29 of the medication days. In the MIDY pigs, the targeted dosage was ingested on 87% ± 3 of the medication days and thus almost twice as often **(Fig. 21A)**. Complete MMF uptake occurred in the WT pigs on 17% ± 17 of the medication days and in the MIDY pigs on 52% ± 7 of the medication days. Thus, the MIDY pigs were three times more likely to take up MMF completely than the WT pigs **(Fig. 21B)**.

Both groups took up TAC more consistently than MMF (factor difference WT: 2.6, factor difference MIDY: 1.7)

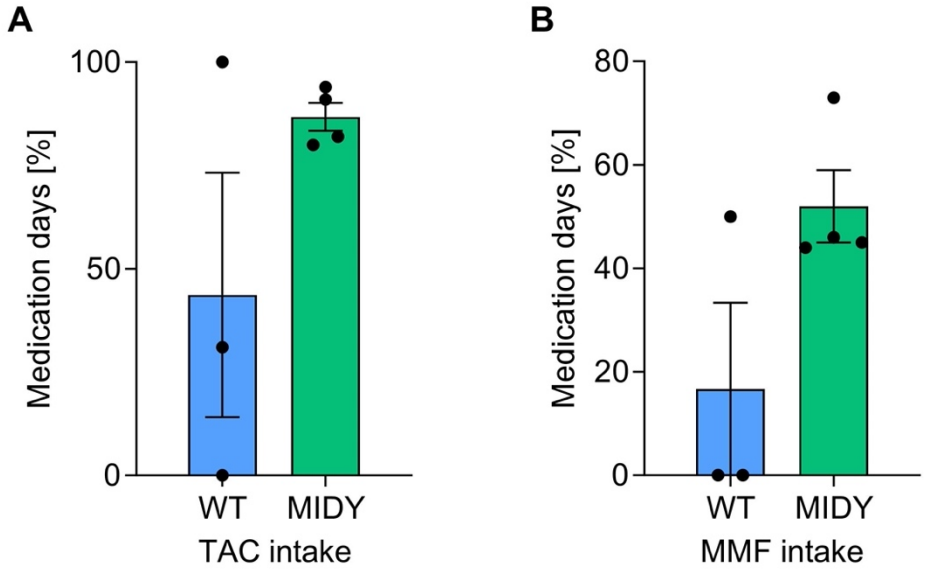

Figure 21: *Intake of immunosuppressants in WT group and MIDY group.*

(A) *Intake of TAC.* ***(B)*** *Intake of MMF. MIDY group showed distinct higher intake of immunosuppressants than WT group. MMF less absorbed than TAC in both groups.*

2.4. Influence of islet transplantation on liver function and inflammation parameters

Clinical-chemical analyses, with a particular focus on liver enzymes, were performed to determine whether liver damage occurred as a result of the islet graft infusion or in the post-transplant period. In addition, the effects of long-term immunosuppression on liver function were investigated and systemic inflammation was ruled out. The reference range for the liver enzymes in pigs were taken from Moritz & Kraft, 2014 (MORITZ & KRAFT, 2014).

2.4.1. Short-term effect of islet transplantation on liver function

Blood samples for the investigation of the short-term effect of ITx on liver function were obtained directly after the islet infusion (Txd 0) and included samples from #12401 #12580, #12582, #13062 and #13064. Aspartate aminotransferase (AST), gamma-glutamyl transferase (GGT), alkaline phosphatase (AP) and ALT levels were determined as liver function parameters. A WT control, and additionally, a MIDY control in the case of ALT from pigs that didn’t receive an ITx were

measured for reference. ALT values of Txd 0 could only be determined for #12582, #13062, #13064 due to insufficient sample material in the other ITx animals.

The AST value of the WT control was 35.6 U/l. In ITx pigs, an exceedance of the upper limit of the normal (ULN) (up to 35 U/l) was detected in animal #13064 (63.7 U/l) **(Fig. 22A)**.

The GGT reference range goes up to 45 U/l. The value of the WT control was 11.5 U/l. An increased value was measured in #12582 (81.9 U/l) **(Fig. 22B)**.

The AP value of the WT control was 25 U/l. In the ITx group, there were two values that exceeded the ULN (up to 170 U/l) clearly: 211 U/l (#12582) and 227 U/l (#13062). One value (172 U/l; #13064) was only slightly increased **(Fig. 22C)**.

ALT control values of WT and MIDY pig were 51.4 U/l and 33.8 U/l, respectively. In the ITx pigs, if measured, the ULN of 68 U/l was not exceeded **(Fig. 22D)**.

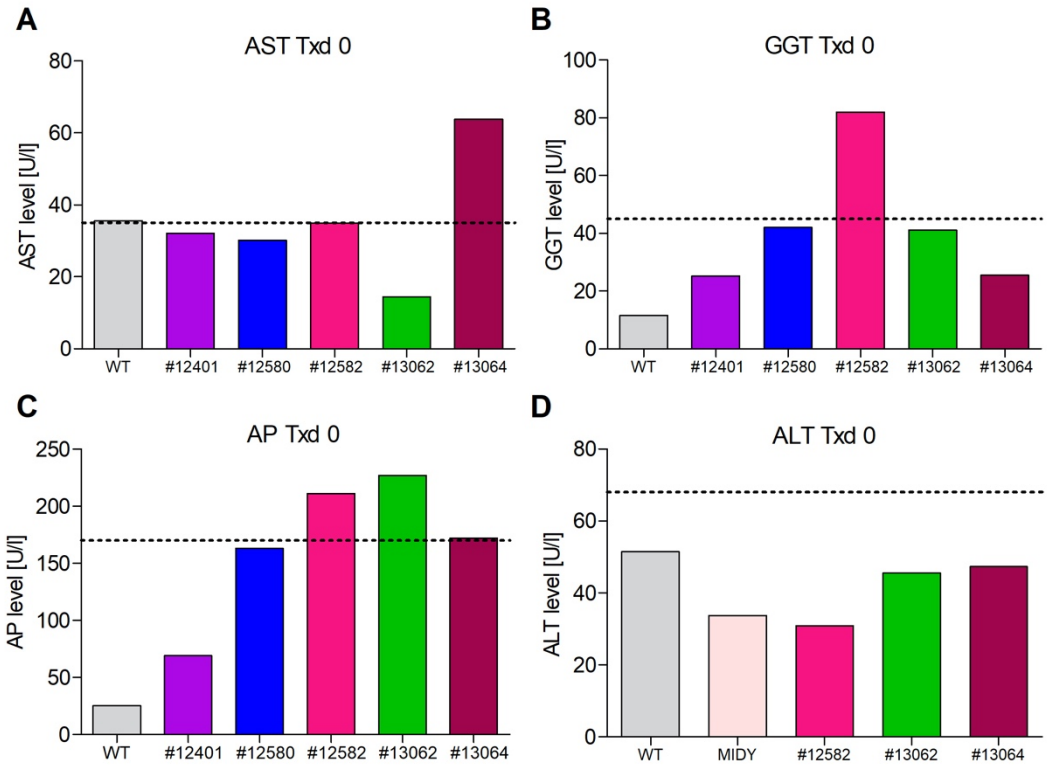

Figure 22: *Liver enzymes on Txd 0.*

(A) *AST levels, increased value in #13064.* ***(B)*** *GGT levels, increased value in #12582.* ***(C)*** *AP levels, clearly increased values in #12582 and #13062, slightly elevated value in #13064.* ***(D)*** *ALT levels, no increased values.*

2.4.2. Long-term effect of islet transplantation on liver function and inflammation parameters

Longitudinal analysis of AST values revealed that in #13064, the elevated AST value (63.7 U/I) directly post-ITx returned to the reference frame from Txd 41 (22.8 U/l) onwards. #11821 had an increased AST level on Txd 2 (61.5 U/l), which dropped to a physiological level until Txd 7 (32.1 U/l). In #12401 the AST level exceeded the ULN at Txd 15 (37.1 U/l) and rose again to Txd 31 (39.52 U/l). The values of #12580 and #12582 showed a continuous increase beginning on Txd 38 and Txd 52, respectively and exceeding the ULN at Txd 103 for #12580 (38.7 U/l) and at Txd 83 for #12582 (45.1 U/l). #11822 and #13062 had physiological AST values **(Fig. 23A)**.

#11821 had an increased GGT level on Txd 2 (75.2 U/l), which normalized until Txd 7 (34.8 U/l). In #12582 the increased GGT value on Txd 0 fell consistently back into the physiological range from Txd 52 onwards (33.3 U/l). The GGT levels of #11822, #12401, #12580, #13062 and #13064 were physiological at all times **(Fig. 23B)**.

The elevated AP values on Txd 0 of #12582, #13062 and #13064 normalized during the observation period. For #12582, the value on Txd 52 was 111 U/l and therefore in the physiological range, dropping further to 61 U/l at Txd 77 and 50 U/l at Txd 83. #13062 showed a physiological value of 38 U/l at Txd 100. #13064 had a value of 116 U/l on Txd 41 and 83 U/l on Txd 71. #11822, #12401 and #12580 had physiological AP values **(Fig. 23C)**.

There was a single elevated ALT value in #11821 (90.6 U/l). Since only this value was measured in this animal, there is no information on how ALT values developed. No ALT values deviating from the norm were measured in the other ITx pigs **(Fig. 23D)**.

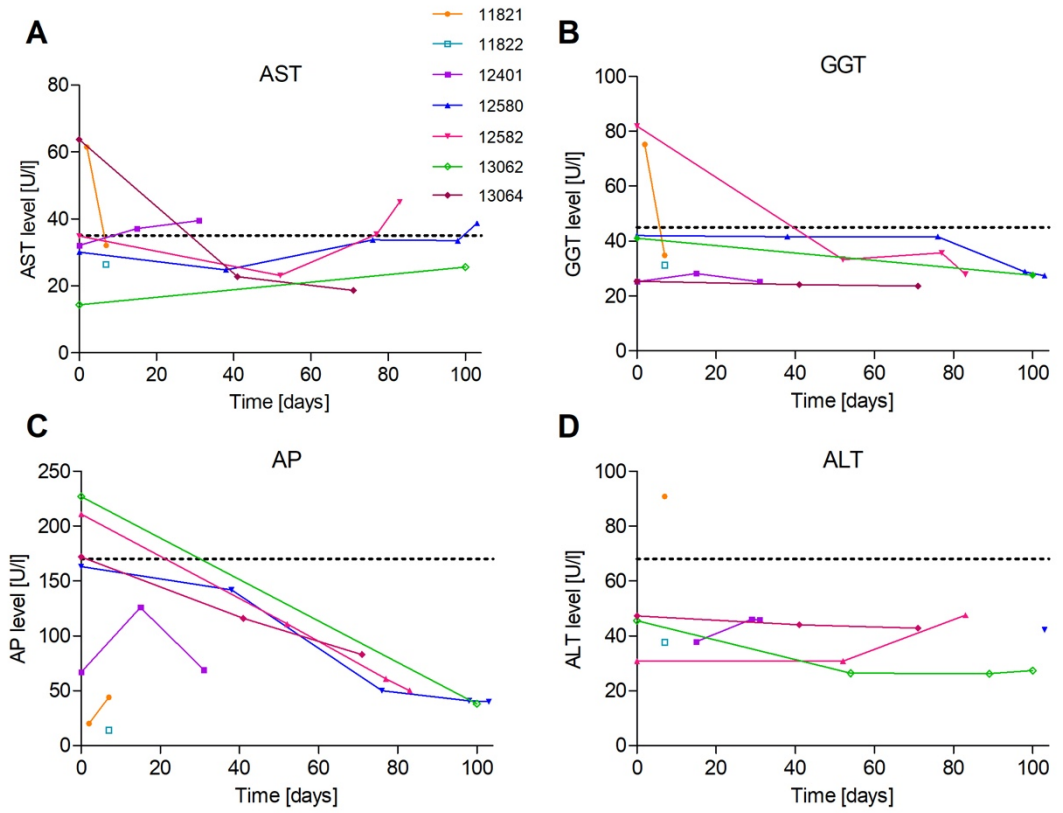

Figure 23: *Longitudinal development of liver function parameters.*

(A) *AST levels; #11821 and #12401 had a decreasing trend from initially elevated values. #12401, #12580 and #12582 showed increasing values, that exceeded the ULN at later time points.* ***(B)*** *GGT levels; Initially elevated values in #11821 and #12582 normalized over time.* ***(C)*** *AP levels; Elevated values were seen in #12582, #13062 and to a lesser extent in #13064. All values dropped to a physiological level over time.* ***(D)*** *ALT levels; The only increased value was measured in #11821, for which there is no information on the development.*

CRP values were determined in order to obtain information about a possible inflammatory process in the ITx recipients. There are no official reference values for CRP in pigs. Therefore, in addition to blood samples collected in the observation period after ITx, control values were measured. These consisted of a WT control, a MIDY control and Txd 0 samples from #12582, #13064 and #13062, collected directly after ITx. The values measured in the control group were between 3.3 µg/ml and 7.2 µg/ml. The measurements in the observation period after ITx revealed that most of the values were clustered, with a range of 0.6 µg/ml - 4.6 µg/ml. Two values that fall outside this range were striking, 11.9 µg/ml and 16.1 µg/ml. These values were both measured in pig #13064 **(Fig. 24A)**. The course of the CRP values of #13064 showed an increase from 3.3 µg/ml, measured directly after ITx, to 16.1 µg/ml at Txd 71, i.e. there was an increase by a factor of 4.9 **(Fig. 24B)**. #13064 is the only pig for which the values have risen continuously after ITx. The mean value

of the >Txd 1 group (4.1 µg/ml ± 1.1) was even lower than the mean value (5.6 µg/ml ± 0.8) of the control group **(Fig. 20A)**.

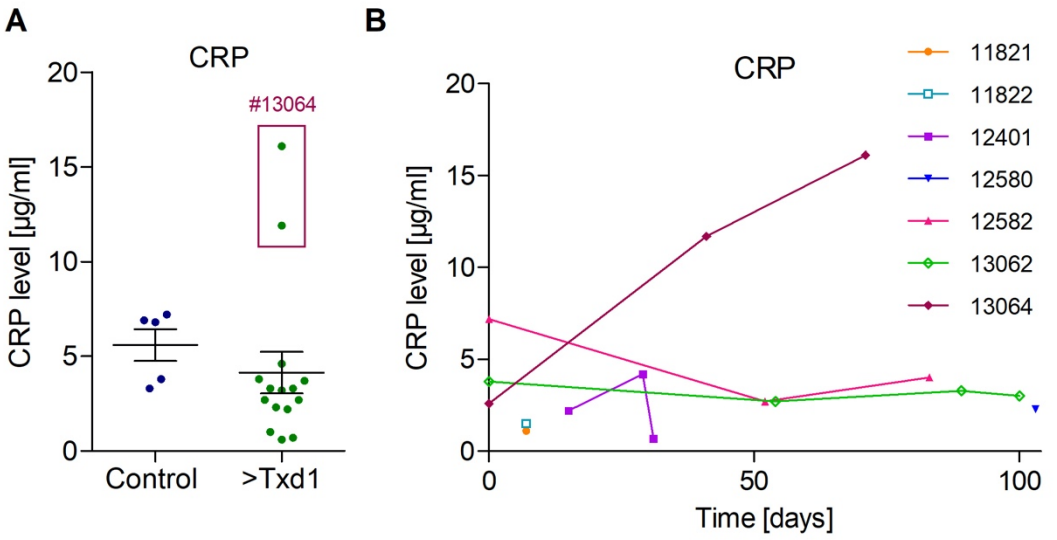

Figure 24: *CRP values.*

(A) *CRP measurements divided into control group and >Txd 1 group. CRP levels cluster in both groups with a total range of 0.6 µg/ml – 7.2 µg/ml. Two values in the >Txd 1 group fell out of the clustered distribution scheme, being strikingly higher. Both measurements stem from pig #13064.* ***(B)*** *Development of CRP values over time. There was a distinct increase of CRP levels in pig #13064. The other values showed a constant trend, with decreasing tendencies. For #11821, #11822 and #12580, there was only one measurement and therefore no information of the CRP courses.*

2.5. Impact of islet transplantation on diabetic phenotype of MIDY pigs

2.5.1. Diabetic phenotype of MIDY pigs prior to islet transplantation

All pigs in the MIDY group exhibited hyperglycemia at least 3-7 weeks before ITx was performed. Insulin therapy was started 1-4 weeks before ITx. In detail, in #12580, hyperglycemia was recorded 29 days prior to ITx, and insulin therapy commenced eleven days before ITx **(Fig. 25A)**. In #12582, hyperglycemia was observed 50 days before ITx, and insulin therapy was initiated 28 days prior to ITx **(Fig. 25B)**. In #13062, hyperglycemia was noted 30 days before ITx, and insulin therapy was started 16 days prior to ITx **(Fig. 25C)**. In #13064, hyperglycemia was recorded 23 days before ITx, and insulin therapy commenced six days before ITx **(Fig. 25D)**.

On the day of ITx, the MIDY pigs exhibited a hyperglycemic FBG and reached a dose of exogenous insulin consisting of LAIA and SAIA of 5-2 (#12580), 30-15 (#12582), 8-4 (#13062) and 2-1 (#13064) **(Table 22)**. It should be noted that no

insulin (#12580 and #13062) or a reduced insulin dose (#12582 and #13064) was administered on the day of the ITx itself due to the food restriction that was necessary because of the anesthesia.

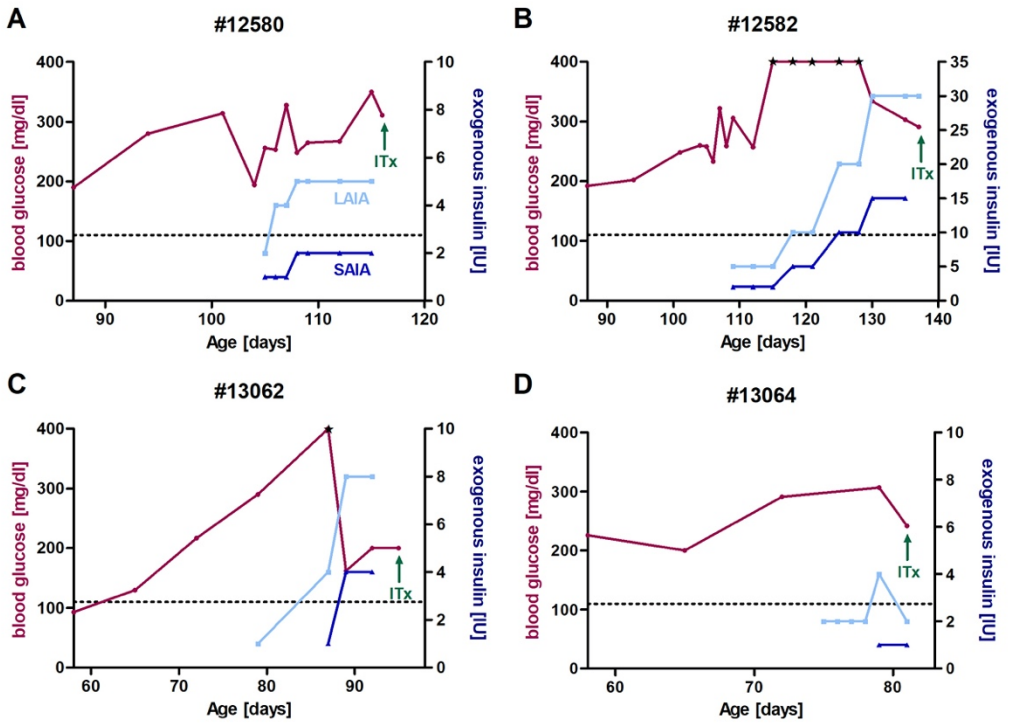

Figure 25: *FBG levels and exogenous insulin therapy of MIDY pigs prior to ITx.*

(A) *#12580, hyperglycemia recorded 29 days prior to ITx, insulin therapy started 11 days before ITx.* ***(B)*** *#12582, hyperglycemia recorded 50 days before ITx, insulin therapy started 28 days before ITx.* ***(C)*** *#13062, hyperglycemia recorded 30 days prior to ITx, insulin therapy started 16 days before ITx.* ***(D)*** *#13064, hyperglycemia recorded 23 days prior to ITx, insulin therapy started 6 days before ITx.*

Animal ID	FBG value at ITx day	Dose of LAIA	Dose of SAIA
12580	311	5	2
12582	291	30	15
13062	200	8	4
13064	242	4	1

Table 22: *FBG values of MIDY pigs at day of ITx and dose of exogenous insulin reached.*

2.5.2. Development of diabetic state of MIDY pigs after islet transplantation

In three out of four MIDY pigs, normoglycemic levels were first achieved within 18-47 days post-ITx and were constantly obtained from 37-72 days post-ITx onwards. Within 16-45 days, SAIA could be discontinued, LAIA was omitted between day 54 and 100 after ITx, or continuously reduced to 2 IU until Txd 61.

In detail, the first normoglycemic value in pig #12580 was measured at Txd 47, constant normoglycemia persisted from Txd 72. A single elevated value was measured at Txd 94 (132 mg/dl). SAIA was dispensed with from Txd 45 and LAIA from Txd 100 **(Fig. 26A)**. In #12582, a normoglycemic value was detected for the first time at Txd 23. After that, the values remained in a near-normoglycemic range (110-141 mg/dl) from Txd 37 onwards. From day 16, the animal no longer received SAIA. It was constantly treated with LAIA, whereby the dose could be continuously reduced to 2 IU **(Fig. 26B)**. A first normoglycemic value in #13062 was reached at Txd 18. Constant normoglycemia occurred in this animal from Txd 64 onwards. Therapy with SAIA was discontinued at Txd 32 and with LAIA at Txd 54 **(Fig. 26C)**. In pig #13064, FBG levels <200 mg/dl were mostly observed from week four post ITx, normoglycemia did not occur. The insulin dose showed a plateau from Txd 29 of 10-11 IU LAIA and 3 IU SAIA per day **(Fig. 26D)**.

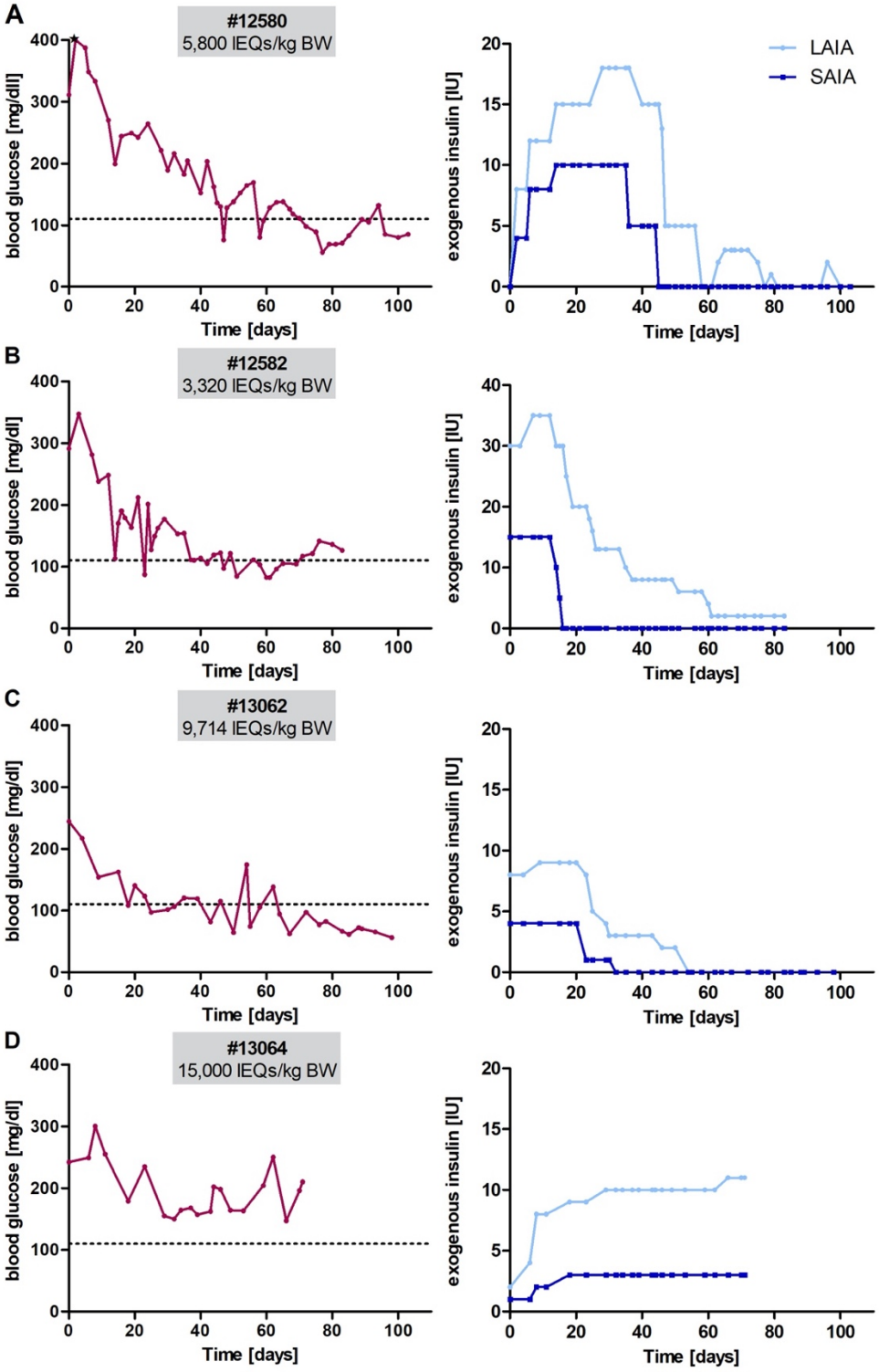

Figure 26: *FBG levels and exogenous insulin therapy of MIDY pigs after ITx.*

(A) *#12580, first normoglycemic value at Txd 47, constant normoglycemia from Txd 72, except one elevated value at Txd 94, omission of SAIA from Txd 45, omission of LAIA from Txd 100.* ***(B)*** *#12582, first normoglycemic value at Txd 23, subsequently near-normoglycemic values from Txd 37, omission of SAIA from Txd 16, continuous reduction of LAIA to 2 IU.* ***(C)*** *#13062, first normoglycemic value at Txd 18, constant normoglycemia from Txd 64, omission of SAIA at Txd 32, omission of LAIA at Txd 54.* ***(D)*** *#13064, mainly FBG levels <200 mg/dl from week 4 post ITx, no normoglycemic values recorded, plateau of insulin dose from Txd 29. Adapted from Pilz et al., 2024.*

2.6. Longitudinal *in vivo* monitoring of islet grafts in ITx recipient pigs by [^{68}Ga]Ga-DOTA-Exendin-4 PET/CT imaging

The non-invasive *in vivo* monitoring of endogenous pancreatic BCM in pigs using [^{68}Ga]Ga-DOTA-Exendin-4-PET/CT imaging with histological validation is addressed in the scientific work and dissertation of Ms. Nicol Gloddek. The results of this study are also relevant for the present study. Therefore, a summary of the results is presented in the "proof-of-concept" section.

The i.v. injection of [^{68}Ga]Ga-DOTA-Exendin-4 did not cause any noticeable side effects. The pigs' vital parameters were stable during anesthesia. The recovery phase after anesthesia was undisturbed. An exception to this occurred in #13064, that died in the recovery phase after the third PET/CT scan due to a gastrointestinal emergency. Tachycardia (> 100 beats/minute) already occurred during the PET/CT examination.

2.6.1. Proof-of-concept study for imaging of endogenous pancreatic beta cells in pigs by [^{68}Ga]Ga-DOTA-Exendin-4 PET/CT

The time-activity curves of the baseline scans showed a rapid increase of SUV in kidney, pancreas and liver within the first 3.5 minutes. The strongest tracer accumulation in the entire scan with a plateau from minute 20 onwards was detected in the kidneys, through which the tracer was excreted (LINDHEIMER et al., 2023). The mean SUV of the kidneys was 17.5 ± 5.7. There was also a clear accumulation of [^{68}Ga]Ga-DOTA-Exendin-4 in the pancreas, which reached a SUV plateau with a range of 2.5 - 5.2 after 36 minutes. The mean SUV in the pancreas was 2.8 ± 0.75. For the liver, the SUV first ranged between 2.5 and 3.9 and had a mean SUV of 1.5 ± 0.9. After 30 minutes it dropped to values <1. There was no increase in SUV in the *longissimus dorsi* muscle, the values remained constantly at a low background level (mean: 0.2 ± 0.06) **(Fig. 27)**.

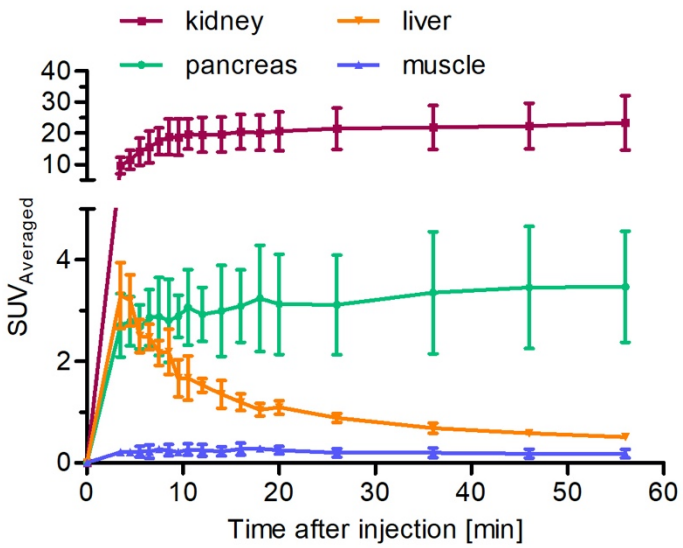

Figure 27: *Proof-of-concept: Imaging of endogenous, pancreatic beta cells by [^{68}Ga]Ga-DOTA-Exendin-4 PET/CT in MIDY pigs.*

Time-activity curves within 60 minutes post injection. Shown are the mean SUVs of the pigs #12580, #12582, #13062, #13064 measured in the baseline scans. Mean SUVs were determined in kidneys, liver, pancreas and longissimus dorsi muscle. This graph shows the SD of mean values.

Rapid and strongest uptake of radiotracer in kidney. Distinct radiotracer uptake with plateau in the pancreas. Decreasing SUVs in liver after a first increase. Constant background levels in longissimus dorsi muscle.

From Pilz et al., 2024

The dynamic distribution of the radiotracer was visualized in axial and coronal images, showing that [^{68}Ga]Ga-DOTA-Exendin-4 was initially mainly located in the blood vessels (aorta, organs) and then accumulated in the target organs, mainly the kidney and the pancreas, where it caused a distinct signal. The kidney signal was clearly visible during the entire scan, whereas a clear signal appeared in the pancreas from minute 20 onwards, which intensified up to minute 50 **(Fig. 28)**.

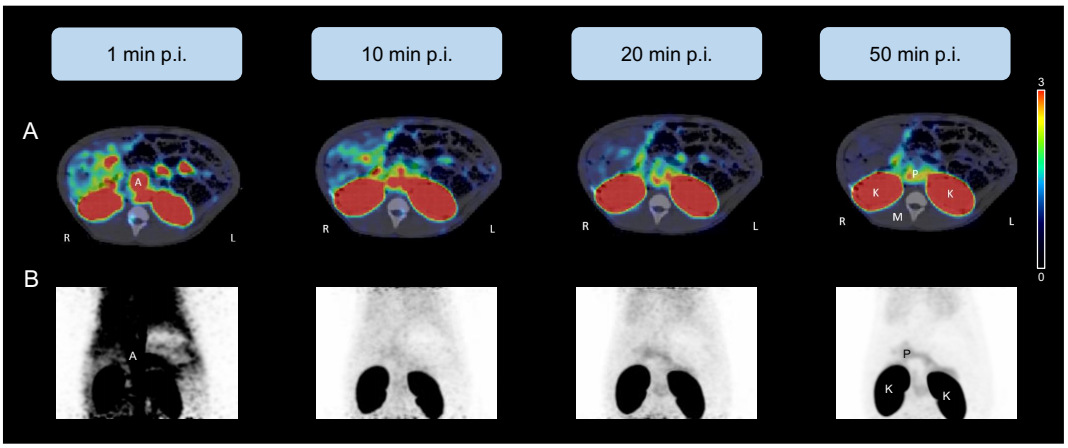

Figure 28: *Examples of axial and coronal [^{68}Ga]Ga-DOTA-Exendin-4 PET/CT images.*

(A) *Pig #13062, shown are axial images at minute 1 (A: aorta), 10, 20 and 50 post injection, normalized to SUV=3.* ***(B)*** *Pig #13062, maximum intensity projection in coronal images at minute 1, 10, 20 and 50 post injection. Images visualize the dynamic distribution of the radiotracer, which quickly accumulated from the bloodstream in the kidneys and from minute 20 visibly in the pancreas.*

Adapted from Pilz et al., 2024.

2.6.2. Dynamic development of liver SUV in ITx recipient pigs in longitudinal [^{68}Ga]Ga-DOTA-Exendin-4 PET/CT imaging

A total of three PET/CT examinations were performed for #12580 and #13064 after ITx and two PET/CT examinations each for #12582 and #13062. On average, the whole-liver SUV of the baseline scans was 0.46 (range: 0.39 - 0.52). This corresponds to the background accumulation of [^{68}Ga]Ga-DOTA-Exendin-4 in the liver.

After the ITx, a continuous and significant increase in the whole-liver SUV could be determined in the longitudinal [^{68}Ga]Ga-DOTA-Exendin-4 PET/CT imaging. Pig #12580 showed a consistent elevation of whole-liver SUV, reaching a total increase of 115% at the last PET/CT scan compared to the baseline scan (Baseline: 0.44, Txd 98: 0.95). In pig #12582, a 111% increase in whole-liver SUV was observed between the baseline scan (0.39) and the first imaging post-ITx (0.82), after which the value plateaued. #13062 exhibited consistently increasing whole-liver SUVs with a 66% increase from the baseline scan to the last PET/CT scan (Baseline: 0.52, Txd 89: 0.86). In #13064, only a slight increase of 12% in whole-liver SUV was observed between baseline scan (0.47) and Txd 71 (0.53). No liver SUV data exist for the second PET/CT measurement at Txd 41 in this animal due to a setting error **(Fig. 29A)**.

The mean of the baseline whole-liver SUVs added with the twofold SD resulted in a threshold of 0.47, which was implemented for the hotspot analysis. The hotspot analysis revealed a continuous increase in hotspot-liver SUVs for pigs #12580, #12582 and #13062. In detail, the value increased for #12580 from 0.64 to 0.96 (50%), for #12582 from 0.66 to 1.50 (127%) and for #13062 from 0.63 to 0.91 (42%). In contrast, there was hardly any increase in the hotspot-liver SUV of #13064 from 0.65 to 0.66, which corresponds to 2% **(Fig. 29B)**.

Overall, #12580 had the strongest intensification in the whole-liver SUV and #12582 in the hotspot-liver SUV. #13064 had the weakest effect on the SUV. The p-value of the whole-liver SUV analysis was 0.008 and that of the hotspot-liver SUV analysis 0.0197, which is why both developments can be classified as significant.

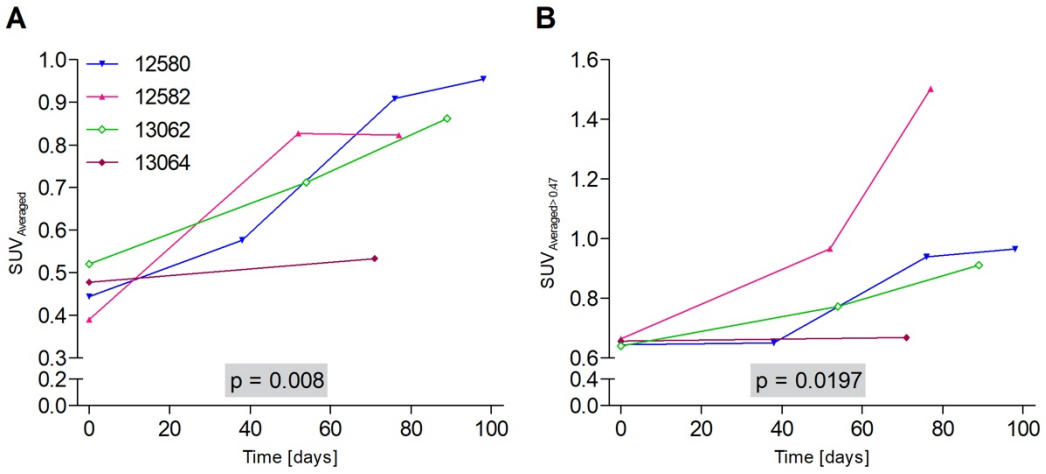

Figure 29: *Development of liver SUV in MIDY pigs post-ITx.*

(A) *Development of whole-liver SUV in MIDY pigs after ITx.* ***(B)*** *Development of hotspot-liver SUV in MIDY pigs after ITx. Both graphs show significantly increasing SUVs over time in #12580, #12582 and #13062 and hardly any increase in SUV in #13064.*

Adapted from Pilz et al., 2024.

Coronal PET/CT images of ITx recipient pigs indicated diffuse, multifocal increase in liver signal from baseline scan to the last scans, which was particularly pronounced in #13062 **(Fig. 30)**.

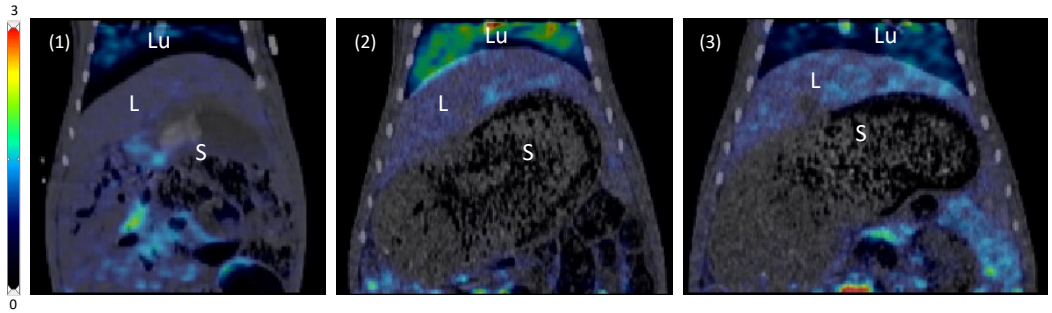

Figure 30: *Coronal [^{68}Ga]Ga-DOTA-Exendin-4 PET/CT images.*

Pig #13062; ***(1)*** *Baseline scan,* ***(2)*** *Txd 54,* ***(3)*** *Txd 89. To enable direct comparison, coronal images are normalized to SUV=3. (L = liver; Lu = lung; S = stomach). Images show diffuse, multifocal increase in liver SUV.*

From Pilz et al., 2024.

3. Validation of islet graft properties in the liver *in situ*

The sampling procedure was individually adapted for each animal, e.g. to liver size, length of the observation period and circumstances of the dissection. RNAlater® samples were only taken in the MIDY group. An average of 125 samples/liver were obtained in the WT group. In the MIDY group, an average of 258 samples/liver were generated. For this study, histological examinations were carried out using PFA-fixed, paraffin-embedded samples. The distribution and total amount of PFA-fixed samples is considered representative of the entire liver and is hereinafter referred to as "all liver segments". **Table 23** shows an overview of the number of the liver samples obtained for each fixative or storage method.

Animal ID	PFA	ME	-80°C	TissueTek®	RNAlater®
11821	54	53	47	48	0
11822	37	30	19	0	0
12401	42	12	0	34	0
12580	65	47	51	48	46
12582	67	55	54	53	55
13062	88	76	70	71	68
13064	68	0	49	0	0

Table 23: *Overview of liver samples collected from ITx recipient pigs.*

3.1. Overview of histological ITx outcome

Animal ID	Main findings of overview stainings	Linear connection between number of IEQs/kg BW and ICC+ liver segments	Localization of ICCs	Distribution pattern of ICCs	*In vivo* maturation into alpha, beta and delta cells	Occurrence of alpha and beta cells according to ICCs distribution	Extent of immune response
11821	Engraftment and re-endothelization	Yes	Periportal, left liver lobes	Broad distribution, <50% of liver segments ICC+, mainly 1-5 ICCs/slide	-/-	Yes	Mild - moderate T-cell response
11822	Lymphocytic cell infiltrations	Yes	Periportal, left liver lobes	Broad distribution, <50% of liver segments ICC+, mainly 1-5 ICCs/slide	-/-	Yes	Strong T-cell response
12401	Lymphocytic cell infiltrations	Yes	Periportal, left-centered, slight right tendency	Broad distribution, <50% of liver segments ICC+, mainly 1-5 ICCs/slide	-/-	Yes	Moderate-strong T-cell response
12580	Engraftment and re-endothelization	Yes	Periportal, left liver lobes	Broad distribution, <50% of liver segments ICC+, mainly 1-5 ICCs/slide	Yes	Yes	Mild T-cell response
12582	Engraftment and re-endothelization	No, comparable lower number of ICC+ liver segments	Periportal, left liver lobes	Broad distribution, <50% of liver segments ICC+, mainly 1-5 ICCs/slide, sporadically >15 ICCs/slide	Increased proportion of liver segments with 6-15 alpha cell clusters	Yes	Mild T-cell response
13062	Engraftment and re-endothelization	Yes	Periportal, whole liver	Broad distribution, >50% of liver segments ICC+, mainly 1-5 ICCs/slide	Yes	Yes	Mild T-cell response
13064	Engraftment and re-endothelization	No, comparable lower number of ICC+ liver segments	Periportal, left liver lobes	Broad distribution, <50% of liver segments ICC+, mainly 1-5 ICCs/slide, sporadically >15 ICCs/slide	Yes	Yes	Mild T-cell response, strikingly high abundance of macro-phages

Table 24: *Overview of histological ITx outcome.*

3.2. H&E and Giemsa stains for first assessment of graft-bearing livers

H&E stainings were performed on all PFA-fixed liver samples for each animal as an initial overview stain. The liver parenchyma was unsuspicious in all animals, exhibiting no abnormalities, except for areas with islet-graft-associated mononuclear cell infiltration, that were predominantly found in #11822 and #12401. ICCs could occasionally be identified in the periportal region, exhibiting signs of reendothelialization during the early islet engraftment process. Reendothelialization was detectable as early as seven days post-ITx and persisted throughout the long-term experiment. However, H&E staining did not reliably enable the identification of ICCs in the portal vein system, particularly in cases where engraftment and graft maturation occurred. The identification of ICCs in H&E staining was therefore facilitated by comparing conspicuous sites with serial liver sections immunohistochemically stained with the neuroendocrine marker protein SYP, detecting ICCs. Well engrafted and revascularized ICCs were found in the periportal area mainly in animals #11821, #12580, #12582, #13062, and #13064 **(Fig. 31)**.

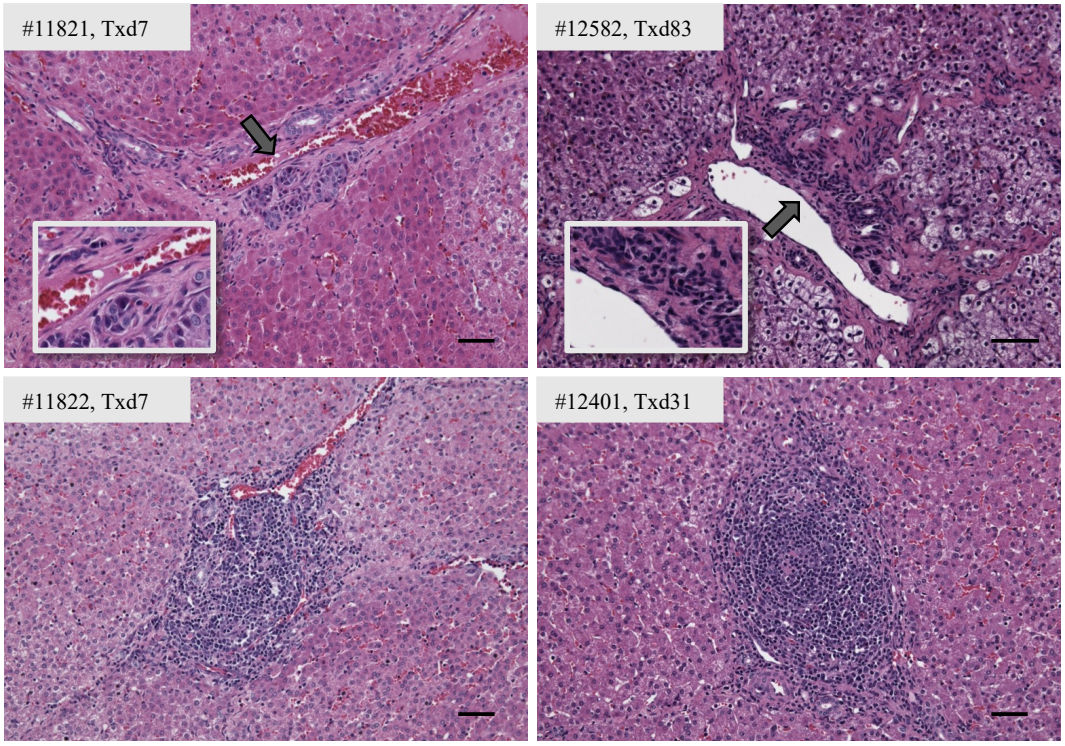

Figure 31: *H&E staining of ITx livers.*

(Upper row) *Representative liver sections of #11821 and #12582 showing reendothelization at early and late time points during islet engraftment process. Arrows point to ICCs surrounding endothelium, for which a zoomed view is provided in the left picture corner.*

(Lower row) *Representative liver sections of animals #11822 and #12401 showing periportal regions with intense mononuclear cell infiltrates. Time points of tissue sampling post-ITx are indicated as Txd. Bars = 50 µm.*

Giemsa staining was performed on a small subset of liver sections displaying areas of cellular infiltrations for each animal. The infiltrating cells turned out to be dark blue stained, round cells, indicating lymphocytes. These infiltrates were particularly prominent in the livers of #11822 and #12401 **(Fig. 32)**.

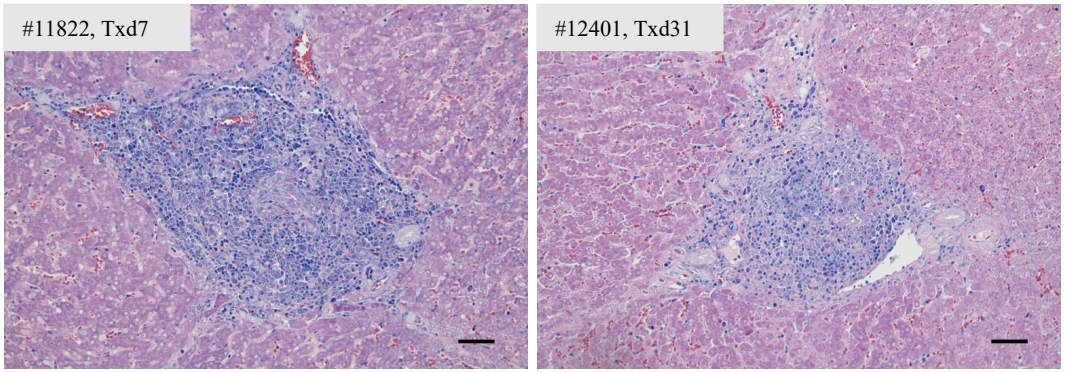

Figure 32: *Giemsa staining of ITx livers.*

Lymphocyte infiltrations in representative liver sections of #11822 and #12401. Time points of tissue sampling post-ITx are indicated as Txd. Bars = 50 µm.

3.3. Abundance and distribution of islet grafts in the liver

ICCs in the portal vein system were reliably identified by immunohistochemical detection of the neuroendocrine marker protein synaptophysin, that is expressed in pancreatic islets (WIEDENMANN et al., 1986). With the exception of nerves that innervated the liver, no other hepatic cell types showed a positive stain for SYP. It was possible to reliably distinguish the neuronal structures from pancreatic islets based on staining intensity and staining pattern. On this basis, islet-containing liver segments, referred to as “SYP + liver segments”, could be distinguished from liver segments without an islet transplant. The ICCs were characterized by a heterogeneous size, with an average cross-sectional area range between 19 µm x 44 µm – 250 µm x 453 µm **(Fig. 33)**.

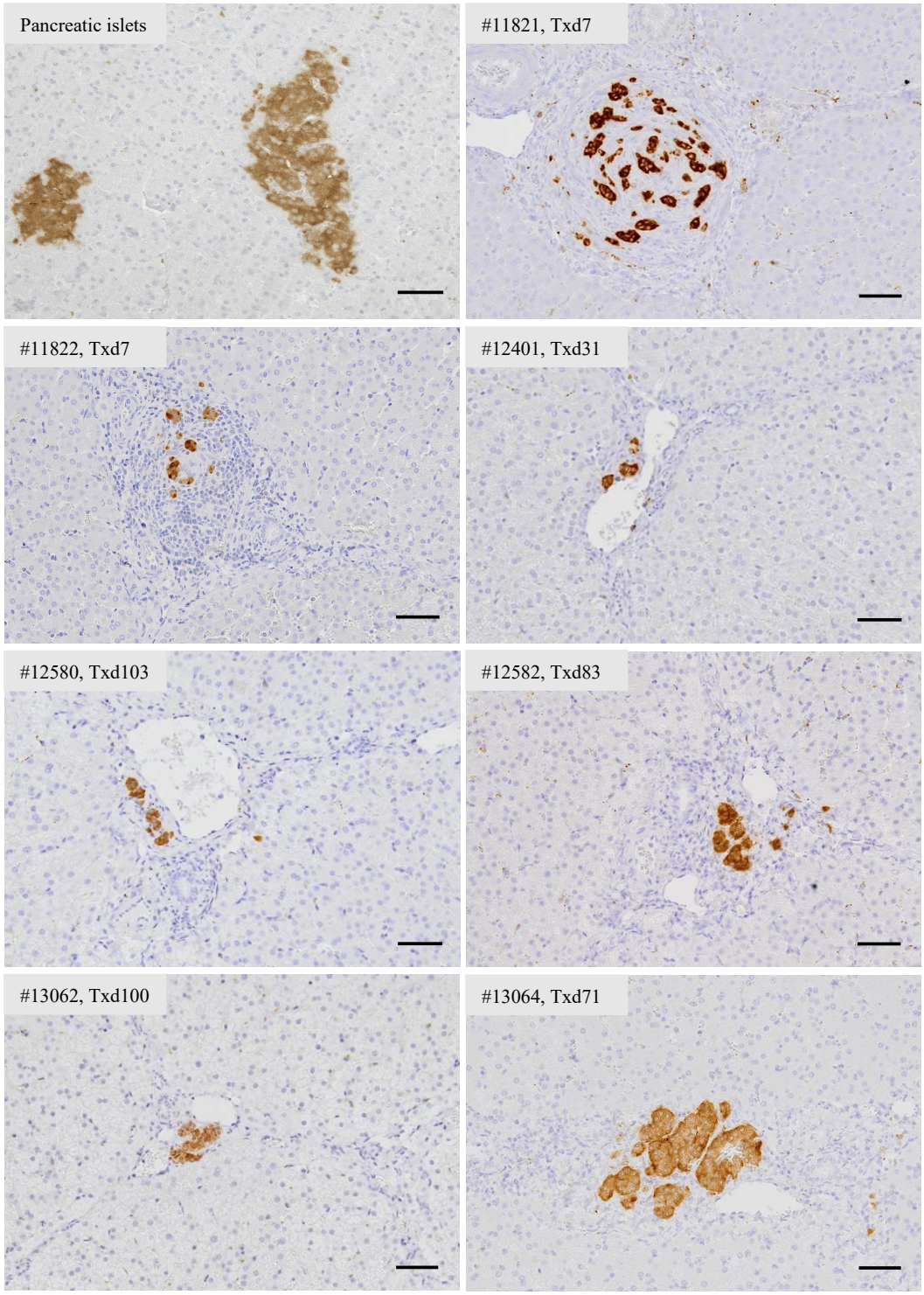

Figure 33: *Immunohistochemical staining of ICCs (SYP).*

Shown are representative liver sections of each ITx pig containing periportal ICCs. Pancreatic islets are shown for reference. SYP was stained in brown color, whereas nuclei were stained in purple color. Time points of tissue sampling post-ITx are indicated as Txd. Bars = 50 µm.

Overall, the ITx recipients of the WT pigs had the following proportion of SYP+ slides within all liver segments: 41% (#11821 and #11822) and 23% (#12401) **(Fig. 34A)**. In the MIDY group, the percentage of SYP+ slides was 42% (#12580), 20%

(#12582), 64% (#13062) and 38% (#13064) **(Fig. 34B)**. On average, 35% of all liver slides analyzed in the WT group and 40% of the liver slides of the MIDY group contained SYP+ ICCs, indicating a broad distribution of ICCs upon intraportal infusion. Of note, #11821 and #11822 had a 1.8x higher proportion of SYP+ liver segments than #12401. In the MIDY pigs, #13062 had the highest proportion of SYP+ liver segments and #12582 the lowest, differing by a factor of 3.2.

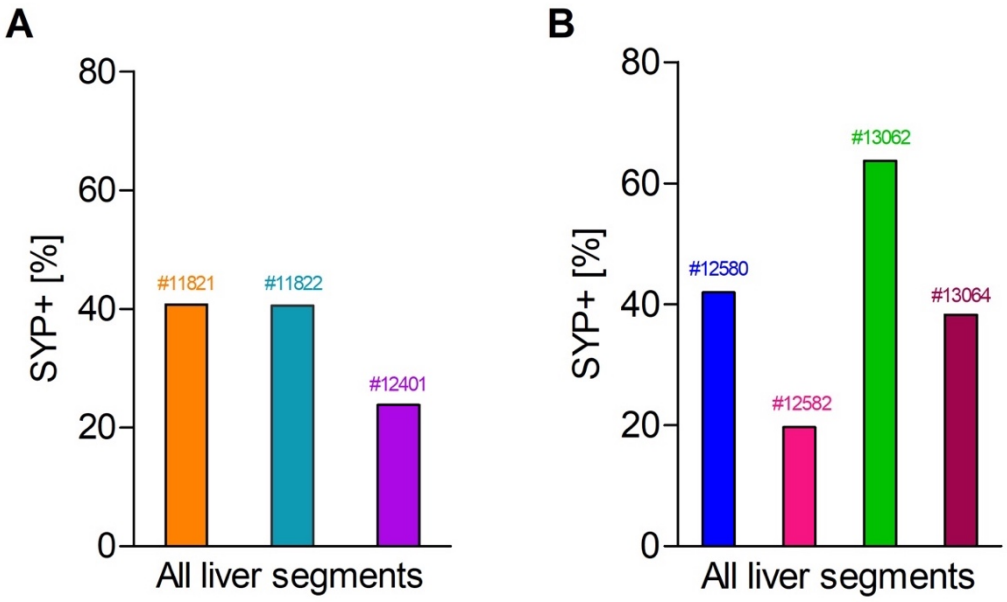

Figure 34: *Proportion of SYP+ liver segments within all liver segments.*

(A) *Proportion of SYP+ liver segments within all analyzed liver segments in WT group.* ***(B)*** *Proportion of SYP+ liver segments within all analyzed liver segments in MIDY group.*

The greater the number of IEQs/kg BW transplanted, the higher the percentage of SYP+ liver segments in animals #11821, #11822, #12401, #12580 and #13062. #12582 and #13064 had a lower percentage of SYP+ liver segments with comparatively more IEQs/kg BW transplanted **(Fig. 35)**. Of note, catheter position at NPI transplant infusion into the liver differed between the animals (see **Table 20**).

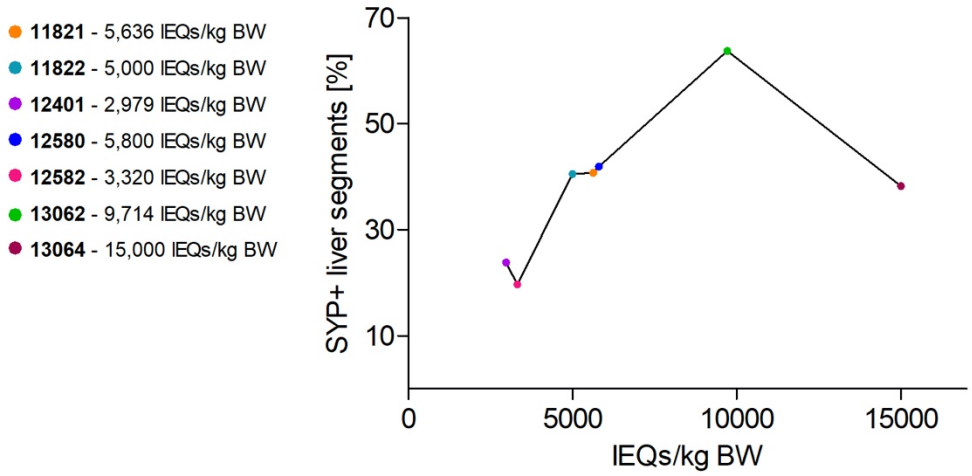

Figure 35: *Connection between transplanted IEQs/kg BW and percentage of SYP+ liver segments.*

In principle, a higher number of transplanted IEQs/kg BW resulted in a higher number of SYP+ liver segments. Exceptions are #12582 and #13064.

In the WT group, ICCs were enriched in the left liver lobes of pigs #11821 and #11822. In pig #12401 the islets were mostly left-centered, with some ICCs showing a slight rightward tendency. In the MIDY group, ICCs were localized in the left liver lobes of pigs #12580, #12582 and #13064. In pig #13062, ICCs were distributed over the whole liver **(Fig. 36).**

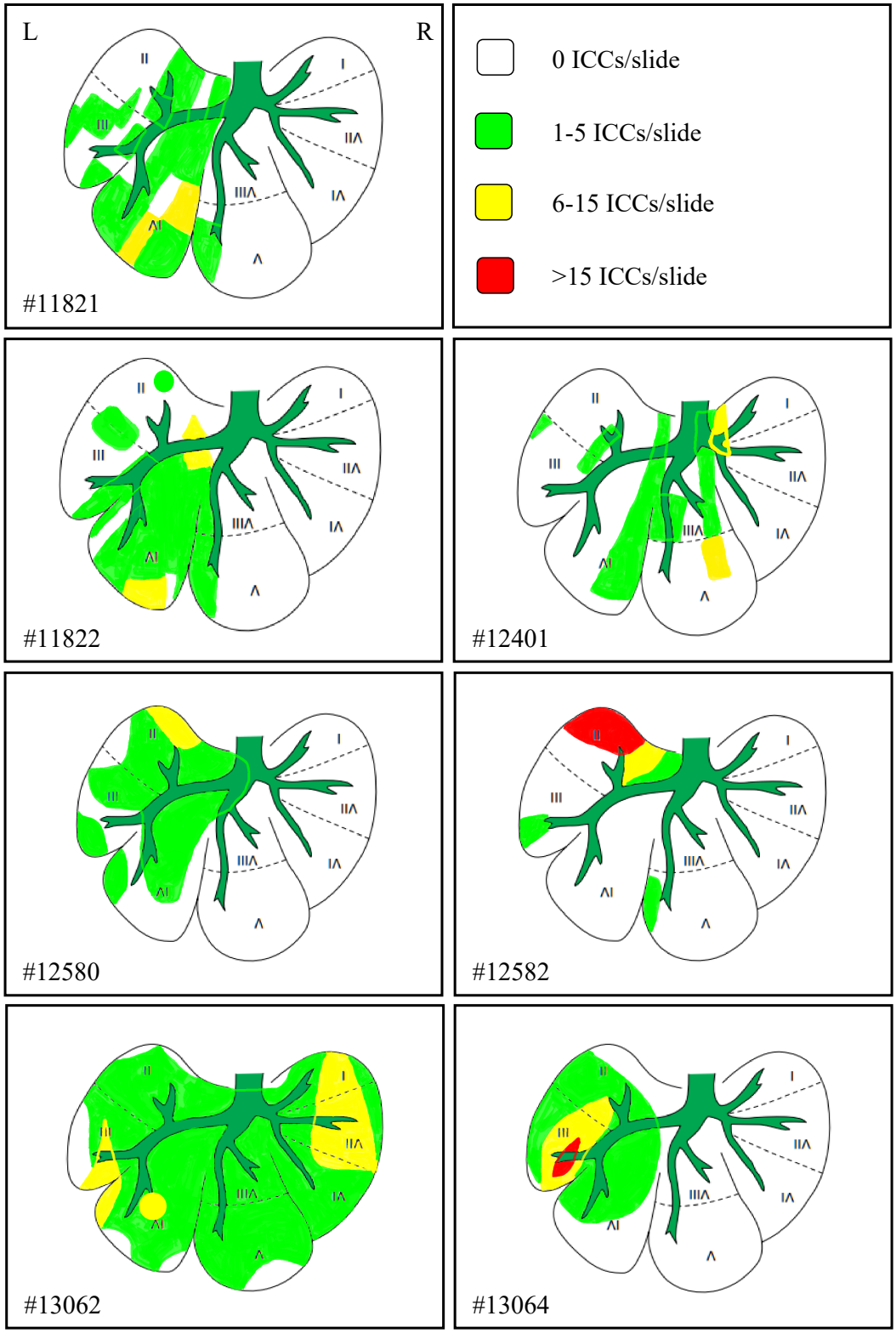

Figure 36: *Distribution and incidence of ICCs in livers of ITx pigs.*

ICCs located in left liver lobes of pigs #11821, #11822, #12580, #12582 and #13064. #12401 showed left-centered ICCs with slight right tendency. In #13062, ICCs were distributed throughout the entire liver.

Adapted from Pilz et al., 2024.

In the WT pigs, 65% ± 5.6 of the liver segments did not contain any ICCs (score 0), 30% ± 5.7 of the liver segments contained 1-5 ICCs/slide (score I) and 5% ± 0.5 of the liver segments contained 6-15 ICCs/slide (score II). No segment contained > 15 ICCs/slide (score III) **(Fig. 37A)**. In the MIDY group, 59% ± 9.0 of the liver segments had no ICCs, 31% ± 8.6 of the liver segments were classified as score I, 8% ± 1.3 as score II and 1% ± 0.7 as score III **(Fig. 37B)**. The proportion of score 0 segments was highest in both groups, although it was 1.1 times lower in the MIDY pigs. Score 0 occurred twice as often as the following score I, that was the most frequent score within the cluster-containing segments in both groups. It showed an almost identical proportion in the two groups. Reduced by a factor of 6 (WT) or 4 (MIDY) this was followed by score II slides, that were slightly more frequent in the MIDY pigs (factor 1.6). Score III only occurred in the MIDY pigs and had the lowest proportion overall.

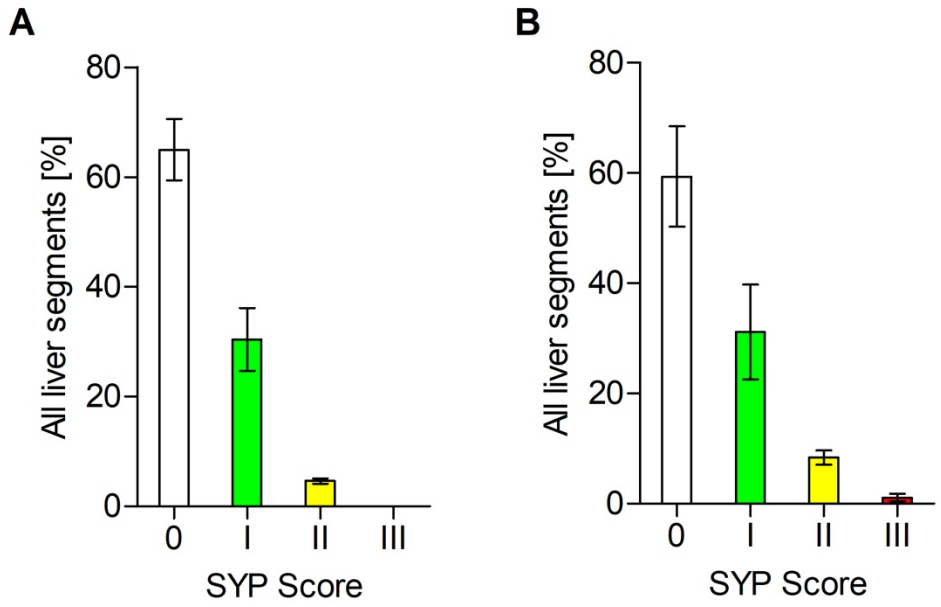

Figure 37: *Scoring of SYP+ ICCs within all liver segments..*

(A) *Scoring of SYP+ ICCs within all analyzed liver segments in WT group.* ***(B)*** *Scoring of SYP+ ICCs within all analyzed liver segments in MIDY group. Liver segments without ICCs were most common in both groups (0), followed by segments with 1-5 ICCs (I) and then segments with 6-15 ICCs (II). Liver segments with > 15 ICCs occurred only sporadically and only in the MIDY group.*

3.4. *In vivo* maturation of NPIs into pancreatic endocrine cell types

In vivo maturation of NPIs, still immature at the time of ITx, was investigated by 4-color IF staining on representative graft-bearing liver segments of the MIDY group. This staining included SYP for identification of the islet graft, INS-staining for beta cells, GCG staining for alpha cells and SST staining for delta cells. The IF stainings revealed INS+ beta cells, GCG+ alpha cells and SST+ delta cells within the individual ICCs, identified by SYP **(Fig. 38)**. This observation was true for the ICCs of all MIDY pigs in the liver sections examined. The INS+ beta cells occupied the largest area, followed by the GCG+ alpha cells and then the SST+ delta cells.

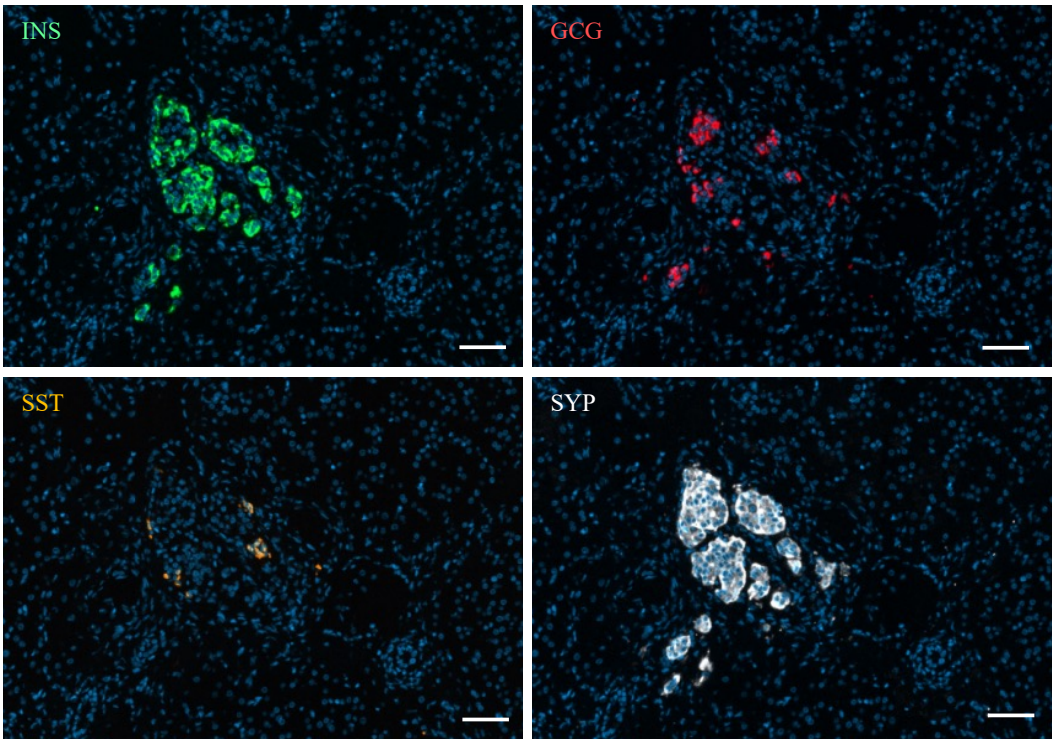

Figure 38: *4-color IF staining of INS, GCG, SST and SYP.*

Shown is a representative ICC of MIDY pig #13064. Identification of ICC by SYP staining. ICC consisted of beta cells, alpha cells and delta cells. Beta cells occupied the largest area.
Bars = 50 µm.

From Pilz et al., 2024.

3.5. Abundance and distribution of beta and alpha cells in the liver

To evaluate in more detail the distribution and abundance of endocrine cells of the islet graft in WT and MIDY group, immunohistochemical detection of INS+ and GCG+ positive cells within SYP+ slides was performed and systematically evaluated.

INS+ beta cells were detected in varying intensity in all animals. #11821, #11822, #12580, #12582, #13062 and #13064 showed strong INS+ beta cells. With #12401 only a very weak DAB signal was obtained in a few positive cells for INS **(Fig. 39)**.

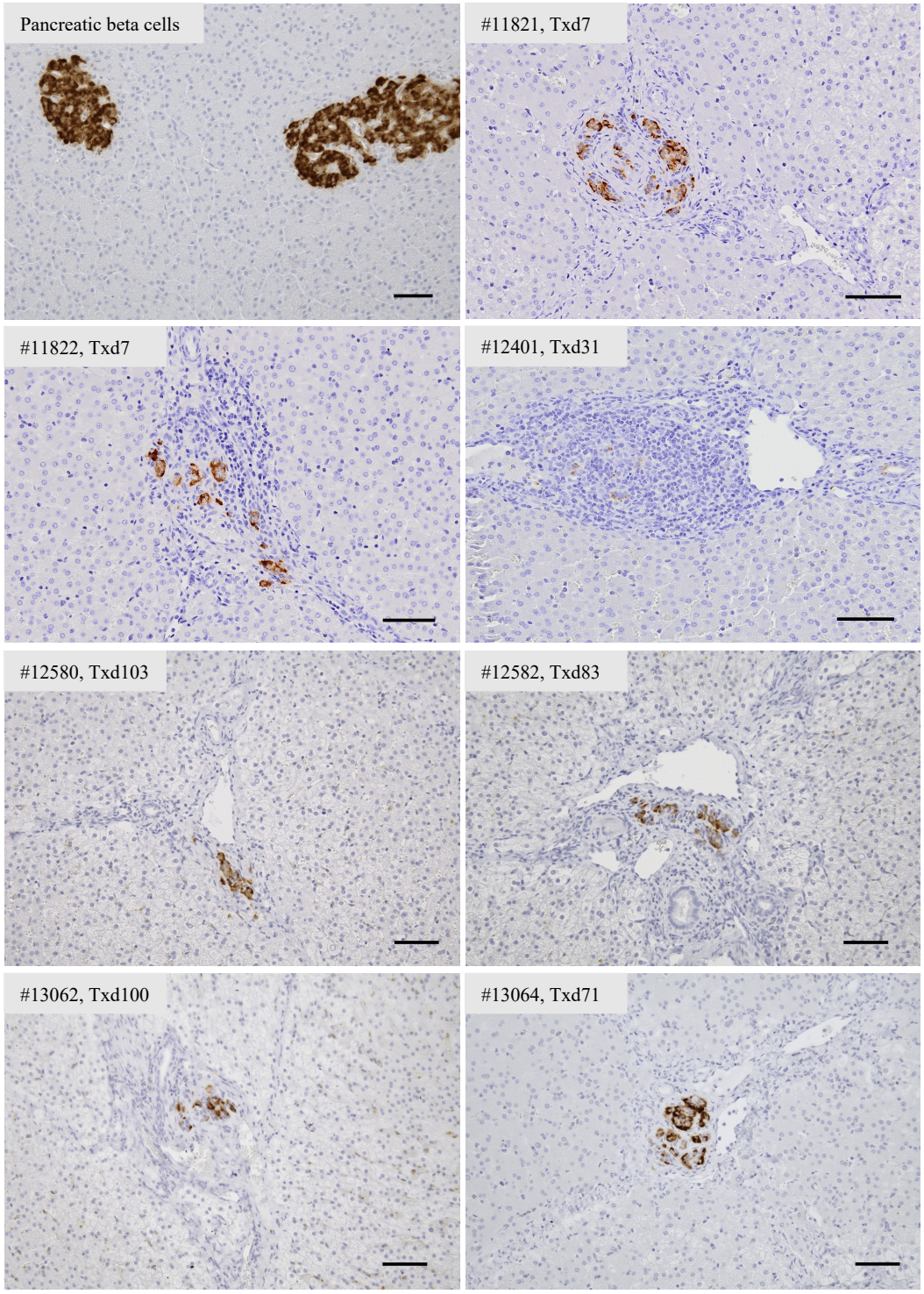

Figure 39: *Immunohistochemical staining of beta cells (INS).*

Shown are representative liver sections of each ITx pig, containing INS+ ICCs. Pancreatic beta cells are shown for reference. INS was stained in brown color, whereas nuclei were stained in purple color. Time points of tissue sampling post-ITx are indicated as Txd. Bars = 50 µm.

In the WT group, the following percentages of INS+ liver slides were found within the SYP+ liver segments: 95% (#11821), 80% (#11822), 30% (#12401) **(Fig. 40A)**. This corresponds to an average of 68% INS+ slides. In the MIDY group, there were

65% (#12580), 46% (#12582), 84% (#13062) and 81% (#13064) INS+ slides within the SYP+ segments, corresponding to an average of 69% **(Fig. 40B)**. In the WT group, #11821 had the highest proportion of INS+ slides within the SYP+ segments and #12401 the lowest, with a factor difference of 3.2. Among the MIDY pigs, the most INS+ slides were found in pig #13062 and the least in pig #12582 (factor difference: 1.8).

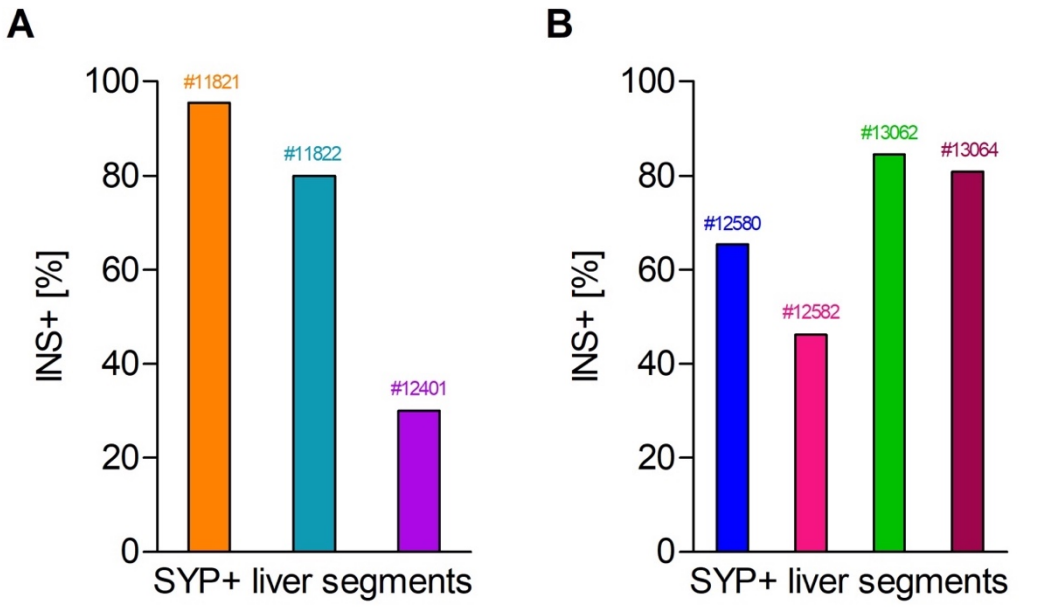

Figure 40: *Proportion of INS+ liver segments within SYP+ liver segments.*

(A) *Proportion of INS+ liver segments within SYP+ liver segments in WT group.* ***(B)*** *Proportion of INS+ liver segments within SYP+ liver segments in MIDY group.*

In the WT group, 31% ± 19.7 of the SYP+ segments contained no INS+ ICCs. 55% ± 15 contained 1-5 INS+ ICCs and 13% ± 7.7 contained 6-15 INS+ ICCs. Score III did not occur in this group **(Fig. 41A)**. In the MIDY group, 30% ± 9.0 of the slides were classified as score 0, 53% ± 9.0 as score I, 14% ± 0.8 as score II and 2% ± 1.9 as score III **(Fig. 41B)**. The sequence of the individual scores according to frequency was identical for both groups: Within the SYP+ liver segments, most slides examined for INS had score I, occurring with almost identical percentages in both groups. Next was score 0, also with almost identical percentages. This was followed by score II, again with almost the same percentage in both groups. Score III was only recorded in the MIDY group.

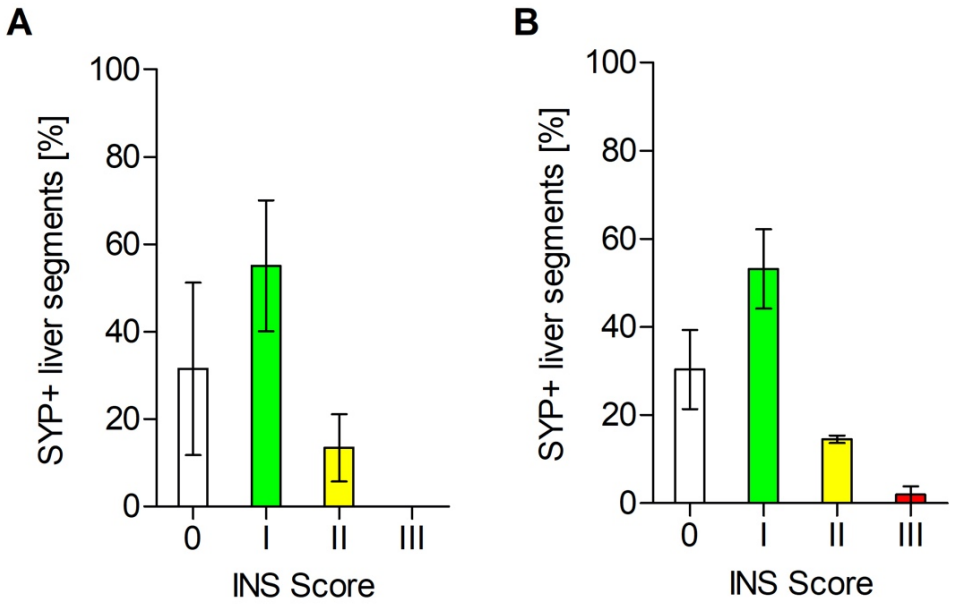

Figure 41: *Scoring of INS+ ICCs in SYP+ liver segments.*

(A) *Scoring of INS+ ICCs within SYP+ liver segments in WT group.* ***(B)*** *Scoring of INS+ ICCs within SYP+ liver segments in MIDY group.*

The immunohistochemical staining against GCG in the SYP+ liver segments identified alpha cells in all animals, showing strong staining intensity **(Fig. 42)**.

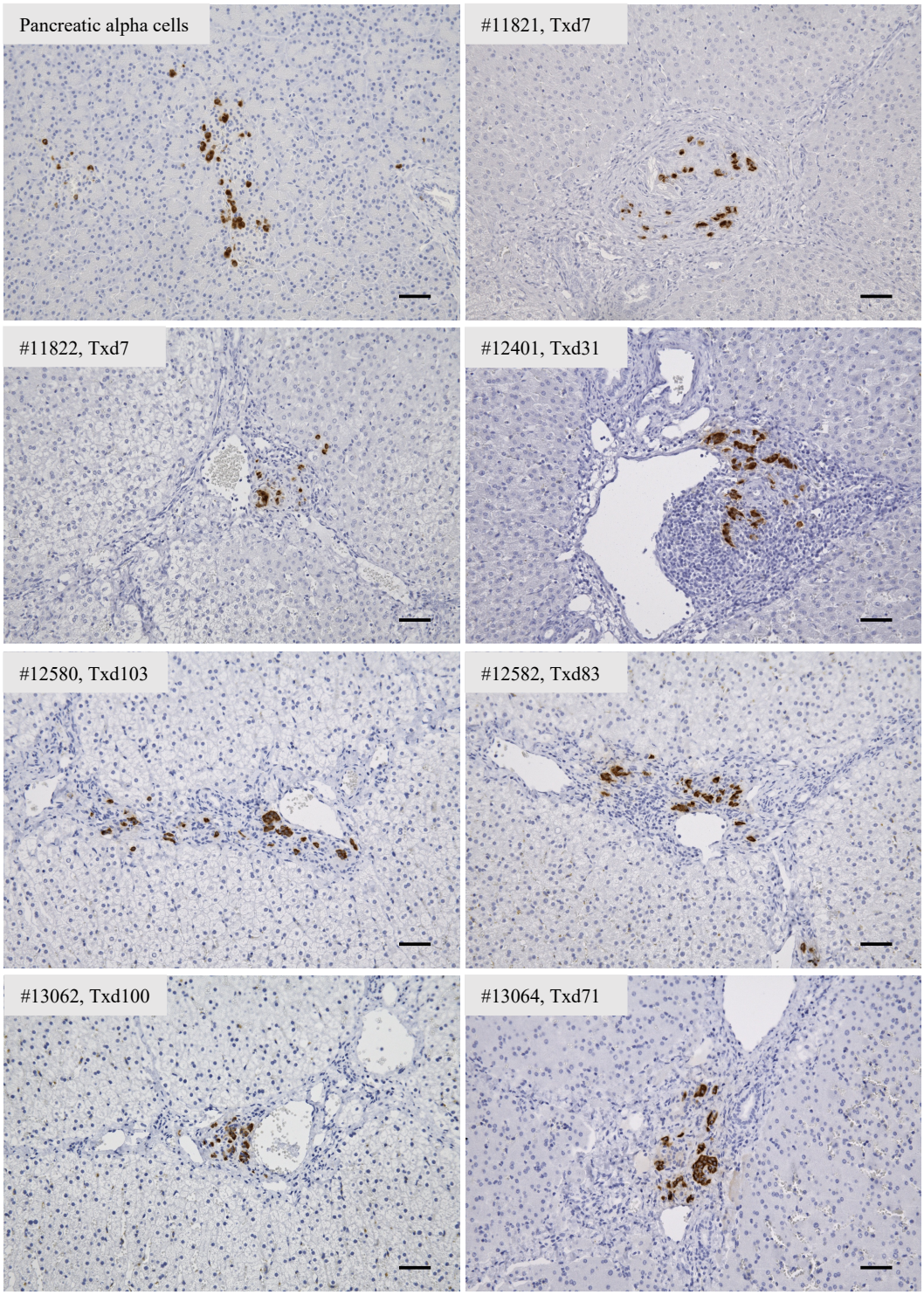

Figure 42: *Immunohistochemical staining of alpha cells (GCG).*

Shown are representative liver sections of each ITx pig, containing GCG+ ICCs. Pancreatic alpha cells are shown for reference. GCG was stained in brown color, whereas nuclei were stained in purple color. Time points of tissue sampling post-ITx are indicated as Txd. Bars = 50 µm.

The alpha cells occurred with a frequency of 95% (#11821), 87% (#11822) and 60% (#12401) within SYP+ liver segments in the WT pigs **(Fig. 43A)**, corresponding to an average of 81%. In the MIDY pigs, this was 69% in #12580

and #12582, 81% in #13062 and 77% in #13064 **(Fig. 43B)**, which corresponds to an average of 74%. The highest proportion of GCG+ slides within SYP+ liver segments was found in the WT group in the liver of pig #11821 and the lowest in #12401 (factor difference: 1.6). In the MIDY pig group, #13062 had the highest proportion of GCG+ slides compared to #12580 and #12582 with the lowest proportion (factor difference: 1.2).

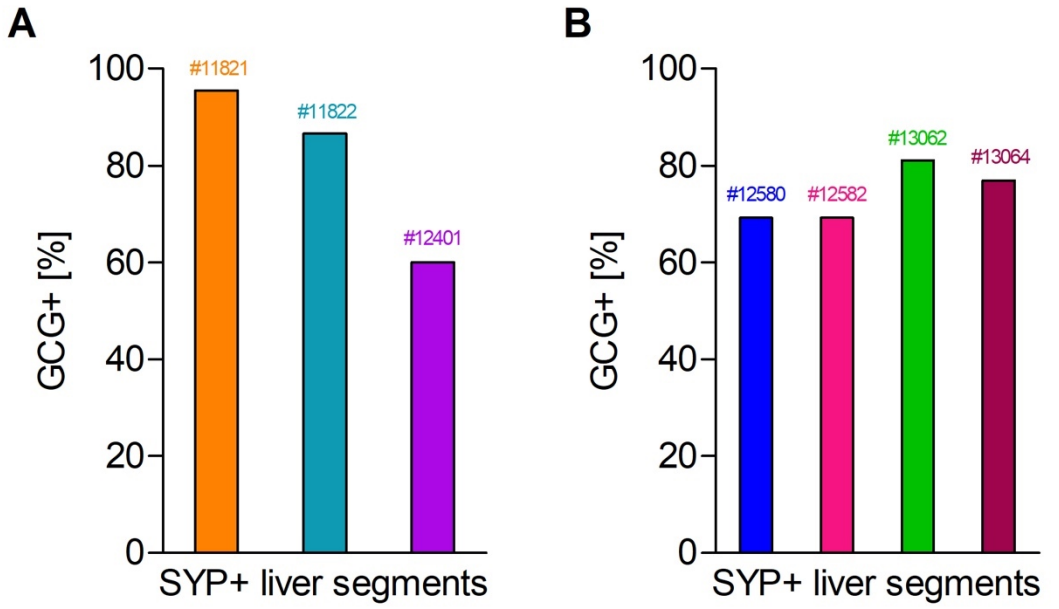

Figure 43: *Proportion of GCG+ liver segments within SYP+ liver segments.*

(A) *Proportion of GCG+ liver segments within SYP+ liver segments in WT group.* ***(B)*** *Proportion of GCG+ liver segments within SYP+ liver segments in MIDY group.*

The GCG+ clusters within the SYP+ liver segments were distributed as follows: in the WT pigs, 19% ± 10.7 score 0, 60% ± 15.1 score I and 20% ± 4.9 score II. There were no slides that belonged to score III **(Fig. 44A)**. In the MIDY pigs, 26% ± 2.3 score 0, 52% ± 10.9 score I, 20% ± 9.2 score II, and 2% ± 1.9 score III could be assigned **(Fig. 44B)**. Score I slides occurred most frequently in both groups. This score occurred 1.1 times more frequently in the WT pigs. In the WT pigs, score II came next, with almost the same proportion as the following score 0. In the MIDY pigs, score 0 was the second most frequent score, followed by score II and then score III.

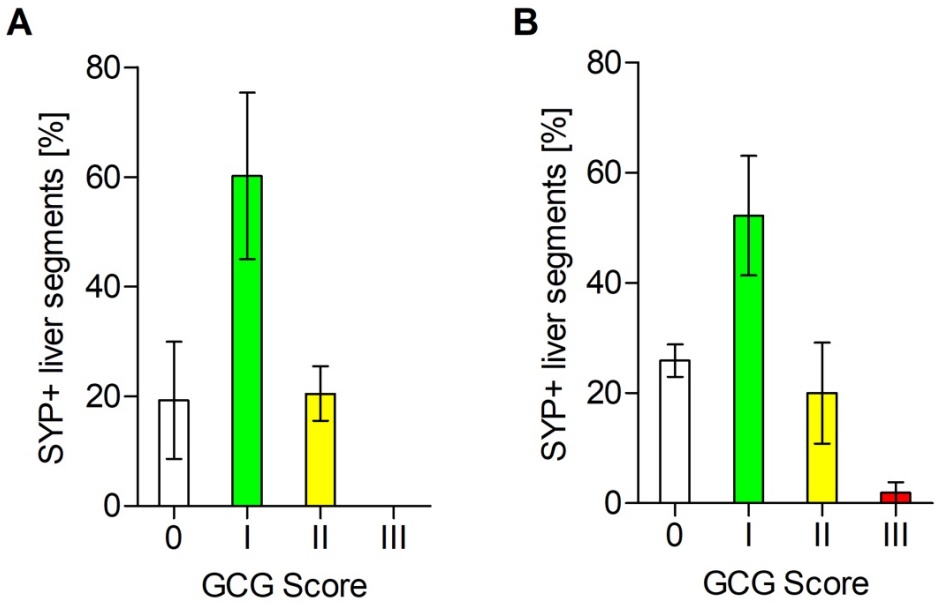

Figure 44: *Scoring of GCG+ ICCs within SYP+ liver segments.*

(A) *Scoring of GCG+ ICCs within SYP+ liver segments in WT group.* ***(B)*** *Scoring of GCG+ ICCs within SYP+ liver segments in MIDY group.*

Overall, the distribution pattern of endocrine cell types in islet transplant-containing liver segments was similar for beta cells and alpha cells and corresponded to islet occurrence in general. The only exception is #12582, in which the percentage of liver segments with 6-15 alpha cell clusters was increased. On average, GCG+ segments were slightly more common than INS+ segments in both groups (WT: 81% *vs*. 68%, MIDY 74% *vs*. 69%).

4. Characterization and quantification of the immune response in graft-bearing livers

A stepwise characterization of immune cells revealed that within the periportal cell infiltrates of the ITx pigs almost all cells stained positive for CD45 and therefore consisted mainly of leukocytes. In addition to the periportal cell infiltrates, isolated cells in the liver sinusoids also stained positive for CD45. Within the periportal CD45+ cell infiltrates, a large proportion of the cells stained positive for CD3, which is why the majority of the immune cells were identified as T cells. A smaller proportion of the CD45+ cells did not stain for CD3, which is why these cells are to be classified as other leukocytes. In addition to the periportal infiltrates, there

were also isolated CD3+ cells in the liver sinusoids **(Fig. 45)**. These staining patterns could be detected for all animals.

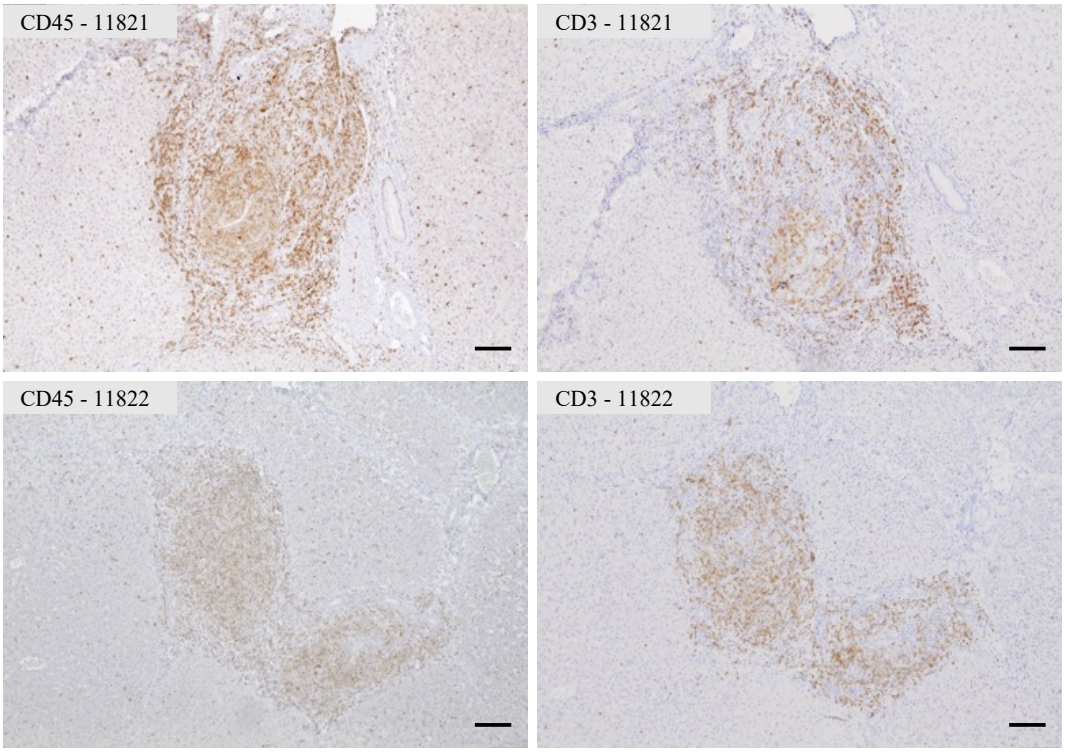

Figure 45: *Immunohistochemical staining of leukocytes (CD45) and T cells (CD3).*

Shown are identical and representative liver sections of #11821 and #11822. Majority of CD45+ leukocytes consisted of CD3+ T cells. CD45 and CD3 were stained in brown color, whereas nuclei were stained in purple color. Bars = 100µm.

The association between the appearance of CD3+ cell infiltrates and occurrence of the islet graft was investigated by immunohistochemical co-staining of CD3 and SYP in representative liver segments with high levels of SYP+ cell clusters and CD3+ cell infiltrates. The following staining patterns were identified in the analysis: (A) mostly SYP+ cells, associated with isolated CD3+ cells **(Fig. 46A)** , (B) mixed SYP/CD3 cell cluster with strong SYP staining intensity **(Fig. 46B)**, (C) mixed SYP/CD3 cell cluster with weak SYP staining intensity **(Fig. 46C)**, (D) strictly CD3+ cell cluster **(Fig. 46D)**. The staining intensity of CD3 was uniform.

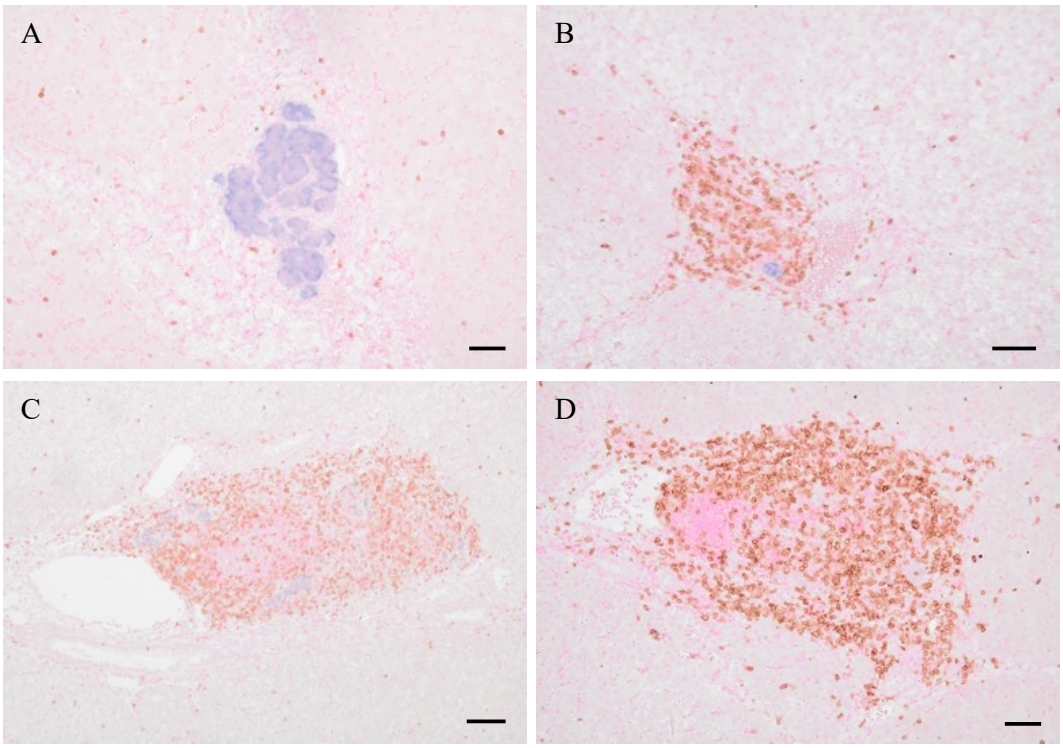

Figure 46: *Immunohistochemical co-staining of islet graft (SYP) and T cells (CD3).*

Shown are exemplary liver sections. ***(A)*** *SYP+ cell cluster with sporadic occurrence of CD3+ cells (#13064).* ***(B)*** *Mixed CD3+/SYP+ cells, strong SYP staining intensity (#11822).* ***(C)*** *Mixed CD3+/SYP+ cells, weak SYP staining intensity (#12401).* ***(D)*** *Strictly CD3+ cell infiltrate (#11822). SYP was stained in blue color, whereas CD3 was stained in brown color. Cell nuclei were stained in red color. Bars (A-C)= 50µm; Bar (D) = 100µm.*

The distribution of the staining pattern in the individual animals was as follows: In #11821, CD3+/weakly SYP+ cell clusters dominated. In #11822, the majority of cell infiltrates were stained exclusively for CD3, although some mixed CD3+/SYP+ cell clusters were detected, mainly weakly SYP+. In #12401, there was a balanced proportion of strictly CD3+ infiltrates and SYP+ clusters with mild CD3+ infiltration. In addition mixed CD3+/weakly SYP+ cell clusters were found. #12580 showed mainly SYP+ cell cluster including sporadic CD3+ cells. In addition, pure CD3+ cell infiltrates were sporadically seen. #12582 had mainly SYP+ clusters with mild infiltration of CD3+ cells. In addition mixed CD3+/SYP+ clusters occurred sporadically. Mainly strict SYP+ clusters including single CD3+ cells also occurred in #13062, in addition to two pure CD3+ accumulations. In #13064, mainly SYP+ clusters including single CD3+ cells were identified. A mixed cluster of CD3+/strong SYP+ and a pure CD3+ infiltrate were also found **(Table 25)**.

Animal ID	Predominant staining pattern of SYP/CD3 according to Fig. 46
11821	C
11822	D
12401	Mixed, no predominant staining pattern
12580	A
12582	A
13062	A
13064	A

Table 25: *Predominant staining pattern of SYP/CD3 co-staining in ITx pigs.*

50% (#11821), 87% (#11822), and 80% (#12401) of the SYP+ liver segments in the WT group contained CD3+ cell infiltrates **(Fig. 47A)**. Thus, on average, 72% of SYP+ liver segments were CD3+. #11822 had the highest proportion and 1.7x more CD3+ cell infiltrate containing liver segments than #11821 with the lowest proportion. The MIDY pigs had 46% (#12580), 38% (#12582), 67% (#13062) and 58% (#13064) CD3+ cell infiltrate containing slides within the SYP+ liver segments, respectively **(Fig. 47B)**. This corresponds to an average of 52%. The highest percentage was found in #13062 and the lowest in #12582 (factor difference: 1.8).

Overall, the WT pigs had on average a 1.4-fold higher incidence of CD3+ cell infiltrate containing liver segments than the MIDY pigs.

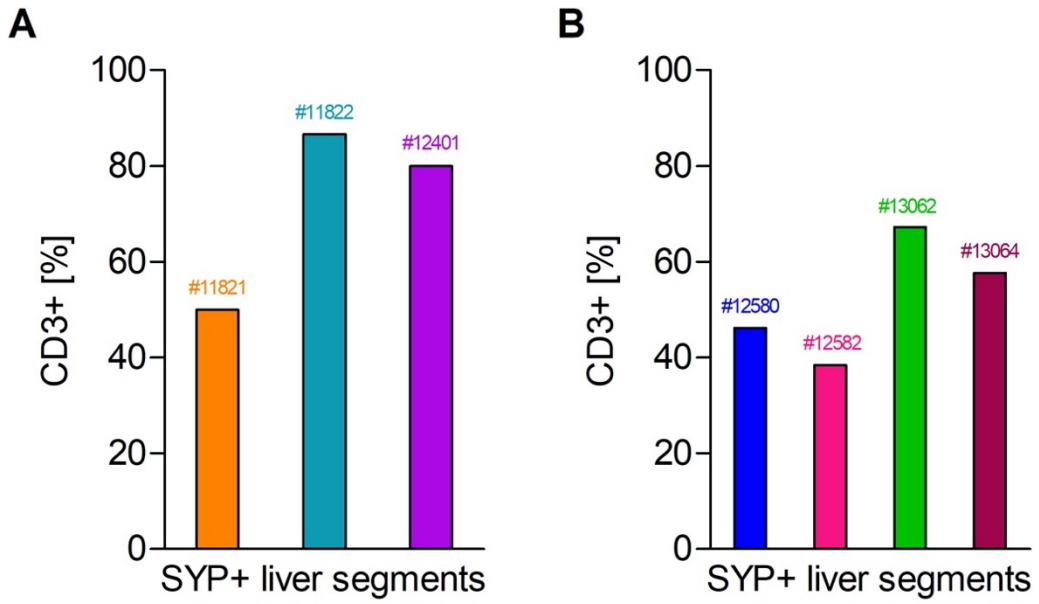

Figure 47: *Proportion of CD3+ liver segments within SYP+ liver segments.*

(A) *Proportion of CD3+ liver segments within SYP+ liver segments in WT group.* ***(B)*** *Proportion of CD3+ liver segments within SYP+ liver segments in MIDY group.*

In WT pigs, 28% ± 11.3 of SYP+ segments contained no CD3+ cell infiltrates (-), 39% ± 6.7 contained 1-5 cell infiltrates/slide (+), 24% ± 12.4 contained 6-15 cell infiltrates/slide (++) and 9% ± 8.9 contained >15% cell infiltrates/slide (+++) **(Fig. 48A).** In the MIDY group, the distribution was as follows: 48% ± 6.1 (-), 51% ± 5.5 (+), 1% ± 0.9 (++) and 0% (+++) **(Fig. 48B)**. In both groups, (+) slides occurred most frequently, followed by (-) slides, (++) slides and (+++) slides only in the WT group. The gradation from (+) slides to (++) slides occurred in the WT group by a factor of 1.6 and to (+++) slides by a factor of 2.7. In contrast, in the MIDY group, (+) slides occurred on average 51 times more frequently than (++) slides.

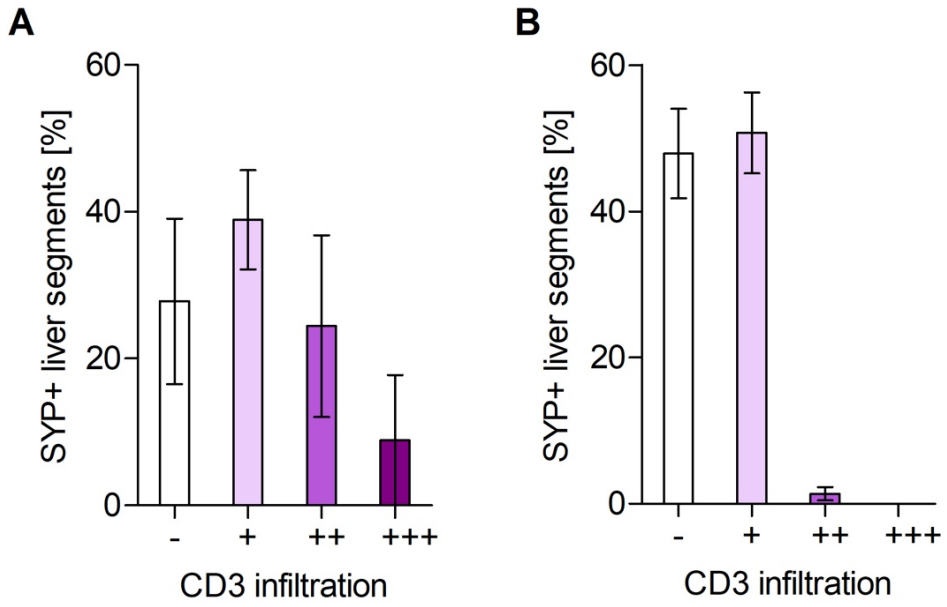

Figure 48: *Degree of infiltration with CD3+ cell infiltrates.*

(A) *Degree of infiltration with CD3+ cell infiltrates in SYP+ liver segments in WT group.*
(B) *Degree of infiltration with CD3+ cell infiltrates in SYP+ liver segments in MIDY group.*

FoxP3+ cells as a marker for regulatory T cells occurred, if then, sporadically in association with cell infiltrates. They occurred most strongly in #11822 and #12401 **(Fig. 49)**.

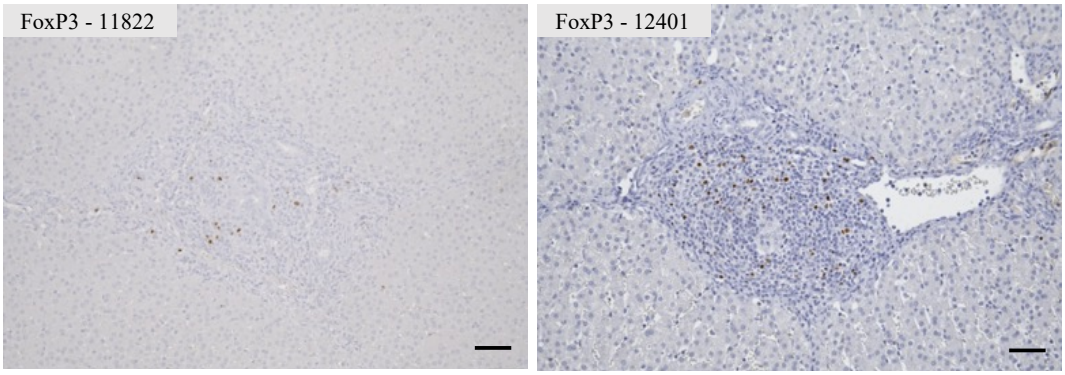

Figure 49: *Immunohistochemical staining of regulatory T cells (FoxP3).*

Sporadic occurrence of Fox P3+ cells in representative liver segments of #11822 and #12401. FoxP3+ cells were stained in brown color, whereas nuclei were stained in purple color.
Bars = 50µm.

L1/Calprotectin+ cells were identified as macrophages. The macrophages occurred mostly locally independent of the ICCs and were heterogeneously distributed in the liver sinusoids. Macrophages were found in association with CD45+ cell infiltrates only sporadically. Of note, an apparently different overall intensity of macrophages between individual liver segments and different animals was observed. #11821, for

example, showed a sporadic occurrence of macrophages in the liver sinusoids. A particularly high incidence of macrophages was observed in pig #13064 **(Fig. 50)**.

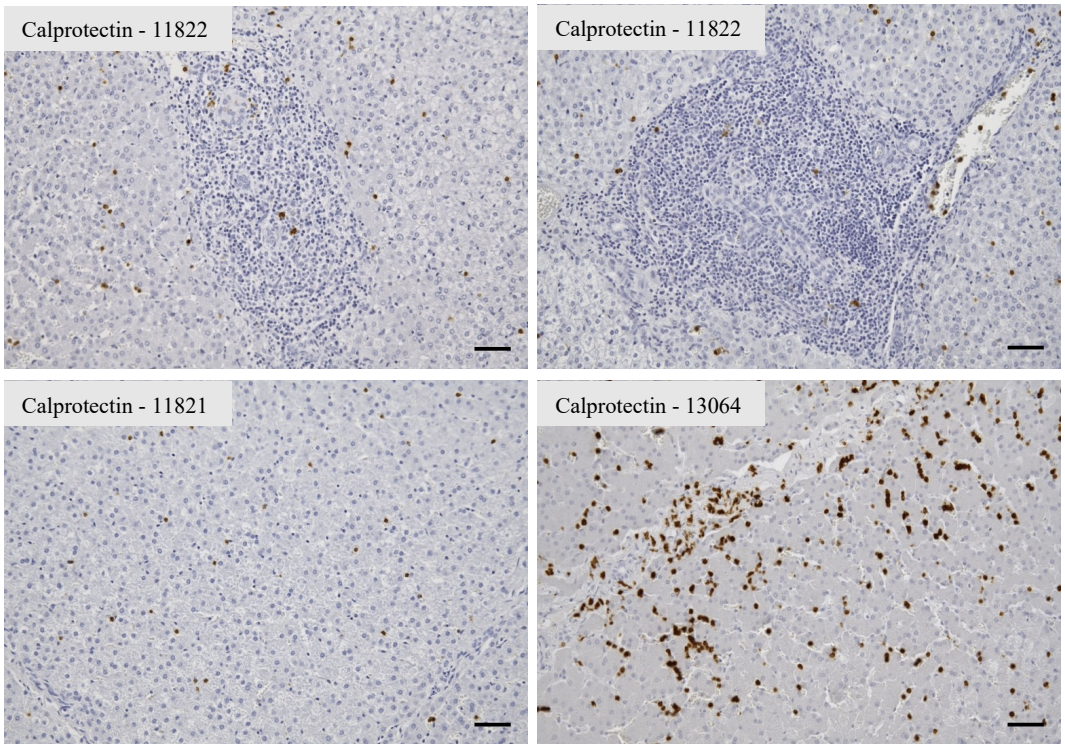

Figure 50: *Immunohistochemical staining of macrophages (L1/Calprotectin).*

(Upper row) *Mild infiltration of cell infiltrates with macrophages in representative liver segments of pig #11822.*

(Lower row) *Examples for minor presence of macrophages in liver sinusoids of liver segment 10b (#11821) and for high incidence of macrophages in liver sinusoids of liver segment 4d (#13064). L1/Calprotectin+ cells were stained in brown color, whereas nuclei were stained in purple color. Bars = 50µm.*

Macrophage detection in the WT group revealed 73 ± 6 (#11821), 134 ± 15 (#11822) and 118 ± 8 (#12401) macrophages$_{OD>0.6}$/mm^2 within the analyzed liver segments **(Fig. 51A)**. Within the analyzed liver segments of the MIDY group, there were 111 ± 8 (#12580), 146 ± 9 (#12582), 111 ± 6 (#13062), and 861 ± 80 (#13064) macrophages$_{OD>0.6}$/mm^2, respectively **(Fig. 51B)**. The mean value of 13064 deviated significantly from the mean values of the other pigs, that showed a range of 73-146 macrophages$_{OD>0.6}$/mm^2.

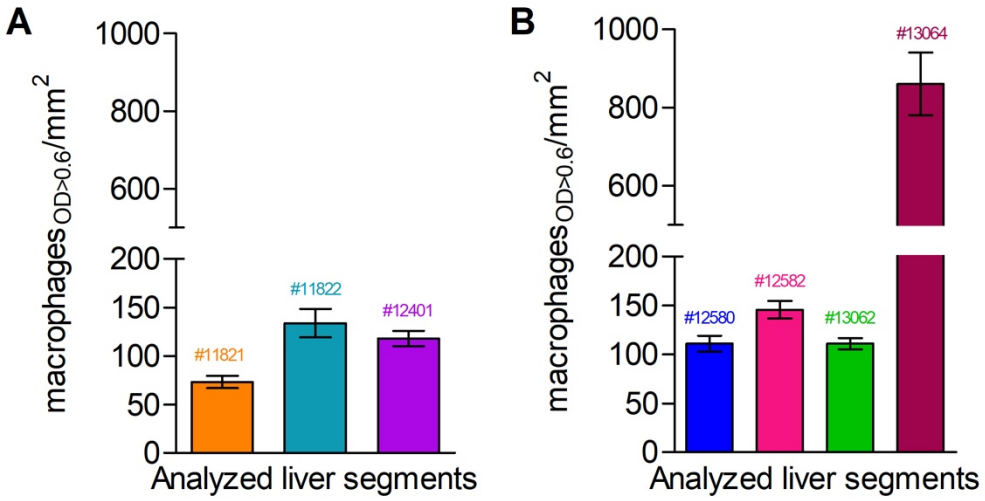

Figure 51: *Quantitative assessment of macrophages incidence.*

(A) *Macrophages$_{OD>0.6}$/mm^2 in representative liver segments of WT pigs.* ***(B)*** *Macrophages$_{OD>0.6}$/mm^2 in representative liver segments of MIDY pigs. Strikingly elevated macrophages abundance in pig #13064.*

The control group of pigs without islet transplant (n=5) had 36 ± 10 macrophages$_{OD>0.6}$/mm^2 on average, whereby the values between control WT and control MIDY pigs were all < 100 and comparable, ranging from 16 to 75. The ITx WT group had an average of 108 ± 7 macrophages$_{OD>0.6}$/mm^2 and the ITx MIDY group had an average of 307 ± 55 macrophages$_{OD>0.6}$/mm^2. Thus, the WT group had a 3-fold higher incidence of macrophages$_{OD>0.6}$/mm^2 than the control group which resulted in a P-value of 0.0015. The MIDY group had an 8-fold higher incidence of macrophages$_{OD>0.6}$/mm^2 than the control group with a p-value of 0.0003 and a 3-fold higher incidence of macrophages$_{OD>0.6}$/mm^2 than the WT group. Accordingly, the occurrence of macrophages in the liver sinusoids was significantly increased in pigs that received ITx compared to pigs without ITx. This applies to both the WT and the MIDY group, with the effect being stronger in the MIDY group. **(Fig. 52A)**.

Within the WT group, the liver sections with islet transplant had 95 ± 11 macrophages$_{OD>0.6}$/mm^2 and the liver sections without islet transplant had 121 ± 9 macrophages$_{OD>0.6}$/mm^2. Therefore, the sections without islet transplant had a slightly higher incidence of macrophages$_{OD>0.6}$/mm^2 by a factor of 1.3 **(Fig. 52B)**. The difference was not significant (p-value: 0.1).

In the MIDY group, the liver segments with islet transplant contained 263 ± 58 macrophages$_{OD>0.6}$/mm^2, while the liver segments without islet transplant contained

351 ± 94 macrophages$_{OD>0.6}$/mm^2. Thus, as in the WT group, the liver segments without islet transplant had 1.3x more macrophages$_{OD>0.6}$/mm^2 than the liver segments with islet transplant. The difference was not significant (p-value: 0.7) **(Fig. 52C)**.

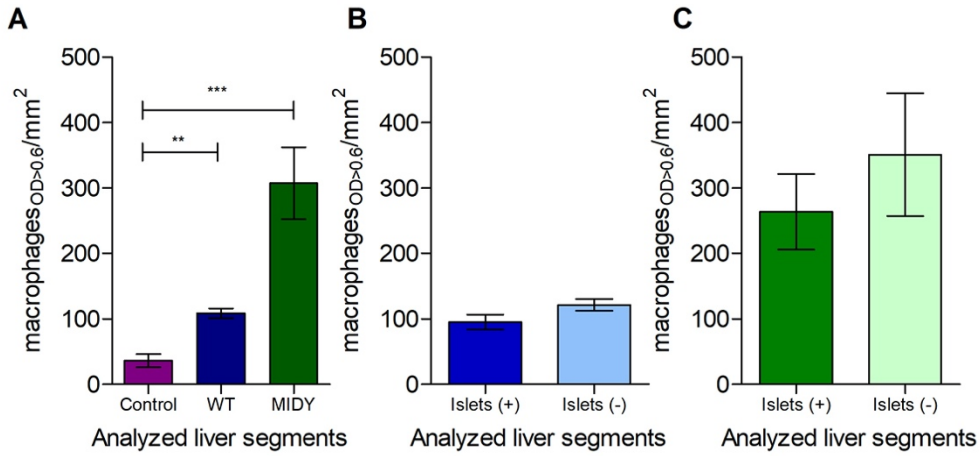

Figure 52: *Comparison of macrophages incidence.*

(A) *Occurrence of macrophages$_{OD>0.6}$/mm^2 in representative liver sections of control group, WT group and MIDY group. Significantly increased macrophages number in WT and MIDY group compared to control group without ITx. Stronger effect in MIDY group.* ***(B)*** *Incidence of macrophages$_{OD>0.6}$/mm^2 in representative liver sections with islet transplant (islets (+)) and without islet transplant (islets (-)) from WT pigs. No significant difference.* ***(C)*** *Incidence of macrophages$_{OD>0.6}$/mm^2 in representative liver sections with islet graft (islets (+)) and without islet graft (islets (-)) from MIDY pigs. No significant difference.*

VI. DISCUSSION

T1D represents a public health crisis and is increasing at an alarming rate in many nations, especially in low- and middle-income countries (GREGORY et al., 2022; GUO & SHAO, 2022). Medical and economic burden for those affected remain high, despite increased knowledge of the pathophysiology and progress in disease management and treatment (SUSSMAN et al., 2020; GUO & SHAO, 2022; reviewed in QUATTRIN, MASTRANDREA & WALKER, 2023). Intraportal ITx is an effective treatment option for restoring insulin independence and preventing severe hypoglycemic episodes in selected T1D patients. Nevertheless, there are still major challenges to this therapeutic approach that prevent its widespread clinical application, in particular the substantial loss of islet graft mass in the early phase after ITx, but also in the long term course (reviewed in GAMBLE et al., 2018; reviewed in WALKER, APPARI & FORBES, 2022).

The aim of the present study was to address this obstacle by establishing a genetically diabetic large animal model for intraportal transplantation and longitudinal monitoring of NPIs with high comparability to human ITx.

1. The pig as a suitable ITx animal model

Preclinical research in the field of ITx is mostly performed in rodent or NHP models, although their transferability to humans is limited (PILZ et al., 2023). Morphology, physiology and pathology of pancreatic islets in rodents differ from those in humans (CABRERA et al., 2006; RODRIGUEZ-DIAZ et al., 2011b; RODRIGUEZ-DIAZ et al., 2011a; reviewed in ARROJO E DRIGO et al., 2015). In addition, rodent models are of limited value when it comes to the development of clinically applicable imaging techniques of islet grafts, due to their small body size. NHPs largely show similarities with humans in terms of the structure and function of pancreatic islets (reviewed in ARROJO E DRIGO et al., 2015). However, they have a considerably higher insulin requirement/kg BW for proper glycemic control compared to humans, due to different eating habits and dietary energy requirements (GRAHAM et al., 2011; reviewed in COE, MARKMANN & RICKERT, 2020).

The pig is particularly well suited as an animal model for ITx, as it shares many similarities with humans in terms of anatomy and physiology, as well as having a similar pancreatic system and similar glucose metabolism. Furthermore, porcine insulin varies from human insulin by just a single amino acid (reviewed in WOLF et al., 2014; reviewed in ZETTLER et al., 2020). In addition, the adequate body size enables research into imaging procedures with great translational value. Resembling MIDY in humans, transgenic *INS*^{C94Y} pigs show a stable diabetic phenotype without further intervention, which is why they are particularly well suited for ITx studies (RENNER et al., 2013).

2. Establishment of intraportal allotransplantation of NPIs

The first objective of the present study was to establish a novel intraportal allotransplantation model in pigs using NPIs.

PIPIT was successfully performed in all recipient pigs of the present study. Since the minimally invasive transplantation procedure overall did not lead to any undesirable side effects, PIPIT turned out to be a safe and reproducible method. It is remarkable, that relatively small IEQ quantities of ~3.0k-15k IEQs NPIs/kg BW were used for ITx, with the majority of the pigs receiving clearly below 10k IEQs/kg BW. For comparison, >300 IEQs of adult mouse islets are used for intrahepatic allotransplantation in mouse models (reviewed in CANTARELLI et al., 2013), corresponding to at least 10k IEQs/kg BW, assuming a mouse BW of 30g. 25k IEQs/kg BW are usually used for allotransplantations in NHPs (reviewed in COE, MARKMANN & RICKERT, 2020). In xenotransplantation studies, 100k IEQs/kg BW APIs and a range of 9.6k-115k IEQs/kg BW NPIs are reported to be used for NHP trials (SHIN et al., 2017; GAO et al., 2021; HAWTHORNE et al., 2022). These differences in the amount of IEQs required can be attributed to the different metabolic demands, with pigs having the lowest glucose-induced insulin response compared to humans and especially compared to NHPs (GRAHAM et al., 2011). An ITx animal model in which smaller quantities of IEQs are required, is to be welcomed, as this can reduce the number of animals used for the experiments in line with the 3Rs (Replacement, Reduction, Refinement) (reviewed in LEWIS, 2019). The range of transplanted IEQs used for ITx in this study results from the variation in the recipient pigs BW and variable NPI yield in the individual

isolations. Since intraportal ITx in pigs had never been tested before, the amount of NPI IEQs/kg BW was not standardized. Instead, a broader range of islet dosages was tested to assess efficacy in normalizing blood glucose. In this context, it was encouraging, that in a NHP ITx study a range of 9.6k-56.9k IEQs NPIs/kg BW led to reliable glycemic control (HAWTHORNE et al., 2022).

The animals showed no disturbances in their general condition after the procedure. However, intermittent diarrhea occurred in the MIDY group in three pigs, which were subjected to long-term observation, finally leading to weight loss. This could not be observed in the WT group, which only had a short experiment duration. Weight loss and diarrhea are known to be one of the main side effects associated with chronic immunosuppressive treatment in ITx studies in humans and NHPs (HIRSHBERG et al., 2003; GRAHAM et al., 2022; HAWTHORNE et al., 2022). Compared to the WT group, the MIDY group showed a higher degree of compliance with oral immunosuppressant intake, particularly with TAC. The considerably more reliable drug intake by the MIDY pigs was helped by the fact that two ITx recipient pigs were kept in parallel in one group, which promoted drug intake due to feed envy. In addition, the MIDY pigs are more accustomed to human handling and therefore more trusting than WT pigs due to the blood glucose measurements that begin at piglet age. TAC levels of 5-15 µg/ml (trough levels) are considered suitable target concentrations for effective immunosuppression in pigs (equivalent to 5-15 ng/ml) (JENSEN-WAERN, KRUSE & LUNDGREN, 2012). The two pigs most affected by diarrhea had final trough levels of TAC that exceeded the recommended serum concentration of 5-15 ng/ml. A connection between the symptoms and chronic immunosuppression is therefore plausible. However, diarrhea in pigs is considered a multifactorial symptom, so that, for example, pathogens, dietary factors or stress may also have been involved in the pathogenesis (reviewed in PANAH et al., 2021). Interestingly, pig #13064, which had a very reliable TAC intake, was not affected by chronic diarrhea or weight loss. However, there is no final TAC trough value available for this animal, making it challenging to definitively assess whether it reached a sufficient therapeutic level, given the distinct inter- and intraindividual differences in TAC pharmacokinetics (THONGPRAYOON et al., 2020). This underlines the importance of close monitoring of TAC trough levels in order to ensure the drug’s efficacy and at the

same time to prevent overdosing. This could only be implemented to a limited extent in this study, as successful blood sampling was challenging with awake and non-fixed pigs; thus, it was primarily conducted on anesthetized animals. However, the timepoint of anesthesia, required for PET/CT assessments did not necessarily allow trough levels to be obtained.

A short-term effect of PIPIT on the liver function parameters could be observed in some of the pigs, likely indicating hepatocyte damage during ITx. Zhang et al. reported in this context, that the increase in AST after ITx in human patients depended on the volume of the transplanted islet tissue and therefore also on the purity of the islets, since they influenced the extent of the liver injury (ZHANG et al., 2019). This is in line with the observation that pig #13064, which received the highest graft mass within a comparable restricted liver area, was the only one with an increased blood AST value after PIPIT. In this pig an increased AST level seemed to be associated with diminished ITx outcome, probably attributed to liver injury that impaired engraftment. However, there were no reference values taken before the procedure that would definitively confirm PIPIT as the cause of the elevated liver parameters. Increased AST, AP, and GGT values observed in blood samples taken shortly after the intervention, normalized spontaneously during the post-ITx observation period.

A long-term impact of ITx on liver function parameters was mainly evident in the AST levels. An increase in AST within four weeks post-ITX occurred in two WT pigs, one of them with spontaneous recovery; this pig also exhibited an increased ALT and GGT level. After more than one month post-ITx, two MIDY pigs showed a continuous increase in AST. Rafael and coworkers investigated the development of liver enzymes in 42 ITx patients within 40 days after ITx. It can be summarized, that there was a significant increase in AST and ALT levels in > 50% of the patients within the first four weeks post ITx. AP increased to a lesser extent (12% of the transplantations). In 90% of the recipients, the values normalized spontaneously within the first four weeks and no correlation with graft characteristics and function was found (RAFAEL et al., 2003). An increase in AST and ALT with spontaneous recovery within one month post-ITx was also reported in other human ITx studies (MALOSIO et al., 2015; AHN et al., 2018). The transient increase in liver enzymes may be attributed to hypoxic injury of presinusoidal hepatocytes following islet

infusion, as well as to cell damage caused by local inflammatory reactions, particularly involving innate immunity (IBMIR). Furthermore, a possible explanation for elevated transaminase levels that do not recover spontaneously could be indirect damage to the hepatocytes due to the toxicity of immunosuppressive drugs (RAFAEL et al., 2003; AHN et al., 2018). Because of the different time courses and development of AST increases in the WT and MIDY group, different pathogenetic mechanisms appear to be involved. The WT pigs had a short-term, partially self-limiting transaminitis, which indicates a hypoxic and/or inflammatory damage to the hepatocytes early after ITx. In contrast, the MIDY pigs had a delayed but progressive increase in AST levels. Therefore, in this case, chronic, progressive damage to the hepatocytes, e.g. by the immunosuppressants, is more likely, especially in view of the final elevated trough levels of TAC in these two pigs.

The interpretation of the CRP values is complicated by the fact that there is no official CRP reference frame for pigs. Previous studies in human patients with allogeneic ITx and in NHPs after xenogeneic ITx of porcine islets have described that CRP as a standard marker for inflammatory processes can increase transiently in the blood after ITx or can be detected immunohistochemically (MALOSIO et al., 2015; MAFFI et al., 2019; MIN et al., 2018; GRAHAM et al., 2022). In the case of immunohistochemical detection of CRP, this was not limited to the xenograft but could also be detected in the kidney, from which it was concluded that a systemic inflammatory process was present. CRP levels correlated with the occurrence of severe side effects, like weight loss and diarrhea, while liver enzymes remarkably remained within a range of twice the baseline value (GRAHAM et al., 2022). In the present study, there were two outliers in the measured CRP values, both in pig #13064, indicating the presence of a chronic, systemic inflammatory process. Contrary to the results from the study of Graham and coworkers no correlation between elevated CRP levels and severe side effects was found in this pig. At the same time, the pigs in which side effects occurred did not show any striking CRP values. The exact cause of the elevated CRP levels in pig #13064 remained unclear.

Overall, the analysis of the blood samples provided important initial insights into the influence of ITx and drug treatment regime on liver function and inflammation parameters in pigs. Systematic and more intensive sampling would have been

important for more in-depth findings, a consideration that should be taken into account in future studies.

3. Intraportal transplantation of NPIs cures diabetes of genetically diabetic pigs

The second objective of the present study was to implement the novel established porcine islet allotransplantation model in genetically diabetic *INS*^{C94Y} transgenic pigs.

All MIDY pigs developed insulin-dependent diabetes mellitus before ITx. In three pigs, a quantity of 3.3k-9.7k IEQs NPIs/kg BW was sufficient to cure the diabetic symptoms and lower the need for exogenous insulin after 5-10 weeks. Two pigs reached complete independence from exogenous insulin. Therefore, the range of 3k-10k IEQs/kg BW appeared to be an effective amount of NPIs for reliable glycemic control in this allotransplantation model.

Transplantation of APIs led to immediate normalization of blood glucose levels in STZ-induced diabetic NHPs (SHIN et al., 2015). In contrast, the NPIs were not yet mature at the time of transplantation, so *in vivo* maturation and volume expansion was essential to achieve critical mass of the islet graft before the recipients' blood glucose levels normalized. The time span in which effects on blood glucose and finally normoglycemia occurred and the amount of exogenous insulin was reduced varied between the pigs. A maturation period until the onset of glycemic control with individual variation between recipients was also observed when NPIs were transplanted into STZ-induced NHPs. NHPs showed a comparable range of days to discontinue insulin (20-189 days) as observed in the pigs in the present study (16-100 days) (HAWTHORNE et al., 2022). Remarkably, in pig #13064, which received the highest amount of IEQs, neither normoglycemia occurred nor could the exogenous insulin dose be reduced. It can therefore be concluded that, similar to observations in NHP ITx models, there is no direct correlation between the amount of IEQs NPI/API transplanted and the achievement and maintenance of glycemic control (SHIN et al., 2015; GAO et al., 2021; HAWTHORNE et al., 2022). This can be attributed to the fact that many factors can interfere with proper engraftment, e.g. inflammation, especially IBMIR, hypoxic graft damage or

allogeneic immune rejection (reviewed in SUSZYNSKI, AVGOUSTINIATOS & PAPAS, 2014; reviewed in WALKER, APPARI & FORBES, 2022). Inflammation is generally considered an important cause of islet damage and loss in the pre-, peri-, and post-ITx period (reviewed in KANAK et al., 2014). Although elevated CRP levels after diagnosis of T1D do not appear to have an aggravating effect on islet destruction and beta-cell loss, but rather reflect insulin resistance (SCHÖLIN et al., 2004) the chronic inflammatory state of pig #13064 might have had a negative impact on engraftment and thus prevented the development of normoglycemia. However, the exact effect of elevated CRP levels on the function of intraportal islet grafts has not yet been researched.

4. Increased hepatic uptake of [^{68}Ga]Ga-DOTA-Exendin-4 in PET/CT imaging after islet transplantation

The third objective of the present study was to test the feasibility of [^{68}Ga]Ga-DOTA-Exendin-4 PET/CT imaging for longitudinal, morphological imaging of intraportal islet grafts.

The fate of intraportal islet cell grafts after transplantation remains largely unclear, and is limited to functional parameters, that can only indirectly illustrate BCM (JANSEN et al., 2023). Therefore, there is an urgent need to establish non-invasive longitudinal imaging procedures of the islet graft. To date, there are only a few clinical studies on islet graft imaging in human patients. Malosio and coworkers conducted MRI on four human patients who received superparamagnetic iron oxide (SPIO)-labelled islets intrahepatically. The islet graft appeared as hypointense areas distributed within the liver parenchyma on MRI. There was a significant decrease of hypointense spots in the early post-ITx phase, indicating early graft loss, also described by Saudek and coworkers (SAUDEK et al., 2010). Although slowing down, the amount of detectable hypointense spots decreased further from one month post-ITx, while functionality of the islet graft was preserved, questioning its suitability for long-term islet graft monitoring (MALOSIO et al., 2015). A MRI study by Toso and coworkers also found no correlation between islet graft function and MRI signal. Furthermore, concomitant i.v. iron therapy or a spontaneous high liver iron content hindered the MRI signal and a high inter-individual variability of the hypointense spots counted was reported (TOSO et al., 2008). There was also no

correlation between the number of transplanted islets and the appearance of hypointense spots (TOSO et al., 2008; SAUDEK et al., 2010). Another limitation of the MRI imaging approach is, that SPIO-MRI cannot distinguish between viable and dying cells nor between single islets or multiple islet clusters (reviewed in ARIFIN & BULTE, 2021), limiting its potential for quantification of BCM. Furthermore, islets have to be labelled with SPIO prior to ITx and therefore the application for long-term monitoring of islet graft fate by SPIO-MRI is limited.

Tracing of islets by PET/CT can be achieved e.g. by [^{18}F]-fluorodeoxyglucose ([^{18}F]FDG)-labelling of islets shortly prior to ITx, followed by dynamic PET/CT after ITx (ERIKSSON et al., 2009). This approach provides important information about the islet distribution within the liver, as well as the actual amount of islet mass transplanted, based on the comparison of administered radioactivity and radioactivity detected directly after ITx. In this way, it was found that islets were distributed broadly and heterogeneously in the liver and accumulated multifocally. Furthermore, it was demonstrated that the radioactivity directly after ITx corresponded to only 53% of administered radioactivity or didn't reach the expected level. From this it can be concluded that approximately half of the transplanted islets were lost within minutes (EICH, ERIKSSON & LUNDGREN, 2007; ERIKSSON et al., 2009). Pre-labeling of islets with subsequent PET/CT examination can therefore be an important tool for real-time measurement of islet survival and distribution. However, it cannot provide information about long-term survival of islet grafts due to the half-life of [^{18}F]FDG (109.8 min) (ERIKSSON et al., 2009).

Another PET/CT radiotracer tested by Eriksson and coworkers in a clinical study with eight ITx patients, is the serotonin precursor [^{11}C]5-hydroxytryptophan ([^{11}C]5-HTP), that can be used as a clinical routine marker for beta cells. In this study, a correlation between hepatic uptake of [^{11}C]5-HTP and islet graft functionality was established, confirming the potential of *in vivo* targeting of islet grafts with beta-cell specific PET/CT radiotracers (ERIKSSON et al., 2016).

Since GLP-1R analogs such as exendin-4 bind specifically to the GLP-1R, which is highly enriched on beta cells, their use promises to be a valuable tool for *in vivo* nuclear medicine imaging of transplanted islets and quantification of BCM (TORNEHAVE et al., 2008; reviewed in CHEN et al., 2022). In rodent models

using Indium-111-exendin, *in vivo* SPECT imaging demonstrated the binding of radiolabeled exendin to pancreatic beta cells with a high correlation between pancreatic tracer uptake and BCM (BROM et al., 2014). Furthermore, a correlation between Indium-111-exendin tracer uptake of i.m. allo-transplanted islets and BCM of the islet graft could be confirmed by *in vivo* SPECT imaging in mice (ETER et al., 2017). Gallium-labelled exendin-4 can also bind to porcine GLP-1R which was recently demonstrated in the study of Lindheimer and coworkers (LINDHEIMER et al., 2023). In this study, porcine islet grafts were successfully imaged in mice by [^{68}Ga]Ga-Exendin-4 PET/CT. Imaging was performed at the time point when STZ-induced diabetic NSG mice reached normalization of blood glucose levels after i.m. xenotransplantation of WT NPIs. The high clinical relevance of targeting the GLP-1R for PET/CT imaging of transplanted islets was also demonstrated in a recently published proof-of-concept-study by Jansen and coworkers (JANSEN et al., 2023). In this study the hepatic uptake of [^{68}Ga]Ga-NODAGA-Exendin-4 in hotspot regions was significantly increased in T1D patients with a functional islet graft (n=9), compared to a T1D control group without islet transplant (n=4) (median 0.55 vs. 0.43). No correlation between tracer uptake and transplanted IEQ quantity or functional parameters was found in this study.

In the present study, longitudinal PET/CT imaging of intraportal islet cell transplants was performed for the first time in a genetically diabetic pig model. In contrast to the proof-of-concept study by Jansen et al., which included one PET/CT assessment per ITx recipient, up to four [^{68}Ga]Ga-DOTA-Exendin-4 PET/CT examinations per ITx recipient pig were performed in the present study, including a baseline measurement. In this way, it was possible to obtain information about development and changes of the PET/CT signal within a recipient over time. An increase in the hepatic uptake of [^{68}Ga]Ga-DOTA-Exendin-4 with the onset of glycemic control as an indicator for *in vivo* maturation of the NPIs was expected.

The baseline imaging of the ITx recipient pigs confirmed a low liver signal at background levels and showed a distinct signal in the pancreas. The strong signal in the kidneys as excretory organs illustrates the need for a large animal model when abdominal organs are the imaging target, as otherwise signal overlaps can occur (LINDHEIMER et al., 2023). The binding of [^{68}Ga]Ga-DOTA-Exendin-4 to

porcine pancreatic beta cells with only weak background signal in the liver was an important prerequisite for the imaging of the intraportal islet graft.

Imaging of MIDY pigs after ITx revealed a gradual intensification in liver signal over time, manifesting as a multifocal hotspot pattern, consistent with observations from SPIO-MRI, [^{18}F]FDG PET/CT, and [^{68}Ga]Ga-NODAGA-Exendin-4 PET/CT studies mentioned above. In addition, there was a constant and significant increase in both the whole-liver SUV and the hotspot-liver SUV for three pigs. In other studies (ERIKSSON et al., 2016; JANSEN et al., 2023), the hotspot-liver SUV analysis was preferred to the whole-liver SUV analysis in order to avoid a "dilution effect" of the liver tissue on the signal generated by the islet transplant. In contrast, the findings of the present study demonstrated that the increasing trend of SUV over time was clearly pronounced and largely comparable for both evaluation methods. Furthermore, a clear temporal and qualitative association was observed between the increase in liver SUV and the extent of glycemic control. This also applies to the pig #13064, which showed practically no increase in SUV and was the only one that did not exhibit a reduction in blood glucose, indicating insufficient engraftment. Similar to the study of Jansen et al., no correlation between the amount of IEQ transplanted and the hepatic uptake of the radiotracer was observed in this study either, which corresponds to the findings from the [^{18}F]FDG PET/CT study, confirming high graft loss in the early post-transplant period.

The main limitation of the PET/CT imaging approach in general is that the spatial resolution of clinical PET/CT devices is usually 3-4 mm, which is why imaging of individual ICCs that are at least ten times smaller is not possible due to technical limitations. With regard to the present study, the identification of ICCs was complicated by the fact, that the total volume of islet graft required to cure diabetes was vanishingly small compared to the volume of the entire liver. Another limitation is, that although the SUVs harmonized with the clinical development of the ITx recipients, no direct correlation between SUV and BCM could be established in this study. In this context, the present study would have benefited from detailed analysis of the cell surface GLP-1R abundance of the transplanted islets, which was not possible due to the lack of species reactivity of numerous anti-GLP-1R antibodies tested. An antibody that was used in the past to detect GLP-1R on porcine beta cells is no longer available (RENNER et al., 2010). However,

preclinical validation studies confirmed, that exendin uptake linearly correlates with BCM without being impacted by inflammatory conditions (BROM et al., 2014; BROM et al., 2015; BROM et al., 2018; JOOSTEN et al., 2019; JANSEN et al., 2023). This emphasizes, that the changes in the pigs' liver SUVs harmonized with changes in viable BCM.

5. *In vivo* maturation of NPIs into all pancreatic endocrine cell types required for glycemic control

The fourth objective of the present study was to histologically prove clinical ITx outcome by characterization of islet graft properties.

Histologic examinations confirmed the presence of well-engrafted ICCs in the livers of all ITx recipient pigs, and there was largely a link between the amount of IEQs/kg BW transplanted and the proportion of ICC-containing liver segments. Interestingly, the two animals in which this linear relationship did not apply had the most condensed distribution of ICCs and, in contrast to the other pigs, had liver segments with more than 15 ICCs/slide. This could explain the relatively lower proportion of liver segments containing ICCs. Of note, the combination of a very low relative amount of islet graft in the large recipient's liver and the heterogeneous distribution of ICCs complicates the absolute quantification of graft mass through stereological analyses. The broad distribution of transplanted islets throughout the liver was consistent with observations from other ITx studies (EICH, ERIKSSON & LUNDGREN, 2007; ERIKSSON et al., 2009). Final engraftment localization of ICCs was depended on the Tx site. When islet grafts were identified within liver segments, the majority contained a maximum of five ICCs per slide. This illustrates the heterogeneous, sporadic occurrence of ICCs and at the same time proves the difficulty of histologic examination of ICCs in human patients obtained by liver needle biopsy, that is complicated by low pick-up rates (TOSO et al., 2009; KIM et al., 2020b). Remarkably, liver segments with more than 15 ICCs occurred only in the long-term group, emphasizing the *in vivo* proliferation capacity of NPIs at appropriate maturation time (KLYMIUK et al., 2016). Of note, *in vivo* maturation of the transplanted NPIs occurred into beta, alpha, and delta cells within individual ICCs, resembling the mature islets of Langerhans in the pancreas. This is of great importance as proper glycemic control requires a fine interplay of the hormones

INS, GCG and SST, produced by these endocrine cell types (reviewed in JOHNSON & JONES, 2012).

The considerable proportion of INS+ liver segments within the islet graft containing liver segments confirmed insulin secretion by transplanted beta cells and harmonizes with the restoration of glycemic control in three diabetic recipient pigs. The occurrence of INS+ beta cells also in the short-term experiment group can be explained by the fact, that ICCs already contain insulin producing beta cells at the time of ITx (KORBUTT et al., 1996). The progressive increase of glycemic control in the MIDY pigs reflects *in vivo* proliferation, differentiation and maturation of beta cells, till a critical BCM for curing diabetes is achieved. The differentiation and maturation of the NPI graft might have been promoted by the initially present hyperglycemic status in the pigs (KIN & KORBUTT, 2007; LI et al., 2018). Remarkably, #13064 showed an above-average proportion of insulin-positive liver segments without achieving glycemic control. It can therefore be concluded that the presence of viable beta cells alone does not necessarily guarantee their proper functionality, as described also in other studies (KEENAN et al., 2010; YU et al., 2019; JANSEN et al., 2023). It is also possible that the BCM critical for curing the pig's diabetes has not been reached. The distribution pattern of INS+ ICCs harmonized with the distribution of ICCs in general, indicating homogenous differentiation and maturation of ICCs.

Within islet containing liver segments, GCG+ liver segments were slightly more common than INS+ liver segments, suggesting that alpha cells occurred moderately more often than beta cells. One possible explanation could be that alpha cells differentiated at a higher rate than beta cells. This observation differs from the composition of human pancreatic islets and human islet cell transplants, which consist mainly of beta cells (TOSO et al., 2009; reviewed in ARROJO E DRIGO et al., 2015). On the other hand, this could also be due to different probabilities with which the cell types were present on the individual tissue sections. In total, the distribution pattern of GCG+ ICCs were largely comparable to INS+ ICCs, which allow the assumption that different pancreatic cell types differentiated homogenously within individual ICCs.

The main limitation in this context is that only the proportion of GCG+ and INS+ segments within the islet-containing segments was recorded, but no area determination of the respective cell types was carried out, which is why the area-related proportion of alpha and beta cells within the ICCs cannot be commented on.

6. Peri- and posttransplant treatment regime is essential for ITx outcome and to prevent graft rejection

The final objective of the present study was to characterize and quantify the immune response in graft-bearing livers.

Histological markers for leukocytes, T cells, regulatory T cells and macrophages are commonly used in ITx studies, since these cell types are known to be involved in immunological rejection of islet grafts (TOSO et al., 2009; GRAHAM et al., 2022; HAWTHORNE et al., 2022; reviewed in CHEN et al., 2023; LEI et al., 2024). In line with findings from the literature (reviewed in CHEN et al., 2023), inflammatory cell infiltrates in the present study turned out to be leukocytes, consisting largely of T cells. They occurred either in islet graft surrounding or infiltrative within the islet graft, whereby the latter can be interpreted as allogeneic transplant rejection. Of note, strong T-cell infiltration with up to complete displacement of the islet graft occurred much more pronounced in the WT group, in line with insufficient uptake of immunosuppressive drugs. In contrast, in the MIDY group with a more solid uptake of the immunosuppressants, T cells were detected rather sporadically in the islet graft surrounding. It can therefore be concluded that the combination of TAC and MMF, when adequately absorbed, was able to reliably attenuate T cell mediated rejection of the islet transplants. Given the mild immune response recorded despite irregular MMF intake but consistent TAC intake, it appears that TAC played a decisive role in T-cell suppression. However, since a constant, complete uptake of both drugs in their full dose could not be realized in any pig, the presence of T cells in all recipient pigs could be explained. Remarkably, regulatory T cells appeared in low numbers only in association with strong T-cell graft infiltration, so their presence could be an indicator of pronounced, destructive immune processes, as also described by Graham and coworkers (GRAHAM et al., 2022). An important difference of the present study compared to immunosuppressive regime in human ITx is that no induction therapy

was performed in the ITx recipient pigs. This was dispensed with as the available agents have a human-specific effect due to their antibody-based action and are not species-compatible with pigs. The fact that the animals therefore had a potentially activated immune system is a further limitation of this study.

The analysis of the macrophage abundance in ITx livers was interesting in order to shed light on the involvement of the innate immune system, especially since macrophages are known as main contributor to IBMIR and immune rejection after ITx (reviewed in CHEN et al., 2023; reviewed in DUAN et al., 2023). Liver resident macrophages (Kupffer cells) and inflammatory macrophages contribute to the demise of the islet graft by secreting proinflammatory cytokines (GOU et al., 2021). Macrophages infiltrated ICCs only to a minor degree. However, they were present in significantly increased amounts in livers of animals with islet transplants compared to animals that did not receive ITx, highlighting their pivotal role in immune response after ITx. The increased occurrence of macrophages was not associated with islet-containing liver segments, so that the effect is rather to be classified as a global phenomenon of the entire islet graft containing liver. Contrary to the T cell based immune response, this phenomenon was more pronounced in the MIDY pigs. This is mainly due to the outlier of #13064, which had a substantially higher proportion of macrophages than the remaining MIDY pigs. This emphasizes that an inflammatory process was present in #13064, which is also reflected in the elevated CRP values. The presence of massive inflammation, systemic but also localized in the liver, driven by innate immunity, could also be an explanation for the lack of glycemic control and SUV increase in this pig, since innate immune response creates an adverse environment for islet graft survival (reviewed in HUANG et al., 2008). The example of this pig also shows that reliable suppression of T cell mediated immune response by immunosuppression does not necessarily suppress systemic inflammation, as also described by Graham and coworkers (GRAHAM et al., 2022). The fact that innate immune reactions based on monocyte signaling pathway occur after organ transplantation despite immunosuppression with TAC and MMF is also described by Kannegieter and coworkers (KANNEGIETER et al., 2017).

The characterization of the immune response in the present study is limited to the detection of leukocytes in general and T cells, regulatory T cells and macrophages

in particular. Further characterization of the T cells into $CD4^+$ T helper cells and $CD8^+$ cytotoxic T cells was attempted, but was not achievable due to the lack of species reactivity of numerous antibodies tested. A limitation of the statistical comparison of macrophage abundance is the low number of analyzed livers from pigs without ITx, which are therefore underrepresented compared to the livers of pigs with ITx.

7. Conclusion and outlook

Summarizing the findings of this study, a novel large animal model for allogenic intraportal ITx in genetically diabetic pigs was established, exhibiting a high translational value to human ITx. Remarkably, a relatively small NPI graft volume was sufficient to restore normoglycemia in the diabetic recipient pigs. In addition, longitudinal monitoring of intraportal islet grafts by [^{68}Ga]Ga-DOTA-Exendin-4 PET/CT imaging was successfully performed for the first time in a large animal model, emphasizing its high clinical relevance. Clinical findings were confirmed by histological proof of mature and fully functional ICCs, consisting of all endocrine cell types required for proper glycemic control. ITx led to the activation of innate and acquired immunity, with adequate and sufficient immune suppressive regime proving to be a key criterion for suppressing T cell mediated transplant rejection also in the pig model.

As this study was designed as an orientation study to establish an allogenic intraportal ITx model in pigs and to assess the feasibility of non-invasive monitoring of the islet graft fate by PET/CT, all objectives were successfully achieved.

There is room for improvement. One example is the optimization of the immunosuppressive regime, which as in humans and other animal models, poses a significant challenge. The model could also benefit from characterization of the graft prior to ITx, such as determination of viability, metabolic capacity or cell composition, as graft properties before transplantation impact the ITx outcome. Further, *in vivo* functional testing, e.g. by IVGTT with C-peptide determination, would also be valuable for further evaluation of the graft condition. With regard to PET/CT imaging, further insights into the GLP-1R expression of the transplanted

beta cells would be of great importance in order to be able to establish a correlation between hepatic tracer uptake and BCM.

In conclusion, based on the established porcine allo-ITx model including longitudinal, non-invasive islet graft imaging, more important insights can be gained in the future with the aim of further expanding the clinical success of ITx as a curative therapy for T1D.

VII. SUMMARY

Establishment of intraportal islet allotransplantation in a diabetic pig model

Type 1 diabetes (T1D) is one of the most common metabolic and endocrinological diseases in children and adolescents worldwide. The development of the disease is based on an autoimmune-mediated destruction of pancreatic beta cells, which leads to an absolute insulin deficiency and therefore to a derailment of glycemic control. A diagnosis of T1D requires lifelong therapy with exogenous insulin to slow the onset of long-term diabetic complications. However, intensified insulin therapy as the current standard of care cannot fully mimic pancreatic insulin secretion pattern and increases the risk of severe hypoglycemia, which particularly affects patients with Brittle diabetes. Since the establishment of the Edmonton protocol, intraportal islet transplantation (ITx) as a beta-cell replacement therapy is a potentially curative treatment option for T1D. However, its clinical use is currently limited due to several hurdles, especially the multifactorial significant loss of islet graft mass after ITx. Therefore there is a great need for non-invasive imaging techniques for morphological long-term monitoring of the graft, for timely therapeutic intervention in the event islet graft loss. A promising approach in this context is PET/CT imaging of the GLP-1 receptor (GLP-1R), which is highly enriched on beta cells and can be visualized using exendin analogues as GLP-1R agonists.

The animal models used to date in ITx research have limited transferability to humans due to considerable anatomical and metabolic differences. The pig, on the other hand, is considered to be an animal model of high translational value due to its great anatomical and physiological similarity to humans. Transgenic *INS*^{C94Y} pigs, which represent a model for human mutant *INS* gene-induced diabetes of youth (MIDY), are particularly suitable for ITx studies due to their stable diabetic phenotype.

To address current limitations of ITx research, the aim of this study was to establish a large animal model for intraportal ITx with high transferability to human ITx and to test a non-invasive imaging technique based on PET/CT for the visualization of intraportal islet cell grafts.

For this purpose, neonatal porcine islets (NPI) were first transplanted intraportally into immunosuppressed wildtype (WT) pigs and, after successful establishment of the transplantation method, into immunosuppressed, insulin-dependent transgenic *INS*^{C94Y} pigs (MIDY pigs). This was followed by an observation period of up to three months, during which blood parameters and blood glucose levels were measured regularly. In addition, longitudinal [^{68}Ga]Ga-DOTA-Exendin-4 PET/CT imaging was performed to visualize the islet graft and to quantify changes in the hepatic uptake of a beta cell specific radiotracer (unit of measurement: standard uptake value (SUV)). The results were compared with a baseline PET/CT before ITx. Finally, the liver was extensively sampled. The subsequent detailed histological examination focused on graft distribution and properties as well as on a characterization of immunological processes

The intraportal transplantation of NPIs in a diabetic pig model was successfully established. In the largely unremarkable clinical course, transiently elevated liver enzymes and, to some extent, presumably immunosuppression-related side effects were noted. In three out of four MIDY pigs, normalization of blood glucose with (almost) complete independence from an exogenous insulin source was observed. PET/CT examination showed a diffuse, multifocal increase in liver signal over time as well as a significant increase in SUV in the whole liver and in hepatic hotspot regions. Histologic analysis revealed islet cell clusters (ICCs) widely distributed throughout the portal system that consisted of beta cells, alpha cells and delta cells, resembling mature islets of Langerhans in the pancreas. ITx activated innate and acquired immunity, which was reflected by increased macrophage abundance and islet-associated T-cell infiltrates in graft-bearing livers. The quality of the immune suppressive regime proved to be a decisive criterion for the suppression of T cell mediated transplant rejection.

Taken together, the results show that transplantation of NPIs led to the recovery of diabetic symptoms in transgenic *INS*^{C94Y} pigs. The development of glycemic control was associated with a significant increase in hepatic uptake of a beta cell-specific radiotracer, emphasizing the clinical relevance of GLP-1R imaging by PET/CT for morphological assessment of transplanted beta cells. The clinical findings could be confirmed by the detection of mature, functional ICCs.

The large animal model established in this study bridges the gap between preclinical research and clinical application, both in questions of ITx and in terms of morphological, non-invasive long-term monitoring of islet grafts. It could therefore play an important role in the optimization of ITx as a curative therapy for T1D, especially due to its high transferability to human ITx.

VIII. ZUSAMMENFASSUNG

Etablierung der intraportalen Allotransplantation von Inselzellen in einem diabetischen Schweinemodell

Typ 1 Diabetes (T1D) kommt weltweit als eine der häufigsten metabolischen und endokrinologischen Erkrankungen von Kindern und Jugendlichen vor. Die Entstehung der Krankheit beruht auf einer autoimmun-vermittelten Zerstörung der pankreatischen Betazellen, welche zu absoluten Insulinmangel und damit zur Entgleisung der glykämische Kontrolle führt. Eine Diagnose mit T1D macht eine lebenslange Therapie mit exogenem Insulin erforderlich, um das Auftreten von diabetischen Langzeitkomplikationen zu verlangsamen. Die intensivierte Insulintherapie als aktueller Behandlungsstandard kann die Insulin-Sekretionsmuster des Pankreas jedoch nicht vollständig imitieren, außerdem steigert sie das Risiko für schwere Hypoglykämien, von denen besonders Patienten mit Brittle Diabetes betroffen sind. Seit der Etablierung des Edmonton-Protokolls stellt die intraportale Inselzelltransplantation (ITx) als Betazellersatztherapie potentiell eine kurative Behandlungsmöglichkeit für T1D dar. Ihr klinischer Einsatz ist aktuell jedoch aufgrund mehrerer Hürden, v.a. dem multifaktoriell bedingten erheblichen Verlust an Inseltransplantatmasse nach ITx, begrenzt. Daher besteht ein großer Bedarf an nicht-invasiven bildgebenden Verfahren zur morphologischen Langzeitüberwachung des Transplantats, um im Falle eines Verlustes von Inseltransplantat rechtzeitig therapeutisch eingreifen zu können. Ein vielversprechender Ansatz in diesem Zusammenhang ist die PET/CT-Bildgebung des GLP-1 Rezeptors (GLP-1R), der auf Betazellen stark angereichert ist, und unter Verwendung von Exendin-Analoga als GLP-1R Agonisten dargestellt werden kann.

Die bisher in der ITx Forschung eingesetzten Tiermodelle weisen aufgrund teils erheblicher anatomischer und metabolischer Unterschiede eine limitierte Übertragbarkeit auf den Menschen auf. Das Schwein hingegen gilt aufgrund seiner großen anatomischen und physiologischen Ähnlichkeit mit dem Menschen als ein Tiermodell von hohem translationalem Wert.

Aufgrund ihres stabilen diabetischen Phänotyps sind transgene *INS*^{C94Y} Schweine, die ein Modell für „mutant *INS* gene-induced diabetes of youth (MIDY)“ des Menschen darstellen, besonders geeignet für ITx Studien.

Um aktuell bestehende Limitationen der ITx Forschung zu adressieren, war das Ziel dieser Studie, ein Großtiermodell für intraportale ITx mit hoher Übertragbarkeit zur menschlichen ITx zu etablieren. Außerdem sollte ein nichtinvasives PET/CT Bildgebungsverfahren für die Darstellung von intraportalen Inselzelltransplantaten getestet werden.

Dazu wurden neonatale porzine Inselzellen (NPI) zunächst in immunsupprimierte Wildtyp (WT) Schweine und nach erfolgreicher Etablierung der Transplantationsmethodik in immunsupprimierte, insulinpflichtige transgene *INS*^{C94Y} Schweine (MIDY Schweine) intraportal transplantiert. Anschließend folgte ein Beobachtungszeitraum von bis zu drei Monaten, in denen Blutparameter und Blut Glucosespiegel regelmäßig ermittelt wurden. Zusätzlich wurde longitudinales [^{68}Ga]Ga-DOTA-Exendin-4 PET/CT Imaging zur Darstellung des Inseltransplantates und zur Quantifizierung von Veränderungen der hepatischen Aufnahme eines Beta Zell spezifischen Radiotracers durchgeführt (Messeinheit: Standard uptake value (SUV)). Die Ergebnisse wurden mit einem Baseline PET/CT vor ITx verglichen. Schließlich erfolgte eine ausführliche Beprobung der Leber. Die anschließende detaillierte histologische Untersuchung fokussierte sich auf Transplantat Verteilung und Eigenschaften sowie auf eine Charakterisierung von immunologischen Vorgängen.

Die intraportale Transplantation von NPIs im diabetischen Schweine Modell konnte erfolgreich etabliert werden. Im weitgehend unauffälligen klinischen Verlauf fielen transient erhöhte Leberwerte sowie in gewissem Umfang wahrscheinlich immunsuppressionsbedingte Nebeneffekte auf. In drei von vier MIDY Schweinen konnte eine Normalisierung der Blutglukose mit (beinahe) vollständiger Unabhängigkeit von einer exogenen Insulinquelle festgestellt werden. Die PET/CT Untersuchung zeigte über die Zeit eine diffuse, multifokale Zunahme des Lebersignals sowie einen signifikanten Anstieg des SUV in der Gesamtleber und in hepatischen Hotspot Regionen. Die histologische Analyse ergab weit über das Pfortader System verteilte Inselzellcluster (ICCs), die wie reife Langerhans’sche

Inseln im Pankreas aus Betazellen, Alphazellen und Deltazellen bestanden. Die ITx aktivierte die angeborene und erworbene Immunität, was sich in einem erhöhten Makrophagen Aufkommen und inselassoziierten T-Zell-Infiltraten in den Transplantat-haltigen Lebern äußerte. Die Qualität des immunsuppressiven Regimes erwies sich hierbei als entscheidendes Kriterium für die Unterdrückung der T-Zell-vermittelten Transplantatabstoßung.

Zusammengefasst zeigen die Ergebnisse, dass die Transplantation von NPIs zur Heilung der diabetischen Symptomatik von transgenen *INS*^{C94Y} Schweinen führte. Die Entwicklung der glykämischen Kontrolle war verbunden mit einem signifikanten Anstieg der hepatischen Aufnahme eines betazell-spezifischen Radiotracers, was die klinische Relevanz der Darstellung des GLP-1R mittels PET/CT zur morphologischen Abbildung von transplantierten Betazellen unterstreicht. Die klinischen Befunde konnten durch den Nachweis von reifen, funktionsfähigen ICCs bestätigt werden.

Das in dieser Studie etablierte Großtiermodell schließt eine Lücke zwischen präklinischer Forschung und klinischer Anwendung in Hinblick auf ITx generell sowie auf morphologische, nicht-invasive Langzeitüberwachung von Inselzelltransplantaten. Ihm könnte daher, vor allem aufgrund seiner großen Übertragbarkeit zur menschlichen ITx, eine bedeutende Rolle bei der Optimierung der ITx als kurative Therapie von T1D zukommen.

IX. INDEX OF FIGURES

X. INDEX OF TABLES

XI. REFERENCES

Ahamed A, Unnikrishnan AG, Pendsey SS, Nampoothiri S, Bhavani N, Praveen VP, Kumar H, Jayakumar RV, Nair V, Ellard S, Edghill EL. Permanent neonatal diabetes mellitus due to a C96Y heterozygous mutation in the insulin gene. A case report. Jop 2008; 9: 715-8.

Ahn CH, Jang JY, Lee SO, Yoon JW, Kim SW, Park KS, Jung HS. Liver transaminase levels after intraportal autologous islet transplantation after partial pancreatectomy were associated with long-term metabolic outcomes. Diabetes Res Clin Pract 2018; 143: 232-8.

Aigner B, Renner S, Kessler B, Klymiuk N, Kurome M, Wünsch A, Wolf E. Transgenic pigs as models for translational biomedical research. J Mol Med (Berl) 2010; 88: 653-64.

Al Hezaimi K, Naghshbandi J, Nooh N, Schupbach P, Nevins M. Buccal Bone Remodeling Around Immediate Implants in STZ-Induced Diabetic Dogs: A Histologic and Microcomputed Tomographic Analysis. Int J Periodontics Restorative Dent 2021; 41: 683-90.

Al-Awar A, Kupai K, Veszelka M, Szűcs G, Attieh Z, Murlasits Z, Török S, Pósa A, Varga C. Experimental Diabetes Mellitus in Different Animal Models. J Diabetes Res 2016; 2016: 9051426.

Arifin DR, Bulte JWM. In Vivo Imaging of Pancreatic Islet Grafts in Diabetes Treatment. Front Endocrinol (Lausanne) 2021; 12: 640117.

Arnold R, Pussell BA, Pianta TJ, Lin CS, Kiernan MC, Krishnan AV. Association between calcineurin inhibitor treatment and peripheral nerve dysfunction in renal transplant recipients. Am J Transplant 2013; 13: 2426-32.

Arrojo e Drigo R, Ali Y, Diez J, Srinivasan DK, Berggren PO, Boehm BO. New insights into the architecture of the islet of Langerhans: a focused cross-species assessment. Diabetologia 2015; 58: 2218-28.

Aubin AM, Lombard-Vadnais F, Collin R, Aliesky HA, McLachlan SM, Lesage S. The NOD Mouse Beyond Autoimmune Diabetes. Front Immunol 2022; 13: 874769.

Badin JK, Kole A, Stivers B, Progar V, Pareddy A, Alloosh M, Sturek M. Alloxan-induced diabetes exacerbates coronary atherosclerosis and calcification in Ossabaw miniature swine with metabolic syndrome. J Transl Med 2018; 16: 58.

Ballinger WF, Lacy PE. Transplantation of intact pancreatic islets in rats. Surgery 1972; 72: 175-86.

Bamoulid J, Staeck O, Halleck F, Khadzhynov D, Brakemeier S, Dürr M, Budde K. The need for minimization strategies: current problems of immunosuppression. Transpl Int 2015; 28: 891-900.

Barton FB, Rickels MR, Alejandro R, Hering BJ, Wease S, Naziruddin B, Oberholzer J, Odorico JS, Garfinkel MR, Levy M, Pattou F, Berney T, Secchi A, Messinger S, Senior PA, Maffi P, Posselt A, Stock PG, Kaufman DB, Luo X, Kandeel F, Cagliero E, Turgeon NA, Witkowski P, Naji A, O'Connell PJ, Greenbaum C, Kudva YC, Brayman KL, Aull MJ, Larsen C, Kay TW, Fernandez LA, Vantyghem MC, Bellin M, Shapiro AM. Improvement in outcomes of clinical islet transplantation: 1999-2010. Diabetes Care 2012; 35: 1436-45.

Bellin MD, Barton FB, Heitman A, Harmon JV, Kandaswamy R, Balamurugan AN, Sutherland DE, Alejandro R, Hering BJ. Potent induction immunotherapy promotes long-term insulin independence after islet transplantation in type 1 diabetes. Am J Transplant 2012; 12: 1576-83.

Bennet W, Sundberg B, Groth CG, Brendel MD, Brandhorst D, Brandhorst H, Bretzel RG, Elgue G, Larsson R, Nilsson B, Korsgren O. Incompatibility between human blood and isolated islets of Langerhans: a finding with implications for clinical intraportal islet transplantation? Diabetes 1999; 48: 1907-14.

Bennet W, Sundberg B, Lundgren T, Tibell A, Groth CG, Richards A, White DJ, Elgue G, Larsson R, Nilsson B, Korsgren O. Damage to porcine islets of Langerhans after exposure to human blood in vitro, or after intraportal transplantation to cynomologus monkeys: protective effects of sCR1 and heparin. Transplantation 2000; 69: 711-9.

Bergen WG. Pigs (Sus Scrofa) in Biomedical Research. Adv Exp Med Biol 2022; 1354: 335-43.

Berney T, Toso C. Monitoring of the islet graft. Diabetes Metab 2006; 32: 503-12.

Berney T, Wassmer CH, Lebreton F, Bellofatto K, Fonseca LM, Bignard J, Hanna R, Peloso A, Berishvili E. From islet of Langerhans transplantation to the bioartificial pancreas. Presse Med 2022; 51: 104139.

Bertera S, Knoll MF, Knoll CA, Cooper DKC, Trucco M, Bottino R. Pig-to-Macaque Islet Xenotransplantation. Methods Mol Biol 2020; 2110: 289-314.

Biarnés M, Montolio M, Nacher V, Raurell M, Soler J, Montanya E. Beta-cell death and mass in syngeneically transplanted islets exposed to short- and long-term hyperglycemia. Diabetes 2002; 51: 66-72.

Birkenfeld A, Fritsche A, Roden M, Vosseler A. Insulin therapy for diabetes. diabinfo. Das Diabetesinformationsportal: Helmholtz München, DDZ, DZD 2021; 26.07.2021: https://www.diabinfo.de/en/living-with-diabetes/treatment/insulin-therapy.html. 17.11.2023.

Bloch K, Assa S, Lazard D, Abramov N, Shalitin S, Weintrob N, Josefsberg Z, Rapoport M, Vardi P. Neonatal pig islets induce a lower T-cell response than adult pig islets in IDDM patients. Transplantation 1999; 67: 748-52.

Boss M, Buitinga M, Jansen TJP, Brom M, Visser EP, Gotthardt M. PET-Based Human Dosimetry of (68)Ga-NODAGA-Exendin-4, a Tracer for β-Cell Imaging. J Nucl Med 2020; 61: 112-6.

Brennan DC, Schnitzler MA. Long-term results of rabbit antithymocyte globulin and basiliximab induction. N Engl J Med 2008; 359: 1736-8.

Brom M, Woliner-van der Weg W, Joosten L, Frielink C, Bouckenooghe T, Rijken P, Andralojc K, Göke BJ, de Jong M, Eizirik DL, Béhé M, Lahoutte T, Oyen WJ, Tack CJ, Janssen M, Boerman OC, Gotthardt M. Non-invasive quantification of the beta cell mass by SPECT with ^{111}In-labelled exendin. Diabetologia 2014; 57: 950-9.

Brom M, Joosten L, Frielink C, Boerman O, Gotthardt M. (111)In-exendin uptake in the pancreas correlates with the β-cell mass and not with the α-cell mass. Diabetes 2015; 64: 1324-8.

Brom M, Joosten L, Frielink C, Peeters H, Bos D, van Zanten M, Boerman O, Gotthardt M. Validation of (111)In-Exendin SPECT for the Determination of the β-Cell Mass in BioBreeding Diabetes-Prone Rats. Diabetes 2018; 67: 2012-8.

Brooks AM, Walker N, Aldibbiat A, Hughes S, Jones G, de Havilland J, Choudhary P, Huang GC, Parrott N, McGowan NW, Casey J, Mumford L, Barker P, Burling K, Hovorka R, Walker M, Smith RM, Forbes S, Rutter MK, Amiel S, Rosenthal MJ, Johnson P, Shaw JA. Attainment of metabolic goals in the integrated UK islet transplant program with locally isolated and transported preparations. Am J Transplant 2013; 13: 3236-43.

Brozzi F, Eizirik DL. ER stress and the decline and fall of pancreatic beta cells in type 1 diabetes. Ups J Med Sci 2016; 121: 133-9.

BTS (2019) British Transplantation Society. UK Guidelines on Pancreas and Islet Transplantation

Buerck LW, Schuster M, Oduncu FS, Baehr A, Mayr T, Guethoff S, Abicht J, Reichart B, Klymiuk N, Wolf E, Seissler J. LEA29Y expression in transgenic neonatal porcine islet-like cluster promotes long-lasting xenograft survival in humanized mice without immunosuppressive therapy. Sci Rep 2017; 7: 3572.

Cabrera O, Berman DM, Kenyon NS, Ricordi C, Berggren PO, Caicedo A. The unique cytoarchitecture of human pancreatic islets has implications for islet cell function. Proc Natl Acad Sci U S A 2006; 103: 2334-9.

Caldara R, Tomajer V, Monti P, Sordi V, Citro A, Chimienti R, Gremizzi C, Catarinella D, Tentori S, Paloschi V, Melzi R, Mercalli A, Nano R, Magistretti P, Partelli S, Piemonti L. Allo Beta Cell transplantation: specific features, unanswered questions, and immunological challenge. Front Immunol 2023; 14: 1323439.

Campbell PM, Salam A, Ryan EA, Senior P, Paty BW, Bigam D, McCready T, Halpin A, Imes S, Al Saif F, Lakey JR, Shapiro AM. Pretransplant HLA antibodies are associated with reduced graft survival after clinical islet transplantation. Am J Transplant 2007; 7: 1242-8.

Cantarelli E, Citro A, Marzorati S, Melzi R, Scavini M, Piemonti L. Murine animal models for preclinical islet transplantation: No model fits all (research purposes). Islets 2013; 5: 79-86.

Cantley J, Eizirik DL, Latres E, Dayan CM. Islet cells in human type 1 diabetes: from recent advances to novel therapies - a symposium-based roadmap for future research. J Endocrinol 2023; 259:

Cao ZH, Wu Z, Hu C, Zhang M, Wang WZ, Hu XB. Endoplasmic reticulum stress and destruction of pancreatic beta cells in type 1 diabetes. Chin Med J (Engl) 2020; 133: 68-73.

Carlsson PO, Palm F, Andersson A, Liss P. Markedly decreased oxygen tension in transplanted rat pancreatic islets irrespective of the implantation site. Diabetes 2001; 50: 489-95.

Cellini J, Zaura Jukic AM, LePard KJ. Neostigmine-induced contraction and nitric oxide-induced relaxation of isolated ileum from STZ diabetic guinea pigs. Auton Neurosci 2011; 165: 178-90.

Chen H, Carlson EC, Pellet L, Moritz JT, Epstein PN. Overexpression of metallothionein in pancreatic beta-cells reduces streptozotocin-induced DNA damage and diabetes. Diabetes 2001; 50: 2040-6.

Chen J, Mei A, Wei Y, Li C, Qian H, Min X, Yang H, Dong L, Rao X, Zhong J. GLP-1 receptor agonist as a modulator of innate immunity. Front Immunol 2022; 13: 997578.

Chen QD, Liu L, Zhao XH, Liang JB, Li SW. Challenges and opportunities in the islet transplantation microenvironment: a comprehensive summary of inflammatory cytokine, immune cells, and vascular endothelial cells. Front Immunol 2023; 14: 1293762.

Chen YG, Mathews CE, Driver JP. The Role of NOD Mice in Type 1 Diabetes Research: Lessons from the Past and Recommendations for the Future. Front Endocrinol (Lausanne) 2018; 9: 51.

CITR (2022) Collaborative Islet Transplant Registry Eleventh Allograft Report (2022), 11 edn. National Institute of Diabetes and Digestive and Kidney Diseases National Institutes of Health

Citro A, Cantarelli E, Maffi P, Nano R, Melzi R, Mercalli A, Dugnani E, Sordi V, Magistretti P, Daffonchio L, Ruffini PA, Allegretti M, Secchi A, Bonifacio E, Piemonti L. CXCR1/2 inhibition enhances pancreatic islet survival after transplantation. The Journal of Clinical Investigation 2012; 122: 3647-51.

Citro A, Cantarelli E, Piemonti L. Anti-inflammatory strategies to enhance islet engraftment and survival. Curr Diab Rep 2013; 13: 733-44.

Coe TM, Markmann JF, Rickert CG. Current status of porcine islet xenotransplantation. Curr Opin Organ Transplant 2020; 25: 449-56.

Colombo C, Porzio O, Liu M, Massa O, Vasta M, Salardi S, Beccaria L, Monciotti C, Toni S, Pedersen O, Hansen T, Federici L, Pesavento R, Cadario F, Federici G, Ghirri P, Arvan P, Iafusco D, Barbetti F. Seven mutations in the human insulin gene linked to permanent neonatal/infancy-onset diabetes mellitus. J Clin Invest 2008; 118: 2148-56.

Court FG, Wemyss-Holden SA, Morrison CP, Teague BD, Laws PE, Kew J, Dennison AR, Maddern GJ. Segmental nature of the porcine liver and its potential as a model for experimental partial hepatectomy. Br J Surg 2003; 90: 440-4.

Czarnecka Z, Dadheech N, Razavy H, Pawlick R, Shapiro AMJ. The Current Status of Allogenic Islet Cell Transplantation. Cells 2023; 12

D'Amour KA, Bang AG, Eliazer S, Kelly OG, Agulnick AD, Smart NG, Moorman MA, Kroon E, Carpenter MK, Baetge EE. Production of pancreatic hormone-expressing endocrine cells from human embryonic stem cells. Nat Biotechnol 2006; 24: 1392-401.

Damyar K, Farahmand V, Whaley D, Alexander M, Lakey JRT. An overview of current advancements in pancreatic islet transplantation into the omentum. Islets 2021; 13: 115-20.

Daniel C. Wie verbreitet ist Diabetes Typ 1? diabinfo. Das Diabetesinformationsportal: Helmholtz München, DDZ, DZD 2019; 31.10. 2019: https://www.diabinfo.de/leben/typ-1-diabetes/grundlagen/verbreitung.html. 26.09.2023.

Davalli AM, Scaglia L, Zangen DH, Hollister J, Bonner-Weir S, Weir GC. Vulnerability of islets in the immediate posttransplantation period. Dynamic changes in structure and function. Diabetes 1996; 45: 1161-7.

DCCT RG. Hypoglycemia in the Diabetes Control and Complications Trial. The Diabetes Control and Complications Trial Research Group. Diabetes 1997; 46: 271-86.

De Beaufort C, Besançon S, Balde N. Management of type 1 diabetes. Med Sante Trop 2018; 28: 359-62.

de Mesquita GHA, Jardim YJ, Iuamoto LR, Suguita FY, Essu FF, Oliveira LT, Meyer A, Crescenzi A, Rocha-Santos V, Galvão FHF, Andraus W, Chaib E, D'Albuquerque LAC. Gastric fundus submucosa as a site for islets transplantation: An experimental study. Ann Med Surg (Lond) 2018; 28: 1-5.

De Paep DL, Van Hulle F, Ling Z, Vanhoeij M, Pirenne J, Keymeulen B, Pipeleers D, Jacobs-Tulleneers-Thevissen D. Lower beta cell yield from donor pancreases after controlled circulatory death prevented by shortening acirculatory warm ischemia time and by using IGL-1 cold preservation solution. PLoS One 2021; 16: e0251055.

Deeds MC, Anderson JM, Armstrong AS, Gastineau DA, Hiddinga HJ, Jahangir A, Eberhardt NL, Kudva YC. Single dose streptozotocin-induced diabetes: considerations for study design in islet transplantation models. Lab Anim 2011; 45: 131-40.

Delaune V, Berney T, Lacotte S, Toso C. Intraportal islet transplantation: the impact of the liver microenvironment. Transpl Int 2017; 30: 227-38.

Desai T, Shea LD. Advances in islet encapsulation technologies. Nat Rev Drug Discov 2017; 16: 338-50.

DGFG. Islet cell donation and transplantation. DGFG - Deutsche Gesellschaft für Gewebetransplantation - Gemeinnützige Gesellschaft mbH 2022: https://gewebenetzwerk.de/en/inselzellspende/. 17.02.2024.

DiMeglio LA, Evans-Molina C, Oram RA. Type 1 diabetes. Lancet 2018; 391: 2449-62.

Dimitrioglou N, Kanelli M, Papageorgiou E, Karatzas T, Hatziavramidis D. Paving the way for successful islet encapsulation. Drug Discov Today 2019; 24: 737-48.

Ding HX, Dong NX, Zhou CX, Wang FJ, Xing N, Ma HF, Hou L. Liraglutide Attenuates Restenosis After Vascular Injury in Rabbits With Diabetes Via the TGF-β/Smad3 Signaling Pathway. Altern Ther Health Med 2022; 28: 22-8.

Du X, He S, Jiang Y, Wei L, Hu W. Adiponectin prevents islet ischemia-reperfusion injury through the COX2-TNFα-NF-κB-dependent signal transduction pathway in mice. J Endocrinol 2013; 218: 75-84.

Duan K, Liu J, Zhang J, Chu T, Liu H, Lou F, Liu Z, Gao B, Wei S, Wei F. Advancements in innate immune regulation strategies in islet transplantation. Front Immunol 2023; 14: 1341314.

Dufrane D, van Steenberghe M, Guiot Y, Goebbels RM, Saliez A, Gianello P. Streptozotocin-induced diabetes in large animals (pigs/primates): role of GLUT2 transporter and beta-cell plasticity. Transplantation 2006; 81: 36-45.

Echeverri GJ, McGrath K, Bottino R, Hara H, Dons EM, van der Windt DJ, Ekser B, Casu A, Houser S, Ezzelarab M, Wagner R, Trucco M, Lakkis FG, Cooper DK. Endoscopic gastric submucosal transplantation of islets (ENDO-STI): technique and initial results in diabetic pigs. Am J Transplant 2009; 9: 2485-96.

Eckhard M, Martin I, Eich T, Weimer R, Zinn S, Bretzel RG, Brendel MD. Incidence of cytomegalovirus infections after immunosuppression induction in clinical islet transplantation and impact on graft function. Transplant Proc 2002; 34: 1922-4.

Edgerton DS, Moore MC, Gregory JM, Kraft G, Cherrington AD. Importance of the route of insulin delivery to its control of glucose metabolism. Am J Physiol Endocrinol Metab 2021; 320: E891-e7.

Edghill EL, Flanagan SE, Patch AM, Boustred C, Parrish A, Shields B, Shepherd MH, Hussain K, Kapoor RR, Malecki M, MacDonald MJ, Støy J, Steiner DF, Philipson LH, Bell GI, Hattersley AT, Ellard S. Insulin mutation screening in 1,044 patients with diabetes: mutations in the INS gene are a common cause of neonatal diabetes but a rare cause of diabetes diagnosed in childhood or adulthood. Diabetes 2008; 57: 1034-42.

Eguchi N, Damyar K, Alexander M, Dafoe D, Lakey JRT, Ichii H. Anti-Oxidative Therapy in Islet Cell Transplantation. Antioxidants (Basel) 2022; 11

Eich T, Eriksson O, Lundgren T. Visualization of early engraftment in clinical islet transplantation by positron-emission tomography. N Engl J Med 2007; 356: 2754-5.

Elliott RB, Escobar L, Garkavenko O, Croxson MC, Schroeder BA, McGregor M, Ferguson G, Beckman N, Ferguson S. No evidence of infection with porcine endogenous retrovirus in recipients of encapsulated porcine islet xenografts. Cell Transplant 2000; 9: 895-901.

Emamaullee JA, Rajotte RV, Liston P, Korneluk RG, Lakey JR, Shapiro AM, Elliott JF. XIAP overexpression in human islets prevents early posttransplant apoptosis and reduces the islet mass needed to treat diabetes. Diabetes 2005; 54: 2541-8.

Engin F. ER stress and development of type 1 diabetes. J Investig Med 2016; 64: 2-6.

Eriksson O, Eich T, Sundin A, Tibell A, Tufveson G, Andersson H, Felldin M, Foss A, Kyllönen L, Langstrom B, Nilsson B, Korsgren O, Lundgren T. Positron emission tomography in clinical islet transplantation. Am J Transplant 2009; 9: 2816-24.

Eriksson O, Alavi A. Imaging the islet graft by positron emission tomography. Eur J Nucl Med Mol Imaging 2012; 39: 533-42.

Eriksson O, Selvaraju R, Eich T, Willny M, Brismar TB, Carlbom L, Ahlstrom H, Tufvesson G, Lundgren T, Korsgren O. Positron Emission Tomography to Assess the Outcome of Intraportal Islet Transplantation. Diabetes 2016; 65: 2482-9.

Ernst AU, Wang LH, Ma M. Islet encapsulation. J Mater Chem B 2018; 6: 6705-22.

Esievo KAN, Num-Adom SM, Adamu S, Ogbuagu NE, Aluwong T, Umar IA. Elevated serum sialic acids, a potent biomarker of alloxan-induced type 1 diabetes in dogs by ethanolic extract of Anogeissus leiocarpus. J Diabetes Metab Disord 2021; 20: 179-86.

Estil Les E, Téllez N, Nacher M, Montanya E. A Model for Human Islet Transplantation to Immunodeficient Streptozotocin-Induced Diabetic Mice. Cell Transplant 2018; 27: 1684-91.

Eter WA, Van der Kroon I, Andralojc K, Buitinga M, Willekens SMA, Frielink C, Bos D, Joosten L, Boerman OC, Brom M, Gotthardt M. Non-invasive in vivo determination of viable islet graft volume by (111)In-exendin-3. Sci Rep 2017; 7: 7232.

Forbes S, Bond AR, Thirlwell KL, Burgoyne P, Samuel K, Noble J, Borthwick G, Colligan D, McGowan NWA, Lewis PS, Fraser AR, Mountford JC, Carter RN, Morton NM, Turner ML, Graham GJ, Campbell JDM. Human umbilical cord perivascular cells improve human pancreatic islet transplant function by increasing vascularization. Sci Transl Med 2020; 12

Frost PA, Chen S, Mezzles MJ, Voruganti VS, Nava-Gonzalez EJ, Arriaga-Cazares HE, Freed KA, Comuzzie AG, DeFronzo RA, Kent JW, Jr., Grayburn PA, Bastarrachea RA. Successful pharmaceutical-grade streptozotocin (STZ)-induced hyperglycemia in a conscious tethered baboon (Papio hamadryas) model. J Med Primatol 2015; 44: 202-17.

Fu H, Li G, Liu C, Li J, Cheng L, Yang W, Tse G, Zhao J, Liu T. Probucol prevents atrial ion channel remodeling in an alloxan-induced diabetes rabbit model. Oncotarget 2016; 7: 83850-8.

Furman BL. Streptozotocin-Induced Diabetic Models in Mice and Rats. Curr Protoc 2021; 1: e78.

Gaba RC, Garcia-Roca R, Oberholzer J. Pancreatic islet cell transplantation: an update for interventional radiologists. J Vasc Interv Radiol 2012; 23: 583-94; quiz 94.

Gamble A, Pepper AR, Bruni A, Shapiro AMJ. The journey of islet cell transplantation and future development. Islets 2018; 10: 80-94.

Gangemi A, Salehi P, Hatipoglu B, Martellotto J, Barbaro B, Kuechle JB, Qi M, Wang Y, Pallan P, Owens C, Bui J, West D, Kaplan B, Benedetti E, Oberholzer J. Islet transplantation for brittle type 1 diabetes: the UIC protocol. Am J Transplant 2008; 8: 1250-61.

Gao Q, Davis R, Fitch Z, Mulvihill M, Ezekian B, Schroder P, Schmitz R, Song M, Leopardi F, Ribeiro M, Miller A, Moris D, Shaw B, Samy K, Reimann K, Williams K, Collins B, Kirk AD. Anti-thymoglobulin induction improves neonatal porcine xenoislet engraftment and survival. Xenotransplantation 2021; 28: e12713.

Gołąb K, Kizilel S, Bal T, Hara M, Zielinski M, Grose R, Savari O, Wang XJ, Wang LJ, Tibudan M, Krzystyniak A, Marek-Trzonkowska N, Millis JM, Trzonkowski P, Witkowski P. Improved coating of pancreatic islets with regulatory T cells to create local immunosuppression by using the biotin-polyethylene glycol-succinimidyl valeric acid ester molecule. Transplant Proc 2014; 46: 1967-71.

Gorray KC, Fujimoto WY. In vitro toxicity of alloxan for guinea pig B cells: comparison with rat B cells. Proc Soc Exp Biol Med 1983; 173: 606-12.

Goto M, Groth CG, Nilsson B, Korsgren O. Intraportal pig islet xenotransplantation into athymic mice as an in vivo model for the study of the instant blood-mediated inflammatory reaction. Xenotransplantation 2004; 11: 195-202.

Gotthardt M, Lalyko G, van Eerd-Vismale J, Keil B, Schurrat T, Hower M, Laverman P, Behr TM, Boerman OC, Göke B, Béhé M. A new technique for in vivo imaging of specific GLP-1 binding sites: first results in small rodents. Regul Pept 2006; 137: 162-7.

Gou W, Wang J, Song L, Kim DS, Cui W, Strange C, Wang H. Alpha-1 antitrypsin suppresses macrophage activation and promotes islet graft survival after intrahepatic islet transplantation. Am J Transplant 2021; 21: 1713-24.

Goyal SN, Reddy NM, Patil KR, Nakhate KT, Ojha S, Patil CR, Agrawal YO. Challenges and issues with streptozotocin-induced diabetes - A clinically relevant animal model to understand the diabetes pathogenesis and evaluate therapeutics. Chem Biol Interact 2016; 244: 49-63.

Graham ML, Bellin MD, Papas KK, Hering BJ, Schuurman HJ. Species incompatibilities in the pig-to-macaque islet xenotransplant model affect transplant outcome: a comparison with allotransplantation. Xenotransplantation 2011; 18: 328-42.

Graham ML, Schuurman HJ. Validity of animal models of type 1 diabetes, and strategies to enhance their utility in translational research. Eur J Pharmacol 2015; 759: 221-30.

Graham ML, Ramachandran S, Singh A, Moore MEG, Flanagan EB, Azimzadeh A, Burlak C, Mueller KR, Martins K, Anazawa T, Appakalai BN, Bansal-Pakala P, Murtaugh MP, O'Brien TD, Papas KK, Spizzo T, Schuurman HJ, Hancock WW, Hering BJ. Clinically available immunosuppression averts rejection but not systemic inflammation after porcine islet xenotransplant in cynomolgus macaques. Am J Transplant 2022; 22: 745-60.

Gregory GA, Robinson TIG, Linklater SE, Wang F, Colagiuri S, de Beaufort C, Donaghue KC, Magliano DJ, Maniam J, Orchard TJ, Rai P, Ogle GD. Global incidence, prevalence, and mortality of type 1 diabetes in 2021 with projection to 2040: a modelling study. Lancet Diabetes Endocrinol 2022; 10: 741-60.

Groth CG, Korsgren O, Tibell A, Tollemar J, Möller E, Bolinder J, Ostman J, Reinholt FP, Hellerström C, Andersson A. Transplantation of porcine fetal pancreas to diabetic patients. Lancet 1994; 344: 1402-4.

Guo SJ, Shao H. Growing global burden of type 1 diabetes needs multitiered precision public health interventions. Lancet Diabetes Endocrinol 2022; 10: 688-9.

Haak T, Gölz S, Fritsche A, Füchtenbusch M, Siegmund T (2018) S3-Leitlinie Therapie des Typ-1-Diabetes, 2 edn. Deutsche Diabetes Gesellschaft, AWMF online

Haak T, Gölz S, Fritsche A, Füchtenbusch M, Siegmund T, Schnellbächer E, Klein HH, Uebel T, Droßel D. Therapy of Type 1 Diabetes. Exp Clin Endocrinol Diabetes 2019; 127: S27-s38.

Hacke K, Falahati R, Flebbe-Rehwaldt L, Kasahara N, Gaensler KM. Suppression of HLA expression by lentivirus-mediated gene transfer of siRNA cassettes and in vivo chemoselection to enhance hematopoietic stem cell transplantation. Immunol Res 2009; 44: 112-26.

Han Q, Sun J, Xie W, Bai Y, Wang S, Huang J, Zhou S, Li Q, Zhang H, Tang Z. Repeated Low-Dose Streptozotocin and Alloxan Induced Long-Term and Stable Type 1 Diabetes Model in Beagle Dogs. Biomed Res Int 2022; 2022: 5422287.

Hanafusa T, Miyagawa J, Nakajima H, Tomita K, Kuwajima M, Matsuzawa Y, Tarui S. The NOD mouse. Diabetes Res Clin Pract 1994; 24 Suppl: S307-11.

Hao L, Mi J, Song L, Guo Y, Li Y, Yin Y, Zhang C. SLC40A1 Mediates Ferroptosis and Cognitive Dysfunction in Type 1 Diabetes. Neuroscience 2021; 463: 216-26.

Harreiter J, Roden M. Diabetes mellitus: definition, classification, diagnosis, screening and prevention (Update 2023). Wiener Klinische Wochenschrift 2023; 135: 7-17.

Hatchell DL, Reiser HJ, Bresnahan JF, Whitworth UG, Jr. Resistance of cats to the diabetogenic effect of alloxan. Lab Anim Sci 1986; 36: 37-40.

Hawthorne WJ, Salvaris EJ, Chew YV, Burns H, Hawkes J, Barlow H, Hu M, Lew AM, Nottle MB, O'Connell PJ, Cowan PJ. Xenotransplantation of Genetically Modified Neonatal Pig Islets Cures Diabetes in Baboons. Front Immunol 2022; 13: 898948.

Haynes R, Harden P, Judge P, Blackwell L, Emberson J, Landray MJ, Baigent C, Friend PJ. Alemtuzumab-based induction treatment versus basiliximab-based induction treatment in kidney transplantation (the 3C Study): a randomised trial. Lancet 2014; 384: 1684-90.

He S, Chen Y, Wei L, Jin X, Zeng L, Ren Y, Zhang J, Wang L, Li H, Lu Y, Cheng J. Treatment and risk factor analysis of hypoglycemia in diabetic rhesus monkeys. Exp Biol Med (Maywood) 2011; 236: 212-8.

Heinke S, Ludwig B, Schubert U, Schmid J, Kiss T, Steffen A, Bornstein S, Ludwig S. Diabetes induction by total pancreatectomy in minipigs with simultaneous splenectomy: a feasible approach for advanced diabetes research. Xenotransplantation 2016; 23: 405-13.

Hering BJ, Kandaswamy R, Ansite JD, Eckman PM, Nakano M, Sawada T, Matsumoto I, Ihm SH, Zhang HJ, Parkey J, Hunter DW, Sutherland DE. Single-donor, marginal-dose islet transplantation in patients with type 1 diabetes. JAMA 2005; 293: 830-5.

Hering BJ, Clarke WR, Bridges ND, Eggerman TL, Alejandro R, Bellin MD, Chaloner K, Czarniecki CW, Goldstein JS, Hunsicker LG, Kaufman DB, Korsgren O, Larsen CP, Luo X, Markmann JF, Naji A, Oberholzer J, Posselt AM, Rickels MR, Ricordi C, Robien MA, Senior PA, Shapiro AM, Stock PG, Turgeon NA. Phase 3 Trial of Transplantation of Human Islets in Type 1 Diabetes Complicated by Severe Hypoglycemia. Diabetes Care 2016; 39: 1230-40.

Hilbrands R, Huurman VA, Gillard P, Velthuis JH, De Waele M, Mathieu C, Kaufman L, Pipeleers-Marichal M, Ling Z, Movahedi B, Jacobs-Tulleneers-Thevissen D, Monbaliu D, Ysebaert D, Gorus FK, Roep BO, Pipeleers DG, Keymeulen B. Differences in baseline lymphocyte counts and autoreactivity are associated with differences in outcome of islet cell transplantation in type 1 diabetic patients. Diabetes 2009; 58: 2267-76.

Hirshberg B, Rother KI, Digon BJ, 3rd, Lee J, Gaglia JL, Hines K, Read EJ, Chang R, Wood BJ, Harlan DM. Benefits and risks of solitary islet transplantation for type 1 diabetes using steroid-sparing immunosuppression: the National Institutes of Health experience. Diabetes Care 2003; 26: 3288-95.

Hornaschewitz N (2023) Impact of LEA29Y expression on myocardial infarction outcome in pigs. In: Faculty of Veterinary Medicine. LMU Munich, Electronic Theses of LMU Munich

Huang K, Liang L, Fu JF, Dong GP. Permanent neonatal diabetes mellitus in China. BMC Pediatr 2014; 14: 188.

Huang X, Moore DJ, Ketchum RJ, Nunemaker CS, Kovatchev B, McCall AL, Brayman KL. Resolving the conundrum of islet transplantation by linking metabolic dysregulation, inflammation, and immune regulation. Endocr Rev 2008; 29: 603-30.

Jansen TJP, Buitinga M, Boss M, Nijhoff MF, Brom M, de Galan BE, van der Graaf M, van Koeverden S, Vantyghem MC, Beron A, Pattou F, Engelse MA, Velikyan I, Eriksson O, de Koning EJP, Gotthardt M. Monitoring beta-Cell Survival After Intrahepatic Islet Transplantation Using Dynamic Exendin PET Imaging: A Proof-of-Concept Study in Individuals With Type 1 Diabetes. Diabetes 2023; 72: 898-907.

Jansson L, Carlsson PO. Graft vascular function after transplantation of pancreatic islets. Diabetologia 2002; 45: 749-63.

Javadi S, Asri-Rezaei S, Allahverdizadeh M. Interrelationship of βeta-2 microglobulin, blood urea nitrogen and creatinine in streptozotocin-induced diabetes mellitus in rabbits. Vet Res Forum 2014; 5: 7-11.

Javed F, Al-Daghri NM, Wang HL, Wang CY, Al-Hezaimi K. Short-term effects of non-surgical periodontal treatment on the gingival crevicular fluid cytokine profiles in sites with induced periodontal defects: a study on dogs with and without streptozotocin-induced diabetes. J Periodontol 2014; 85: 1589-95.

Jensen-Waern M, Kruse R, Lundgren T. Oral immunosuppressive medication for growing pigs in transplantation studies. Lab Anim 2012; 46: 148-51.

Jeong SH, Jung BH, Yoo KY, Um HS, Chang BS, Lee JK, Choi WY. Determination of the optimal diabetes duration for bone regeneration experiments in an alloxan-induced diabetic rabbit calvarial defect model. J Periodontal Implant Sci 2018; 48: 383-94.

Jin C, Luo X, Li X, Zhou R, Zhong Y, Xu Z, Cui C, Xing X, Zhang H, Tian M. Positron emission tomography molecular imaging-based cancer phenotyping. Cancer 2022; 128: 2704-16.

Johnson PR, Jones KE. Pancreatic islet transplantation. Semin Pediatr Surg 2012; 21: 272-80.

Jones GL, Juszczak MT, Hughes SJ, Kooner P, Powis SH, Press M. Time course and quantification of pancreatic islet revascularization following intraportal transplantation. Cell Transplant 2007; 16: 505-16.

Joosten L, Brom M, Peeters H, Bos D, Himpe E, Bouwens L, Boerman O, Gotthardt M. Measuring the Pancreatic β Cell Mass in Vivo with Exendin SPECT during Hyperglycemia and Severe Insulitis. Mol Pharm 2019; 16: 4024-30.

Kanak MA, Takita M, Kunnathodi F, Lawrence MC, Levy MF, Naziruddin B. Inflammatory response in islet transplantation. Int J Endocrinol 2014; 2014: 451035.

Kannegieter NM, Hesselink DA, Dieterich M, Kraaijeveld R, Rowshani AT, Leenen PJ, Baan CC. The Effect of Tacrolimus and Mycophenolic Acid on CD14+ Monocyte Activation and Function. PLoS One 2017; 12: e0170806.

Katsarou A, Gudbjörnsdottir S, Rawshani A, Dabelea D, Bonifacio E, Anderson BJ, Jacobsen LM, Schatz DA, Lernmark Å. Type 1 diabetes mellitus. Nat Rev Dis Primers 2017; 3: 17016.

Keenan HA, Sun JK, Levine J, Doria A, Aiello LP, Eisenbarth G, Bonner-Weir S, King GL. Residual insulin production and pancreatic ß-cell turnover after 50 years of diabetes: Joslin Medalist Study. Diabetes 2010; 59: 2846-53.

Kemter E, Cohrs CM, Schäfer M, Schuster M, Steinmeyer K, Wolf-van Buerck L, Wolf A, Wuensch A, Kurome M, Kessler B, Zakhartchenko V, Loehn M, Ivashchenko Y, Seissler J, Schulte AM, Speier S, Wolf E. INS-eGFP transgenic pigs: a novel reporter system for studying maturation, growth and vascularisation of neonatal islet-like cell clusters. Diabetologia 2017; 60: 1152-6.

Kemter E, Wolf E. Recent progress in porcine islet isolation, culture and engraftment strategies for xenotransplantation. Curr Opin Organ Transplant 2018; 23: 633-41.

Kemter E, Denner J, Wolf E. Will Genetic Engineering Carry Xenotransplantation of Pig Islets to the Clinic? Curr Diab Rep 2018; 18: 103.

Kikawa K, Sakano D, Shiraki N, Tsuyama T, Kume K, Endo F, Kume S. Beneficial effect of insulin treatment on islet transplantation outcomes in Akita mice. PLoS One 2014; 9: e95451.

Kilworth L, Crane D, Masters C. The influence of insulin on the flux of lipid metabolism in vivo. Biochem Int 1985; 10: 539-47.

Kim GS, Lee JH, Shin DY, Lee HS, Park H, Lee KW, Yang H-M, Kim SJ, Park JB. Integrated whole liver histologic analysis of the allogeneic islet distribution and characteristics in a nonhuman primate model. Scientific reports 2020a; 10: 1-9.

Kim GS, Lee JH, Shin DY, Lee HS, Park H, Lee KW, Yang HM, Kim SJ, Park JB. Integrated whole liver histologic analysis of the allogeneic islet distribution and characteristics in a nonhuman primate model. Sci Rep 2020b; 10: 793.

Kim JM, Shin JS, Min BH, Kang SJ, Yoon IH, Chung H, Kim J, Hwang ES, Ha J, Park CG. JAK3 inhibitor-based immunosuppression in allogeneic islet transplantation in cynomolgus monkeys. Islets 2019; 11: 119-28.

Kim S, Whitener RL, Peiris H, Gu X, Chang CA, Lam JY, Camunas-Soler J, Park I, Bevacqua RJ, Tellez K, Quake SR, Lakey JRT, Bottino R, Ross PJ, Kim SK. Molecular and genetic regulation of pig pancreatic islet cell development. Development 2020c; 147

Kim YH, Kastner K, Abdul-Wahid B, Izaguirre JA. Evaluation of conformational changes in diabetes-associated mutation in insulin a chain: a molecular dynamics study. Proteins 2015; 83: 662-9.

Kin T, Korbutt GS. Delayed functional maturation of neonatal porcine islets in recipients under strict glycemic control. Xenotransplantation 2007; 14: 333-8.

Kin T, Shapiro AM. Surgical aspects of human islet isolation. Islets 2010; 2: 265-73.

King AJ. The use of animal models in diabetes research. Br J Pharmacol 2012; 166: 877-94.

King JL, Mason JO, 3rd, Cartner SC, Guidry C. The influence of alloxan-induced diabetes on Müller cell contraction-promoting activities in vitreous. Invest Ophthalmol Vis Sci 2011; 52: 7485-91.

Klymiuk N, Ludwig B, Seissler J, Reichart B, Wolf E. Current Concepts of Using Pigs as a Source for Beta-Cell Replacement Therapy of Type 1 Diabetes. Current Molecular Biology Reports 2016; 2: 73-82.

Koh A, Senior P, Salam A, Kin T, Imes S, Dinyari P, Malcolm A, Toso C, Nilsson B, Korsgren O, Shapiro AMJ. Insulin-Heparin Infusions Peritransplant Substantially Improve Single-Donor Clinical Islet Transplant Success. Transplantation 2010; 89: 465-71.

Korbutt GS, Elliott JF, Ao Z, Smith DK, Warnock GL, Rajotte RV. Large scale isolation, growth, and function of porcine neonatal islet cells. J Clin Invest 1996; 97: 2119-29.

Kordonouri O, Kerner W. Type 1 diabetes: an update. Internist (Berl) 2021; 62: 627-37.

Korsgren O, Christofferson R, Jansson L. Angiogenesis and angioarchitecture of transplanted fetal porcine islet-like cell clusters. Transplantation 1999; 68: 1761-6.

Kosinova L, Patikova A, Jirak D, Galisova A, Vojtiskova A, Saudek F, Kriz J. A novel model for in vivo quantification of immediate liver perfusion impairment after pancreatic islet transplantation. Islets 2019; 11: 129-40.

Kourtzelis I, Magnusson PU, Kotlabova K, Lambris JD, Chavakis T. Regulation of Instant Blood Mediated Inflammatory Reaction (IBMIR) in Pancreatic Islet Xeno-Transplantation: Points for Therapeutic Interventions. Adv Exp Med Biol 2015; 865: 171-88.

Kroon E, Martinson LA, Kadoya K, Bang AG, Kelly OG, Eliazer S, Young H, Richardson M, Smart NG, Cunningham J, Agulnick AD, D'Amour KA, Carpenter MK, Baetge EE. Pancreatic endoderm derived from human embryonic stem cells generates glucose-responsive insulin-secreting cells in vivo. Nat Biotechnol 2008; 26: 443-52.

Laiteerapong N, Ham SA, Gao Y, Moffet HH, Liu JY, Huang ES, Karter AJ. The Legacy Effect in Type 2 Diabetes: Impact of Early Glycemic Control on Future Complications (The Diabetes & Aging Study). Diabetes Care 2019; 42: 416-26.

Lampe EW, Sutherland DE, Najariam HS. Autotransplantation of porcine islets of Langerhans. Surgery 1976; 79: 138-43.

Landstra CP, Nijhoff MF, Roelen DL, de Vries APJ, de Koning EJP. Diagnosis and treatment of allograft rejection in islet transplantation. Am J Transplant 2023; 23: 1425-33.

Leech CA, Dzhura I, Chepurny OG, Kang G, Schwede F, Genieser HG, Holz GG. Molecular physiology of glucagon-like peptide-1 insulin secretagogue action in pancreatic β cells. Prog Biophys Mol Biol 2011; 107: 236-47.

Lei Y, Wolf-van Buerck L, Honarpisheh M, Zhang Y, Schwinzer R, Petersen B, Seissler J. Neonatal islets from human PD-L1 transgenic pigs reduce immune cell activation and cellular rejection in humanized nonobese diabetic-scid IL2rγ(null) mice. Am J Transplant 2024; 24: 20-9.

Lenzen S, Freytag S, Panten U. Inhibition of glucokinase by alloxan through interaction with SH groups in the sugar-binding site of the enzyme. Mol Pharmacol 1988; 34: 395-400.

Lenzen S, Tiedge M, Elsner M, Lortz S, Weiss H, Jörns A, Klöppel G, Wedekind D, Prokop CM, Hedrich HJ. The LEW.1AR1/Ztm-iddm rat: a new model of spontaneous insulin-dependent diabetes mellitus. Diabetologia 2001; 44: 1189-96.

Lenzen S. The mechanisms of alloxan- and streptozotocin-induced diabetes. Diabetologia 2008; 51: 216-26.

Lewis DI. Animal experimentation: implementation and application of the 3Rs. Emerg Top Life Sci 2019; 3: 675-9.

Li B, Cui W, Yang J. Enhanced skeletal muscle growth in myostatin-deficient transgenic pigs had improved glucose uptake in stretozotocin-induced diabetes. Transgenic Res 2020; 29: 253-61.

Li W-C, Chen C-Y, Kao C-W, Huang P-C, Hsieh Y-T, Kuo T-Y, Chen T-Y, Chia H-Y, Juang J-H. Porcine Neonatal Pancreatic Cell Clusters Maintain Their Multipotency in Culture and After Transplantation. Scientific reports 2018; 8: 8212.

Li X, Chen H, Epstein PN. Metallothionein protects islets from hypoxia and extends islet graft survival by scavenging most kinds of reactive oxygen species. J Biol Chem 2004; 279: 765-71.

Lindheimer F, Lindner MJ, Oos R, Honarpisheh M, Zhang Y, Lei Y, Wolf-van Buerck L, Gildehaus FJ, Lindner S, Bartenstein P, Kemter E, Wolf E, Seissler J, Ziegler S. Non-invasive in vivo imaging of porcine islet xenografts in a preclinical model with [68Ga]Ga-exendin-4. Frontiers in Nuclear Medicine 2023; 3

Liu M, Hodish I, Haataja L, Lara-Lemus R, Rajpal G, Wright J, Arvan P. Proinsulin misfolding and diabetes: mutant INS gene-induced diabetes of youth. Trends Endocrinol Metab 2010; 21: 652-9.

Liu M, Sun J, Cui J, Chen W, Guo H, Barbetti F, Arvan P. INS-gene mutations: from genetics and beta cell biology to clinical disease. Mol Aspects Med 2015; 42: 3-18.

Liuwantara D, Chew YV, Favaloro EJ, Hawkes JM, Burns HL, O'Connell PJ, Hawthorne WJ. Characterizing the Mechanistic Pathways of the Instant Blood-Mediated Inflammatory Reaction in Xenogeneic Neonatal Islet Cell Transplantation. Transplant Direct 2016; 2: e77.

Lobo PI, Spencer C, Simmons WD, Hagspiel KD, Angle JF, Deng S, Markmann J, Naji A, Kirk SE, Pruett T, Brayman KL. Development of anti-human leukocyte antigen class 1 antibodies following allogeneic islet cell transplantation. Transplant Proc 2005; 37: 3438-40.

Lu Y, Zou S, Bertera S, Bottino R, Cooper DKC, Liu Z, Huang Y, Wang C, Hong C, He T, Zhang H, Huo Q, Fu H, Cai Z, Mou L. A Method for Islet Transplantation to the Omentum in Mouse. J Vis Exp 2019;

Ludwig B, Reichel A, Kruppa A, Ludwig S, Steffen A, Weitz J, Bornstein SR. Islet transplantation at the Dresden diabetes center: five years' experience. Horm Metab Res 2015; 47: 4-8.

Ludwig B, Wolf E, Schönmann U, Ludwig S. Large Animal Models of Diabetes. Methods Mol Biol 2020; 2128: 115-34.

Ma X, Ye B, Gao F, Liang Q, Dong Q, Liu Y, Rong P, Wang W, Yi S. Tissue factor knockdown in porcine islets: an effective approach to suppressing the instant blood-mediated inflammatory reaction. Cell Transplant 2012; 21: 61-71.

Maahs DM, West NA, Lawrence JM, Mayer-Davis EJ. Epidemiology of type 1 diabetes. Endocrinol Metab Clin North Am 2010; 39: 481-97.

Maffi P, Nano R, Monti P, Melzi R, Sordi V, Mercalli A, Pellegrini S, Ponzoni M, Peccatori J, Messina C, Nocco A, Cardillo M, Scavini M, Magistretti P, Doglioni C, Ciceri F, Bloem SJ, Roep BO, Secchi A, Piemonti L. Islet Allotransplantation in the Bone Marrow of Patients With Type 1 Diabetes: A Pilot Randomized Trial. Transplantation 2019; 103: 839-51.

Magliano D, Boyko E, Balkau B (2021) IDF Diabetes Atlas 10th Edition 2021

Makino S, Kunimoto K, Muraoka Y, Mizushima Y, Katagiri K, Tochino Y. Breeding of a non-obese, diabetic strain of mice. Jikken Dobutsu 1980; 29: 1-13.

Malik FS, Taplin CE. Insulin therapy in children and adolescents with type 1 diabetes. Paediatr Drugs 2014; 16: 141-50.

Mallone R, Eizirik DL. Presumption of innocence for beta cells: why are they vulnerable autoimmune targets in type 1 diabetes? Diabetologia 2020; 63: 1999-2006.

Malosio ML, Esposito A, Brigatti C, Palmisano A, Piemonti L, Nano R, Maffi P, De Cobelli F, Del Maschio A, Secchi A. MR imaging monitoring of iron-labeled pancreatic islets in a small series of patients: islet fate in successful, unsuccessful, and autotransplantation. Cell Transplant 2015; 24: 2285-96.

Marfil-Garza BA, Imes S, Verhoeff K, Hefler J, Lam A, Dajani K, Anderson B, O'Gorman D, Kin T, Bigam D, Senior PA, Shapiro AMJ. Pancreatic islet transplantation in type 1 diabetes: 20-year experience from a single-centre cohort in Canada. Lancet Diabetes Endocrinol 2022; 10: 519-32.

Markmann JF, Rickels MR, Eggerman TL, Bridges ND, Lafontant DE, Qidwai J, Foster E, Clarke WR, Kamoun M, Alejandro R, Bellin MD, Chaloner K, Czarniecki CW, Goldstein JS, Hering BJ, Hunsicker LG, Kaufman DB, Korsgren O, Larsen CP, Luo X, Naji A, Oberholzer J, Posselt AM, Ricordi C, Senior PA, Shapiro AMJ, Stock PG, Turgeon NA. Phase 3 trial of human islet-after-kidney transplantation in type 1 diabetes. Am J Transplant 2021; 21: 1477-92.

Mathews CE, Langley SH, Leiter EH. New mouse model to study islet transplantation in insulin-dependent diabetes mellitus. Transplantation 2002; 73: 1333-6.

Matsumoto S, Takita M, Chaussabel D, Noguchi H, Shimoda M, Sugimoto K, Itoh T, Chujo D, SoRelle J, Onaca N, Naziruddin B, Levy MF. Improving efficacy of clinical islet transplantation with iodixanol-based islet purification, thymoglobulin induction, and blockage of IL-1β and TNF-α. Cell Transplant 2011; 20: 1641-7.

Matsumoto S, Tan P, Baker J, Durbin K, Tomiya M, Azuma K, Doi M, Elliott RB. Clinical porcine islet xenotransplantation under comprehensive regulation. Transplant Proc 2014; 46: 1992-5.

Matsumoto S, Shimoda M. Current situation of clinical islet transplantation from allogeneic toward xenogeneic. J Diabetes 2020; 12: 733-41.

Meglasson MD, Burch PT, Berner DK, Najafi H, Matschinsky FM. Identification of glucokinase as an alloxan-sensitive glucose sensor of the pancreatic beta-cell. Diabetes 1986; 35: 1163-73.

Mellert J, Hering BJ, Liu X, Brandhorst D, Brandhorst H, Brendel M, Ernst E, Gramberg D, Bretzel RG, Hopt UT. Successful islet auto- and allotransplantation in diabetic pigs. Transplantation 1998; 66: 200-4.

Meloni AR, DeYoung MB, Lowe C, Parkes DG. GLP-1 receptor activated insulin secretion from pancreatic β-cells: mechanism and glucose dependence. Diabetes Obes Metab 2013; 15: 15-27.

Menger MD, Jaeger S, Walter P, Feifel G, Hammersen F, Messmer K. Angiogenesis and hemodynamics of microvasculature of transplanted islets of Langerhans. Diabetes 1989; 38 Suppl 1: 199-201.

Millman JR, Xie C, Van Dervort A, Gürtler M, Pagliuca FW, Melton DA. Generation of stem cell-derived β-cells from patients with type 1 diabetes. Nat Commun 2016; 7: 11463.

Min BH, Shin JS, Kim JM, Kang SJ, Kim HJ, Yoon IH, Park SK, Choi JW, Lee MS, Park CG. Delayed revascularization of islets after transplantation by IL-6 blockade in pig to non-human primate islet xenotransplantation model. Xenotransplantation 2018; 25

Moberg L, Johansson H, Lukinius A, Berne C, Foss A, Källen R, Østraat Ø, Salmela K, Tibell A, Tufveson G, Elgue G, Nilsson Ekdahl K, Korsgren O, Nilsson B. Production of tissue factor by pancreatic islet cells as a trigger of detrimental thrombotic reactions in clinical islet transplantation. Lancet 2002; 360: 2039-45.

Moberg L, Korsgren O, Nilsson B. Neutrophilic granulocytes are the predominant cell type infiltrating pancreatic islets in contact with ABO-compatible blood. Clin Exp Immunol 2005; 142: 125-31.

Mohanakumar T, Narayanan K, Desai N, Ramachandran S, Shenoy S, Jendrisak M, Susskind BM, Olack B, Benshoff N, Phelan DL, Brennan DC, Fernandez LA, Odorico JS, Polonsky KS. A significant role for histocompatibility in human islet transplantation. Transplantation 2006; 82: 180-7.

Molven A, Ringdal M, Nordbø AM, Raeder H, Støy J, Lipkind GM, Steiner DF, Philipson LH, Bergmann I, Aarskog D, Undlien DE, Joner G, Søvik O, Bell GI, Njølstad PR. Mutations in the insulin gene can cause MODY and autoantibody-negative type 1 diabetes. Diabetes 2008; 57: 1131-5.

Mordes JP, Bortell R, Blankenhorn EP, Rossini AA, Greiner DL. Rat models of type 1 diabetes: genetics, environment, and autoimmunity. Ilar j 2004; 45: 278-91.

Morel P, Kaufmann DB, Matas AJ, Tzardis P, Field MJ, Lloveras JK, Sutherland DE. Total pancreatectomy in the pig for islet transplantation. Technical alternatives. Transplantation 1991; 52: 11-5.

Moritz A, Kraft W (2014) Klinische Labordiagnostik in der Tiermedizin. Schattauer

Morozov VA, Wynyard S, Matsumoto S, Abalovich A, Denner J, Elliott R. No PERV transmission during a clinical trial of pig islet cell transplantation. Virus Res 2017; 227: 34-40.

Mysore TB, Shinkel TA, Collins J, Salvaris EJ, Fisicaro N, Murray-Segal LJ, Johnson LE, Lepore DA, Walters SN, Stokes R, Chandra AP, O'Connell PJ, d'Apice AJ, Cowan PJ. Overexpression of glutathione peroxidase with two isoforms of superoxide dismutase protects mouse islets from oxidative injury and improves islet graft function. Diabetes 2005; 54: 2109-16.

Nagaya M, Hasegawa K, Uchikura A, Nakano K, Watanabe M, Umeyama K, Matsunari H, Osafune K, Kobayashi E, Nakauchi H, Nagashima H. Feasibility of large experimental animal models in testing novel therapeutic strategies for diabetes. World J Diabetes 2021; 12: 306-30.

Najarian JS, Sutherland DE, Baumgartner D, Burke B, Rynasiewicz JJ, Matas AJ, Goetz FC. Total or near total pancreatectomy and islet autotransplantation for treatment of chronic pancreatitis. Ann Surg 1980; 192: 526-42.

Nalin L, Selvaraju RK, Velikyan I, Berglund M, Andréasson S, Wikstrand A, Rydén A, Lubberink M, Kandeel F, Nyman G, Korsgren O, Eriksson O, Jensen-Waern M. Positron emission tomography imaging of the glucagon-like peptide-1 receptor in healthy and streptozotocin-induced diabetic pigs. Eur J Nucl Med Mol Imaging 2014; 41: 1800-10.

Nathan DM, Genuth S, Lachin J, Cleary P, Crofford O, Davis M, Rand L, Siebert C. The effect of intensive treatment of diabetes on the development and progression of long-term complications in insulin-dependent diabetes mellitus. N Engl J Med 1993; 329: 977-86.

Nijhoff MF, Engelse MA, Dubbeld J, Braat AE, Ringers J, Roelen DL, van Erkel AR, Spijker HS, Bouwsma H, van der Boog PJ, de Fijter JW, Rabelink TJ, de Koning EJ. Glycemic Stability Through Islet-After-Kidney Transplantation Using an Alemtuzumab-Based Induction Regimen and Long-Term Triple-Maintenance Immunosuppression. Am J Transplant 2016; 16: 246-53.

Nilsson B, Ekdahl KN, Korsgren O. Control of instant blood-mediated inflammatory reaction to improve islets of Langerhans engraftment. Curr Opin Organ Transplant 2011; 16: 620-6.

Niu M, Liu Y, Xiang L, Zhao Y, Yuan J, Jia Y, Dai X, Chen H. Long-term case study of a Wuzhishan miniature pig with diabetes. Animal Model Exp Med 2020; 3: 22-31.

Noble JA. Immunogenetics of type 1 diabetes: A comprehensive review. J Autoimmun 2015; 64: 101-12.

Noguchi H. Pancreatic islet transplantation. World J Gastrointest Surg 2009; 1: 16-20.

Nørgaard SA, Søndergaard H, Sørensen DB, Galsgaard ED, Hess C, Sand FW. Optimising streptozotocin dosing to minimise renal toxicity and impairment of stomach emptying in male 129/Sv mice. Laboratory Animals 2020; 54: 341-52.

Ogle G, Wang F, Gregory G, Maniam J (2022) IDF ATLAS REPORTS - Type 1 diabetes estimates in children and adults

Oram RA, Sims EK, Evans-Molina C. Beta cells in type 1 diabetes: mass and function; sleeping or dead? Diabetologia 2019; 62: 567-77.

Othonos N, Choudhary P. Who Should Be Considered for Islet Transplantation Alone? Curr Diab Rep 2017; 17: 23.

Ou Y, Ren Z, Wang J, Yang X. Phycocyanin ameliorates alloxan-induced diabetes mellitus in mice: Involved in insulin signaling pathway and GK expression. Chem Biol Interact 2016; 247: 49-54.

Owen RJ, Ryan EA, O'Kelly K, Lakey JR, McCarthy MC, Paty BW, Bigam DL, Kneteman NM, Korbutt GS, Rajotte RV, Shapiro AM. Percutaneous transhepatic pancreatic islet cell transplantation in type 1 diabetes mellitus: radiologic aspects. Radiology 2003; 229: 165-70.

Ozmen L, Ekdahl KN, Elgue G, Larsson R, Korsgren O, Nilsson B. Inhibition of thrombin abrogates the instant blood-mediated inflammatory reaction triggered by isolated human islets: possible application of the thrombin inhibitor melagatran in clinical islet transplantation. Diabetes 2002; 51: 1779-84.

Pagliuca FW, Millman JR, Gürtler M, Segel M, Van Dervort A, Ryu JH, Peterson QP, Greiner D, Melton DA. Generation of functional human pancreatic β cells in vitro. Cell 2014; 159: 428-39.

Pamidi N, Satheesha Nayak BN. Effect of streptozotocin induced diabetes on rat hippocampus. Bratisl Lek Listy 2012; 113: 583-8.

Panah FM, Lauridsen C, Højberg O, Nielsen TS. Etiology of Colitis-Complex Diarrhea in Growing Pigs: A Review. Animals (Basel) 2021; 11

Parlakpinar H, Gunata M. Transplantation and immunosuppression: a review of novel transplant-related immunosuppressant drugs. Immunopharmacol Immunotoxicol 2021; 43: 651-65.

Paschou SA, Papadopoulou-Marketou N, Chrousos GP, Kanaka-Gantenbein C. On type 1 diabetes mellitus pathogenesis. Endocr Connect 2018; 7: R38-R46.

Piemonti L, Pileggi A. 25 YEARS OF THE RICORDI AUTOMATED METHOD FOR ISLET ISOLATION. CellR4 Repair Replace Regen Reprogram 2013; 1

Piemonti L, Everly MJ, Maffi P, Scavini M, Poli F, Nano R, Cardillo M, Melzi R, Mercalli A, Sordi V, Lampasona V, Espadas de Arias A, Scalamogna M, Bosi E, Bonifacio E, Secchi A, Terasaki PI. Alloantibody and autoantibody monitoring predicts islet transplantation outcome in human type 1 diabetes. Diabetes 2013; 62: 1656-64.

Piemonti L (2022) Islet Transplantation [Updated 2022 Sep 16]. In: Endotext [Internet]. Eds Feingold K, Anawalt B, Blackman M, et a, South Dartmouth (MA): MDText.com, Inc.

Pilz J, Gloddek N, Puhr-Westerheide D, Ümütlü M, Wolf E, Kemter E. 118.3: Intraportal transplantation of neonatal porcine islets cures diabetes mellitus of INSC94Y transgenic pigs. Transplantation 2023; 107: 31. (Published congress abstract)

Pilz J, Gloddek N, Lindheimer F, Lindner MJ, Puhr-Westerheide D, Ümütlü M, Cyran C, Seidensticker M, Lindner R, Kraetzl M, Renner S, Merkus D, Teupser D, Bartenstein P, Ziegler SI, Wolf E, Kemter E. Functional maturation and longitudinal imaging of intraportal neonatal porcine islet grafts in genetically diabetic pigs. Am J Transplant 2024;

Podell BK, Ackart DF, Richardson MA, DiLisio JE, Pulford B, Basaraba RJ. A model of type 2 diabetes in the guinea pig using sequential diet-induced glucose intolerance and streptozotocin treatment. Dis Model Mech 2017; 10: 151-62.

Polak M, Dechaume A, Cavé H, Nimri R, Crosnier H, Sulmont V, de Kerdanet M, Scharfmann R, Lebenthal Y, Froguel P, Vaxillaire M. Heterozygous missense mutations in the insulin gene are linked to permanent diabetes appearing in the neonatal period or in early infancy: a report from the French ND (Neonatal Diabetes) Study Group. Diabetes 2008; 57: 1115-9.

Ponte GM, Pileggi A, Messinger S, Alejandro A, Ichii H, Baidal DA, Khan A, Ricordi C, Goss JA, Alejandro R. Toward maximizing the success rates of human islet isolation: influence of donor and isolation factors. Cell Transplant 2007; 16: 595-607.

Posselt AM, Szot GL, Frassetto LA, Masharani U, Tavakol M, Amin R, McElroy J, Ramos MD, Kerlan RK, Fong L, Vincenti F, Bluestone JA, Stock PG. Islet Transplantation in Type 1 Diabetic Patients Using Calcineurin Inhibitor-Free Immunosuppressive Protocols Based on T-Cell Adhesion or Costimulation Blockade. Transplantation 2010; 90: 1595-601.

Quattrin T, Mastrandrea LD, Walker LSK. Type 1 diabetes. Lancet 2023; 401: 2149-62.

Radenković M, Stojanović M, Prostran M. Experimental diabetes induced by alloxan and streptozotocin: The current state of the art. J Pharmacol Toxicol Methods 2016; 78: 13-31.

Rafael E, Ryan EA, Paty BW, Oberholzer J, Imes S, Senior P, McDonald C, Lakey JR, Shapiro AM. Changes in liver enzymes after clinical islet transplantation. Transplantation 2003; 76: 1280-4.

Rahmim A, Zaidi H. PET versus SPECT: strengths, limitations and challenges. Nucl Med Commun 2008; 29: 193-207.

Rajab A. Islet transplantation: alternative sites. Curr Diab Rep 2010; 10: 332-7.

Reckard CR, Barker CF. Transplantation of isolated pancreatic islets across strong and weak histocompatibility barriers. Transplant Proc 1973; 5: 761-3.

Rees DA, Alcolado JC. Animal models of diabetes mellitus. Diabet Med 2005; 22: 359-70.

Reid L, Baxter F, Forbes S. Effects of islet transplantation on microvascular and macrovascular complications in type 1 diabetes. Diabet Med 2021; 38: e14570.

Renner S, Fehlings C, Herbach N, Hofmann A, von Waldthausen DC, Kessler B, Ulrichs K, Chodnevskaja I, Moskalenko V, Amselgruber W, Göke B, Pfeifer A, Wanke R, Wolf E. Glucose intolerance and reduced proliferation of pancreatic beta-cells in transgenic pigs with impaired glucose-dependent insulinotropic polypeptide function. Diabetes 2010; 59: 1228-38.

Renner S, Braun-Reichhart C, Blutke A, Herbach N, Emrich D, Streckel E, Wünsch A, Kessler B, Kurome M, Bähr A, Klymiuk N, Krebs S, Puk O, Nagashima H, Graw J, Blum H, Wanke R, Wolf E. Permanent Neonatal Diabetes in INSC94Y Transgenic Pigs. Diabetes 2013; 62: 1505-11.

Renner S, Blutke A, Clauss S, Deeg CA, Kemter E, Merkus D, Wanke R, Wolf E. Porcine models for studying complications and organ crosstalk in diabetes mellitus. Cell Tissue Res 2020; 380: 341-78.

Reusser F. Mode of action of streptozotocin. J Bacteriol 1971; 105: 580-8.

Rewers M, Ludvigsson J. Environmental risk factors for type 1 diabetes. Lancet 2016; 387: 2340-8.

Richards TM, Sun A, Hayat H, Robertson N, Zhang Z, Fan J, Wang P. Current Progress and Perspective: Clinical Imaging of Islet Transplantation. Life (Basel) 2020; 10

Richardson SJ, Rodriguez-Calvo T, Gerling IC, Mathews CE, Kaddis JS, Russell MA, Zeissler M, Leete P, Krogvold L, Dahl-Jorgensen K, von Herrath M, Pugliese A, Atkinson MA, Morgan NG. Islet cell hyperexpression of HLA class I antigens: a defining feature in type 1 diabetes. Diabetologia 2016; 59: 2448-58.

Rickels MR, Stock PG, de Koning EJP, Piemonti L, Pratschke J, Alejandro R, Bellin MD, Berney T, Choudhary P, Johnson PR, Kandaswamy R, Kay TWH, Keymeulen B, Kudva YC, Latres E, Langer RM, Lehmann R, Ludwig B, Markmann JF, Marinac M, Odorico JS, Pattou F, Senior PA, Shaw JAM, Vantyghem MC, White S. Defining Outcomes for β-cell Replacement Therapy in the Treatment of Diabetes: A Consensus Report on the Igls Criteria From the IPITA/EPITA Opinion Leaders Workshop. Transplantation 2018; 102: 1479-86.

Rickels MR, Robertson RP. Pancreatic Islet Transplantation in Humans: Recent Progress and Future Directions. Endocr Rev 2019; 40: 631-68.

Ricordi C, Lacy PE, Finke EH, Olack BJ, Scharp DW. Automated method for isolation of human pancreatic islets. Diabetes 1988; 37: 413-20.

Ricordi C, Lacy PE, Scharp DW. Automated islet isolation from human pancreas. Diabetes 1989; 38 Suppl 1: 140-2.

Ricordi C, Japour A. Transplanting islet cells can fix brittle diabetes. Why isn't it available in the U.S.? CellR4 Repair Replace Regen Reprogram 2019; 7

Robinson NB, Krieger K, Khan FM, Huffman W, Chang M, Naik A, Yongle R, Hameed I, Krieger K, Girardi LN, Gaudino M. The current state of animal models in research: A review. Int J Surg 2019; 72: 9-13.

Rodriguez-Calvo T, Richardson SJ, Pugliese A. Pancreas Pathology During the Natural History of Type 1 Diabetes. Curr Diab Rep 2018; 18: 124.

Rodriguez-Diaz R, Dando R, Jacques-Silva MC, Fachado A, Molina J, Abdulreda MH, Ricordi C, Roper SD, Berggren PO, Caicedo A. Alpha cells secrete acetylcholine as a non-neuronal paracrine signal priming beta cell function in humans. Nat Med 2011a; 17: 888-92.

Rodriguez-Diaz R, Abdulreda MH, Formoso AL, Gans I, Ricordi C, Berggren PO, Caicedo A. Innervation patterns of autonomic axons in the human endocrine pancreas. Cell Metab 2011b; 14: 45-54.

Roep BO, Stobbe I, Duinkerken G, van Rood JJ, Lernmark A, Keymeulen B, Pipeleers D, Claas FH, de Vries RR. Auto- and alloimmune reactivity to human islet allografts transplanted into type 1 diabetic patients. Diabetes 1999; 48: 484-90.

Roep BO, Thomaidou S, van Tienhoven R, Zaldumbide A. Type 1 diabetes mellitus as a disease of the beta-cell (do not blame the immune system?). Nat Rev Endocrinol 2021; 17: 150-61.

Rooden Rv, Doppenberg JB, van Dijk MC, De Goeij FH, van der Heijden FJ, Alwayn IP, De Koning EJ, Jonge JD, Engelse MA, Huurman VA. 310.1: Improved pancreatic islet isolation yield after abdominal normothermic regional perfusion of controlled donation after circulatory death donors. Transplantation 2023; 107: 83.

Ryan EA, Paty BW, Senior PA, Bigam D, Alfadhli E, Kneteman NM, Lakey JR, Shapiro AM. Five-year follow-up after clinical islet transplantation. Diabetes 2005; 54: 2060-9.

Sageshima J, Ciancio G, Chen L, Dohi T, El-Hinnawi A, Paloyo S, Misawa R, Ekwenna O, Yatawatta A, Burke GW, 3rd. Everolimus with low-dose tacrolimus in simultaneous pancreas and kidney transplantation. Clin Transplant 2014; 28: 797-801.

Sahin GS, Lee H, Engin F. An accomplice more than a mere victim: The impact of beta-cell ER stress on type 1 diabetes pathogenesis. Mol Metab 2021; 54: 101365.

Sakata N, Yoshimatsu G, Tsuchiya H, Egawa S, Unno M. Animal models of diabetes mellitus for islet transplantation. Exp Diabetes Res 2012; 2012: 256707.

Saudek F, Jirák D, Girman P, Herynek V, Dezortová M, Kríz J, Peregrin J, Berková Z, Zacharovová K, Hájek M. Magnetic resonance imaging of pancreatic islets transplanted into the liver in humans. Transplantation 2010; 90: 1602-6.

Schölin A, Siegbahn A, Lind L, Berne C, Sundkvist G, Björk E, Karlsson FA. CRP and IL-6 concentrations are associated with poor glycemic control despite preserved beta-cell function during the first year after diagnosis of type 1 diabetes. Diabetes Metab Res Rev 2004; 20: 205-10.

Shah RB, Patel M, Maahs DM, Shah VN. Insulin delivery methods: Past, present and future. Int J Pharm Investig 2016; 6: 1-9.

Shapiro AM, Lakey JR, Ryan EA, Korbutt GS, Toth E, Warnock GL, Kneteman NM, Rajotte RV. Islet transplantation in seven patients with type 1 diabetes mellitus using a glucocorticoid-free immunosuppressive regimen. N Engl J Med 2000; 343: 230-8.

Shapiro AM. State of the art of clinical islet transplantation and novel protocols of immunosuppression. Curr Diab Rep 2011; 11: 345-54.

Shapiro AM. Islet transplantation in type 1 diabetes: ongoing challenges, refined procedures, and long-term outcome. Rev Diabet Stud 2012; 9: 385-406.

Shapiro AM, Ricordi C. Islet Cell Transplantation Procedure and Surgical Technique. In: Textbook of Organ Transplantation. Kirk AD, Knechtle SJ, Larsen CP, Madsen JC, Pearson TC, Webber SA, eds.: 2014: 682-90.

Shapiro AM, Pokrywczynska M, Ricordi C. Clinical pancreatic islet transplantation. Nat Rev Endocrinol 2017; 13: 268-77.

Shapiro J. Eighty years after insulin: parallels with modern islet transplantation. CMAJ 2002; 167: 1398-400.

Shin J-S, Kim J-M, Min B-H, Kim J-S, Yoon I-H, Chung H, Lee W-W, Kang HJ, Park C-G. Pig-to-Nonhuman Primate (NHP) Naked Islet Xenotransplantation. In: Xenotransplantation. Shuji M, ed. Rijeka: IntechOpen 2017: Ch. 6.

Shin JS, Kim JM, Kim JS, Min BH, Kim YH, Kim HJ, Jang JY, Yoon IH, Kang HJ, Kim J, Hwang ES, Lim DG, Lee WW, Ha J, Jung KC, Park SH, Kim SJ, Park CG. Long-term control of diabetes in immunosuppressed nonhuman primates (NHP) by the transplantation of adult porcine islets. Am J Transplant 2015; 15: 2837-50.

Shojaeian A, Mehri-Ghahfarrokhi A. An overview of the Epidemiology of Type 1 Diabetes Mellitus. International Journal of Metabolic Syndromes 2018;

Smith KE, Purvis WG, Davis MA, Min CG, Cooksey AM, Weber CS, Jandova J, Price ND, Molano DS, Stanton JB, Kelly AC, Steyn LV, Lynch RM, Limesand SW, Alexander M, Lakey JRT, Seeberger K, Korbutt GS, Mueller KR, Hering BJ, McCarthy FM, Papas KK. In vitro characterization of neonatal, juvenile, and adult porcine islet oxygen demand, β-cell function, and transcriptomes. Xenotransplantation 2018; 25: e12432.

Soleimanpour SA, Sekiguchi DR, LaRosa DF, Luning Prak ET, Naji A, Rickels MR. Hypersensitivity to rabbit antithymocyte globulin in an islet transplant recipient: a case report. Transplant Proc 2011; 43: 3302-6.

Stegall MD, Lafferty KJ, Kam I, Gill RG. Evidence of recurrent autoimmunity in human allogeneic islet transplantation. Transplantation 1996; 61: 1272-4.

Støy J, Edghill EL, Flanagan SE, Ye H, Paz VP, Pluzhnikov A, Below JE, Hayes MG, Cox NJ, Lipkind GM, Lipton RB, Greeley SA, Patch AM, Ellard S, Steiner DF, Hattersley AT, Philipson LH, Bell GI. Insulin gene mutations as a cause of permanent neonatal diabetes. Proc Natl Acad Sci U S A 2007; 104: 15040-4.

Sussman M, Benner J, Haller MJ, Rewers M, Griffiths R. Estimated Lifetime Economic Burden of Type 1 Diabetes. Diabetes Technol Ther 2020; 22: 121-30.

Suszynski TM, Avgoustiniatos ES, Papas KK. Intraportal islet oxygenation. J Diabetes Sci Technol 2014; 8: 575-80.

Swindle MM, Makin A, Herron AJ, Clubb FJ, Jr., Frazier KS. Swine as models in biomedical research and toxicology testing. Vet Pathol 2012; 49: 344-56.

Szempruch KR, Banerjee O, McCall RC, Desai CS. Use of anti-inflammatory agents in clinical islet cell transplants: A qualitative systematic analysis. Islets 2019; 11: 65-75.

Szkudelski T. The mechanism of alloxan and streptozotocin action in B cells of the rat pancreas. Physiol Res 2001; 50: 537-46.

Takahashi K, Yamanaka S. Induction of pluripotent stem cells from mouse embryonic and adult fibroblast cultures by defined factors. Cell 2006; 126: 663-76.

Taylor GD, Kirkland T, Lakey J, Rajotte R, Warnock GL. Bacteremia due to transplantation of contaminated cryopreserved pancreatic islets. Cell Transplant 1994; 3: 103-6.

Thongprayoon C, Hansrivijit P, Kovvuru K, Kanduri SR, Bathini T, Pivovarova A, Smith JR, Cheungpasitporn W. Impacts of High Intra- and Inter-Individual Variability in Tacrolimus Pharmacokinetics and Fast Tacrolimus Metabolism on Outcomes of Solid Organ Transplant Recipients. J Clin Med 2020; 9

Tornehave D, Kristensen P, Rømer J, Knudsen LB, Heller RS. Expression of the GLP-1 receptor in mouse, rat, and human pancreas. J Histochem Cytochem 2008; 56: 841-51.

Toso C, Vallee JP, Morel P, Ris F, Demuylder-Mischler S, Lepetit-Coiffe M, Marangon N, Saudek F, James Shapiro AM, Bosco D, Berney T. Clinical magnetic resonance imaging of pancreatic islet grafts after iron nanoparticle labeling. Am J Transplant 2008; 8: 701-6.

Toso C, Isse K, Demetris AJ, Dinyari P, Koh A, Imes S, Kin T, Emamaullee J, Senior P, Shapiro AM. Histologic graft assessment after clinical islet transplantation. Transplantation 2009; 88: 1286-93.

Tritschler S, Thomas M, Böttcher A, Ludwig B, Schmid J, Schubert U, Kemter E, Wolf E, Lickert H, Theis FJ. A transcriptional cross species map of pancreatic islet cells. Mol Metab 2022; 66: 101595.

Trivedi N, Hollister-Lock J, Lopez-Avalos MD, O'Neil JJ, Keegan M, Bonner-Weir S, Weir GC. Increase in beta-cell mass in transplanted porcine neonatal pancreatic cell clusters is due to proliferation of beta-cells and differentiation of duct cells. Endocrinology 2001; 142: 2115-22.

Turan A, Zhang L, Tarique M, Ulker V, Arguc FN, Badal D, Yolcu ES, Shirwan H. Engineering pancreatic islets with a novel form of thrombomodulin protein to overcome early graft loss triggered by instant blood-mediated inflammatory reaction. Am J Transplant 2023; 23: 619-28.

Tydén G, Reinholt FP, Sundkvist G, Bolinder J. Recurrence of autoimmune diabetes mellitus in recipients of cadaveric pancreatic grafts. N Engl J Med 1996; 335: 860-3.

Umeyama K, Watanabe M, Saito H, Kurome M, Tohi S, Matsunari H, Miki K, Nagashima H. Dominant-negative mutant hepatocyte nuclear factor 1alpha induces diabetes in transgenic-cloned pigs. Transgenic Res 2009; 18: 697-706.

Urakami T. Severe Hypoglycemia: Is It Still a Threat for Children and Adolescents With Type 1 Diabetes? Front Endocrinol (Lausanne) 2020; 11: 609.

Vajkoczy P, Menger MD, Simpson E, Messmer K. Angiogenesis and vascularization of murine pancreatic islet isografts. Transplantation 1995a; 60: 123-7.

Vajkoczy P, Olofsson AM, Lehr HA, Leiderer R, Hammersen F, Arfors KE, Menger MD. Histogenesis and ultrastructure of pancreatic islet graft microvasculature. Evidence for graft revascularization by endothelial cells of host origin. Am J Pathol 1995b; 146: 1397-405.

Valdés-González RA, Dorantes LM, Garibay GN, Bracho-Blanchet E, Mendez AJ, Dávila-Pérez R, Elliott RB, Terán L, White DJ. Xenotransplantation of porcine neonatal islets of Langerhans and Sertoli cells: a 4-year study. Eur J Endocrinol 2005; 153: 419-27.

Van Belle T, von Herrath M. Immunosuppression in islet transplantation. J Clin Invest 2008; 118: 1625-8.

van der Windt DJ, Echeverri GJ, Ijzermans JN, Cooper DK. The choice of anatomical site for islet transplantation. Cell Transplant 2008; 17: 1005-14.

Vanderschelden R, Sathialingam M, Alexander M, Lakey JRT. Cost and Scalability Analysis of Porcine Islet Isolation for Islet Transplantation: Comparison of Juvenile, Neonatal and Adult Pigs. Cell Transplant 2019; 28: 967-72.

Vantyghem MC, de Koning EJP, Pattou F, Rickels MR. Advances in β-cell replacement therapy for the treatment of type 1 diabetes. Lancet 2019; 394: 1274-85.

Vendrame F, Pileggi A, Laughlin E, Allende G, Martin-Pagola A, Molano RD, Diamantopoulos S, Standifer N, Geubtner K, Falk BA, Ichii H, Takahashi H, Snowhite I, Chen Z, Mendez A, Chen L, Sageshima J, Ruiz P, Ciancio G, Ricordi C, Reijonen H, Nepom GT, Burke GW, 3rd, Pugliese A. Recurrence of type 1 diabetes after simultaneous pancreas-kidney transplantation, despite immunosuppression, is associated with autoantibodies and pathogenic autoreactive CD4 T-cells. Diabetes 2010; 59: 947-57.

Venturini M, Angeli E, Maffi P, Fiorina P, Bertuzzi F, Salvioni M, De Cobelli F, Socci C, Aldrighetti L, Losio C, Di Carlo V, Secchi A, Del Maschio A. Technique, complications, and therapeutic efficacy of percutaneous transplantation of human pancreatic islet cells in type 1 diabetes: the role of US. Radiology 2005; 234: 617-24.

Venturini M, Maffi P, Querques G, Agostini G, Piemonti L, Sironi S, De Cobelli F, Fiorina P, Secchi A, Del Maschio A. Hepatic steatosis after islet transplantation: Can ultrasound predict the clinical outcome? A longitudinal study in 108 patients. Pharmacol Res 2015; 98: 52-9.

Venturini M, Sallemi C, Marra P, Palmisano A, Agostini G, Lanza C, Balzano G, Falconi M, Secchi A, Fiorina P, Piemonti L, Maffi P, Esposito A, De Cobelli F, Del Maschio A. Allo- and auto-percutaneous intra-portal pancreatic islet transplantation (PIPIT) for diabetes cure and prevention: the role of imaging and interventional radiology. Gland Surg 2018; 7: 117-31.

Vilsbøll T, Agersø H, Krarup T, Holst JJ. Similar elimination rates of glucagon-like peptide-1 in obese type 2 diabetic patients and healthy subjects. J Clin Endocrinol Metab 2003; 88: 220-4.

Wagner LE, Melnyk O, Duffett BE, Linnemann AK. Mouse models and human islet transplantation sites for intravital imaging. Front Endocrinol (Lausanne) 2022; 13: 992540.

Walker S, Appari M, Forbes S. Considerations and challenges of islet transplantation and future therapies on the horizon. Am J Physiol Endocrinol Metab 2022; 322: E109-e17.

Wang C, Du X, Fu F, Li X, Wang Z, Zhou Y, Gou L, Li W, Li J, Zhang J, Liao G, Li L, Han YP, Tong N, Liu J, Chen Y, Cheng J, Cao Q, Ilegems E, Lu Y, Zheng X, Berggren PO. Adiponectin gene therapy prevents islet loss after transplantation. J Cell Mol Med 2022; 26: 4847-58.

Wang W, Mo Z, Ye B, Hu P, Liu S, Yi S. A clinical trial of xenotransplantation of neonatal pig islets for diabetic patients. Zhong Nan Da Xue Xue Bao Yi Xue Ban 2011; 36: 1134-40.

Wang Y, Wang S, Harvat T, Kinzer K, Zhang L, Feng F, Qi M, Oberholzer J. Diazoxide, a K(ATP) channel opener, prevents ischemia-reperfusion injury in rodent pancreatic islets. Cell Transplant 2015; 24: 25-36.

Weimar B, Rauber K, Brendel MD, Bretzel RG, Rau WS. Percutaneous transhepatic catheterization of the portal vein: A combined CT- and fluoroscopy-guided technique. Cardiovasc Intervent Radiol 1999; 22: 342-4.

Wiedenmann B, Franke WW, Kuhn C, Moll R, Gould VE. Synaptophysin: a marker protein for neuroendocrine cells and neoplasms. Proc Natl Acad Sci U S A 1986; 83: 3500-4.

Wild D, Wicki A, Mansi R, Béhé M, Keil B, Bernhardt P, Christofori G, Ell PJ, Mäcke HR. Exendin-4-based radiopharmaceuticals for glucagonlike peptide-1 receptor PET/CT and SPECT/CT. J Nucl Med 2010; 51: 1059-67.

Wise MH, Gordon C, Johnson RW. Intraportal autotransplantation of cryopreserved porcine islets of Langerhans. Cryobiology 1985; 22: 359-66.

Wojtusciszyn A, Branchereau J, Esposito L, Badet L, Buron F, Chetboun M, Kessler L, Morelon E, Berney T, Pattou F, Benhamou PY, Vantyghem MC. Indications for islet or pancreatic transplantation: Statement of the TREPID working group on behalf of the Société francophone du diabète (SFD), Société francaise d'endocrinologie (SFE), Société francophone de transplantation (SFT) and Société française de néphrologie - dialyse - transplantation (SFNDT). Diabetes Metab 2019; 45: 224-37.

Wolf E, Braun-Reichhart C, Streckel E, Renner S. Genetically engineered pig models for diabetes research. Transgenic Res 2014; 23: 27-38.

Yoon KH, Quickel RR, Tatarkiewicz K, Ulrich TR, Hollister-Lock J, Trivedi N, Bonner-Weir S, Weir GC. Differentiation and expansion of beta cell mass in porcine neonatal pancreatic cell clusters transplanted into nude mice. Cell Transplant 1999; 8: 673-89.

Yoshinaga T, Nakatome K, Nozaki J, Naitoh M, Hoseki J, Kubota H, Nagata K, Koizumi A. Proinsulin lacking the A7-B7 disulfide bond, Ins2Akita, tends to aggregate due to the exposed hydrophobic surface. Biol Chem 2005; 386: 1077-85.

Yu L, Zhao Z, Steck AK. T1D Autoantibodies: room for improvement? Curr Opin Endocrinol Diabetes Obes 2017; 24: 285-91.

Yu MG, Keenan HA, Shah HS, Frodsham SG, Pober D, He Z, Wolfson EA, D'Eon S, Tinsley LJ, Bonner-Weir S, Pezzolesi MG, King GL. Residual β cell function and monogenic variants in long-duration type 1 diabetes patients. J Clin Invest 2019; 129: 3252-63.

Zajec A, Trebusak Podkrajsek K, Tesovnik T, Sket R, Cugalj Kern B, Jenko Bizjan B, Smigoc Schweiger D, Battelino T, Kovac J. Pathogenesis of Type 1 Diabetes: Established Facts and New Insights. Genes (Basel) 2022; 13

Zatcepin A, Ziegler SI. Detectors in positron emission tomography. Z Med Phys 2023; 33: 4-12.

Zeng Y, Ricordi C, Lendoire J, Carroll PB, Alejandro R, Bereiter DR, Tzakis A, Starzl TE. The effect of prednisone on pancreatic islet autografts in dogs. Surgery 1993; 113: 98-102.

Zettler S, Renner S, Kemter E, Hinrichs A, Klymiuk N, Backman M, Riedel EO, Mueller C, Streckel E, Braun-Reichhart C, Martins AS, Kurome M, Keßler B, Zakhartchenko V, Flenkenthaler F, Arnold GJ, Fröhlich T, Blum H, Blutke A, Wanke R, Wolf E. A decade of experience with genetically tailored pig models for diabetes and metabolic research. Anim Reprod 2020; 17: e20200064.

Zhang B, Zhang J, Pei G, Wang J, Liu Y, Ding X, Wang Z, Wang S, Shen Z. Effect factors of liver enzymes elevation afterintraportal islet transplantation. Chinese Journal of Organ Transplantation 2019; 40: 519-22.

Zhang S, Yan H, Ma X, Zheng W, Wang W. Effects of different routes of heparin on instant blood-mediated inflammatory reaction after portal vein islet transplantation. Zhong Nan Da Xue Xue Bao Yi Xue Ban 2022; 47: 1-7.

Zheng C, Huang L, Luo W, Yu W, Hu X, Guan X, Cai Y, Zou C, Yin H, Xu Z, Liang G, Wang Y. Inhibition of STAT3 in tubular epithelial cells prevents kidney fibrosis and nephropathy in STZ-induced diabetic mice. Cell Death Dis 2019; 10: 848.

Zhong J, Mao X, Li H, Shen G, Cao X, He N, Wang J, Xu L, Chen J, Song X, Liu S, Zhang X, Shen Y, Wang LL, Xiang C, Chen YY. Single-cell RNA sequencing analysis reveals the relationship of bone marrow and osteopenia in STZ-induced type 1 diabetic mice. J Adv Res 2022; 41: 145-58.

XII. ACKNOWLEDGEMENTS

First of all, I would like to thank Prof. Eckhard Wolf for the opportunity to pursue my doctoral thesis at the Chair for Molecular Animal Breeding and Biotechnology. In particular, I am grateful to Prof. Wolf for the chance to present my research results at the IPITA-IXA-CTMR Joint Congress 2023 in San Diego, which was a special highlight.

My sincere thanks to my doctoral supervisor Prof. Dr. Elisabeth Kemter, for her support, her remarkable commitment, and the pleasant cooperation.

I would like to express my gratitude to my project partner, Nicol Gloddek, for her outstanding efforts and the professional exchange. I thoroughly enjoyed our collaborative work and am grateful to have found a good friend.

A big thank you to everyone working at the Moorversuchsgut. I particularly thank Tatiana Schröter, Florentine Stotz, and Christina Blechinger for their excellent technical support. Special shoutout goes to my colleagues and friends Sarah Grimus, Yasmin Eckstein, and Richard Lindner, who have greatly enriched my time as a doctoral student.

I would also like to thank all iNanoBIT project partners for the constructive and successful cooperation, especially Prof. Sibylle Ziegler, Felix Lindheimer, and Dr. Daniel Puhr-Westerheide. Additionally, I appreciate the excellent care of our laboratory animals provided by the animal husbandry department of the Walter-Brendel-Center.

Of course, my special acknowledgement and big thank you go to Alex, my family and my friends for their support, their interest and their belief in me. My dog Dobby also deserves a special mention, as our walks were a nice balance for me while writing this work.

Last but not least, I would like to direct my focus and gratitude to those who are at the center of this doctoral thesis and without whom no insights would have been gained: my experimental pigs.